

Univerzita Karlova v Praze
Přírodovědecká fakulta

Studijní program: Fyzikální chemie



Mgr. Kristýna Sovová

**Hmotnostní spektrometrie v proudové trubici s vybranými
ionty, SIFT-MS**

Selected ion flow tube mass spectrometry, SIFT-MS

Disertační práce

Školitel: prof. RNDr. Patrik Španěl, Dr. rer. nat.

Konzultant: prof. RNDr. Eva Tesařová, CSc.

Praha 2013

Prohlášení:

Prohlašuji, že jsem závěrečnou práci zpracovala samostatně a že jsem uvedla všechny použité informační zdroje a literaturu. Tato práce ani její podstatná část nebyla předložena k získání jiného nebo stejného akademického titulu.

V Praze, 12.9. 2013

Podpis

*Pouhou mravenčí práci, s obzorem nízko nad stolem, se nic chytrého vymyslet nedá,
i vědec musí mít jistou fantazii.....*

Jiří Drahoš, předseda AVČR

Acknowledgments

I would like to express my gratitude to many people for their support during my studies. Without them, this work would not have been possible.

The first person to whom I wish to thank is my supervisor professor Patrik Španěl. In the last four years he was my mentor in understanding of the principles of the selected ion flow tube mass spectrometry (SIFT-MS) method. He taught me physics, physical chemistry, mathematics and helped me to improve skills in presentation of results including scientific writing. None of my questions were too foolish for him and he always answered them patiently. I hope that I have learned something from him. He is the person who I respect enormously. I would also like to thank professor Eva Tesařová, my supervisor-consultant at Charles University, Faculty of Science for her support starting from bachelor degree up to now. She was always ready to provide me help and advice; her support has also allowed me to successfully obtain funding from Grant Agency of Charles University and finally she has spent her time reading my thesis and provided useful comments.

Furthermore, I would like to thank my two colleagues Ksenyia Dryahina and Violetta Shestivska. I have spent good years in the lab in the company of these two inspirational ladies, realizing several research projects. Kseniya helped me a lot with my first experiments concerning kinetics of ion-molecule reactions and Violetta provided expert insight into plant physiology and phytoremediation. They both became my friends. I would also like to thank to my co-worker Jiří Kubišta I liked very much the discussions with him about good laboratory practice. It was my honour, that I met professor David Smith FRS from Keel University in England, who together with Patrik Španěl developed SIFT-MS method. It was a pleasure to discuss with him my results reached in the field of ion chemistry relevant for SIFT-MS. Last but not least, I really appreciate his help in reading my thesis and correcting the English. My thanks go also to professor Svatopluk Civiš from the department of laser spectroscopy, who supervised me as bachelor student at Heyrovský institute in 2006. In 2007 he allowed me to participate in the research project on explosives and which was an important contribution to this thesis. I am grateful to all co-author of the publications included in this theses for their contributions detailed on the next page.

Finally, I would like to thank Pavel Zimčák, all my friends and family members, especially my parents for their kind support and encouragement.

Contributions to papers included in the thesis

- A.** Sovová K., Dryahina K., Španěl P.: Selected ion flow tube, SIFT, studies of the reactions of H_3O^+ , NO^+ and $\text{O}_2^{+\bullet}$ with six volatile phytogetic esters *Int. J. Mass spectrom.* **300**, 31 (2011).

Conception and design of the study: all authors. Supervision of the study: KS. Experimental set-up: KD, KS. Data collection/analysis: KS, interpretation of results: all authors. Drafting the manuscript: PS, KS. Approval of intellectual content: all authors.

- B.** Smith D., Sovová K. and Španěl P.: A selected ion flow tube study of the reactions of H_3O^+ , NO^+ and $\text{O}_2^{+\bullet}$ with seven isomers of hexanol in support of SIFT-MS *Int. J. Mass spectrom.* **319**, 25 (2012).

Conception and design of the study: all authors. Supervision of the study: KS, PS. Experimental set-up: KS. Data collection/analysis: KS, interpretation of results: all authors. Drafting the manuscript: all authors. Approval of intellectual content: all authors.

- C.** Dryahina K., Španěl P., Pospíšilová V., Sovová K., Hrdlička L., Machková N., Lukáš M. and David Smith: Quantification of pentane in exhaled breath, a potential biomarker of bowel disease, using selected ion flow tube mass spectrometry *Rapid Commun. Mass Spectrom.* **27**, 1983 (2013).

Conception and design of the study: KD, PS. Supervision of the study: KD, PS. Research governance issues including ethics committee approval: LH, ML. Recruitment of patients: LH, NM, ML. Data collection/analysis: KD, KS, VP, interpretation of results including ion chemistry study of pentane: KD, PS, KS. Drafting the manuscript: KS, PS, DS, LH. Approval of intellectual content: all authors.

- D.** Shestivska V., Nemeč A., Dřevínek P., Sovová K., Dryahina K. and Španěl P.: Quantification of methyl thiocyanate in the headspace of *Pseudomonas aeruginosa* cultures and in the breath of cystic fibrosis patients by selected ion flow tube mass spectrometry *Rapid Commun. Mass Spectrom.* **25**, 2459 (2011).

Conception and design of the study: VS, AN, KD, PS. Supervision of the study: VS, KD, PS. Research governance issues including ethics committee approval: PD. Recruitment of patients: PD. Data collection/analysis: VS, KD, KS, interpretation of results including ion chemistry study of methylthiocyanate: VS,

KD, PS, KS. Drafting the manuscript: VS, AN, PS, KD, PD. Approval of intellectual content: all authors.

- E.** Sovová K., Čepl J., Markoš A. and Španěl P.: Real time monitoring of population dynamics in concurrent bacterial growth using SIFT-MS quantification of volatile metabolites *Analyst* **138**, 4795 (2013).

Conception and design of the study: all authors. Supervision of the study: KS, JČ. Sample preparation: JČ. Data collection/analysis using SIFT-MS: KS. Interpretation of results (SIFT-MS): KS, PS. Interpretation of results (innoculation and counting of CFU): JČ. Drafting the manuscript: all authors. Approval of intellectual content: all authors.

- F.** Sovová K., Shestivska V. and Španěl P.: Real-time quantification of traces of biogenic volatile selenium compounds in humid air by selected ion flow tube mass spectrometry *Anal. Chem.* **84**, 4979 (2012).

Conception and design of the study: KS, VS. Supervision of the study: KS. Sample preparation: KS. Data collection/analysis using SIFT-MS: KS. Interpretation of results (SIFT-MS): KS. Interpretation of results (GC/MS): VS. Drafting the manuscript: KS, PS. Approval of intellectual content: all authors.

- G.** Civiš M., Civiš S., Sovová K., Dryahina K., Španěl P., Kyncl M.: Laser Ablation of FOX-7: Proposed Mechanism of Decomposition *Anal. Chem.* **83**, 1069 (2011).

Conception and design of the study: MC, SC. Supervision of the study: MC. Data collection/analysis using UV-Vis: MC. Data collection/analysis using SIFT-MS: KS, KD. Interpretation of results (UV-Vis): MC. Interpretation of results (SIFT-MS): KS. Drafting the manuscript: MC, SC, KS, PS. Approval of intellectual content: all authors.

Hereby I declare that the actual contribution of K. Sovová to these publications was as detailed above. In the terms of percentage her contribution was in my estimation as follows: A. 60%, B. 40%, C. 20%, D. 20%, E. 60%, F: 60%, G: 20%.

Prague 6.9.2013

prof. Dr. Patrik Španěl

List of Abbreviations

SIFT-MS	Selected Ion Flow Tube Mass Spectrometry
VOCs	Volatile Organic Compounds
ppbv	parts per billion by volume
ppmv	parts per million by volume
pptv	parts per trillion by volume
SPME	Solid Phase Micro Extraction
TD	Thermal Desorption
GC/MS	Gas Chromatography Mass Spectrometry
IMS	Ion Mobility Spectrometry
MIMS	Membrane Inlet Mass Spectrometry
APCI	Atmospheric pressure chemical ionisation
TAGA	Trace Atmospheric Gas Analyser
EESI	Extractive Electrospray Ionisation
SESI-MS	Secondary Electrospray Ionization-Mass Spectrometry
PTR-MS	Proton Transfer Reaction Mass Spectrometry
FA	Flowing Afterglow
SRI	Switchable Reagent Ions
QMF	Quadrupole Mass Filter
PEEK	PolyEther Ether Ketone
FS	Full Scan
MIM	Multiple Ion Monitoring
IP	Ionization Potential
RE	Recombination Energy
DMS	Dimethyl Sulphide
EI	Electron Ionisation
MW	Molecular Weight
PA	<i>Pseudomonas aeruginosa</i>
MALDI	Matrix Assisted Laser Desorption and Ionisation
GLVs	Green Leaf Volatiles
MetB	Methyl Benzoate
MeSA	Methyl Salicylate
TBW	Total body water

CF	Cystic Fibrosis
IBD	Inflammatory Bowel Disease
UC	Ulcerative Colitis
CD	Crohn's Disease
CT	Computed Tomography
MRI	Magnetic Resonance Imaging
CFU	Colony forming units
PCA	Principal Component Analysis
PCR	Principal Component Regression
MTBE	Methyl Tertiary Butyl Ether
AAS	Atomic Absorption Spectroscopy
HGAAS	Hydride Generation Atomic Absorption Spectroscopy
DMSe	Dimethyl Selenide
LIBS	Laser Induced Breakdown Spectroscopy
NQR	Nuclear Quadrupole Resonance
FOX-7	1,1-diamino-2,2-dinitroethylene
RDX	1,3,5-trinitro-2-oxo-1,3,5-triazacyclo-hexane
HMX	1,3,5,7-tetranitro-1,3,5,7-tetraazacyclo-octane

Abstract

This thesis describes research that has been carried out during the years 2009-2013 as a part of my PhD project related to the method of selected ion flow tube mass spectrometry (SIFT-MS) and its application in interdisciplinary areas of research. SIFT-MS is a method that allows accurate quantification of trace gases and vapours presented in humid air with the focus on human breath; without any sample preparation and in real time.

The thesis is divided into several parts. The first part reviews the history of mass spectrometry as a background for the quantitative analytical methods as PTR-MS and SIFT-MS. The second part discusses the detailed history of development of SIFT-MS, starting from principles of selected ion flow tube (SIFT) technique that has been used for study of ion-molecule reactions in the gas phase and forms the basis of SIFT-MS. The next part discusses volatile organic compounds of different biological origin: bacterial, plant and human breath metabolites that can be analyzed in real time using SIFT-MS.

The main part "Results and Discussion" is divided into several subsections that serve as commentaries to the enclosed research papers published in peer reviewed journals. The first is a detailed step by step overview of the kinetics of ion molecule reactions which is the basis of SIFT-MS including the determination of rate constants and product branching ratio for several ion-molecule reactions of H_3O^+ , NO^+ and $\text{O}_2^{+\bullet}$ precursor ions with six phytogetic esters and seven isomers of hexanol. Other two sections concern the application of SIFT-MS in the discovery of biomarkers for clinical diagnostic of inflammatory bowel disease and infections complicating cystic fibrosis. Next section covers a study of population dynamics of three different bacterial species based on their volatile signatures. The theme of plant physiology and the volatiles that are released by plants in the process of phytovolatilization is discussed in the following section. The final section discusses an application of SIFT-MS in the field of security research for the study of decomposition of a highly energetic explosive FOX-7.

Contents

1	Aims	17
2	Introduction	18
2.1	Mass spectrometry techniques in analysis of VOCs	18
3	Selected ion flow tube mass spectrometry	21
3.1	Selected ion flow tube	21
3.2	Selected ion flow tube mass spectrometry	23
3.2.1	<i>Profile 3</i> instrument	24
3.2.2	H ₃ O ⁺ reactions	28
3.2.3	NO ⁺ reactions.....	31
3.2.4	O ₂ ⁺ reactions	32
3.2.5	Absolute quantification	34
3.2.6	Format of kinetics library entries used in <i>Profile 3</i> instrument.....	35
4	Volatile organic compounds	38
4.1	Bacterial volatile organic compounds	38
4.1.1	Clinically relevant bacteria.....	39
4.1.2	Bacterial models of interactions	40
4.2	Plant volatiles	41
4.2.1	Hexyl acetate	42
4.2.2	Phenethyl acetate	43
4.2.3	Benzyl acetate.....	44
4.2.4	Methyl benzoate	44
4.2.5	Benzyl benzoate.....	44
4.2.6	Methyl salicylate	44
4.3	Metabolites in human breath	45
4.3.1	Methane and hydrogen	46
4.3.2	Ammonia	47
4.3.3	Acetone.....	48
4.3.4	Hydrogen cyanide.....	49
4.3.5	Methanol.....	49
4.3.6	Ethanol.....	50

4.3.7	Isoprene	51
4.3.8	Acetonitrile	51
5	Results and Discussion	53
5.1	Determination of rate constants and product ion branching ratios	53
5.2	Construction and optimization of kinetics library	68
5.3	Breath analysis.....	72
5.3.1	Inflammatory bowel disease.....	72
5.3.2	Cystic fibrosis	75
5.4	Population dynamics	80
5.5	Phytogetic volatile compounds.....	86
5.5.1	Phytovolatilization of selenium.....	88
5.6	Explosives.....	97
6	Summary and concluding remarks.....	102
	References	104
	Appendix A, Sovová <i>et al.</i> Int. J. Mass. Spectrom. 300 (2011) 31	A
	Appendix B, Smith <i>et al.</i> Int. J. Mass. Spectrom. 319-320 (2012) 25	B
	Appendix C, Dryahina <i>et al.</i> Rapid Commun. Mass Spectrom. 27 (2013) 1983.....	C
	Appendix D, Shestivska <i>et al.</i> Rapid Commun. Mass Spectrom. 25 (2011) 2459	D
	Appendix E, Sovová <i>et al.</i> Analyst 138 (2013) 4795.....	E
	Appendix F, Sovová <i>et al.</i> Anal. Chem. 84 (2012) 4979.....	F
	Appendix G, Civiš <i>et al.</i> Anal. Chem. 83 (2011) 1069.....	G

1 Aims

The aim of my PhD project as formulated at the onset of my postgraduate study was:

“To develop new reaction schemes and methodology for the use of Selected Ion Flow Tube Mass Spectrometry in interdisciplinary areas of research, including environmental science, microbiology, explosive detection and breath analysis for clinical diagnostics and therapeutic monitoring.”

This dissertation shows that I have achieved this aim and obtained some interesting and original results during the experimental work directed towards this goal.

2 Introduction

Immediate measurement of the concentrations of trace amounts of various gases and vapours of volatile organic compounds (VOCs) presented in the matrix of humid air, exemplified by the ambient atmosphere, air containing VOC emissions from biological samples and exhaled human breath, represents a challenge that still has not been fully addressed [1]. The fields of science [2] where interest in such measurements is greatest include food science, environmental monitoring, occupational health and safety and last, but not least, medicine. The medical interest in analysis of VOCs [3] and other gaseous analytes is largely centred on non-invasive breath analysis. The hypothesis is that some of these compounds can serve as biomarkers or indicators of various diseases.

The methods widely used for the analysis of trace VOCs and inorganic gases are chiefly based on principles of mass spectrometry and different forms of spectroscopy. Spectroscopic techniques (such as optical spectroscopy) are not currently suitable for larger molecules that are presented at concentrations in parts-per-billion by volume (ppbv) in air. Analysis of the kind outlined above is traditionally carried out by sampling the gases into bags, metal canisters or by collecting VOCs on solid adsorbents [4, 5]. For sample preconcentration the methods of solid phase micro extraction (SPME) and thermal desorption (TD) are often used in preparation for analyses using gas chromatography mass spectrometry (GC/MS).

2.1 Mass spectrometry techniques in analysis of VOCs

Whilst optical methods have great advantages in absolute quantification and speed of response, and some recently developed methods like ion mobility spectrometry (IMS) [6, 7] and THz spectroscopy [8] have great potential for monitoring of trace amounts of VOCs, they are not within the scope of this dissertation and thus it will focus on a brief review of the history and the main principles of mass spectrometry methods used for this purpose.

The origins of mass spectrometry can be traced back to the 19th century and Lord Thompson's early work on cathode rays – the “discovery” of electrons for which he received in 1906 Nobel Prize in Physics. Later, in 1913 J.J. Thompson, with the help

of Francis Aston built the first mass spectrometer and resolved neon isotopes and thus they are considered to be the founders of mass spectrometry [9]. These fundamental developments helped towards a better understanding of the elements and their physical properties.

An important step in the analytical use of mass spectrometry was the combination of mass spectrometry with **gas chromatography** (GC). The modern GC was invented by Martin and James in 1952 [10]. GC has become a standard analytical method in many fields, especially petrochemical manufacture, environmental, biological and food sciences, and also in drug residue and forensic analysis. The field of GC rapidly expanded in the 1980s.

Currently GC is considered to be the gold standard method for analysis of VOCs; however the method still has some weaknesses. Absolute quantification requires comparison with standards and suffers from so-called matrix effects. The samples must be prepared by some form of extraction or adsorbing the VOCs onto a suitable adsorbent, as mentioned above [11]. The analyses typically take several minutes (10-60 min.) and thus results are not immediately available. The primary objective of chromatographic analysis is to achieve the desired separation of compounds in a mixture in the shortest possible time. Reductions in analysis time have been achieved by **fast GC** [12]. The principles and theory of fast GC were established in the 1960s, but for routine analysis fast GC were used later in 1990s when the adequate commercial instrumentation was available [13]. Currently, analyses of gaseous VOCs in air, gas chromatography mass spectrometry (GC/MS) is usually combined with the extraction methods of thermal desorption (TD) [14] and the above mentioned solid-phase micro-extraction (SPME) [11].

In 1972 **Membrane inlet mass spectrometry** (MIMS) was described and gradually became a relatively well established technique for monitoring gases and VOCs directly from aqueous solutions [15]. But this technique can be considered to be more qualitative than quantitative. For quantitative analysis, soft ionisation techniques, like chemical ionisation, are preferred. One of the methods for direct sample analysis is **atmospheric pressure chemical ionisation** (APCI) followed by mass spectrometry that was originally developed for analysis of trace components in the gas phase [16]. In 1980 TAGA (trace atmospheric gas analyser) based on APCI was used in several environmental applications, explosive detection and even breath analysis [17] and monitoring of CO₂ [18]. Today, APCI is widely used in analysis of trace gases released

by foods [19] and many other trace gas analyses down to the parts-per-trillion by volume (pptv) levels [17]. In spite of their great sensitivity a weakness of APCI methods is again in its lack of absolute quantification and also due to matrix effects that compromise reproducibility. The state of the art methods stemming from this heritage are **extractive electrospray ionisation** (EESI) [20] and **secondary electrospray ionization-mass spectrometry** (SESI-MS) [21].

In the mid-1990s two techniques based on chemical ionization were introduced capable of direct real time trace gas analysis: **selected ion flow tube mass spectrometry** (SIFT-MS) and **proton transfer reaction mass spectrometry** (PTR-MS). The SIFT-MS method was used as a basis for the research described in this dissertation and will be covered in detail in the next Section 3. PTR-MS has been developed mainly for the detection of both biogenic VOCs and anthropogenic VOCs in atmospheric science, in environmental research, food and flavour analysis and also breath analysis [22]. PTR-MS has similar origin as SIFT-MS, both can be traced back to flowing afterglow method, FA [23]. The PTR-MS technique was developed in Innsbruck by Lindinger and co-workers [24] and several reviews about this technique and its application have been published [24-27]. PTR-MS is based on chemical ionization by proton transfer from H_3O^+ to molecules present in a gas sample inside a **drift tube**. Thus, only compounds with higher proton affinity than water could be analysed. In 2009, the so-called “Switchable Reagent Ions“ (SRI) variant of PTR-MS was introduced. Since then it is possible to switch between H_3O^+ , NO^+ or O_2^+ reagent ions [28, 29], albeit the switch takes several seconds. PTR-MS has been also combined with high resolution time-of-flight (TOF) mass spectrometers [30-32].

3 Selected ion flow tube mass spectrometry

3.1 Selected ion flow tube

The SIFT-MS technique is derived from the **selected ion flow tube** (SIFT), method, developed in 1976 by N.G. Adams and D. Smith [33]. The SIFT is a flow tube technique for the studies of kinetics of gas-phase reactions between ions and molecules. The first application of a **flow tube**, specifically the **flowing afterglow** (FA) in this field was described in 1963 by Ferguson, Fehsenfeld and Schmeltekopf [23, 34] at the National Oceanic and Atmospheric Administration laboratories in Boulder, Colorado, USA. The motivation of their research was to obtain quantitative understanding of the ion chemistry that occurs in the terrestrial ionosphere. However, the flowing afterglow method had its limitations, primarily in the form of production of **multiplicity of primary ions** in the flowing afterglow plasma, which then complicates identification of the **product ions** resulting from primary reactions. The complication of multiple reagent ion production in the flowing afterglow technique was resolved by introduction of the SIFT technique. Here, the reagent ion formed in an ion source was first selected according to its mass to charge ratio (m/z) and then injected into fast flowing neutral carrier gas. Thus the main difference between a **SIFT** instrument and a **FA** instrument is the presence of a quadrupole mass filter after the ion source. The SIFT technique became a standard tool for the study of the kinetics of the reactions between ions and neutral molecules in the gas phase under truly thermalised conditions [35, 36]. Research in this area was focused on the study of ion-molecule kinetics important to atmospheric and interstellar ion chemistry [37]. This work has resulted in a large amount of experimental kinetic data for ion-molecule reactions, including rate constants and product ion distributions. These data now represent a foundation for the use of SIFT-MS for analytical purposes, especially for determination of trace gas concentrations in air, with a focus on quantitative analysis of gases in human breath [32, 38].

The principles of the SIFT technique are illustrated in Figure 3.1. Ions (positively or negatively charged) are produced in an external ion source from an appropriate source gas. From the mixture of ions formed by electron ionisation or chemical ionisation a current of ions with a given mass-to-charge ratio is selected by a

quadrupole mass filter and then injected into the flow tube via a Venturi type injector [35].

Helium is usually used as the carrier gas because it is inert and also because its atoms have low mass and thus the composition of the injected ions are not modified (dissociated) when they collide with carrier gas. The main function of the carrier gas is to thermalise and convect the ions along the flow tube. The ions pass entry ports through which neutral reactant gas is introduced. The resulting product ions of the reactions of the injected (precursor) ions with the neutral reaction gas together with remaining reagent ions are sampled via an orifice, are focussed into a downstream quadrupole mass spectrometer and finally detected and counted by the Channeltron electron multiplier/ion counting system [36].

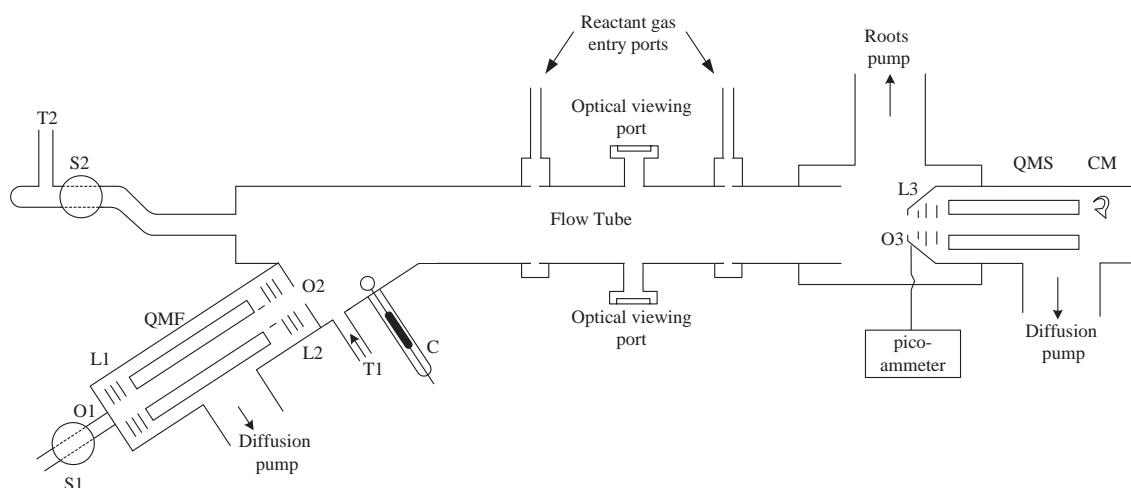


Figure 3.1 –A schematic diagram of the first SIFT apparatus (reproduced from [39]). Ions have been produced in an ion source, by a microwave discharge, S1. Ions effusing from the source through the orifice, O₁ (diameter 0.5 mm), were accelerated and focused into a quadrupole mass filter, QMF, by an electrostatic lens, L1. After selection in this mass filter, the ion species of interest was injected through a second orifice O₂ (diameter 0.5 mm) into the flow tube. The ion current through the orifice, O₂, were monitored by movable collector, C.

In order to determine the rate constants and the ion products for ion-molecule reactions, the neutral gaseous sample is introduced into the carrier gas via a mass flow meter in controlled and measured amounts through an entry port (see Figure 3.1). The decay of the injected ion current and the growth of the product ion count rates are observed using the downstream mass spectrometer/detection system as a function of the reactant gas flow rate [38]. The rate constant for the reaction is then calculated

according to the procedure described in Section 5.1. More than one product ion sometimes results from an ion-molecule reaction, but it is a simple procedure to determine the branching ratios of the true primary product ions as will be described in detailed later.

3.2 Selected ion flow tube mass spectrometry

The SIFT technique formed a basis of a new method for accurate quantification of trace gases using the knowledge of kinetics of ion-molecule reactions. Thus, in 1995 D. Smith and P. Španěl developed the SIFT-MS method for the analysis of trace gases at ppbv concentrations in atmospheric air, with the focus on the detection and quantification of trace gases in human breath. Traditionally, the SIFT instruments were large apparatuses filling the whole laboratory. In 1997, a Transportable Selected Ion Flow Tube (TSIFT) instrument was constructed at Keele University with a short flow tube of about 40 cm long. Further developments have enabled construction of a compact SIFT-MS instrument in 2006 (*Profile 3*, manufactured by Instrument Science Limited, with flow tube of only 5 cm long, easily transportable with a weight of 120 kg). This instrument was used in all experiments discussed in this dissertation.

The SIFT-MS method is based on chemical ionization, in which the ionization of neutral molecules is achieved by “soft ionization“ using a selected species of precursor ions. This approach minimizes fragmentation of product ions of reactions and thus simplifies the analytical mass spectrum [40]. The choice of the appropriate precursor ions was an important step in the analysis of trace gases in atmosphere or human breath. The precursor ions must be relatively unreactive with the major components of the air and breath sample, e.g. N_2 , O_2 , H_2O , Ar and CO_2 in comparison with the trace gases to be analyzed (10-1000 ppbv), because otherwise the precursor ions would be consumed immediately in the reactions with major gases [41]. Thus the precursor ions involved in SIFT-MS ionization were chosen on the basis of understanding of ion chemistry occurring in terrestrial atmosphere (see Figure 3.2) [42]. The flights of rocket-borne mass spectrometers have shown that NO^+ and $\text{O}_2^{+\bullet}$ ions are dominant in the thermosphere and that H_3O^+ (H_2O)_n were the dominant ions in the altitudes around 70 km. This is explained by low reactivity of H_3O^+ , NO^+ and $\text{O}_2^{+\bullet}$ with air molecules. Therefore, these ions are ideal as reagents for selective chemical ionisation of reactive compounds present in air matrix. It has been proved by subsequent

research that the use of these reagents either separately or in combination is the real strength of SIFT-MS [32, 42].

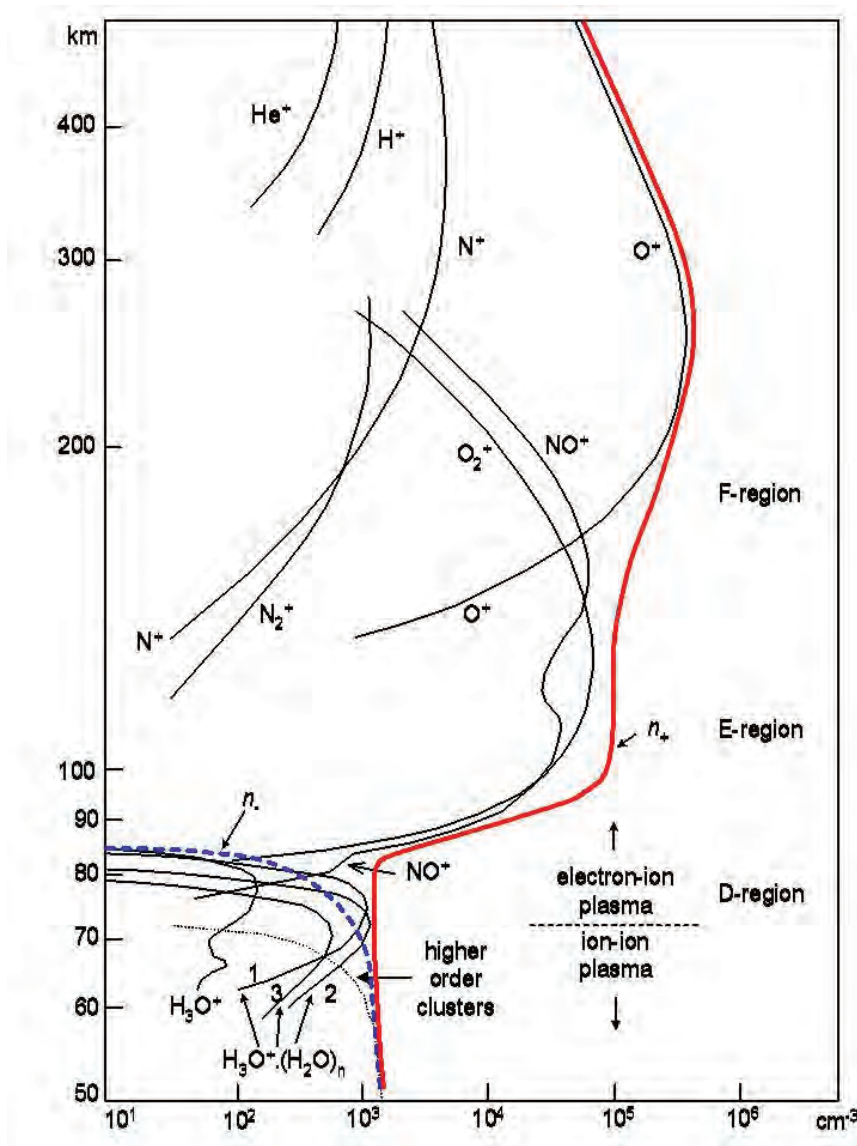


Figure 3.2 The positive ion composition of atmosphere as a function of altitude [42].

3.2.1 Profile 3 instrument

A schematic diagram of the *Profile 3* instrument that was used for all studies discussed in this dissertation is given in Figure 3.3. Positive ions are created in a microwave glow discharge ion source from a mixture of water vapour and air [43] maintained at total pressure of 0.3 mbar. From the mixture of ion species extracted

through the orifice O_1 a current of ions of a given mass-to-charge ratio, m/z , is selected using a quadrupole mass filter.

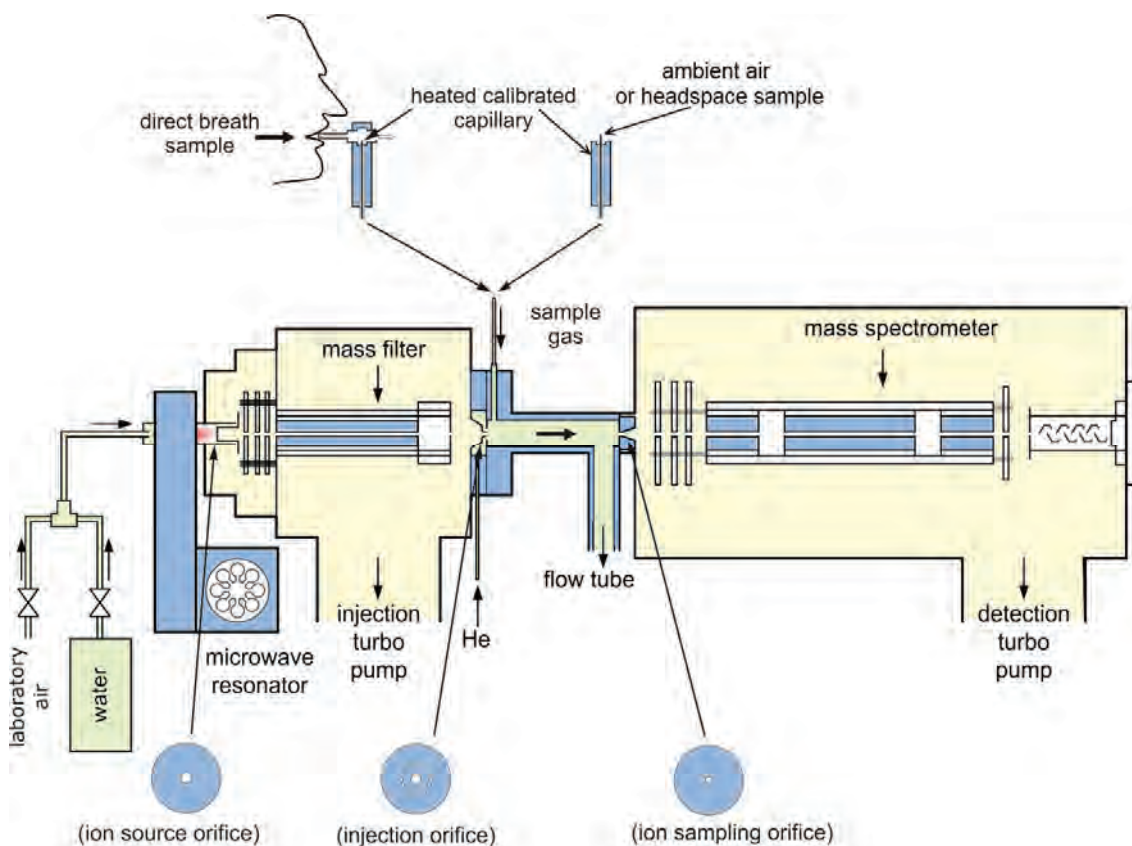


Figure 3.3 Schematic diagram of the Profile 3 SIFT-MS instrument showing the microwave discharge ion source, injection mass filter and the detection quadrupole mass spectrometer and the three metal discs to which ion current can be measured and which support the orifices O_1 , O_2 and O_3 through which, respectively, ions pass from the ion source into the injection mass filter, mass selected ions enter the flow tube and via which ions are sampled into the analytical quadrupole mass spectrometer. Both direct breath sampling into the instrument and sampling from bag samples are illustrated [44].

Note that this filter can be scanned and the current measured at the electrode surrounding the injection orifice O_2 can be used to plot a crude spectrum of the precursor ions, a so called injection scan (see Figure 3.4). A current of selected precursor ions, H_3O^+ , NO^+ or O_2^+ , is then injected into a fast-flowing helium carrier gas via the orifice O_2 and convected along the flow tube (diameter of 1 cm and 5 cm long). A continuous flow of the gas sample (typically 20 to 30 mL/min at standard atmospheric pressure and temperature) can be introduced into the flow tube via a

calibrated capillary. The actual flow rate can be measured by a mass flow meter (manufactured by Voegtlin, Aesch, Switzerland) connected to the sample inlet.

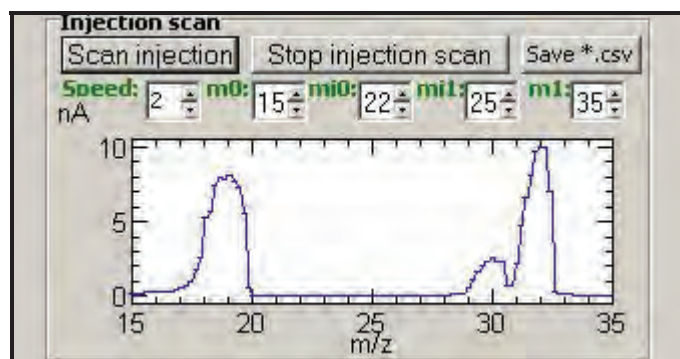


Figure 3.4 An injection scan in SIFT-MS instrument.

The capillary and the connecting tubes (all made from polyether ether ketone, PEEK) are all heated to about 80°C to prevent condensation of water and other condensable species and memory effect. Note that PEEK lines used for the present experiments exhibits much lower memory effects due to surface interactions with VOCs than the stainless steel lines used previously. The precursor ions react with sample gases during a defined reaction time (0.6 ms) which is determined by the carrier gas flow rate and the reaction length. The reactions of the precursor ions with trace gases in the sample diluted in the carrier gas form the product ions that are characteristic of each trace gas compound. The product ions are analysed using the detection (analytical) quadrupole mass spectrometer and are counted by a channeltron multiplier/pulse counting system. The count rates thus obtained are used in calculation of the concentrations of volatile compounds.

The SIFT-MS instrument can be operated in two modes: The **Full Scan** (FS) mode or **Multiple Ion Monitoring** (MIM) mode [45]. In FS, a complete mass spectrum is obtained by sweeping the detection quadrupole ion over a selected m/z range for a chosen time whilst a sample of air or breath is introduced into the carrier gas at a steady flow rate. In the MIM mode, only the count rates of the precursor ions and those of selected product ions are monitored as function of time. This real-time monitoring is possible because of the fast time response of SIFT, approximately 20 ms.

The software that controls the instrument allows switching of the injection mass filter between the selected m/z values of the precursor ions (19, 30 and 32). Worthy of note from the point of view of analytical sensitivity is the effective dwell time, t_d , during

which the product ions of a given m/z are accumulated. In the FS mode the total measurement time, t_d , for each ion (m/z value) is:

$$t_d = 0.3 n_s t_s / (m_1 - m_0) \quad (1)$$

Here, n_s is the number of full scans, t_s is time of each scan, m_0 and m_1 are limit m/z values of the scan. So, for example, for a single scan ($n_s=1$) across the range m/z 10-130 with each scan lasting 60 s, the dwell time for a single product ion is 150 ms. Therefore, at least 7 such scans (whilst maintaining the sample flow for 7 minutes) would have to be integrated to achieve 1 s of integration time. Often it is practical to cycle the precursor ions between the individual full scans (e.g. m/z 19; then 30; then 32; and repeat ...) and obtain 5 full scans for each reagent ion (15 scans total). In this way, representative mass spectra can be obtained even when the composition of the sample is slowly changing with time (for example, as was the case in the study of population dynamics of bacterial cultures discussed in Section 5.4 and Appendix E).

In the MIM mode, which provides more precise quantification of the targeted trace compounds than does the FS mode, the total measurement time per product ion, t_m , is related to the total sampling time, t_i , the precursor and product ion dwell times, t_{pre} and t_{prod} , the number of precursor and product ions recorded, n_{prec} and n_{prod} , the wait time before counting on each ion, t_w , and the fly back time, t_f , by the expression:

$$t_m = t_i t_{prod} / (n_{pre} (t_{pre} + t_w) + n_{prod} (t_{prod} + t_w) + t_f) = t_i t_{prod} / t_{cycle} \quad (2)$$

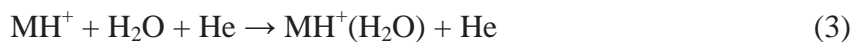
Here, t_{cycle} is the time taken to collect the data for all ions, effectively giving the resolution of the time profiles along the x -axis. As an example, consider the following typical values: **Timings:** $t_i = 10$ s, $t_{pre} = 0.04$ s, $t_{prod} = 0.2$ s, $t_w = 0.02$ s, $t_f = 0.08$ s. **Ions included:** 4 precursors (e.g. $\text{H}_3\text{O}^+(\text{H}_2\text{O})_{0,1,2,3}$) and 10 product ions. Thus, $t_{cycle} = 2.52$ s and the measurement time per ion is 0.8 s. This mode was used, for example, in the study of volatile Se compounds discussed in Section 5.5.1 and Appendix F.

The available count rate of the precursor ions determines the sensitivity and precision of SIFT-MS analysis; 10^6 counts per second is a desired value. Reduction of this count rate by a factor of two results in the precision of the measurement to be lowered 1.4 times (square root dependence). However, a precursor ion count rate that is too large can result in non-linearity of the ion detector (due to its dead time); this can be compensated for [46] and can be checked by the relative intensities of the ^{18}O isotopologues of the H_3O^+ and $\text{O}_2^{+\bullet}$ precursor ions.

3.2.2 H₃O⁺ reactions

The reactions between H₃O⁺ precursor ions and organic molecules (M) proceed predominantly via **proton transfer** and usually result in only one (MH⁺) product ion. However, these MH⁺ ions sometimes dissociate to M-OH. This fragmentation results from elimination of water after protonation of some alcohols or larger aldehydes or carboxylic acids. The important point is that the proton affinity of the molecules must be greater than that of H₂O for proton transfer to occur. The ion chemistry of the H₃O⁺ precursor has been previously comprehensively described in the literature. Many studies have been carried out in order to determine reactivity of all the three available precursor ions (H₃O⁺, NO⁺, O₂⁺) with several groups of organic or inorganic compounds including alcohols [47], aldehydes and ketones [48, 49], esters and carboxylic acids [50], hydrocarbons [51] or more complex molecules such terpenoids [52, 53]. Recent studies summarize the ion chemistry of organosulphur molecules [54], a series of diols [55] and nitrogen containing compounds [56] including amines [57].

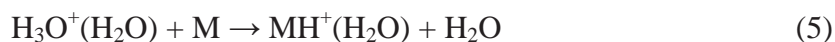
In this section the ion chemistry involving the product ions of the proton transfer reactions and the neutral water molecules is discussed. In the presence of water, the H₃O⁺ ions are partly converted to **hydrated hydronium ions** H₃O⁺(H₂O)_{1,2,3}. These cluster ions can act as precursors, and produce ion products like MH⁺(H₂O)_{1,2,3} via ligand switching reactions [58, 59]. The ion chemistry, which is important for real time and accurate quantification, is influenced by the presence of water vapour and it is necessary to account for this. The efficiency of water cluster formation for the association reactions of MH⁺ ions with H₂O molecules in helium (3) can be described by the three-body rate constant, k_{MH^+} .



It is possible to obtain these rate constants by comparing the decay rate of H₃O⁺ ions, which are described by a three-body rate constant $k_{H_3O^+}$ (4), and the decay rate of MH⁺ ions as they react simultaneously with the added H₂O molecules.



The three body-rate constant for reaction (4) was previously determined to be $k_{H_3O^+} = 6 \cdot 10^{-28} \text{ cm}^6 \text{ s}^{-1}$.



The contribution of the switching reaction (5) to the production of $MH^+ \cdot (H_2O)_{1,2,3}$ ions can be quantified by a parameter (S_{eff}) representing the contribution of switching reactions to their formation taken relatively to the formation of hydrated hydronium ions:

$$S_{eff} = \frac{\ln \frac{[MH^+] + [MH^+(H_2O)_{1,2,3}]_s}{[MH^+]}}{\ln \frac{[H_3O^+]_0}{[H_3O^+]}} \quad (6)$$

The subscript 0 indicates the respective ion count rates in the absence of water as obtained by the direct measurement before introducing water into the helium carrier gas. Thus, the count rate corresponding to $[MH^+]_0$ can be acquired during analysis as the sum of the $[MH^+]$ and $[MH^+ \cdot (H_2O)_n]$ count rates and similarly $[H_3O^+]_0$ can be calculated as the sum of $[H_3O^+]$ and $[H_3O^+ \cdot (H_2O)_n]$.

It is assumed here that the concentrations of ions in the helium carrier gas are proportional to their observed count rates at the detection system (as obtained from data exemplified by Figure 3.5 and corrected for the mass discrimination of the quadrupole mass spectrometer; see Section 3.2.5).

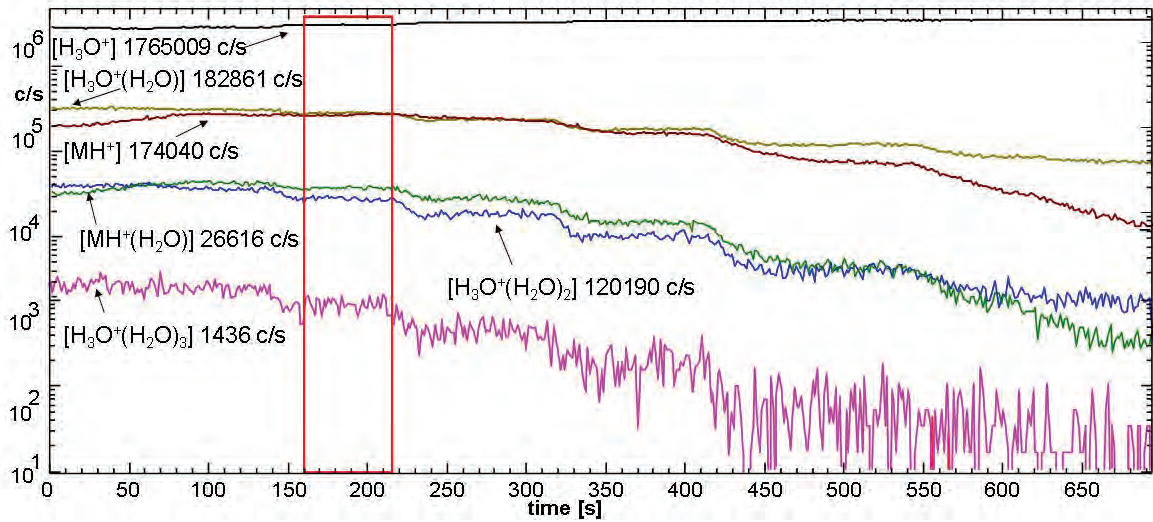


Figure 3.5 Raw data from the SIFT experiment in the form of dependence of the count rates (logarithmic y axis) of the ions indicated on the time (x axis) as the concentration of M is changed. The red box indicates a region in which the average count rates are calculated.

The subscript S in equations (6) and (7) denotes the theoretical count rates of ions formed in switching reactions only as calculated from a linearised kinetic equation:

$$[MH^+(H_2O)_{1,2,3}]_s = [M]t\left([37]\frac{k_{37}}{2} + [55]\frac{k_{55}}{2} + [73]\frac{k_{73}}{2}\right) \quad (7)$$

where k_{37} , k_{55} and k_{73} are the rate constants for the switching reactions of the respective hydrated hydronium ions with M and the [37], [55], and [73] represent the actual count rates of the $H_3O^+(H_2O)_{1,2,3}$ ions as observed in the experiments. The factors 1/2 in equation (7) describe the fact that reactions of the $H_3O^+(H_2O)_{1,2,3}$ ions take place only during a time that is approximately half of that for H_3O^+ due to the continuous formation of the hydrated ions in the flow tube. Thus,

$$S_{eff} = \frac{\ln\left\{1 + \frac{[M]t \cdot \left(\frac{k_{37}}{2} + [55]\frac{k_{55}}{2} + [73]\frac{k_{73}}{2}\right)}{[M]t \cdot [19]k_{19}}\right\}}{\ln\left(1 + \frac{[37] + [55] + [73]}{[19]}\right)} \quad (8)$$

and by simplification of this expression the S_{eff} parameter can be calculated from the known rate constants and experimental data (see Figure 3.5) as follows:

$$S_{eff} = \frac{\ln\left(1 + \frac{[37]\frac{k_{37}}{2} + [55]\frac{k_{55}}{2} + [73]\frac{k_{73}}{2}}{[19]k_{19}}\right)}{\ln\left(1 + \frac{[37] + [55] + [73]}{[19]}\right)} \quad (9)$$

In order to analyse experimental data, it is useful to evaluate the total effect of the three-body association reactions of MH^+ ions with H_2O molecules (reaction (3)) and the above discussed switching reactions that is observed as the ratio of count rates of hydrated ions $[MH^+(H_2O)_n]$ to the primary product ions $[MH^+]$. The most useful way that is not sensitive to the detailed condition of experiments is to express this effect relatively to the hydration of H_3O^+ with H_2O (reaction (4)) as:

$$A_{eff} = \frac{2 \ln \frac{[MH^+] + [MH^+(H_2O)_{1,2,3}]_A}{[MH^+]}}{\ln \frac{[H_3O^+]_0}{[H_3O^+]}} \quad (10)$$

where A_{eff} describes the efficiency of the hydration of MH^+ ions with H_2O molecules (both reactions (3) and (5)) relative to that for H_3O^+ , reaction (5). The factor 2 in

equation (10) corresponds to the reaction time for continuously formed MH^+ ions, which is on average half of that for H_3O^+ .

Because A_{eff} describes the total ion count rates, it can be directly obtained from the experimental data. An important test is that the experimental value for A_{eff} is invariant with $[M]$ and also invariant with $[H_2O]$. The true contribution of the three-body association without switching is then simply calculated as $A_{eff} - S_{eff}$ and the value of the three body association rate constant can be calculated as:

$$k_{MH^+} = (A_{eff} - S_{eff}) \cdot k_{H_3O^+} \quad (11)$$

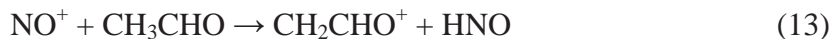
This method was used to calculate three-body rate constants of reactions of protonated esters with H_2O discussed in Appendix A.

3.2.3 NO^+ reactions

The reactions of NO^+ are more diverse in comparison to those of H_3O^+ , but also usually result in one or two primary product ions. Due to the low recombination energy (RE) of NO^+ ions (9.25 eV) they cannot ionize the major air components. Thus, only molecules with ionization potential (IP) less than 9.25 eV can be ionized by charge transfer. One example of **charge transfer** is the reaction (12) with toluene (IP = 8.82 eV) [60].



Another reaction mechanism is **hydride ion transfer** producing $(M-H)^+$ ions. Hydride ion transfer occurs in reactions with aldehydes (see the equation (13)) and esters where the hydrogen is removed from the alpha carbon and the neutral product HNO is produced.



NO^+ reactions often proceed under the SIFT-MS conditions by **association** producing NO^+M ions. This is especially efficient when the IP of the reacting molecule is close to the RE of NO^+ . This can be seen in reactions of NO^+ with carboxylic acids or ketones - a nice example is the acetone reaction:



NO⁺ is in practical SIFT-MS analyses mainly used to **quantify** aldehydes, ketones and carboxylic acids. The use of NO⁺ can help when minimising the effects of isobaric compounds. For example, acetaldehyde is monitored in the headspace of cell cultures and it was commonly quantified using H₃O⁺ precursor [48, 61], but recently dimethyl sulphide, DMS, has also been detected in these samples having the same characteristic product ions with H₃O⁺ [62]. It has been shown that DMS can be separately identified in a humid mixture using NO⁺ precursor ions.

As a part of my PhD programme, a study was carried out of the ion chemistry of H₃O⁺, NO⁺ and also O₂⁺ with several isomers of hexanol in order to find out a method for selective analysis of compounds in this group by SIFT-MS. This ion chemistry and original experimental results are discussed in Section 5.1 and Appendix B.

3.2.4 O₂⁺ reactions

O₂⁺ is a radical cation that reacts with VOCs mainly via **dissociative charge transfer** [38]. The resulting primary product ion is radical cation. The charge transfer is usually dissociative with the fragmentation patterns similar to electron ionisation, EI (see Figure 3.6). Similar fragmentation follows, usually favouring a closed shell ion product. Because the energy is well defined in the charge transfer (in contrast to the wide energy distribution in EI) there are fewer types of fragments. For example, the reaction of methyl salicylate (MW = 152) with O₂⁺ produces three primary product ions with different branching ratio (see the percentages in reactions 15-17 below). One is the radical cation at *m/z* 152 and two are fragments (*m/z* 120 and *m/z* 138).



However, the spectra of VOCs obtained using the O₂⁺ precursor ions are typically more complicated than those obtained using H₃O⁺ or NO⁺. The choice of precursor ion depends on the compounds to be analysed, in the case of O₂⁺ this is the precursor of choice for very small molecules including NH₃ [63] and CH₄ [64] or hydrocarbons like isoprene [65] or pentane researched as a part of this PhD project (see Section 5.3.1). Different product ions are produced in the reactions with the different precursor ions. Such can be used in identification of isobaric compounds [32].

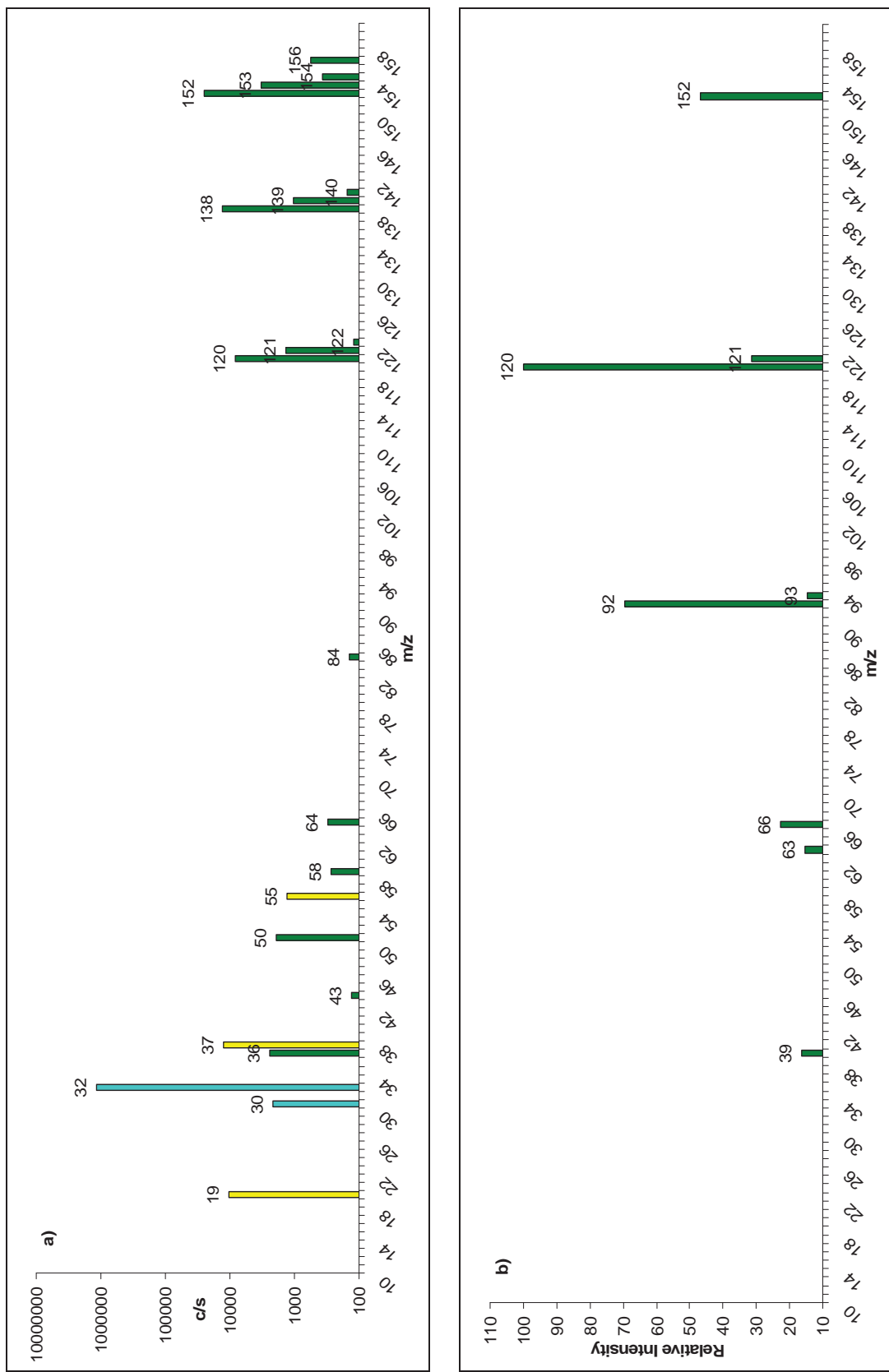


Figure 3.6 The comparison of a) SIFT-MS spectra with three primary product ions: m/z 120-138-152 and b) EI spectra with several fragment ions of methyl salicylate (MW 152).

3.2.5 Absolute quantification

The theoretical background of absolute trace gas quantification in real time is based on first order kinetics. The absolute concentrations are calculated from the known rate constants, count rates of precursor ions and product ions and the known reaction time. Note that the main original use of SIFT was to determine an unknown k for a specific reaction. Once k has been measured for the reaction of a particular analyte gas, this rate constant can then be used in the quantification of that gas using SIFT-MS.

The H_3O^+ reaction can be used as an illustrative example: when only one compound, M , reacts through proton transfer with precursor ion producing one MH^+ product ion.



the reaction proceeds during a well-defined reaction time t_r (being typically 0.6 ms) with the rate constant k . MH^+ is assumed to be the only product ion and if $[\text{H}_3\text{O}^+] \gg [\text{MH}^+]$, then the kinetics can be approximated by the following simple equation (note the [] brackets represent count rates):

$$[\text{MH}^+] = k[M][\text{H}_3\text{O}^+]t_r \quad (19)$$

From this, $[M]$ can be expressed as:

$$[M] = \frac{1}{t_r} \cdot \frac{[\text{MH}^+]}{k[\text{H}_3\text{O}^+]} \quad (20)$$

The measured ion signals are proportional to the ion concentrations and then the measurement of the $\text{MH}^+/\text{H}_3\text{O}^+$ **signal ratio** analysed by the mass spectrometer allow the absolute quantification of M .

However, if the reaction scheme is more complicated and involves ion clusters [46, 66] the general equation is used to calculate the concentration of the trace gas molecule $[M]$:

$$[M] = \frac{1}{t_r} \cdot \frac{f_{p1}I_{p1}/D_{ep1} + f_{p2}I_{p2}/D_{ep2} + \dots}{f_{i1}I_{i1}k_1 + f_{i2}I_{i2}[(k_1 + k_2)/2]/D_{ei2} + \dots} \quad (21)$$

where I_{p1}, I_{p2} etc. are product ion signals (count rates are corrected for the detector dead time and for mass discrimination in the downstream quadrupole mass spectrometer [46]), I_{i1}, I_{i2} etc. are precursor ions signals (e.g. H_3O^+ , $\text{H}_3\text{O}^+(\text{H}_2\text{O})$), again corrected for

mass discrimination and dead time), $k_{1,2}$ are rate constants of ion-molecular reactions between precursor ions and neutral molecule [M]. D_{ep1} , D_{ep2} , D_{ei2} etc. are differential diffusion coefficients of ion products and precursor ions.

If a sufficiently large concentration of [M] is present (typically more than 10 ppmv), secondary reactions of the product ions may occur. In this case it is more accurate to expand equation (21) to a logarithmic form:

$$[M] = \frac{1}{k_1 t_r} \ln \left(1 + k_1 \frac{f_{p1} I_{p1} / D_{ep1} + f_{p2} I_{p2} / D_{ep2} + \dots}{f_{i1} I_{i1} k_1 + f_{i2} I_{i2} [(k_1 + k_2) / 2] / D_{ei2} + \dots} \right) \quad (22)$$

The absolute concentration of [M] in the flow tube can be converted to the relative concentration of the molecule in the gas sample, p_M/p_0 , from the direct consideration of continuous flow dilution of the sampled air (flow rate, Φ_a) in to the carrier gas (flow rate, Φ_c):

$$\frac{p_M}{p_0} = \frac{[M] p_0}{n_0 p_g} \frac{T_g}{T_0} \frac{\Phi_c + \Phi_a}{\Phi_a} \quad (23)$$

Here, $n_0 = 2.687 \times 10^{19} \text{ cm}^{-3}$ is physical constant: Loschmidt's number, which is a reference value of concentration at standard atmospheric pressure, $p_0 = 760 \text{ Torr}$ and temperature $T_0 = 273.15 \text{ K}$ [46]. The ratio of the partial pressures p_M/p_0 is then expressed in the units of ppbv by multiplying by 10^9 .

In summary, SIFT-MS allows the absolute concentrations of the trace amounts of vapours of VOCs in air to be calculated from the measurement of the following physical quantities:

- a) Flow rate of sample, Φ_a
- b) Flow rate of the helium carrier gas, Φ_c
- c) Flow tube pressure, p_g
- d) Flow tube temperature, T_g
- e) Precursor and product ion signals (c/s), I_i , I_p (their ratio)

3.2.6 Format of kinetics library entries used in *Profile 3* instrument

Whilst the equations (22) and (23) allow calculation of the concentrations of any analyte from the measured count rates, for automated and routine immediate calculation it is important to assign to each compound a corresponding set of precursor ions and product ions together with the rate constants and factors f (explained below). These data

(in the case of the *Profile 3* SIFT-MS software) are stored in the so-called kinetics library, a plain text file that consists of an arbitrary (in principle unlimited) number of entries that are labelled by the name of the compound followed by a symbol indicating the precursor ion in parentheses [45]. Examples of the kinetics library entries that are used for the analysis of acetone by the three available precursor ions (H_3O^+ , NO^+ and $\text{O}_2^{+\bullet}$) are given in Table 3.1.

Table 3.1. Sample kinetics library entries describing straightforward calculations of acetone concentrations using the three precursor ions indicated.

compound(ion)	acetone(H3O+)	acetone(NO+)	acetone(O2+)
number of precursors	4 precursors	1 precursor	1 precursor
m/z	19 3.9e-9 1.0	30 1.8e-9 1.0	32 3.1e-9 1.0
k	37 3.3e-9 1.0	1 product	2 products
f_i	55 2.5e-9 1.0	88 1.0	43 1.0
	73 2.4e-9 1.0		58 1.0
number of products	3 products		
m/z	59 1.0		
k	77 1.0		
f_p	95 1.0		

The format of each entry is as follows (see also the first column of Table 3.1): After the name of the compound and the symbol of the injected ion, the number of precursor ions is given. Then, on separate lines, their m/z values are given followed by the rate constants, in units of cm^3s^{-1} , for their reactions with the indicated trace gas (in this example, acetone) and the factors, f_i , as indicated in equation (22). The f_i are simply used to multiply the acquired raw count rate of the ion with its m/z given at the beginning of the row. Normally, f_i values of 1.0 are used, as indicated in the acetone examples. However, such a simple calculation would not provide valid results in the cases when additional ion chemistry occurs (e.g. the removal of the product ions by reactions with H_2O molecules in reverse proton transfer or switching reactions) or when product ions overlap with other ions present. Values other than 1.0 can thus be used to account for the influence of humidity or for optimized calculations that do not sum all product ions (see later in Section 5.2). Then, on another line, the number of product ions used in the calculation is given, and on the required number of following lines the m/z values of the product ions together with the values of factors f_p , as indicated in equation (22). Again, the f_p are simply used to multiply the acquired product ion count rate and are normally set as 1.0, unless corrections for overlapping ions or calculations are used with a partial set of product ions or major isotopologues only. Note, that the values of k

decrease with increasing m/z of the precursor ions. Thus, acetone can be analyzed using all three available precursor ions, but this is an exception rather than the rule for most other compounds, although both H_3O^+ and NO^+ in tandem can be used for a number of compounds [45].

4 Volatile organic compounds

Trace amounts of vapours of VOCs present in the matrix of humid air that are the object of the studies discussed in this dissertation are of interest in several fields including food science, environmental monitoring, occupational health and safety, medical diagnostics and therapeutic monitoring. The medical interest in analysis of VOCs [3] and other gaseous analytes is centred on non-invasive breath analysis. From this wide area of possible interdisciplinary studies three chosen topics were subject of the present experimental work: VOC's emitted by bacterial cultures, by plants and those present in human breath. The background knowledge and the current status of research in these areas important for discussion of the original results reported in this thesis is overviewed in the following sections 5.3 - 5.6 in much more detail, than was reported in the published research articles that resulted from this thesis research work, which are given in the Appendices.

4.1 Bacterial volatile organic compounds

VOCs are produced by bacteria as primary or secondary metabolites or as waste products. The production of VOCs may differ qualitatively and quantitatively according to bacterial type. They can serve a certain function important to the bacterial cell-facilitate communication between cells, promote growth or act as inhibiting agents [67-69]. A variety of bacterial volatile metabolites have been reported on the basis of GC/MS analyses, including carboxylic acids, alcohols, aldehydes, ketones, esters, hydrocarbons and organosulphur compounds [70, 71]. A few years ago, Schulz *et al.* [72, 73] compiled a list of all known volatiles released by bacteria. They classified 75 fatty acid derivatives, 50 aromatic compounds, 74 nitrogen-containing compounds, 30 sulphur compounds, 96 terpenoids, 18 halogenated compounds, and selenium, tellurium, and other metalloid compounds. Bacteria are very important in naturally occurring bio systems, they are an integral part of the healthy human digestive system and are also utilised in many technologies such as food industry. However, some species of bacteria can be harmful and cause or complicate various diseases. As a background to the original results presented in this dissertation, just two relevant areas, viz. medicine and fundamentals of biology will be discussed.

4.1.1 Clinically relevant bacteria

The concentrations of **VOCs** are often considered to be used as **biomarkers** (for the different definitions of the term see Table 4.1) of bacterial growth or infection [74-76].

Table 4.1 Definitions of the term “biomarker”.

<p>Medical Research Council [77]</p> <p>“Objective measurement that acts as an indicator of normal biological processes, pathogenic processes or pharmacologic responses to therapeutic intervention (eg cholesterol, troponin T and I and FDG-PET) and qualification should be taken to mean demonstrating the utility of the marker(s) for use in clinical or public health studies.”</p>
<p>National Institutes of Health in [78]</p> <p>“a characteristic that is objectively* measured and evaluated as an indicator of normal biological processes, pathogenic processes, or pharmacologic responses to an intervention.” Example: cholesterol level.</p> <p>*The committee defines “objectively” to mean “reliably and accurately.”</p>
<p>Cell biology in [79]</p> <p>“a biomarker is a molecule that allows the detection and isolation of a particular cell type (for example, the protein Oct-4 is used as a biomarker to identify embryonic stem cells).”</p>

The knowledge of volatile biomarkers could allow non-invasive early detection of bacterial infection [75, 80]. Zhu *et al.* [81] have very recently used SESI-MS for the detection of bacterial lung infection based on **volatile fingerprints**. They demonstrated that SESI-MS is capable of differentiating mice infected with *Pseudomonas aeruginosa* or *Staphylococcus aureus* against uninfected animals, as well as distinguishing between infections caused by different *P. aeruginosa* (PA) strains. Bacteria belonging to the PA species are important pathogens causing lung infection in cystic fibrosis and they are known to produce several volatiles that are proposed to act as biomarkers of PA infection. Mann *et al.* [82] reported in 1966 that **2-aminoacetophenone** (2-AA) having a grape odour is released by certain strains of PA

and 2-AA is continuously researched as a possible biomarker of PA infection [70, 83-85]. However, it was found that 2-AA is also present in breath of healthy subjects immediately after eating certain types of food, e.g. corn flakes; however after 2 h the level of 2-AA had decreased back to the baseline for each volunteer [86]. **Hydrogen cyanide** is also related to the PA infection of patients suffering from cystic fibrosis [87-89]. However, the experience with breath analysis had shown that the use of HCN as a single biomarker might be negatively affected by several factors (e.g. diet, smoking, oral cavity hygiene). Thus, a combination of several biomarkers, e.g. HCN and 2-AA or the recently identified **methyl thiocyanate** by Shestivska *et al.* [74] would improve diagnostic sensitivity and specificity of diagnosis. Filipiak *et al.* [90] has very recently characterised VOCs released from *Streptococcus pneumoniae* and *Haemophilus influenzae*, recognised as pathogens in the upper airways, by GC/MS. They found 34 volatiles in *S. pneumoniae* and 28 volatiles in *H. influenzae*, including alcohols, aldehydes, esters, hydrocarbons, ketones and sulphur-containing compounds. Highly elevated concentrations were observed of acetic acid, acetaldehyde, methyl methacrylate, 2,3-butanedione and methanethiol. Allardyce *et al.* [91] used SIFT-MS to detect metabolite gases in the headspaces of blood cultures of PA, *S. pneumoniae*, *Escherichia coli*, *S. aureus* and *Neisseria meningitides*. Another interesting field of research is motivated by the possibility that monitoring of VOCs might assist in the early detection of bacterial infection in large scale bioreactors [76, 92].

4.1.2 Bacterial models of interactions

Identification of bacteria based on the composition of VOCs released by their metabolism can be used to diagnose and monitor occurrence and progression of bacterial infections. This ultimately can be used to screen groups of patients at risk of early signs of infection and to choose optimal therapy for its eradication. The theme of bacterial fingerprinting is currently at the forefront of research interest in mass spectrometry [93]; however, most of the approaches require isolation and cultivation of bacteria before the ionisation (usually by matrix assisted laser desorption and ionisation MALDI) which is usually destructive. Thus, an analytical methodology that would shorten time of diagnosis on the basis of immediate analyses of volatile metabolites released *in-vivo* would be of great value. Such methodology could be also used in the field of **population dynamics** in fundamental ecology and biodiversity [94], where

models consisting of several competing bacterial species are used to test theoretical concepts.

The theoretical biologists are interested in the bacterial systems because of its intricate communication capabilities that include quorum sensing [95], chemotactic signalling and plasmid exchange. Jacob *et al.* [96] have proposed that bacterial communication-based cooperation involves colony morphogenesis, which includes coordinate gene expression. “**Social intelligence**” helps bacteria to gain information from the environment and from other organisms; they process the information and develop common knowledge and learn from past experience. Nice example of usage of this concept in **medicine** has been demonstrated by Jacob and co-workers [97]. They were motivated by the idea, that bacterial sociality can serve as a source of inspiration in tumorigenesis. They hypothesised that tumours may be smart society communities. The understanding of the behaviour of these cancer systems could possibly lead to the development of therapeutic approaches with minimised harmful side effects.

As reported in Section 5.4 of this dissertation, a model system of three competing bacterial species: *Serratia rubidaea* (R), *Serratia marcescens* (F) and *Escherichia coli* (Ec), growing in single (R, F and Ec) and binary populations (REc, RF and FEc) in liquid media were studied using their volatile signatures. The ternary system exhibits relationship similar to the children's game rock-paper-scissors [94]. *Serratia* are intensively studied by theoretical biologist [67, 98, 99]. They exhibit a simple model of social interaction and self-organisation.

4.2 Plant volatiles

Since the time of ancient Greeks it has been known that plants and especially flowers have ability to pleasantly perfume the atmosphere around them. Thus floral and other vegetative parts have been used for centuries for the manufacture of perfumes and other fragrant products. Plants produce hundreds of volatile compounds, a comprehensive list of floral scent has been compiled by Knudsen *et al.* [100]. These chemicals are stored in the leaf and plants maintain physiological concentrations of these volatile metabolites, which typically include monoterpenes and sesquiterpenes. Volatiles serve the plants in their developments and growth. The “smell” moves rapidly and thus it is used by plants to attract pollinators or even influenced other plants and animals [101]. These volatiles also attract parasitic and predatory insects that are natural

enemies of plant herbivores (see Figure 4.1) and may induced defence response in other plants [102, 103]. Such chemicals are called semiochemicals, from the Greek semeion a mark or signal [102, 104]. The chemical signalling in plants and among different species is still at the forefront of research interest. The methods used in this field require high sensitivity.

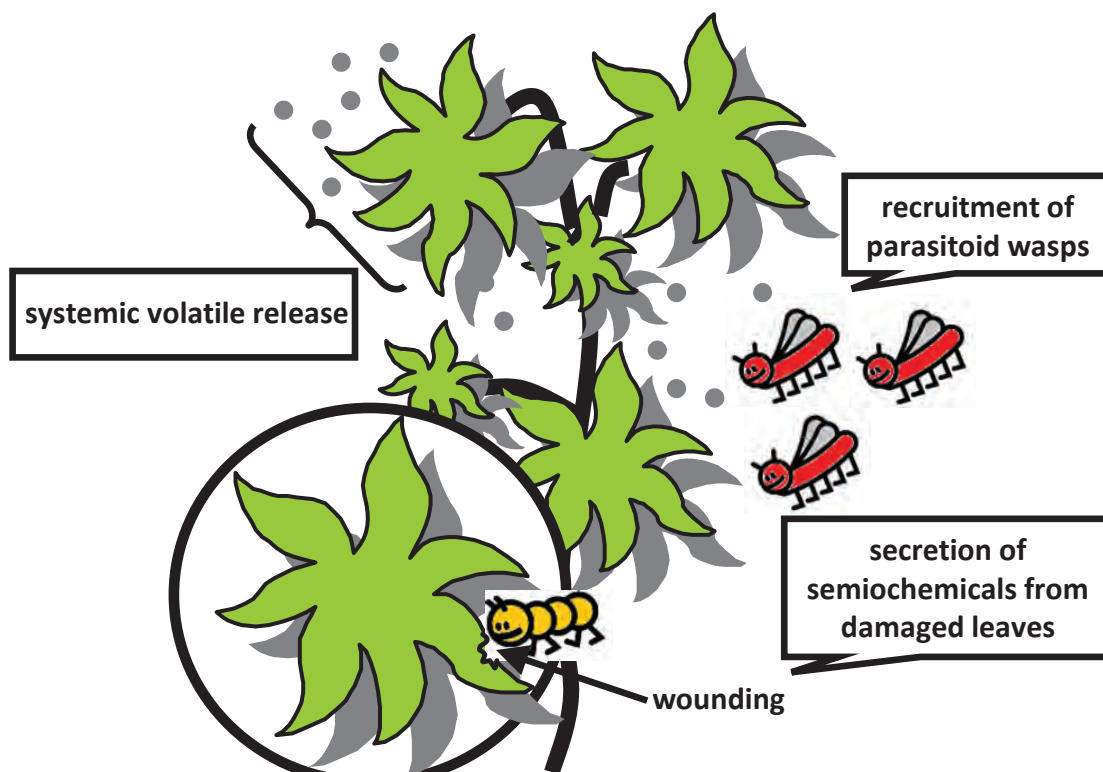


Figure 4.1 An illustration indicating an increase of volatiles from plants in response to herbivore feeding. Volatile semiochemicals are used by natural enemies of herbivores, such as parasitoid wasps, to locate their host. The release of volatiles can be also systemic and not induced by oral secretions of herbivores (inspired by [102]).

In this dissertation, focus is on a group of biogenic esters. The aim was to study the ion chemistry of these substances so that they can be monitored online using SIFT-MS. The compounds included are: hexyl acetate, phenethyl acetate, benzyl acetate, methyl salicylate, methyl benzoate and benzyl benzoate.

4.2.1 Hexyl acetate

The role of hexyl acetate in the plant world is mainly in perfuming the surrounding. But it has been found that this compound is released by plants after wounding of its tissues and plays a role in plant communication [105]. Hexyl acetate belongs to the **green leaf volatiles** (GLVs, terpenoids, benzenoids, and C6-aldehydes)

family and it was found in the headspace of maize seedlings exposed to wound-induced maize, hot pepper and tobacco volatiles [106]. Herbivore attack had also a significant effect on the emission of hexyl acetate from lima beans. De Boer *et al.* [107] have studied the difference between lima beans infected by multi-species herbivory of spider mites (*Tetranychus urticae*) and caterpillars (*Spodoptera exigua*) in comparison to single-species herbivory. The biosynthesis of hexyl acetate is outlined in Figure 4.2.

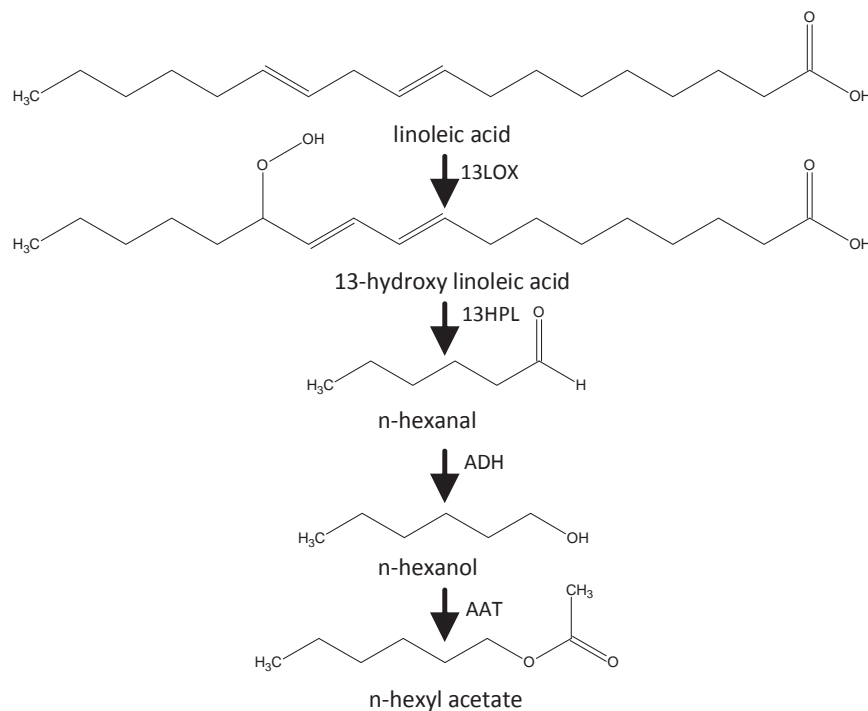


Figure 4.2 Hexyl acetate is biosynthesized from the C18 fatty acids (linoleic acid), which is liberated from the chloroplast membrane by galactolipase. Linoleic acid is oxidized by 13-lipoxygenase (13LOX) to 13-hydroperoxylinolenic acid, which is then cleaved by 13-hydroperoxide lyase (13HPL) to n-hexanal and n-hexanol (derived from [108]).

4.2.2 Phenethyl acetate

Phenethyl acetate is a component of the fragrance of several flowers, for example roses or tillandsia [100], and it is found in the headspace of European orchid *Gymnadenia conopsea* with a characteristic sweet smell of rose and honey. It has been shown that the main role of phenethyl acetate was to attract pollinators [109]. Phenethyl acetate has been identified by GC/MS in the headspace of African maize infested by *Cicadulina storeyi* (it is a China leafhopper vector of maize streak virus). The aim of this study was to develop a novel leafhopper control strategies in sub-Saharan Africa [110].

4.2.3 Benzyl acetate

Benzyl acetate together with phenethyl acetate contributes to the aroma of numerous flowers and fruits [111]. It has been found in the headspace of floral and vegetative fragrances of Nyctaginaceae: *Acleisanthes*, *Mirabilis* and *Selinocarpus* as a scent for pollinators [112]. Guterman *et al.* [113] studied petunia flowers of different transgenic lines and both esters were elevated. Benzyl acetate was recently used as an attractant of various longhorn beetles. The study [114] focused on the evaluation of secondary forests as alternative habitats to primary forests for flower-visiting insects.

4.2.4 Methyl benzoate

Methyl benzoate (MetB) is one of the most common volatiles among the benzenoids [100] and is present in floral scent of many plant species such as *Jasminum*, *Nicotiana*, *Hyacinthus* or *Gardenia*. Horruchi *et al.* [115, 116] found that MetB produced by snapdragon (*Antirrhinum majus*) flowers inhibits root growth in neighbouring *Arabidopsis* seedlings under laboratory conditions. It has also been found that snapdragon flowers emit MetB at a much higher rate during the day than during the night [117].

4.2.5 Benzyl benzoate

Benzyl benzoate is found in a floral blend of *Jasminum* or *Hyacinthus* [100]. It plays a role in benzenoid metabolism in petunia petal tissue [118].

4.2.6 Methyl salicylate

The volatile phytohormone methyl salicylate (MeSA) is recognised to act as a signalling molecule (in contrast with the previously mentioned esters) and together with methyl jasmonate is involved in communication and interactions with other plants to optimize plant defence response [105]. For example, the MeSA production in lima beans is induced either by jasmonic acid or free MeSA (free blend) after infection of lima beans by *Tetranychus urticae* – a prey species of the predatory mite. De Boer and Dicke [119] have shown a significant increase of the mites after adding synthetic MeSA to the MeSA free blend and thus suggested the important role of MeSA.

4.3 Metabolites in human breath

Exhaled air consists of about 73% nitrogen, about 16% oxygen, 3-6% CO₂, 5-6% H₂O, 1% Ar. CO₂ is formed from O₂ and ingested nutrients (carbohydrates, proteins and fats) as the main metabolic waste product. The amount of consumed O₂ and produced CO₂ is a measure of energy expenditure [120] and their ratio is influenced by the type of nutrient ingested. H₂O is to some degree also produced by the burning of fats and proteins, but largely it is ingested in food and drink directly and the water vapour content of breath simply represents evaporation from the surface of airways and its concentration is thus only dependent on the body temperature. In addition to these major components there are multiple compounds at concentrations of ppmv, ppbv or pptv (see the Figure 4.3).

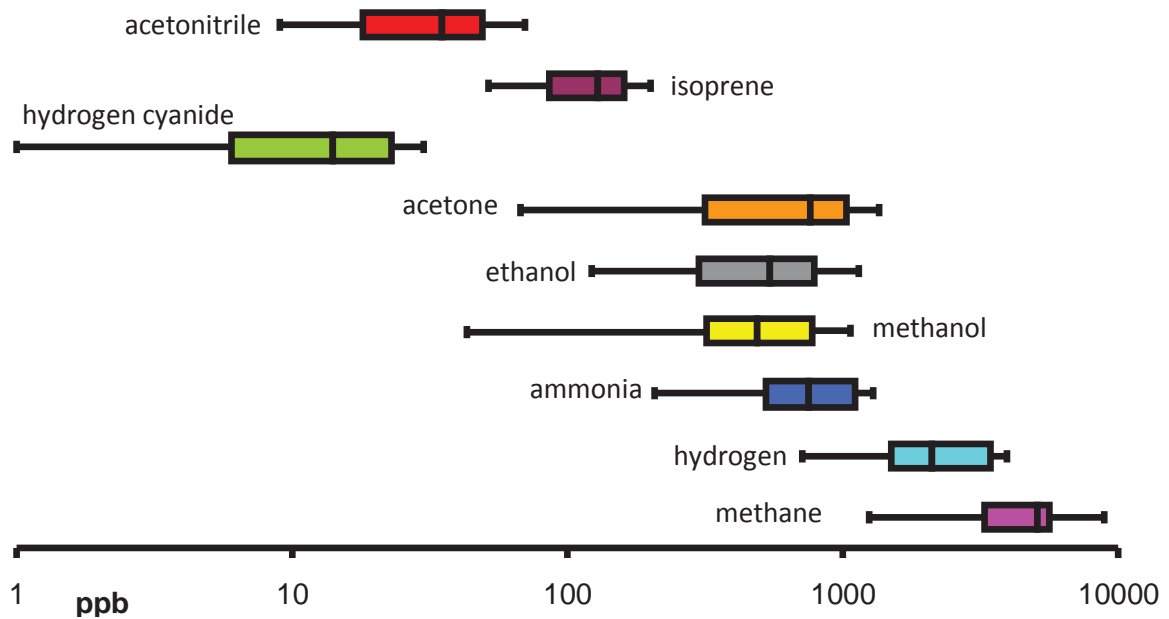


Figure 4.3 Composition of exhaled air excluding the main components (N₂, O₂, CO₂ and H₂O). The concentration distribution is shown via box and whiskers plot.

The metabolites present in human breath can have various origins as indicated in Figure 4.4. Often the same compound can be delivered to the exhaled breath by several parallel pathways, as indicated. For example, ethanol can have an **exogenous** origin simply from ingested drink or food, but it is present in the exhaled breath of all people in concentrations corresponding to less than 0.1 ‰ in blood due to its **endogenous** production by bacteria both in the gut and also in oral cavity; it can be also present as result of inhalation of trace amounts of ethanol vapour present in air.

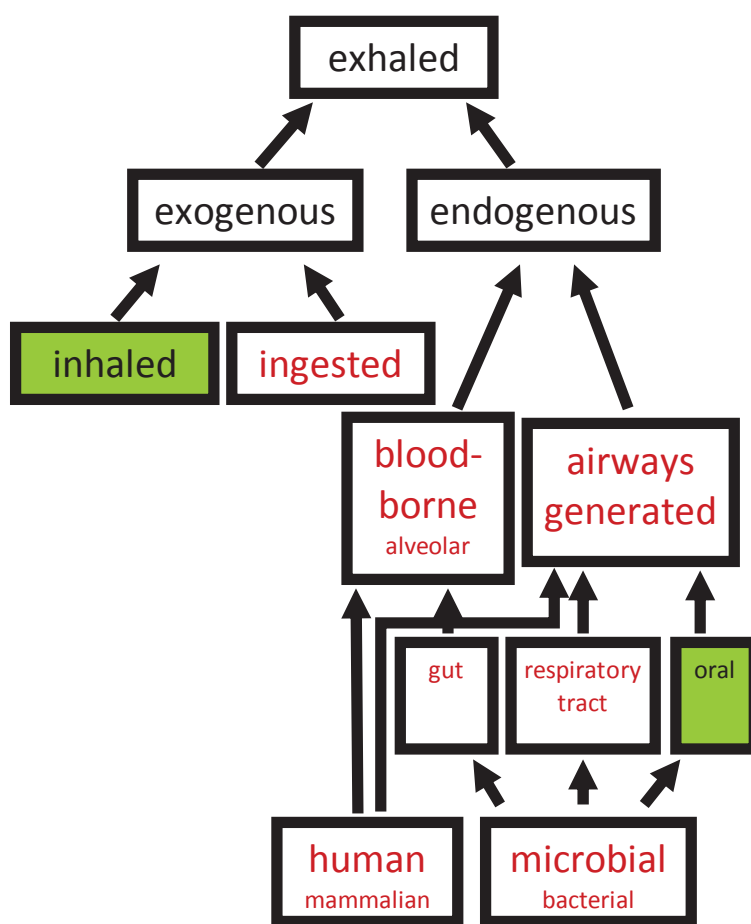


Figure 4.4 The scheme illustrates different origins of trace volatiles present in human breath and demonstrates how complex is the issue of breath analysis that has great potential for clinical diagnostics.

4.3.1 Methane and hydrogen

Methane and hydrogen are generated in the gut by bacteria and thus can be used as indicators of the presence of small intestine bacterial overgrowth and to evaluate carbohydrate maldigestion or malabsorption and intestinal transit time [121, 122]. These compounds are not very soluble in water and thus they can pass through blood stream

and be efficiently released into exhaled breath. The method for methane quantification using SIFT-MS has been described by Dryahina *et al.* [64], the mean methane concentration in exhaled breath is about 6 ppmv with insignificant variation with age and gender.

4.3.2 Ammonia

Ammonia is one of the trace gases present in exhaled breath of all people at concentrations between 100 ppbv and 2 ppmv [123]. It originates to some degree in human metabolism as a breakdown product of protein catabolism [124]. The renal ammonia synthesis is attributed to the renal extraction and catabolism of certain plasma amino acids and other nitrogenous compounds catalyzed by enzymes such as glutamate dehydrogenase. In humans ammonia is detoxified in the liver where is converted to urea (which is less toxic) that is excreted by the kidneys in the urine [125]. A small amount of ammonia is present in the blood and is excreted via the exhaled breath and through the skin [126, 127].

Many previous SIFT-MS studies have shown that breath ammonia to a large degree originates from enzymatic and bacterial activity in the oral cavity [128]. This was well demonstrated by studies of Wang *et al.* [129] and Smith *at al.* [130] when nose-exhaled breath ammonia concentration levels were several times lower than in mouth-exhaled breath and in the static gas in the oral cavity. The study of Boshier *et al.* [131] has shown that variability in repeated on-line breath analysis is lower for metabolites of purely systemic origin (as for example acetone).

Ammonia is, from the perspective of clinical diagnosis, related to end-stage renal failure and may be potentially used in therapeutic monitoring of dialysis [128, 132]. There is a growing interest in the development of dedicated ammonia sensors [133-135] for breath analysis based on the evidence of the correlation of breath ammonia with blood urea nitrogen [136, 137]. Longitudinal studies of ammonia in the breath of several healthy volunteers have been carried out in order to determine the concentration distribution [138, 139] in the healthy population. The median concentration in a cohort of healthy adults has been found to be approximately 1000 ppbv. Španěl *et al.* [139] have shown that ammonia in exhaled breath is dependent on age, the mean level increasing from about 200 ppbv in children to about 1300 ppbv in 80 year old adults.

4.3.3 Acetone

In healthy adults, breath acetone concentrations measured using SIFT-MS have been observed at a median level of 477 ppbv [124]. The studies that have been carried out a few years ago have shown that this compound is truly systemic and not generated to a significant extent in the oral cavity [130, 138]. Acetone is one of the three ketone bodies produced by the liver in lipolysis. Ketone bodies are used in humans as an energy source when glucose is not readily available. The two main ketone bodies are acetoacetate and 3-hydroxybutyrate that are used as a source of energy in the heart and brain. Acetone is the least abundant of the three, and it was even previously considered to be just a waste product [140]; however, it has been suggested that it also plays some role in metabolism as a source of energy [141].

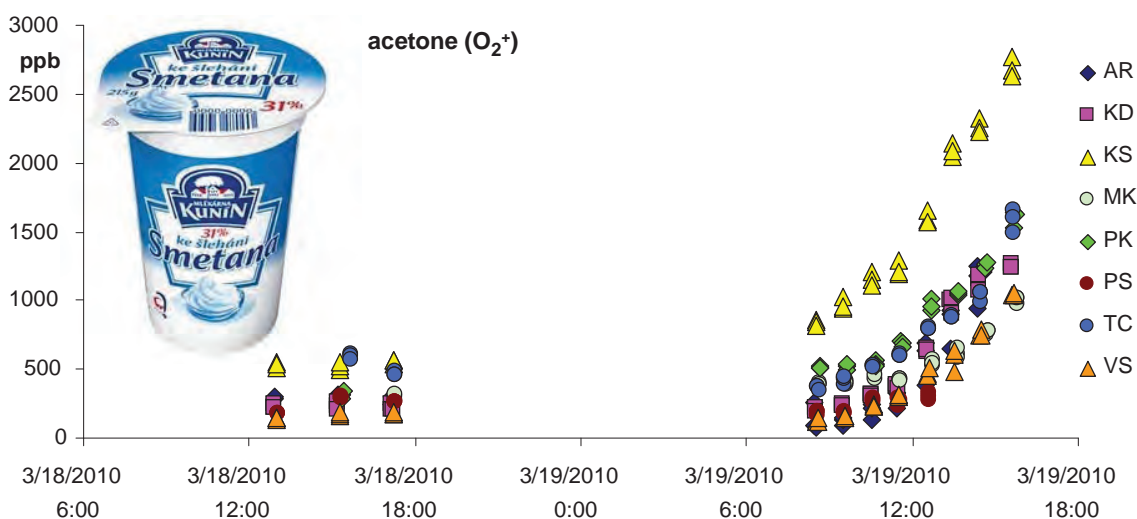


Figure 4.5 The concentrations of acetone (in ppbv) in the exhaled breath of eight healthy volunteers plotted against the time of day, firstly for several hours during the day before the ketogenic meal investigation, and then the following day during the course of the ketogenic diet.

Acetone is historically understood to be related to ketoacidosis in untreated diabetes mellitus [142]. Diabetes mellitus is the most common pathological cause of elevated blood ketones. In diabetic ketoacidosis, high concentrations of ketones are produced in response to low insulin levels. If the levels of both acetoacetate and beta-hydroxybutyrate are elevated, the blood pH drops resulting in potentially fatal metabolic acidosis. Thus, it is often suggested that breath concentration of acetone can be used as a biomarker of diabetes. However, this simple and to some degree naive idea has never

been substantiated because of the high variability of acetone in healthy people. Nevertheless, substantial resources are being invested into development of dedicated sensors for breath acetone measurement [143-147]. One important issue is that breath acetone concentration grows during starvation and decreases after ingestion of carbohydrate. Very recently, an experiment on to investigate the influence of ketogenic diet on exhaled breath acetone has been carried out [148]. Eight healthy individuals took a brief course of a ketogenic diet, which means they ate only dairy cream for 6 hours. Their breath acetone concentrations increased up to five times during this period (see Figure 4.5). These remarkable data forcefully show that diet can have a serious influence, even a dominant influence, of some breath metabolite concentrations.

4.3.4 Hydrogen cyanide

Hydrogen cyanide has been proposed as a biomarker of bacterial infection in the lungs. HCN is produced by PA the main pathogen that colonizes lungs of patients with cystic fibrosis, CF (for more details see Section 5.3.2). Using SIFT-MS, HCN was identified in the headspace of PA cultures [149] and in the breath of patients with cystic fibrosis infected with PA by Enderby *et al.* [87], where the median concentration of breath HCN in children with CF was 13.5 ppbv. Further research has shown that different strains of PA produce HCN at varying concentrations [150]. Recently, significant differences have been reported between HCN concentrations in the exhaled breath of PA infected and uninfected CF patients [88, 151].

The use of SIFT-MS as a tool for early detection of PA infection of those with CF may help in early treatment and thus help to decrease the morbidity and mortality. However, the investigation of such biomarkers is often complicated by several factors and interferences. Dummer *et al.* [152] has reported that HCN is not a reliable biomarker of PA in chronic suppurative lung disease. They found out that HCN is produced by salivary peroxidase in the oral cavity and this increases the orally exhaled concentrations.

4.3.5 Methanol

Methanol has been previously monitored in the exhaled breath of 30 volunteers by Turner *et al.* [153] using SIFT-MS. The median methanol level determined using

H_3O^+ precursor ions was 461 ppbv, the concentrations ranging from 32 to 1684 ppbv. Methanol has several exogenous sources; it is used in manufacturing and is also present in ripe fruits and fruit juices. It has been shown that ingestion of fruit increases the concentration of methanol in exhaled breath [153] by as much as an order-of-magnitude [154]. This is due to the degradation of natural pectin in the human colon by faecal bacteria [155]. Methanol is also produced by the metabolism of the artificial sweetener aspartame and converted to formaldehyde and then to formic acid [156]. The toxicity of methanol derived from aspartame has been discussed many times and it is concluded that it is not possible for a human to ever consume enough aspartame in food products to raise the blood formate concentrations to levels that induce any toxic effect [157]. Very recently, Španěl *et al.* have studied the influence of ambient exhaled air on the concentration of trace compounds in exhaled breath [158], and these studies have revealed that the exhaled concentration of methanol is not significantly influenced by its inhaled concentration. Breath methanol concentration has recently been monitored in patients with esophago-gastric cancer and was found to be statistically significantly different between a cancer cohort and a healthy control group [159].

4.3.6 Ethanol

Ethanol is produced in human both in the mouth and by gut bacteria [128]. Mouth-exhaled ethanol has previously been measured by Diskin *et al.* [160] in five volunteers and the concentration ranged from 0-380 ppbv. The study that was carried out in 2007 monitored the mouth-exhaled breath of volunteers from the different age groups with the following results: young adults (median 317 ppbv), adults (median 638 ppbv) and over 60 (median 1080 ppbv) [124]. Breath analysis of ethanol resulting from the ingestion of alcoholic beverages is routinely used in forensic practice. The detailed kinetics of ethanol decay in mouth- and nose-exhaled breath has been studied using SIFT-MS analyses of direct breath following varying doses of alcohol. It is seen that the ethanol concentration in nose-exhaled breath is generally much lower than in mouth-exhaled breath. The rate at which ethanol decreases in the exhaled breath following the ingestion of a water/ethanol solution was described as the net result of a several processes occurring in parallel:

- a. The retention of the solution in the stomach for a time determined by the gastric emptying rate. The current consensus is that ethanol is not absorbed into the blood stream via the stomach wall.
- b. Absorption of the ethanol from the intestine into the blood stream.
- c. Removal of ethanol from the portal blood stream by metabolic processes in the liver.
- d. The dispersal rate of ethanol into the total body water (TBW) and its partial retention.
- e. Continuous metabolism by ethanol in the general circulation, chiefly in the liver.

4.3.7 Isoprene

The biochemical origin of isoprene in human breath is usually considered to be a side product of cholesterol biosynthesis via the mevalonic acid pathway [161-163]. A longitudinal study of breath isoprene of 30 volunteers using SIFT-MS has shown that the mean concentration is typically 100 ppbv [163]. King *et al.* [164] have used PTR-MS to monitor isoprene and also acetone profile during exercise. They have observed that isoprene reacts very sensitively to changes in pulmonary ventilation, because of its lipophilic character and a low Henry's Law constant, and thus the very fast effect which is visible in the breath during exercise is caused by pulmonary exchange rather than by fluctuations in endogenous synthesis. A recent study [158] of the influence of exogenous concentrations of specific compounds, including isoprene, on exhaled concentrations of the same compounds, revealed that the exhaled end-tidal concentration of isoprene is about three times lower than the concentration corresponding to the equilibrium with blood.

4.3.8 Acetonitrile

It is known that acetonitrile together with benzene and other toxic exogenous compounds is elevated in the exhaled breath of smokers, as was previously studied by PTR-MS [165]. The mean concentration in non-smokers has been found to be 5.6 ± 1.9 ppbv, while that of smokers was significantly higher 69.3 ± 33.3 ppbv. Interestingly, the concentration of acetonitrile in the breath of smokers decreased after one week of abstinence from smoking to values similar to non-smokers.

Using SIFT-MS, acetonitrile was quantified in exhaled breath and urinary headspace from several smokers and also non-smokers [166]. The study confirmed that acetonitrile is detectable in breath and the urine headspace of smokers, but is practically absent for non-smokers. The mean value in the breath of smokers was 69 ppbv ranging from 17 -124 ppbv, which is in very close agreement with the PTR-MS study.

5 Results and Discussion

The section “Results and Discussion” is divided in six subsections that summarize or complement published work that I have worked on during my PhD study. Each subsection thus represents comments on peer reviewed journals included in my dissertation, having the objectives, methods, results and discussion and conclusions

5.1 Determination of rate constants and product ion branching ratios

Objectives

In this section, the details of studies carried out during the PhD project concerning the ion chemistry of a group of esters and a group of hexanol isomers will be discussed. The ion chemistry of these compounds and a provide step by step overview of the whole experimental process starting from observed mass spectra and leading to determination of the rate constants will be described. Predominantly, the material that was not discussed in the research articles published in impacted peer reviewed journals, as included in the Appendices A [167] and B [168], will be discussed. This section is complementing and extending the published work rather than just summarising it. At the onset it is useful to outline the motivation for the choice of compounds:

Selected ion flow tube, SIFT, studies of the reactions of H_3O^+ , NO^+ and O_2^{+} with six volatile phytogetic esters (see Appendix A)*

The ion chemistry study of six volatile phytogetic esters (hexyl acetate, phenethyl acetate, benzyl acetate, methyl salicylate, methyl benzoate and benzyl benzoate) was a prelude to the plant physiology studies, which focused on phytovolatilization (discussed in Section 5.5.1). These esters, together with methanol, isoprene and terpenes, are some of the most ubiquitous natural volatiles. Plants release these VOCs and also some inorganic volatile compounds (e.g. ammonia) to the atmosphere during their growth and development. Some of these compounds are called semiochemicals and play a role in communication between and among species and also as a defence against herbivore enemies of the plants [169, 170].

A selected ion flow tube study of the reactions of H_3O^+ , NO^+ and O_2^{+} with seven isomers of hexanol in support of SIFT-MS (see Appendix B)*

This study was focused on seven isomers of hexanol (1-hexanol, 2-ethyl-1-butanol, 4-methyl-1-pentanol, 2-hexanol, 4-methyl-2-pentanol, 3-hexanol and 3-methyl-3-pentanol). These alcohols are commonly of biogenic origin and are recognised as important flavour components of various produce such as wine and cheese. The main objective was to provide the kinetic data (the rate constants and the product ion branching ratios) to be included in the SIFT-MS kinetics library that would allow separate identification and quantification of these compounds.

Once the esters and hexanols were chosen and prior to the experimental study of ion-molecule reactions, it was necessary to search the literature for all available information about their properties. Values of their proton affinity and ionization energy, the gas phase ion energetics data, were obtained from the NIST database [171]. Other important parameters are their dipole moments and polarisabilities that were obtained from the CRC handbook [172, 173]. These values are used in calculations of the appropriate gas kinetic rate constants.

Methods

In order to determine the product ions and their branching ratios, the headspace of weak aqueous solutions (typically 10 ppmv) of a sample was prepared. The humid headspace was then introduced into the SIFT-MS instrument via a heated calibrated capillary and full scan mass spectra were acquired whilst the three selected precursor ions were alternately injected into the helium carrier gas in the reactor flow tube (see Section 3). The range of mass-to-charge ratio (m/z) was chosen in order to cover all m/z values of the expected primary product ions and any adduct (hydrated) ions that might form. During the experiments with the samples of esters and the isomers of hexanol, five mass spectra were obtained using each precursor ion, during a total integration time of 60 s. Note that switching between the three precursor ions H_3O^+ , NO^+ and O_2^{+*} was controlled electronically by the data system. The major product ions (m/z 85, 121-139 in the case of 1-hexanol) were identified from the full scan mass spectra (Figure 5.1) and their precise count rates were subsequently analysed in separate experiments using the MIM mode [38].

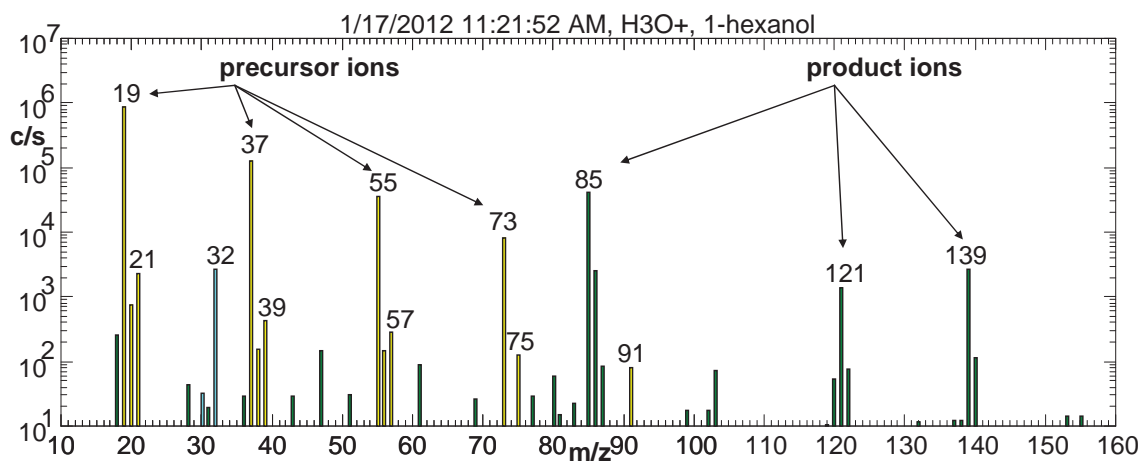


Figure 5.1 The SIFT-MS spectrum obtained as the headspace above 1-hexanol was sampled. The arrows indicate the ions resulting from the reactions of the H_3O^+ precursor ion.

In the MIM mode, the appropriate precursor ion and all the identified product ions were included (see the example of 1-hexanol data in Figure 5.2). The flow rate of the injected gaseous sample was controlled by a needle valve and monitored by a flow-meter (manufactured by Voegtlin, Aesch, Switzerland) to obtain the dependence of ion count rates on the changing amount of the molecules of the VOC/air mixture flowing into the helium carrier gas.

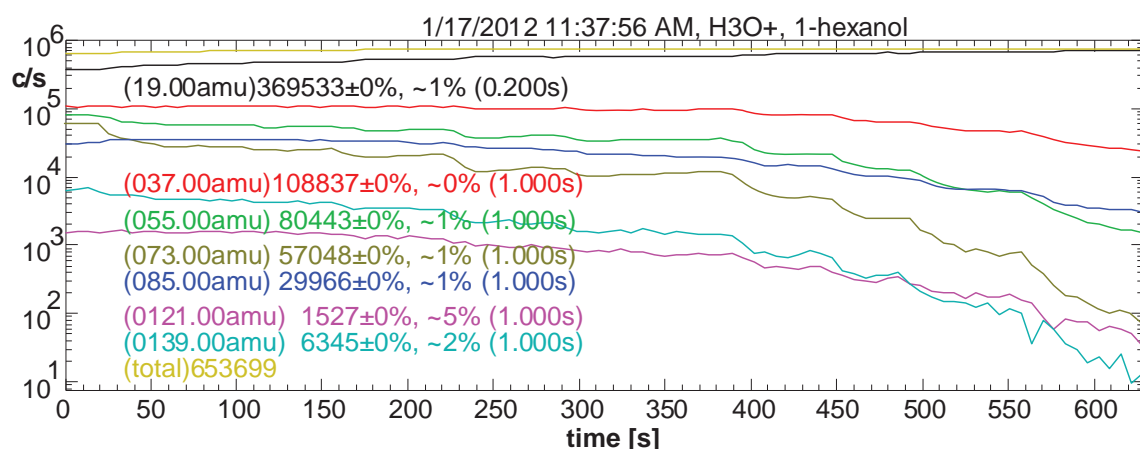


Figure 5.2 The time profile of the decay of signal in c/s of the 1-hexanol primary product ions together with precursor ions (19-37-55-73) obtained using SIFT-MS in the MIM mode.

In order to determine the primary ion product branching ratios of the reaction, it was necessary to plot the percentages of the individual product ions on a linear scale as a function of the sample flow rate. The example of this type of a plot for 1-hexanol is shown in Figure 5.3. By extrapolating to zero sample gas/vapour flow rate (i.e. approaching the limit of zero sample concentration) the true primary branching ratios, excluding any secondary reactions, can be obtained. It is important to exclude any

secondary reactions of the primary product ions, because they distort the observed primary product ion distributions by producing secondary product ions. On the example of Figure 5.3, there is only one primary product ion at m/z 85 and the other two observed ions are secondary product ions. The flow rate of 1-hexanol vapour, which is proportional to the concentration of $C_6H_{14}O$ molecules in the He carrier gas, can most conveniently be expressed in dimensionless units of the logarithm of the reduction of the precursor ion signal $\ln(I_0/I)$ [174].

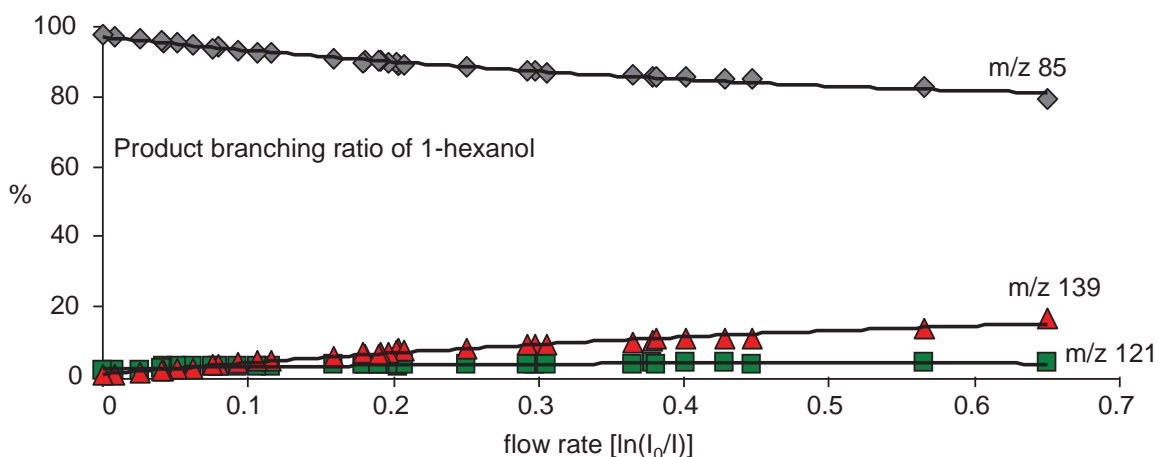


Figure 5.3 A plot of percentages of individual product ions as a function of the flow rate of a mixture of 1-hexanol in humid air introduced into SIFT when H_3O^+ precursor ions are injected. The primary product branching ratios are obtained by extrapolating the lines to zero flow.

The value of the rate constant required for SIFT-MS quantification can be obtained either from original papers or from the Anicich index of the literature for bimolecular gas phase cation-molecule reaction kinetics [175]. But if the required rate constant is not available, as was the case of the biogenic esters, it can be measured by the following procedure. When the reaction occurs on every collision, as is the case for proton transfer reactions that are exothermic by more than some 40 kJ/mol [176], then the rate constant k can be calculated from the polarisability and dipole moment of the neutral molecules using the Su and Chesnavich parameterized trajectory theory and is called the collisional rate constant, k_c [177]. This approach was taken for the reactions of alcohols and esters with H_3O^+ . The rate constants for the reactions with NO^+ and $O_2^{+\bullet}$ (k) are then derived from their experimentally-derived decay rates relatively to that for the H_3O^+ reaction [178]. The SIFT-MS instrument (still in the MIM mode) is in these experiments set up to allow all three precursor ions to react simultaneously with the product ions (Figure 5.4).

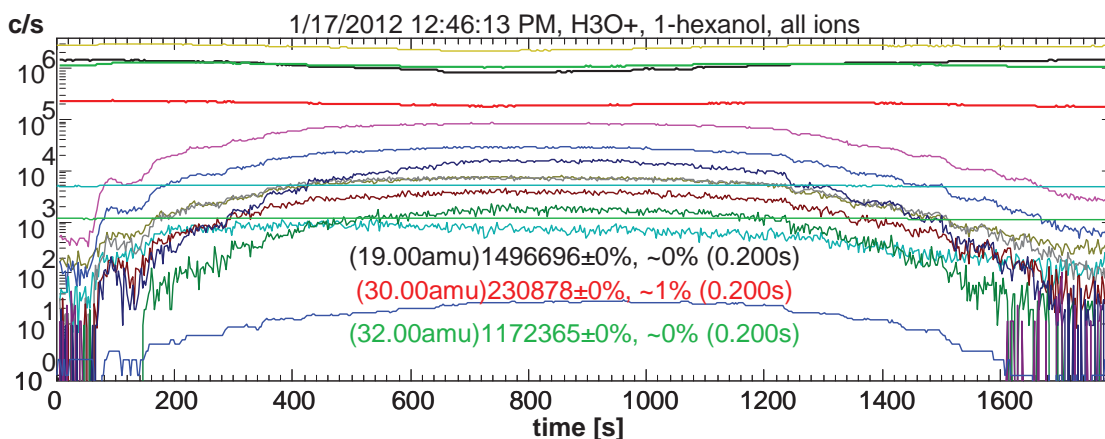


Figure 5.4 MIM profile when all three precursor ions are injected simultaneously into the flow tube where they react with the sample introduced at varied concentration.

This can be achieved by adjusting the mass setting of the injection mass filter to zero value effectively setting the voltage differential between the quadrupole rods to 0 V. The flow rate of injected sample is again controlled by opening and closing the needle valve and is monitored by a flow-meter. The maximum flow rate is typically 25 mL/min at standard atmospheric pressure and temperature. Uncertainties in the absolute values of the determined rate constants are better than 20%, as is typical for SIFT measurements [38]. The plot of experimental dependence of the precursor ion count rates on the sample flow rate is shown in Figure 5.5. The slope reflects the experimental derived relative rate constant which is then multiplied by the theoretically calculated value of k_c of H_3O^+ in order to obtain absolute values for the NO^+ and $\text{O}_2^{+\bullet}$ reactions.

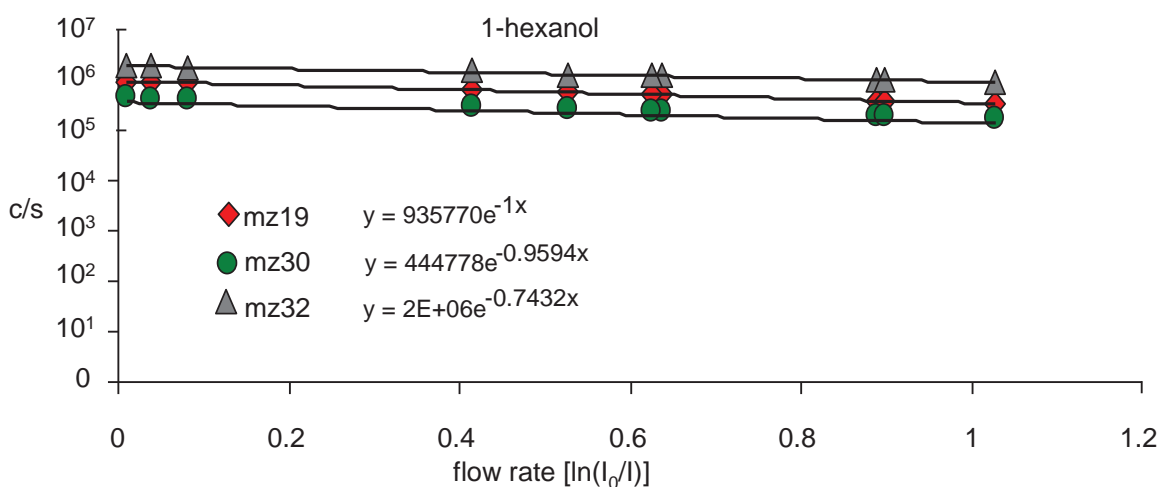


Figure 5.5 The count rates of H_3O^+ , NO^+ and $\text{O}_2^{+\bullet}$ plotted on a semi-logarithmic scale as functions of the sample flow rate. The rate constants (k) for the NO^+ and $\text{O}_2^{+\bullet}$ reactions are then determined from the relative slopes of these plots.

Results and Discussion

This Section presents complementary results, which were not explicitly included in the manuscripts in Appendices A and B. Predominantly, these are examples of mass spectra of the six volatiles phytogetic esters reacting with all three precursors and O_2^+ spectra of isomers of hexanol. Product ions resulting from the ion-molecule reactions are described in the following text. Note that the detailed procedure and an example of the three-body rate constant calculation is described in the Appendix A together with an example of the optimization procedure of the kinetics library entry for the case of overlapping product ions in the spectra.

1. Esters

The major ion products of the H_3O^+ reactions with esters are the protonated molecules, MH^+ , but minor channels involving fragmentation are also evident (see Figure 5.6a-f). These reactions are the results of water molecule elimination and alcohol molecule elimination. The mass spectra were interpreted as follows:

- Five ion products (three primary ions and two ions formed by secondary association with H_2O) are formed in the reaction of **hexyl acetate** (MW 144) with H_3O^+ (Figure 5.6a) with the different product branching ratio (in parenthesis): the protonated molecule and its water cluster at m/z 145 and 163 (77%), an ion fragment $C_6H_{13}^+$ ion at m/z 85 (7%), a fragment and its hydrate at m/z 61 (acetic acid) and 79 (16%).
- **Benzyl acetate** (MW 150) (Figure 5.6b) forms a major product ion at m/z 91 (86%), being interpreted as the tropylium ion, and as a minor channel the protonated molecule and its water cluster at m/z 151 and 169.
- The H_3O^+ reaction with **phenethyl acetate** (MW 164) (Figure 5.6c) produces the ion at m/z 105 (80%) and again, as in the case of hexyl acetate, an acetic acid molecule and its hydrate (m/z 61 and 79) and the protonated molecular ion and its hydrate at m/z 165 and 183. Note that product ions at m/z 61-79 were not included in Table 3 in Appendix A, because their product branching ratio was less than 5 % as was also explained in the manuscript.
- **Methyl salicylate** (MW 152) reacts with H_3O^+ forming the protonated molecule as the only ion product m/z 153 and this ion surprisingly does

not directly associate with H₂O. Methyl salicylate represents a very unusual exception, as can be seen in the mass spectrum in Figure 5.6d demonstrating the absence of an association product. This was confirmed by the experimental determination of the rate constants of the three-body association reactions of the MH⁺ ions with water molecules, k_{MH^+} (in details described in Appendix A). Note the characteristic ion products at m/z 153 and the relatively small peak of the hydrated protonated parent molecule at m/z 171 (1%) that originates entirely from **ligand switching** reactions involving the hydrated hydronium ions at m/z 37, 55 and 73. The hypothesis for this observed anomaly is that it is partly due to steric hindrance and that the charge is not located on an accessible functional group.

The ion products of the NO⁺ reactions with the esters are shown in the mass spectra in Figures 5.7a-f. The reactions of NO⁺ with the esters proceed via three-body association reactions forming M·NO⁺ adduct ions or via charge transfer producing nascent M⁺ ions that in some cases fragment.

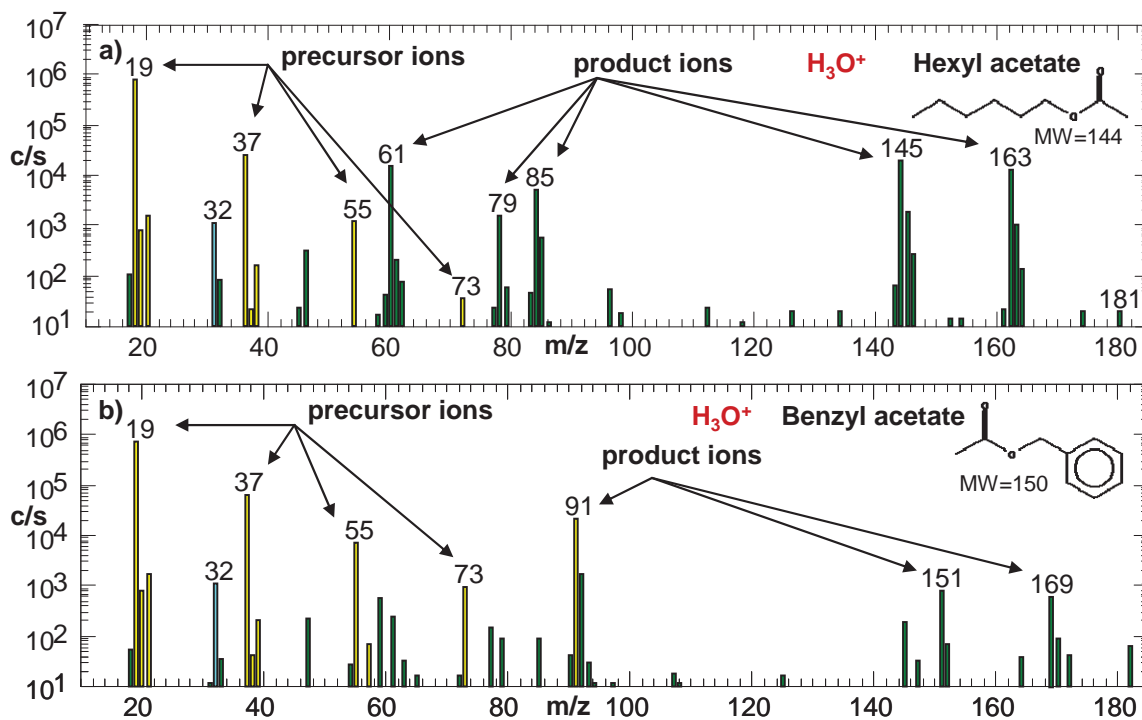


Figure 5.6 a), b) The SIFT-MS spectra obtained as the headspace above a) hexyl acetate, b) benzyl acetate was sampled. The arrows indicate the ions resulting from the reactions of the H₃O⁺.

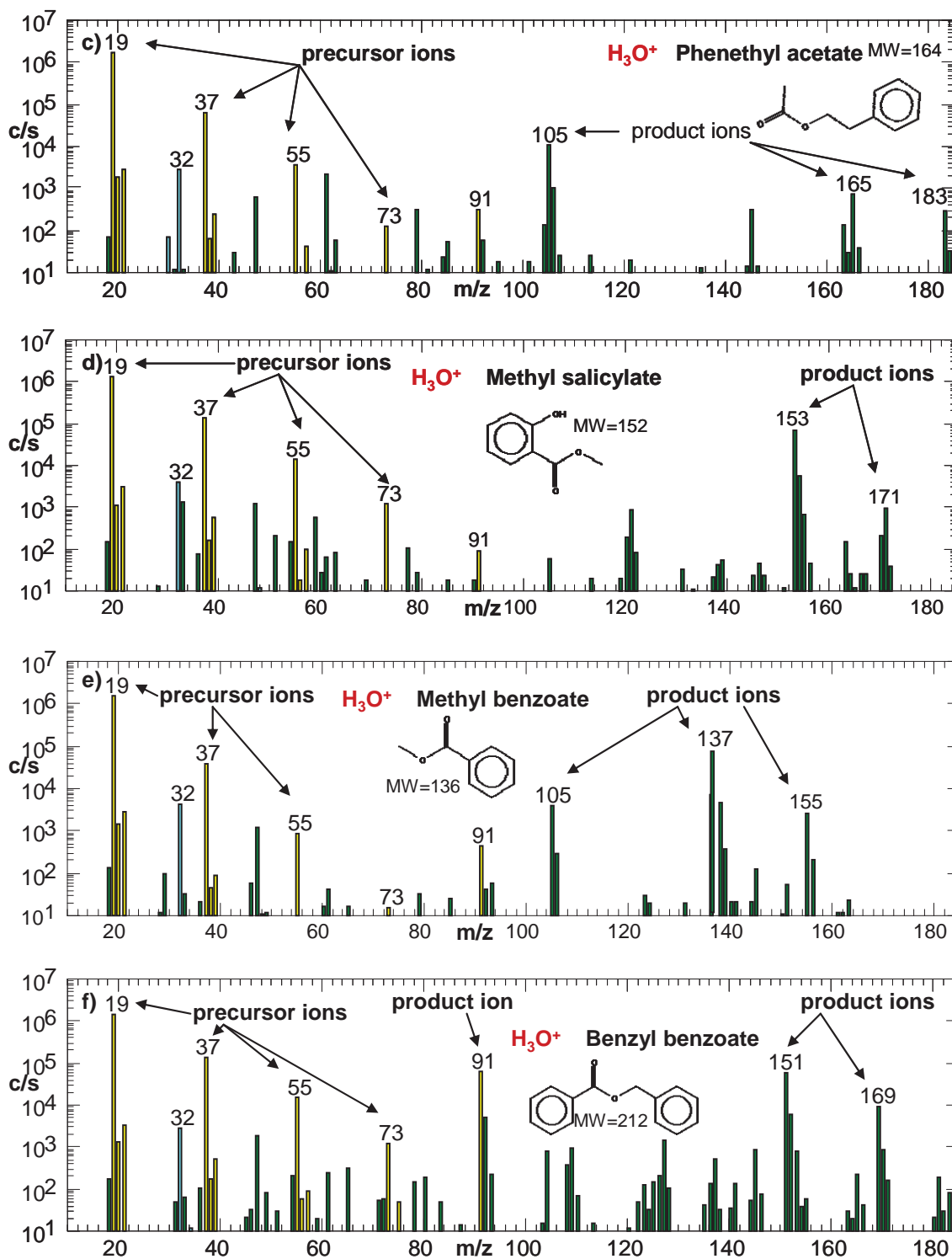


Figure 5.6 c) -f) (continued) The SIFT-MS spectra obtained as the headspace above c) phenethyl acetate, d) methyl salicylate, e) methyl benzoate and f) benzyl benzoate was sampled.

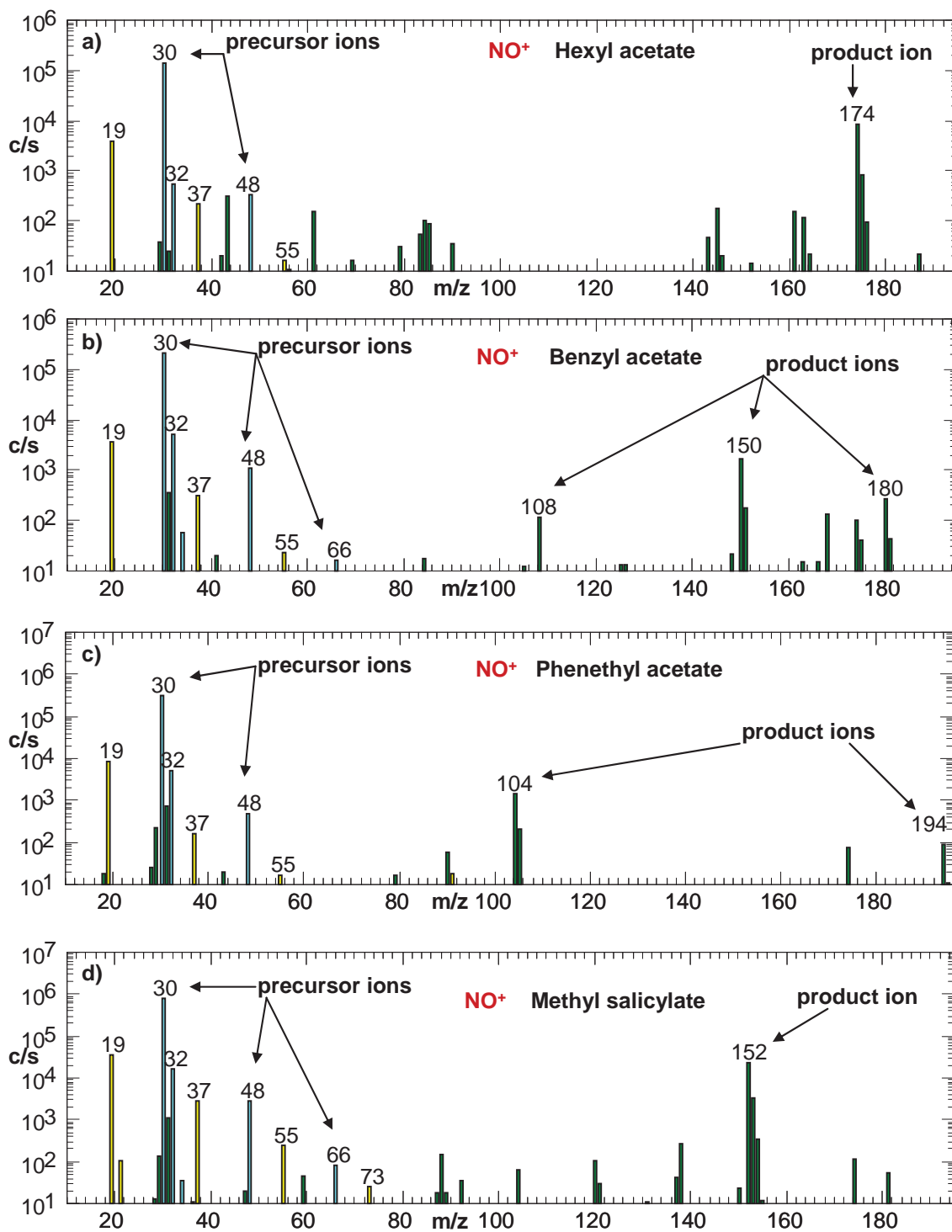


Figure 5.7 The SIFT-MS spectra obtained as the headspace above a) hexyl acetate, b) benzyl acetate, c) phenethyl acetate, d) methyl salicylate was sampled. The arrows indicate the ions resulting from the reactions of the NO⁺.

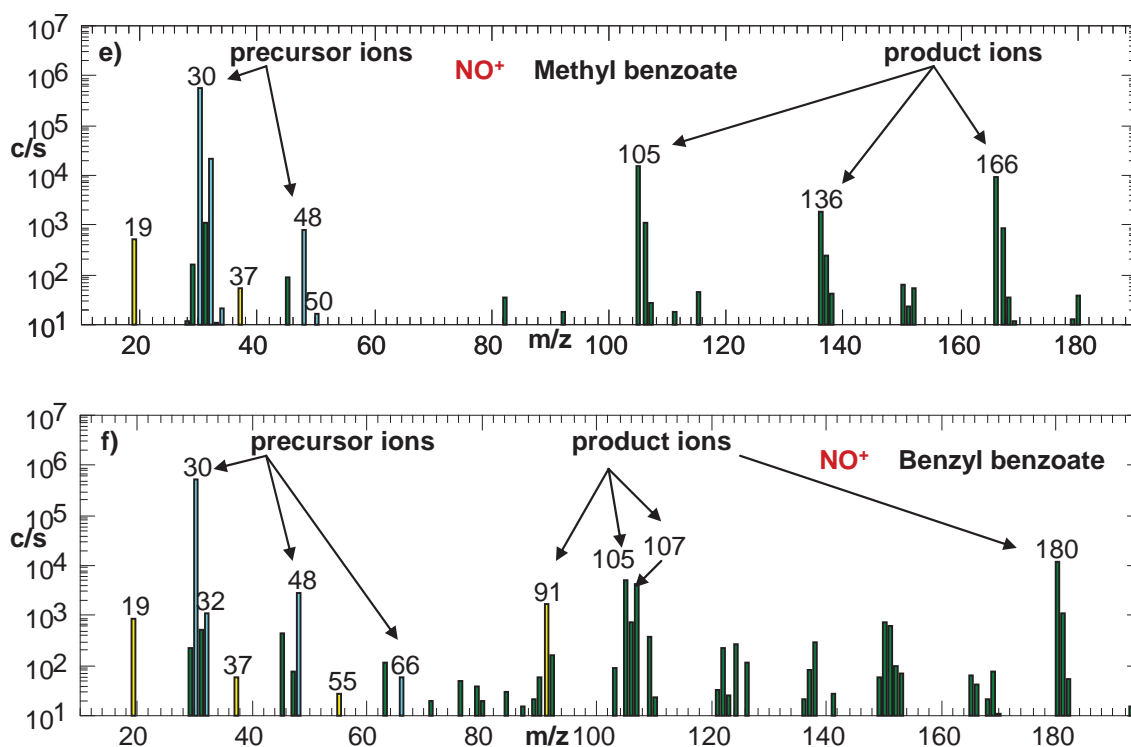


Figure 5.7 (continued) NO⁺ spectra of vapours of e) methyl benzoate and f) benzyl benzoate.

The reactions of these esters with the O₂⁺ precursor ion mostly proceed either via non-dissociative charge transfer producing the parent radical cation M⁺ or via dissociative charge transfer reactions resulting in several fragment ions. The spectra obtained using the O₂⁺ reagent ions are more complicated than those obtained using H₃O⁺ or NO⁺ (Figure 5.8 a-f). It is worthy of note that most of the products of the O₂⁺ reactions are also present in the EI mass spectra of the corresponding compounds [179]. This is because both EI and chemical ionisation using O₂⁺ proceed via the formation of the radical cation followed by its fragmentation.

Note, the detailed information including rate constants, values of k_{MH^+} , and product ion branching ratios are summarized in the Tables in Appendix A.

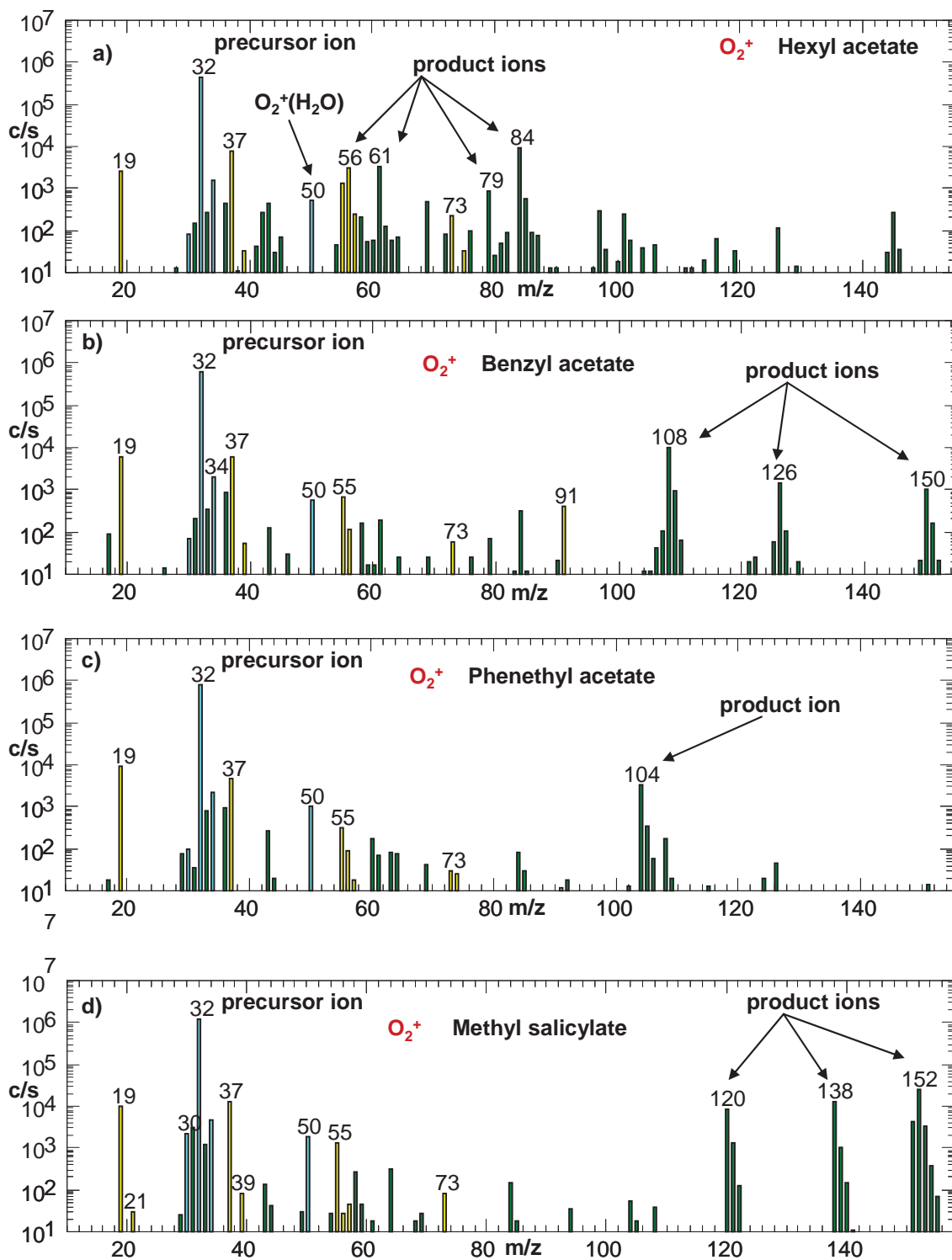


Figure 5.8 The SIFT-MS spectra obtained as the headspace above a) hexyl acetate, b) benzyl acetate c) phenethyl acetate and d) methyl salicylate was sampled. The arrows indicate the ions resulting from the reactions of the O_2^+ precursor ion.

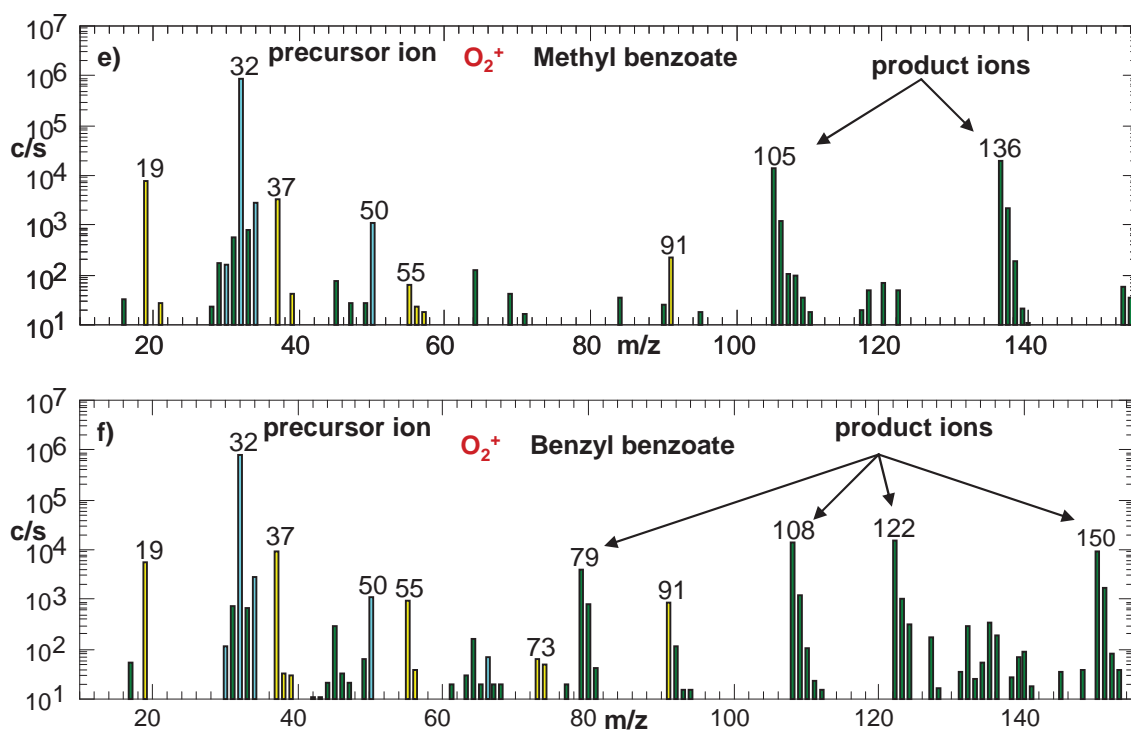


Figure 5.8 (continued) The (O_2^+) spectra of vapours of e) methyl benzoate and f) benzyl benzoate.

2. Hexanol isomers

As previously reported by Španěl and Smith [38, 180], the simplest two aliphatic alcohols methanol and ethanol react with H_3O^+ to produce only the protonated alcohol, MH^+ . For higher order alcohols, including also the isomers of hexanol (MW= 102), MH^+ is no longer the major product and the protonation is followed by H_2O elimination from the $[MH^+]$ * excited nascent product ion occurs producing the $[M-OH]^+$ hydrocarbon ions. The only primary ion product of all isomers appears at m/z 85 is $C_6H_{13}^+$. Note that hydrocarbon ions do not associate with H_2O molecules under SIFT-MS conditions (helium pressure about 1 Torr; room temperature) and this was again the situation for all the isomeric forms of the $C_6H_{13}^+$ produced in these reactions. However, ion products $C_6H_{15}O^+ H_2O$ at m/z 121 (Figure 5.1) were found in air/alcohol samples. This formation is attributed to ligand switching reactions of the alcohol concerned with the hydrated hydronium ions $H_3O^+(H_2O)_{1,2,3}$. Even though the $C_6H_{15}O^+ H_2O$ product ions do not result directly from the reactions of H_3O^+ precursor ions, they must be included for accurate quantification of alcohols by SIFT-MS [46]. The reactions between NO^+ and the hexanol isomers proceed predominantly by hydride ion transfer producing an ion $(M-H)^+$ at m/z 101 and a neutral molecule HNO. The only exception is the reaction of the tertiary alcohol 3-methyl-3-pentanol that does not form this product

ion but results in only one primary ion product $C_6H_{13}^+$ at m/z 85, involving the elimination of an OH group from the nascent $[NO^+C_6H_{14}O]^*$, thus forming a neutral nitrous acid molecule HONO. This can easily be explained: in the case of primary and secondary alcohols in that the hydrogen atom is removed from the alpha C atom forming the $C_6H_{12}OH^+$ cations, but the alpha C atom in the molecule of tertiary alcohol 3-methyl-3-pentanol does not bind to any H and thus this mechanism of hydride ion transfer is not possible.

The reactions of all seven alcohols with O_2^{+*} proceed via dissociative charge transfer resulting in several fragment ions. The product ions are indicated in the mass spectra in Figure 5.9a-g and were compared with the EI spectra obtained from NIST database [179], but as was explained in detail in Appendix B, the major product ions differ. One of the main objectives of this study was to investigate a method for separately identifying the different hexanol isomers and the O_2^{+*} spectra do offer this possibility for some of the isomers.

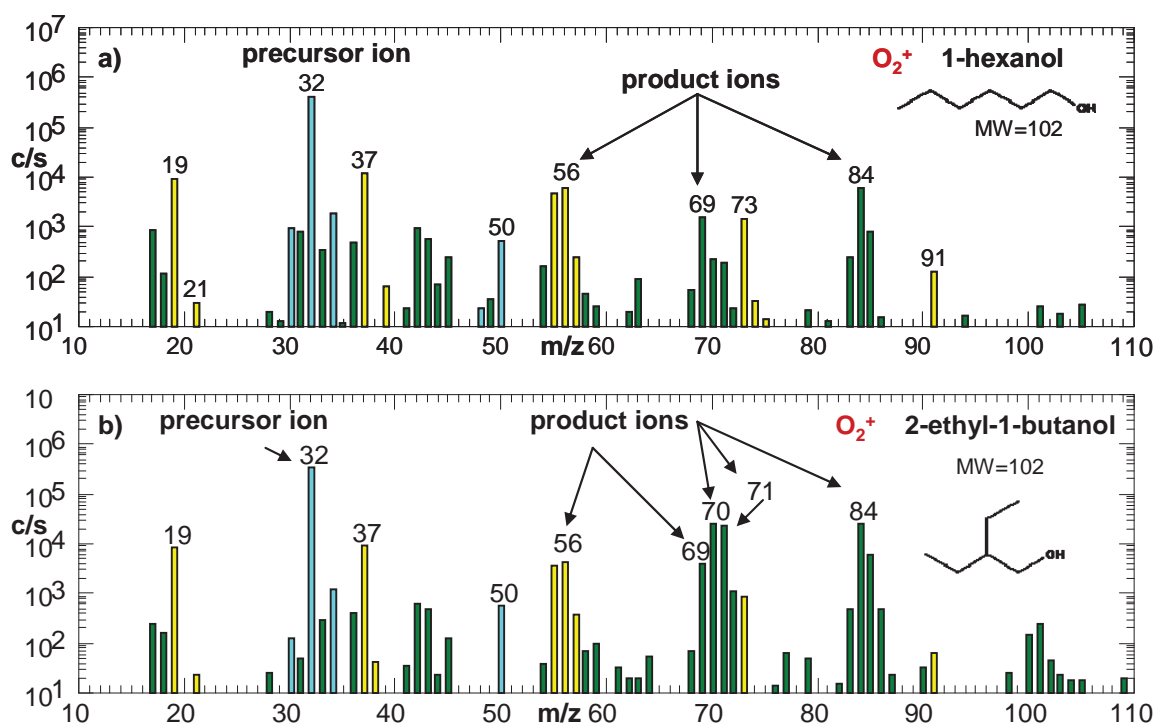


Figure 5.9 a), b) The O_2^{+*} SIFT-MS spectra obtained as the headspace above a) 1-hexanol, b) 2-ethyl-1-butanol was sampled. At axes y ion signal in c/s?

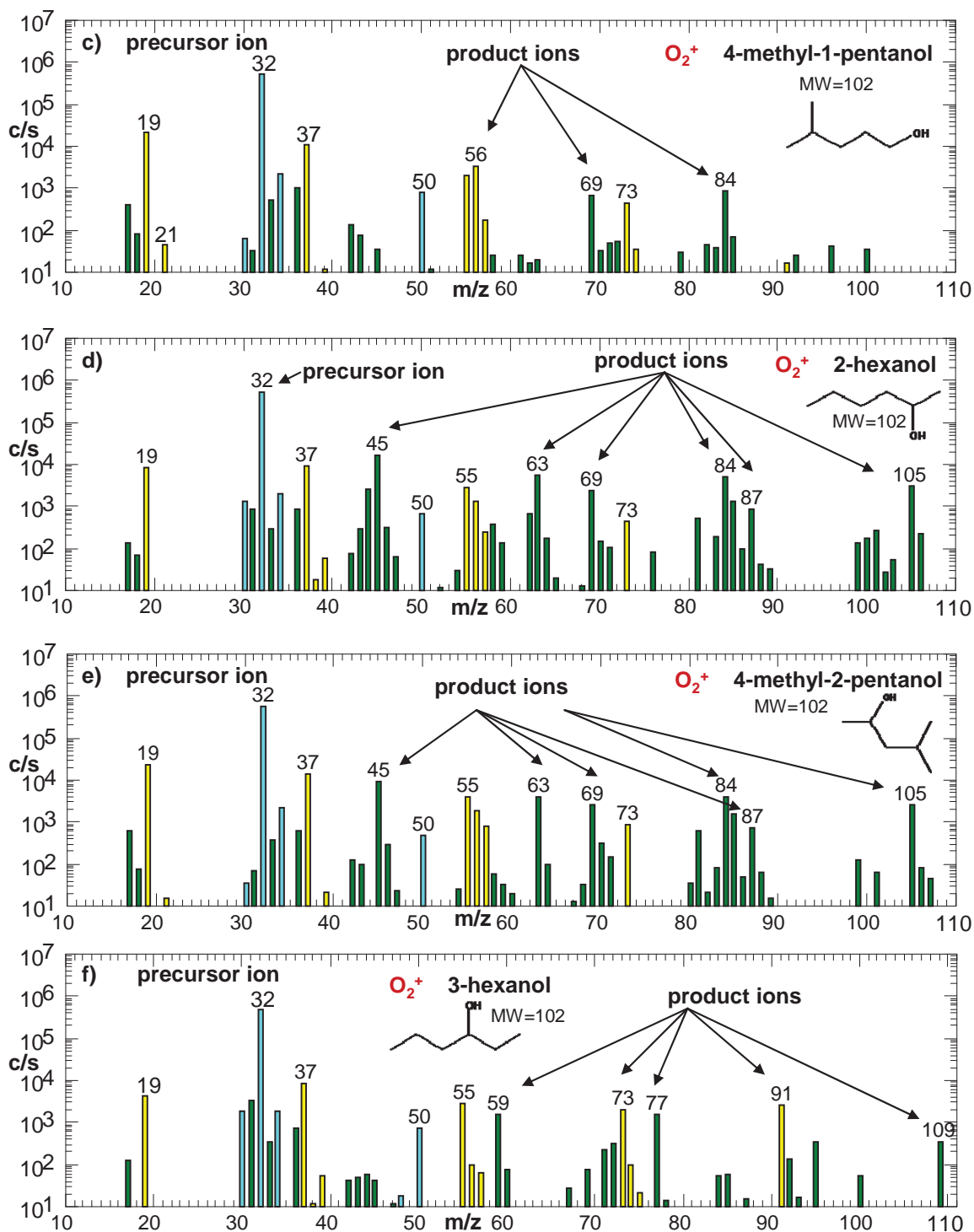


Figure 5.9 c-f) The O_2^+ SIFT-MS spectra obtained as the headspace above c) 4-methyl-1-pentanol, d) 2-hexanol, e) 4-methyl-2-pentanol, f) 3-hexanol was sampled.

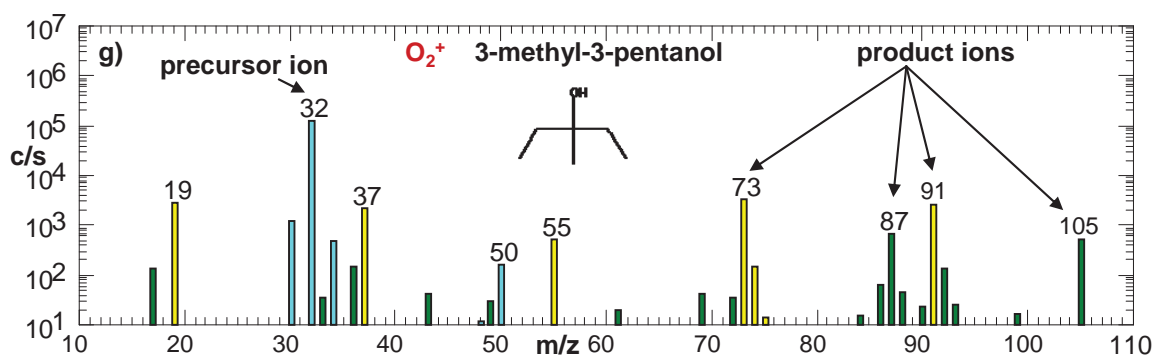


Figure 5.9 g) (continued) The O_2^{+*} spectra of vapours of g) 3-methyl-3-pentanol.

Thus, the varying product ion percentages in the O_2^{+*} reactions offer some support to isomer identification, but the complexity of the product distributions diminishes their value in this pursuit. Similarly, the other two precursor ions provide almost the same product ions, thus the quantification of the selected isomers in mixtures is very difficult. However, the data presented in this study will allow absolute quantification of the total concentration of all hexanol isomers to an acceptable accuracy, because it is shown that the differences between individual rate constants (see Table 2 in Appendix B) of their reactions with H_3O^+ are less than 3%, with NO^+ less than 4%, and with O_2^{+*} less than 10%.

Conclusions

The ion chemistry studies discussed in this section provided some new data for the kinetics of the reactions important for SIFT-MS quantification of biogenic volatile organic compounds in humid air, and so these data can be included in the kinetics library used for automated immediate quantification. However, before that can be done it is important to consider the effect of possible overlaps of product ions from different compounds at the same m/z , as it will be discussed in the following section.

5.2 Construction and optimization of kinetics library

Concentrations of compounds in SIFT-MS analysis are calculated from the ratios of count rates of characteristic product ions to the count rates of the precursor ion using a library of kinetic data [46, 181]. The construction of such kinetics library entries requires information about the appropriate precursor ions, the rate constants and the m/z values of the characteristic product ions. An example of such kinetics data in the format required for the SIFT-MS software was presented in Table 3.1. In the present section a construction of more advanced entries accounting for overlaps of the product ions will be shown for the six volatile phytogetic esters: hexyl acetate, phenethyl acetate, benzyl acetate, methyl salicylate, methyl benzoate and benzyl benzoate. The fundamental kinetics of the reactions of H_3O^+ , NO^+ and $\text{O}_2^{+\bullet}$ with these esters was discussed in the previous Section 5.1. The results obtained can be used to construct an initial simple version of the kinetics library entries as given in Table 5.1. For example, for hexyl acetate the following details are given according to the format described in Section 3.2.6: appropriate precursor ion (H_3O^+), which means listing all four m/z values including the H_3O^+ hydrates (19-37-55-73) together with the appropriate rate constant obtained theoretically or derived experimentally; then the f_p coefficient at the default value of 1.0 (values other than 1.0 can be used to multiply the corresponding ion count rates in order to optimize kinetics entries, as it will be shown below); then the number of product ions (m/z 61, 79, 85, 145, 163) formed by primary and secondary ion-molecular reactions with each m/z value followed by the default f_i coefficient of 1.0.

It was then important to test the constructed kinetics library entries for the effect of ion overlaps by analysing real samples. Thus, reference mixtures (at approximately 10 ppmv concentrations) of all six esters were analyzed subsequently in the MIM mode, see Figure 5.10. As it can be seen, in this plot of concentrations calculated using the kinetics library in Table 5.1, there is evidence of cross sensitivity between different compounds. These validations of this initial library thus indicated m/z overlaps between hexyl acetate and phenethyl acetate and also amongst the group of benzoates. Only methyl salicylate was quantified without any signs of overlaps. The m/z overlaps between hexyl acetate and phenethyl acetate related to the m/z 61 and 79 ions. To allow selective measurements of the concentration of these esters, the kinetics library must be optimised in order to minimise or avoid overlaps. To avoid this overlap problem, these m/z values were excluded from the final kinetics library entry, because the product

branching ratios for phenethyl acetate was less than 5%. Other overlaps amongst the benzoates were caused by the same m/z values of the ion products of the benzyl acetate and benzyl benzoate reactions (m/z 91, 151, and 169). The methyl benzoate reaction leads to a small m/z 91 product (less than 2%) and thus this product ion was excluded from the methyl benzoate entry. More challenging was to resolve the m/z overlaps between benzyl acetate and benzyl benzoate. This was resolved by linear combinations of product ion count rates, the f_p coefficients were determined that allows selective real time quantification of these two compounds even in the mixture. The detailed procedure of these calculations is discussed in Appendix A. The optimized kinetics library is given in Table 5.2 and the final MIM profile concentration calculated using the optimised library is shown in Figure 5.11.

Table 5.1 Kinetics library entries describing straightforward calculations of six esters concentrations using the H_3O^+ precursor ion.

Hexylacetate (H_3O^+)	Benzylacetate (H_3O^+)	Phenethylacetate (H_3O^+)	Methylsalicylate (H_3O^+)	Methylbenzoate (H_3O^+)	Benzylbenzoate (H_3O^+)
4 precursors	4 precursors	4 precursors	4 precursors	4 precursors	4 precursors
19 3.2e-9 1.0	19 3.4e-9 1.0	19 3.5e-9 1.0	19 3.8e-9 1.0	19 3.3e-9 1.0	19 3.7e-9 1.0
37 2.4e-9 1.0	37 2.5e-9 1.0	37 2.6e-9 1.0	37 2.9e-9 1.0	37 2.5e-9 1.0	37 2.8e-9 1.0
55 2.1e-9 1.0	55 2.2e-9 1.0	55 2.2e-9 1.0	55 2.5e-9 1.0	55 2.2e-9 1.0	55 2.4e-9 1.0
73 1.9e-9 1.0	73 2.0e-9 1.0	73 2.0e-9 1.0	73 2.2e-9 1.0	73 2.0e-9 1.0	73 2.1e-9 1.0
5 products	6 products	3 products	3 products	3 products	3 products
61 1.0	105 1.0	121 1.0	121 1.0	137 1.0	91 1.0
79 1.0	137 1.0	153 1.0	153 1.0	155 1.0	151 1.0
85 1.0	169 1.0	171 1.0	171 1.0	153 1.0	169 1.0
145 1.0	163 1.0				
163 1.0	165 1.0				
	183 1.0				

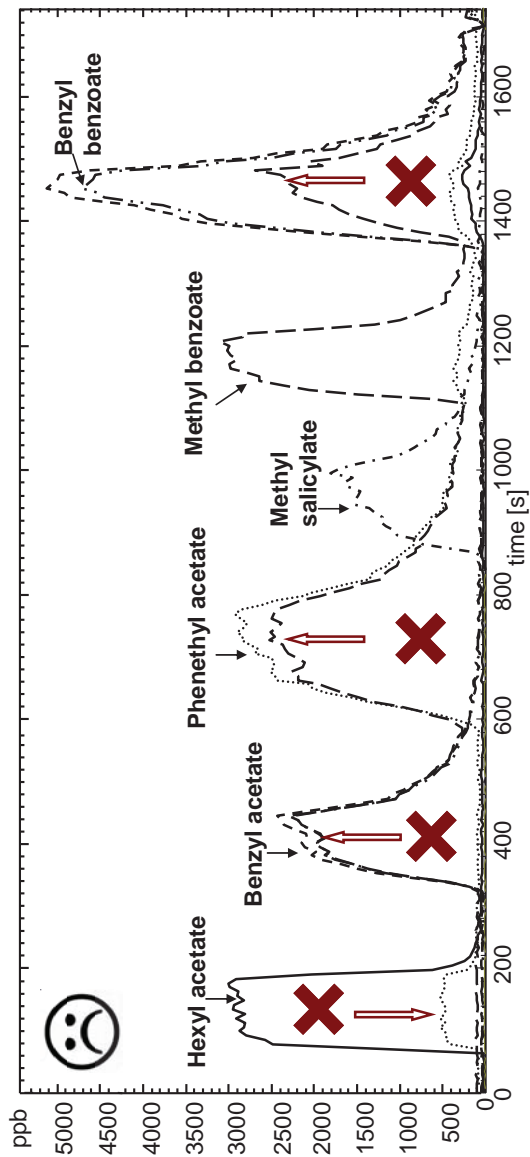


Figure 5.10 A test of the initial simple kinetic library entries given in Table 5.1.

Table 5.2 Optimized kinetics library entries.

Hexylacetate (H_3O^+)	Benzylacetate (H_3O^+)	Phenethylacetate (H_3O^+)	Methylsalicylate (H_3O^+)	Methylbenzoate (H_3O^+)	Benzylbenzoate (H_3O^+)
4 precursors	4 precursors	4 precursors	4 precursors	4 precursors	4 precursors
19 3.2e-9 1.0	19 3.4e-9 1.0	19 3.5e-9 1.0	19 3.8e-9 1.0	19 3.3e-9 1.0	19 3.7e-9 1.0
37 2.4e-9 1.0	37 2.5e-9 1.0	37 2.6e-9 1.0	37 2.9e-9 1.0	37 2.5e-9 1.0	37 2.8e-9 1.0
55 2.1e-9 1.0	55 2.2e-9 1.0	55 2.2e-9 1.0	55 2.5e-9 1.0	55 2.2e-9 1.0	55 2.4e-9 1.0
73 1.9e-9 1.0	73 2.0e-9 1.0	73 2.0e-9 1.0	73 2.2e-9 1.0	73 2.0e-9 1.0	73 2.1e-9 1.0
5 products	3 products	6 products	3 products	3 products	3 products
61 1.0	91 1.38	105 1.088	121 1.077	137 1.236	91 -0.30
79 1.0	151 -0.86	137 -0.06	153 1.088	155 1.088	151 1.96
85 1.066	169 -0.86	155 -0.06	171 1.088	153 -0.16	169 1.96
145 1.088		163 -0.01			
163 1.088		165 1.1			
		183 1.1			

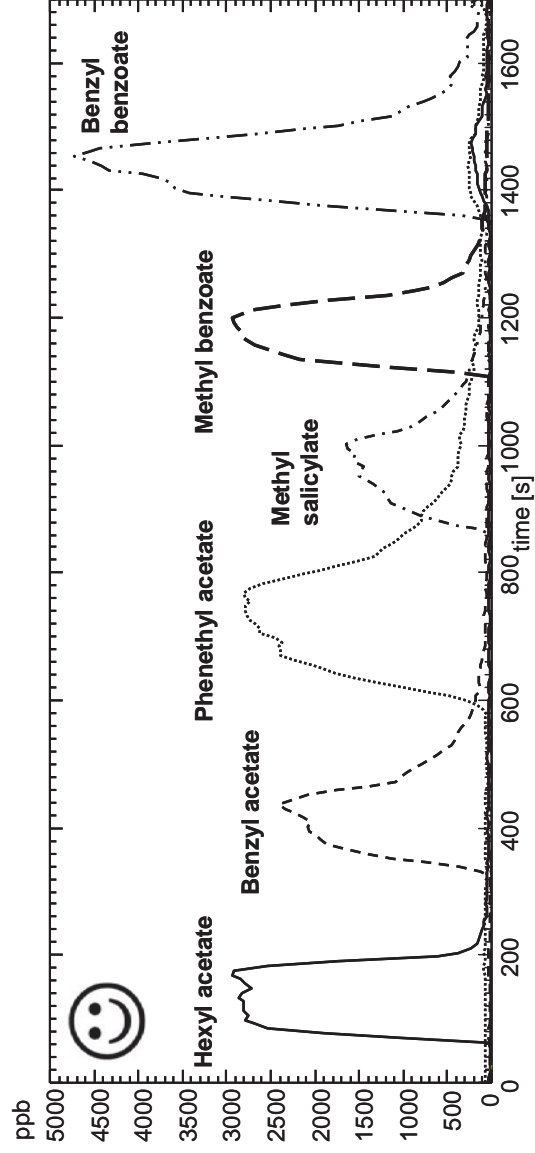


Figure 5.11 A test of the optimized kinetic library entries given in Table 5.2.

5.3 Breath analysis

5.3.1 Inflammatory bowel disease

Objectives

Inflammatory bowel disease (IBD) is a term covering a group of chronic disorders of the gastrointestinal tract that cause extensive damage and inflammation of the intestines and rectum. The primary forms of IBD are **ulcerative colitis** (UC) and **Crohn's disease** (CD). The actual cause of IBD has not yet been elucidated, but everything indicates that it is an autoimmune disease precipitated by a complex



Figure 5.12 Illustration of inflammation of the gastrointestinal tract.

combination of genetic predisposition, immune aberrations, environmental factors and lifestyle [182-184]. Strober *et al.* [185] has concluded that IBD is indeed characterized by an abnormal mucosal immune response and that microbial factors can facilitate this response. These diseases are linked with modern life. It is postulated that improved hygiene alters the intestinal flora by decreasing exposure to certain critical bacteria and that intake of fatty acids in the diet can increase the risk of IBD [183, 186].

Cosnes [187] discussed the risk of tobacco smoking in IBD. He suggested that smoking protects against UC, but it is dose dependent, whereas smoking increases the risk of developing CD. Both UC and CD can seriously diminish the quality of life and lead to shorter life expectancy. Interestingly, UC is slightly more common in males, whereas CD is marginally more frequent in women [183]. They primarily affect the age group 15 - 30. The estimated prevalence in Czech population is about 0.3 %, but accurate epidemiological data are not available.

Current treatment of IBD (pharmacological or surgical) can only ameliorate the symptoms such as abdominal pain, weight loss and bloody diarrhoea, but there is no curative therapy available to date. Diagnosis of IBD is based on the presence of architectural distortion by endoscopy, CT and MRI. Although the symptoms of CD and UC are similar, they are not identical. In CD the location of inflammation is anywhere along the digestive tract from the mouth to the anus, mostly in the terminal ileum. In UC

the inflammation involves only superficial layers of the large intestine – the colon and rectum.

Breath analysis carried out by SIFT-MS has the potential to noninvasively diagnose or even monitor the therapy of these diseases. One of the factors that cause the inflammation is free radicals (reactive oxygen species). These molecules react with the polyunsaturated fatty acids in phospholipids, the main components of cell membranes, which leads to the lipid peroxidation. In this process, **pentane** and other alkanes [188, 189] are formed as by-products [190]. The scheme of the radical chemistry is presented in the manuscript given as Appendix C, which was adopted from Spitteler *et al.* [191].

The aim of the study carried out in Prague and reported here was to develop a method for real-time quantification of **pentane** in human breath by SIFT-MS as a potential **biomarker of IBD**. Having achieved this, the method was tested by a pilot study of the analysis of the exhaled breath of a cohort of patients suffering from both CD and UC.

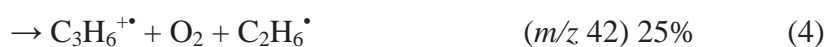
Results and Discussion

Quantification of pentane in exhaled breath, a biomarker of bowel disease, using selected ion flow tube mass spectrometry (see Appendix C)

My specific contribution to this collaborative study was to study ion chemistry of pentane in support of SIFT-MS analyses and I have also participated in the clinical study carried out in the hospital.

Pentane does not react with H_3O^+ and NO^+ precursor ions. Thus, for SIFT-MS analysis, $\text{O}_2^{+\bullet}$ is the only available precursor ion. The kinetics of the reaction of $\text{O}_2^{+\bullet}$ with pentane has been studied previously [192, 193], but the rate constants and percentage of product ions were inconsistent. Thus, one of the objectives of this study was to improve the accuracy of the kinetic data and thus to accurately quantify the concentration of pentane in human breath.

Firstly, dry air mixture of pentane was introduced into the helium carrier gas of the SIFT-MS instrument where it reacted with injected $\text{O}_2^{+\bullet}$ ions. The instrument was operated in the full scan mode in order to identify the primary ion products of the $\text{O}_2^{+\bullet}$ /pentane reaction (Figure 5.13). Four product ions appeared in the spectrum and the percentages of product branching ratio were determined using the methods described in [194] and are given in brackets in equations (1)-(4).



Next, the variation of the count rates of these four product ions was investigated using the MIM mode using SIFT-MS as the pentane flow was varied; see also the detailed procedure described in [194]. For the accurate quantification of pentane in exhaled human breath, only two product ions at m/z 72 and at m/z 42 were chosen. The product ion at m/z 43 cannot be used in analysis because it is also a common fragment ion of the reactions of $\text{O}_2^{+\bullet}$ with acetone (that is present in exhaled breath) and other ketones. The product ion at m/z 57 must be also excluded because it overlaps with ^{18}O isotopologues of the $\text{H}_3\text{O}^+(\text{H}_2\text{O})_2$ ions that are always present when humid samples like breath are being analysed by SIFT-MS. The optimized kinetics library entry is given in the manuscript in Appendix C.

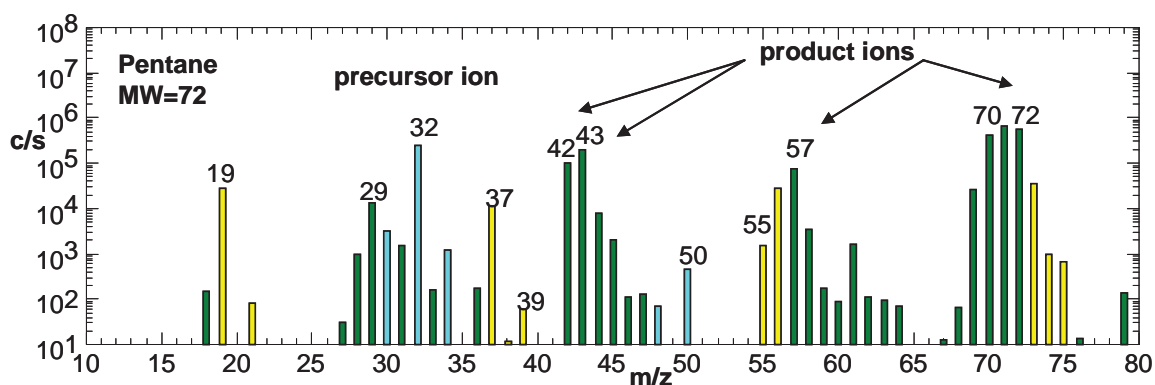


Figure 5.13 The SIFT-MS spectrum obtained as the headspace above pentane was sampled. The primary product ions of the reaction between $\text{O}_2^{+\bullet}$ precursor ion and pentane are indicated.

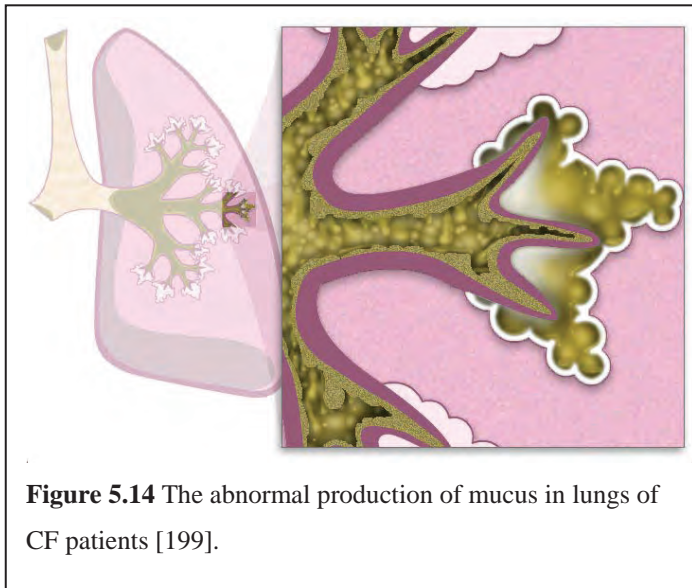
Conclusion

- A method for accurate quantification of pentane in human breath in real time was developed and validated.
- A pilot study of the exhaled breath of a group of patients suffering from IBD (UC and CD) has been carried out. The differences between breath pentane in CD and in healthy controls was significant ($p < 0.001$). In UC the mean pentane concentration was somewhat lower than in CD.

5.3.2 Cystic fibrosis

Objectives

Cystic fibrosis, CF, is an inherited genetic disease that is incurable despite the advances of medicine. It is relatively common (1:3000) [195] and occurs primarily in Caucasians. This disease is caused by mutations in a gene that is responsible for the transfer of ions and salts across the cell membrane [196-198]. Before modern medicine became a science, an observation was made that “*a child that taste salty when kissed will soon die*” (Alonso y de los Ruyzes de Fonteca J. *Diez Privilegios para Mugeres Prenadas*. Henares, Spain, 1606) [197].



These symptoms of CF affect most severely the respiratory and digestive system. The lungs of healthy individuals are covered with a thin layer of mucus, which facilitates airways stretching and allows expectoration. In patients suffering from cystic fibrosis, excessive production

of mucus (see Figure 5.14 [199]) occurs and breathing becomes increasingly harder. The second consequence of abnormal mucus production is a risk of bacterial infection, because the lungs become a rich nutrient medium for bacteria [200, 201]. These bacteria, normally harmless for healthy people, cannot be removed fast enough and cause chronic respiratory infections. Repeated infections cause lung damage, which then fail. Ultimately, lung transplantation is often necessary as CF worsens. Body organs that are damaged in cystic fibrosis are not only the lungs but also the intestine, the salivary glands, the pancreas and in males CF causes infertility. Despite the fact that it is not a curable disease, today patients live for typically for 30 years of age and longer, which in comparison with the earlier common deaths of CF patients in childhood is a great success of treatment, and the progress of CF research is such that further prolongation of life is expected.

As mentioned above, the lungs of patients suffering from CF are often colonized by bacteria, mainly by *Pseudomonas aeruginosa* (PA) [202], which is the major cause

of morbidity and mortality together with *Burkholderia cepacia* in CF patients [203, 204]. Current methods of PA diagnosis are the analysis of sputum or bronchoalveolar lavage that are considered as the “gold standard” methods [205, 206]. But in children who are unable to expectorate sputum these diagnostic methods are unreliable, unpleasant or invasive (the case of bronchoscopy). Initial infection usually occurs with a non-mucoid strain sensitive to antipseudomonal antibiotics. If the infection is diagnosed early, the treatment can help to eradicate the colonization of lungs. Chronic infection makes the treatment by antibiotics unlikely, because the PA phenotype changes to the mucoid variant [207]. Thus there is a need for early, reliable, immediate and non-invasive method of diagnosis of PA.

Breath analysis could potentially be a useful non-invasive diagnostics tool of PA infection and analyses of VOCs emitted from PA cultures are becoming an important part of the search for volatile breath markers of PA lung infection [151]. This approach offers a way since the detection by SIFT-MS of HCN emission from cultures of PA *in vitro* [208, 209]. It was shown that *in-vitro* cultures of PA released several VOC including, and especially, HCN. Subsequently, SIFT-MS was used for the analyses of breath of 40 children suffering from CF. The concentration of HCN in the exhaled breath was in these patients increased significantly in comparison with children who suffered from asthma but not with CF [87]. However, in 2011 a SIFT-MS study of HCN in the headspace of 96 genotyped PA samples showed that different strains of this bacterium produced different amounts of HCN. Also it was observed that the non-mucoid phenotype samples produced more HCN than the mucoid phenotype samples [209-211].

This section describes a part of the research based on searching for volatile biomarkers of PA derived from the sputum of many CF patients in the Czech Republic, the initial results of which have been reported by Shestivska *et al.* [75]. As was mentioned earlier, HCN has been identified and quantified using SIFT-MS in PA cultures and also in the exhaled breath of children with CF. Cyanide produced by bacteria is toxic and PA avoids its toxicity by several enzymatic pathways. One of the recently described mechanisms of detoxification of HCN by PA is its metabolism into **thiocyanate** involving the enzyme thiosulphate sulphurtransferase [212]. The pilot experiment carried out in Španěl’s research group in collaboration with the microbiologists from the National Institute of Public Health using SPME-GC/MS has clearly indicated a presence of methyl thiocyanate in PA cultures (Appendix D).

Results and Discussion

Quantification of methyl thiocyanate in the headspace of Pseudomonas aeruginosa cultures and in the breath of cystic fibrosis patients by selected ion flow tube mass spectrometry (see Appendix D)

My specific contribution to this collaborative study were the experimental determinations of kinetics of reactions of H_3O^+ , NO^+ and $\text{O}_2^{+\bullet}$ with methyl thiocyanate (MW 73) and formulation of a method which allows its real time quantification using SIFT-MS. The primary ion chemistry of methyl thiocyanate is relatively simple (see Figure 5.15): H_3O^+ reacts with this compound only by proton transfer reaction resulting in a primary product ion at m/z 74 CH_3SCNH^+ . This protonated molecule associates and forms hydrates at m/z 92, 110, 128.

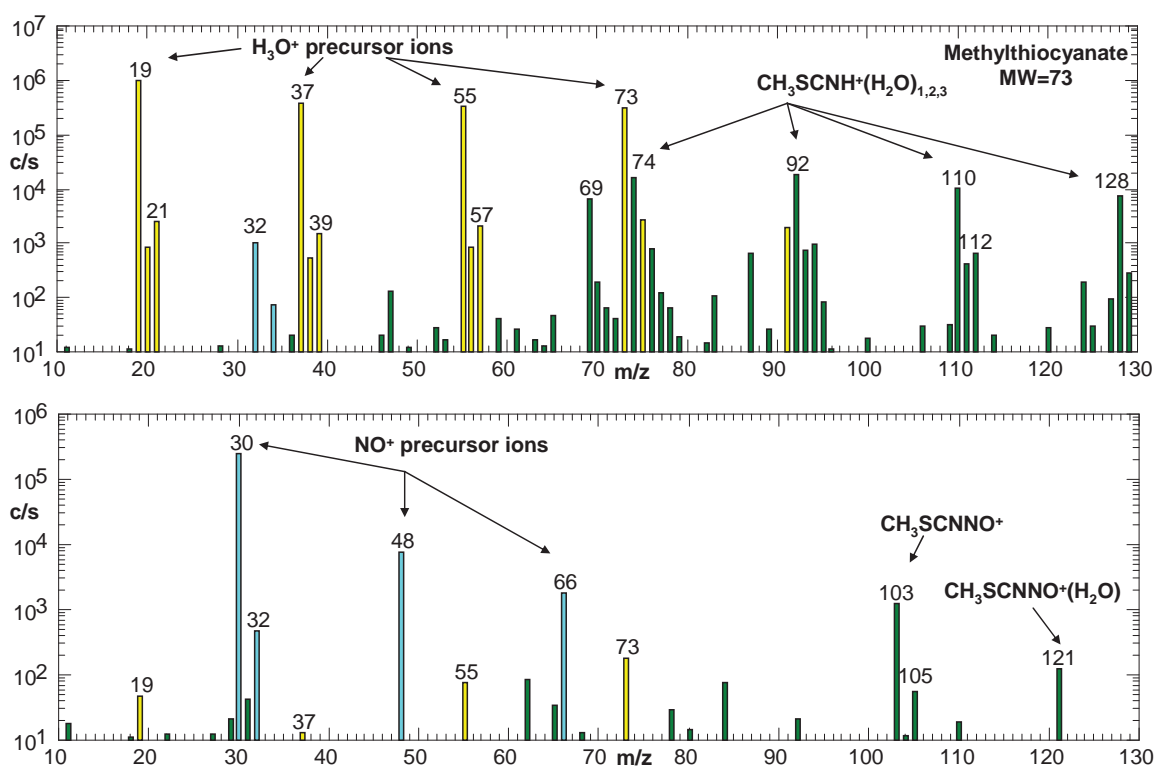


Figure 5.15 SIFT-MS spectra obtained while the headspace weak aqua solution of methyl thiocyanate was introduced into the flow tube. Ion signal intensities are given in counts per second, c/s, plotted against the mass-to-charge ratio, m/z . In these two spectra are shown the major product ions of CH_3SCN with H_3O^+ and NO^+ . Protonated molecule and its hydrates at H_3O^+ spectrum and an adduct at NO^+ spectrum.

The association efficiency, A_{eff} , describing the relative rate constant for three-body association (see Section 3.2.2) of CH_3SCNH^+ with H_2O molecules (using the rate constant of association of H_3O^+ with H_2O , $k_{\text{H}_3\text{O}^+} = 6 \times 10^{-28} \text{ cm}^6 \text{ s}^{-1}$ [66]) was calculated

as 1.6 and thus the three-body rate constant for this reaction is $6.1 \times 10^{-28} \text{ cm}^6 \text{ s}^{-1}$. In comparison with larger organic molecules like esters (Appendix A), this value is relatively small. The collisional rate constant for the formation of the protonated product CH_3SCNH^+ is $4.6 \times 10^{-9} \text{ cm}^3 \text{ s}^{-1}$ according to the calculation using the parameterized trajectory theory [177] (Section 5.1) and the known polarisability and dipole moment of CH_3SCN ($a=7.62 \times 10^{-24} \text{ cm}^3$ and $m=3.56 \text{ D}$, respectively). When using H_3O^+ for SIFT-MS quantification of methyl thiocyanate, it is important to account for the overlap of the product ions with the ^{17}O and D isotopologues of the trihydrated hydronium ions (m/z 74). This can be achieved by including negative f_p coefficients in the kinetics library as given in Table 5.3. Note that such subtraction at m/z 74 leads to a decrease in the precision and thus the kinetics library entry was optimized using the method described in Appendix A. As a result of this only the hydrated products at m/z 92, 110 and 128 are used in the analyses after multiplying the precursor and product ion count rates by optimised coefficients, f_p .

NO^+ reacts with methyl thiocyanate by three-body association only forming the adduct ion $\text{CH}_3\text{SCNNO}^+$ at m/z 103, the effective two-body rate constant for this reaction (proceeding at 1.3mbar of He pressure) is $1.7 \times 10^{-9} \text{ cm}^3 \text{ s}^{-1}$, which is lower than the collisional rate constant $4.4 \times 10^{-9} \text{ cm}^3 \text{ s}^{-1}$. The $\text{O}_2^{+\bullet}$ charge transfer reaction forms the radical cation $\text{CH}_3\text{SCN}^{+\bullet}$ only, and proceeds rapidly with a rate constant equal to the collisional rate constant of $4.3 \times 10^{-9} \text{ cm}^3 \text{ s}^{-1}$. The primary product ion unfortunately overlaps with the $\text{H}_3\text{O}^+(\text{H}_2\text{O})_3$ ion and thus cannot be used for analyses in humid air.

Table 5.3 Rate constants for the reactions of H_3O^+ , NO^+ and $\text{O}_2^{+\bullet}$ with the methyl thiocyanate, given in the units of $10^{-9} \text{ cm}^3\text{s}^{-1}$ together with association efficiencies obtained from experimental data and three body association rate constants calculated from equations in Sections 3.2.2 and 5.1. Also given are the molecular weight, MW, polarisability, α , and the dipole moment, μ_r . Below these data is kinetics library entry in the format required for the SIFT-MS software.

MW	$\alpha(10^{-24} \text{ cm}^3)$	$\mu_r(\text{D})$	$\text{H}_3\text{O}^+ [k_c]$	$\text{NO}^+ k [k_c]$	$\text{O}_2^{+\bullet} k [k_c]$	A_{eff}	$k_{MH^+} (10^{-28} \text{ cm}^6\text{s}^{-1})$
73	7.62	3.56	[4.6]	2.6 [3.9]	2.3 [3.8]	1.6	6.1
Methyl thiocyanate(H_3O^+)							
4 precursors		k		fp			
19		4.6e-9				0.60	
37		3.6e-9				0.50	
55		3.2e-9				1.00	
73		2.9e-9				1.70	
4 products							
91						-0.004	
92						1.20	
110						1.00	
128						1.20	

Conclusions

The presence of methyl thiocyanate in the headspace of genetically diverse PA strains was confirmed by SPME-GC/MS using reference standards. A method for online and real time analysis of methyl thiocyanate based on a careful ion chemistry study was developed and an appropriate kinetics library entry for its analysis by SIFT-MS was constructed. The pilot study of the exhaled breath of CF patients indicated that the concentration of methyl thiocyanate is within the range from zero up to 28 ppbv. The combination of methyl thiocyanate and hydrogen cyanide could be a more robust biomarker of PA and could possibly differentiate different PA strains.

5.4 Population dynamics

Objectives

Another very interesting and challenging experiment concerning bacterial cultures was to develop a model suitable for checking the survival of bacterial colonies in a mixture of several bacterial types/clones (see the publication included in Appendix E). This experiment was done in collaboration with the Department of Philosophy and History of Science at Charles University in Prague, Faculty of Science. This department studies the behaviour of bacteria, which can organise into many interesting multicellular forms, structures and appearance which depends on several factors such as nutrients or even the presence or absence of neighbours [67]. Ostensibly simple unicellular bacteria can thus form fascinating communities of living organisms.

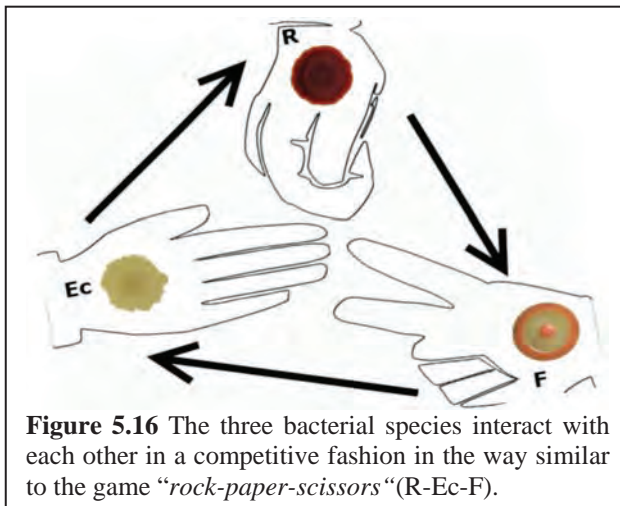


Figure 5.16 The three bacterial species interact with each other in a competitive fashion in the way similar to the game “rock-paper-scissors“(R-Ec-F).

Although bacteria do not have any sensory organs, they somehow can perceive what is happening around them and it is plausible that they are able to communicate using chemical signals. As a model system to investigate such communication we have studied the volatile organic compounds released by bacterial colonies in selected clones of

Serratia rubidaea (R, red and smooth), *Serratia marcescens* (F, fountain shape colonies), which belong to the Gram-negative, facultative anaerobic bacteria of the Enterobacteriaceae family [213], and *Escherichia coli* (Ec) grown on nutrient rich media [67] during 24 hour period. These three organisms form an interesting ecosystem of competing species and their concurrent growth may result in a “*survival of the fittest*” scenario. In a ternary system like this, the interaction can be seen as an analogue of the well-known game “*rock-paper-scissor*” (see Figure 5.16). In this game each item is superior to one other, and inferior to the third one, thus forming a so-called **heterarchy**: rock crushes scissors, scissors cut paper, and paper covers rock [214]. The R colony usually overgrows its F partner; chimeric planting of R and F results in a chimeric colony which looks like R with traces of F in the centre. The Ec colony tends to absorb

the R colony (but it does not directly become overgrown with Ec, as in the previous case) and the resulting chimera contains a mixture of R and Ec in the middle and solely Ec around. In the last possible setting the F colony has a strong tendency to suppress the growth of its Ec partner. The end point state of the FEc chimera consists of F cells only and Ec seems to be driven to extinction. In the chimera consisting of all three clones, F repels Ec, subsequently to be overgrown by R. Thus, there are many possibilities how the bacteria play this game. For example, it is very nice to observe a chimeric colony of R and Ec (it means that Ec absorbed R colony) and to put in its neighbourhood F colonies. The F starts to repel Ec and so the R can escape from the prison of Ec.

Whilst the ultimate result of the population dynamics can be observed by counting the surviving colony forming units, it would be much more instructive to follow them in the real time using volatile signatures (VOCs) of the individual clones. The objective of this study was to identify such VOCs and based on multivariate techniques distinguish among these three bacterial species. It is well known in microbiology that a bacterial colony is a dynamic system that develops in time going through four phases of a so-called growth curve: the lag phase, the exponential or log phase (characterised by the doubling time), the stationary phase (when depletion of nutrients or increasing amounts of waste occur) and the final death phase. The growth dynamics are also influenced by other concurrent organisms that may limit the growth of their neighbours [67, 215, 216].

My specific role in this study was to plan and carry out the SIFT-MS analyses of the VOCs emitted by the bacteria and to analyse the data using traditional and multivariate methods.

Methods

Six different cultures were prepared: monocultures of R, Ec, F, and binary systems of REc, FEc, RF. The SIFT-MS instrument was set in the full scan mode with the scan duration of 120 s in the mass spectral range 10 – 100 m/z and all three precursor ions were cycled. Using this experimental protocol the time evolution of the headspace composition above each sample was monitored and analysed. One experiment took **24 hours** and typically 273 mass spectra were obtained for each precursor ion in each case (for more detail see the published paper in Appendix E). The data were evaluated using the statistical method of principal component analysis (PCA).

Principal component analysis (PCA)

There are several established methods of multivariate data analysis used in chemometrics to enhance data interpretation when a collection of large number of measurements is available. The most common methods are principal component analysis (PCA) and principal component regression (PCR) [217], artificial neural networks and partial least squares regression, PLS-R. Calculation of the principal components, which are linear functions of the measured data, represents the most basic and well understood approach [218]. This method notably forms the mathematical basis of the electronic nose (e-nose) technology, which in the last few years has become an objective tool for discriminating odours. The PCA methods have been previously used for analysis of bacterial culture data obtained using SESI-MS, when it was seen that the species were clearly separated based on their VOC data [21, 81]. Data interpretation using PCA has previously been used in similar PTR-MS analyses [219]. The use of multivariate methods for data analysis in SIFT-MS is still in its infancy and has not yet been described in the published literature and thus this study also serves as a test case for this purpose.

The aim of the principal component analysis is to reduce the dimension of data, which means reducing the number of variables. PCA describes the relationship between variables and observations/cases and also identifies the outliers. If two or more variables in the data table correlate, they can be substituted by one new variable (or factor, or component), PC1. Actually, PC1 becomes a new coordinate axis in the direction of the greatest variability of the data set. Onto this axis the positions of the original data points are projected in multidimensional space. It means that each data point on PC1 has a new coordinate. PC1 is a linear combination of the variables in the original data table. PC2 is then orthogonal coordinate axis to PC1 and has the second highest variance, etc. for additional components. PCA thus rotates the multidimensional coordinate system and projects the data points into fewer dimensions. PCA is very useful for two-dimensional (and sometimes somewhat misleading and questionable three-dimensional) graphical visualization of the multidimensional data, that can be used to reveal differences between groups of data points [220].

For the purpose of PCA analyses the sets of the full scan SIFT-MS mass spectra (combined peak tables of spectra obtained using all three precursors) for different cultures were normalised to a constant total ion count rate. From the count rates of ions

at 90 different m/z values for 3 precursor ions (270 values in total), the precursor ions, their hydrates, ^{13}C isotopologues of the major product ions and all m/z where the mean ion count rate observed was less than 100 c/s were excluded. Thus, 56 characteristic combinations of precursor ion types and product ion m/z values were included in the matrix (273 rows and 56 columns) to be processed by PCA (see Appendix E).

Results and Discussion

Real time monitoring of population dynamics in concurrent bacterial growth using SIFT-MS quantification of volatile metabolites (Appendix E)

An example of PCA visualization which was not included in the published article (Appendix E) is shown in Figure 5.17. From the full scan mass spectra several compounds (ammonia, acetone, acetoin, acetaldehyde, acetic acid, ethanol and propanol) were identified and quantified in the bacterial headspace. PCA was applied on a subset of these data selected from the latter part of the log phases of the bacterial growth curve before the stationary growth phase. As can be seen in Figure 5.17, the PCA plot shows five clusters for the six monitored cultures, in the way that is usually used for PCA visualisation and relatively common in the literature [21, 217, 219]. The single cultures R (red spots) and Ec (grey spots) are clearly separated in the direction of propanol and acetic acid for Ec and in the direction of acetaldehyde, acetoin and ethanol for R. Propanol was, on average, 25 times higher in Ec, compared to the other two monocultures F and R. Thus, propanol can be considered as a marker indicating the presence of Ec in these systems. Acetoin (3-hydroxy butanone) is produced in largest concentration by R and was also detected in the headspace of F in lower concentration, but not in the headspace of Ec. Thus acetoin in the headspace indicates the presence of R in these experiments. The single population F (green spots) and the binary mixture FEc (green spots) overlap. This is caused by the concurrent growth of these two species in one medium; F always overgrows its Ec partner. Thus, the binary mixture FEc has identical headspace composition with the single F sample; actually FEc is not a binary mixture. The RF population is located between the single F and R populations. The REc binary system is located in the direction of acetone and ammonia. PCA is a certainly a very nice tool for visualizing large data tables, but in this experiment, the clear clustering of each sample is a result of the deliberate choice of data from the latter part of the log phases of the bacterial growth curve.

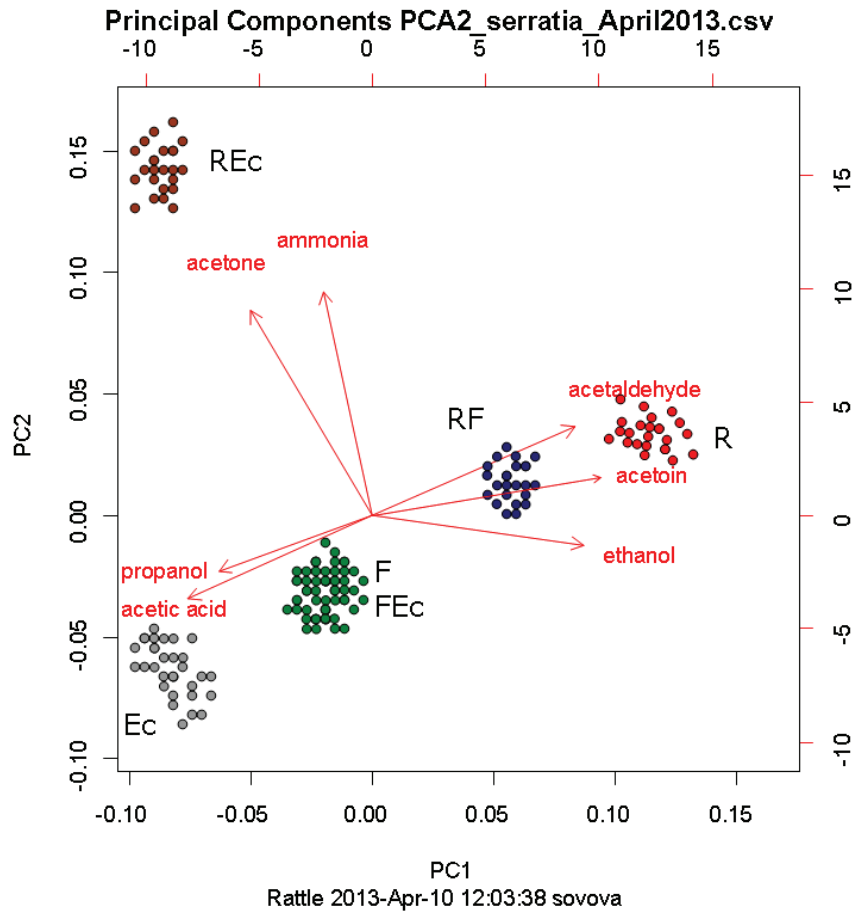


Figure 5.17 PCA analysis of 3 different bacterial species and their binary mixtures. The red arrows indicate the directions of increasing concentrations of variables: acetone, ammonia, acetoin, acetaldehyde, ethanol, propanol and acetic acid. The F colony and FEc binary mixture are located near the middle of the arrows. This means that these two colonies have rather average values of variables concentration in contrast to the other samples. The population of Ec is characterized by a higher concentration of acetic acid and propanol, R colony is dominated by acetoin, acetaldehyde and ethanol. RF goes in the direction which is close to the R colony. The binary system of REc (with the significant reduction of propanol level) is then characterized by acetone and ammonia.

However such a representation that is useful to visualise the clustering of the data does not reveal any time variations in the VOCs. Thus, it was proposed to use a new unorthodox approach and simply to plot the values of the principal components as a function of time. Such plots for the acquired data (Figure 5.18) of the two most important principal components during a 24 hour experiment reveal interesting time profiles that indicate the phases of bacterial growth: the increase of concentrations during the logarithmic phase, maxima specific for the stationary phase of each bacterial strain and finally reduction during the death phase.

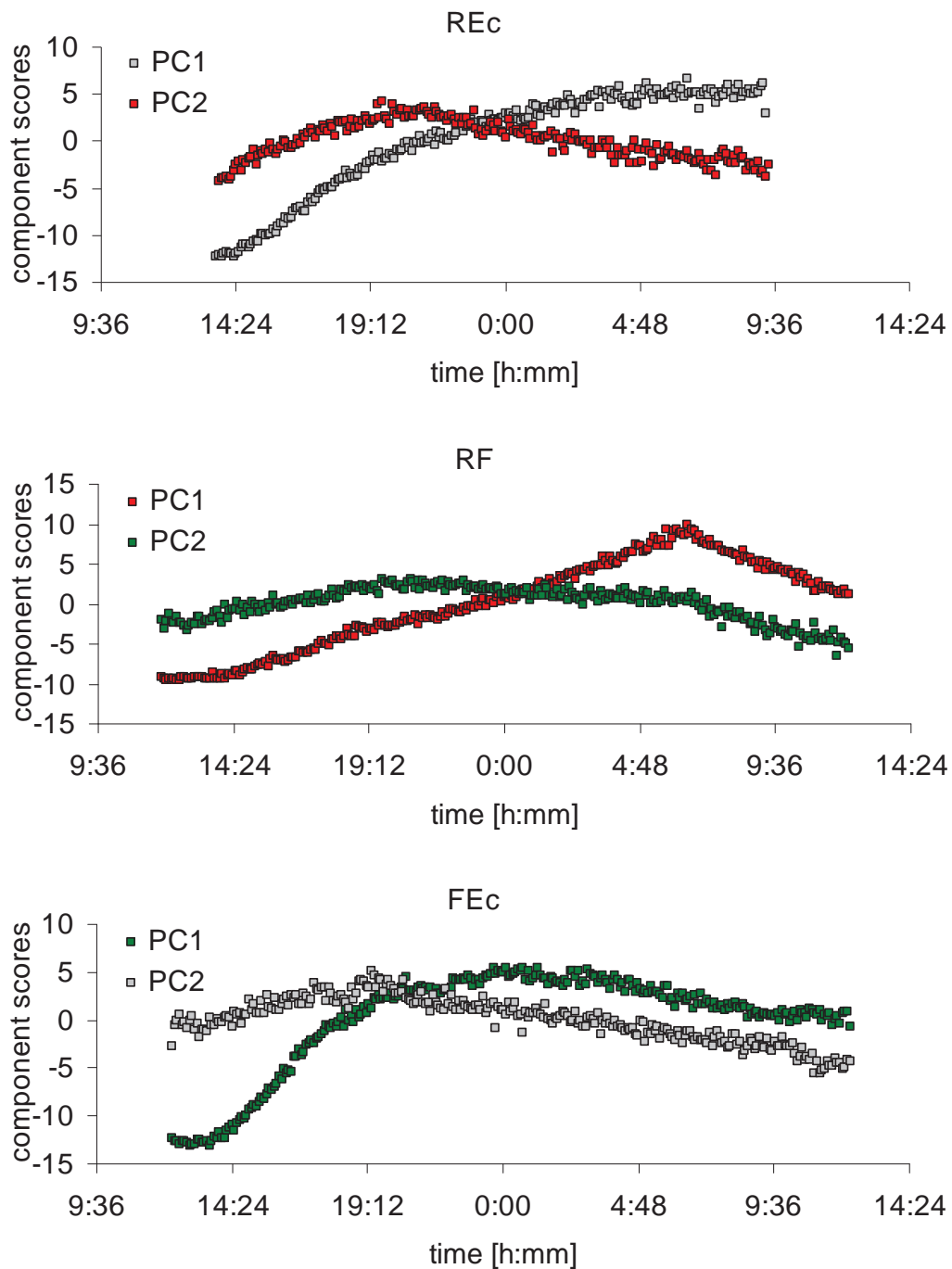


Figure 5.18 Time variation of principal components during the course of cultivation obtained in binary mixtures in real time indicated on the *x* axis. The PCs represent the ion signal of the main variables.

Conclusions

SIFT-MS analyses have been successfully used for non-destructive and quantitative monitoring of the population dynamics of bacterial cultures in real time. Another motivation for this research was that the identification of bacteria based on the composition of VOCs released by their metabolism can be used also to diagnose and monitor the occurrence and progression of bacterial infections. The theme of bacterial fingerprinting is currently at the forefront of research interest in mass spectrometry; however, most of the approaches require isolation and cultivation of bacteria before the ionisation, which is usually destructive. SIFT-MS can potentially be used to screen groups of patients at risk for early signs of infection and to choose optimal therapy for its eradication. Thus, such methodology would be not only applied to the research in the field of population dynamics in fundamental ecology and biodiversity, but also in medicine.

5.5 Phytogetic volatile compounds

As was discussed in Section 4.2, plants emit volatile substances with different odours in order to attract their pollinators or to defend themselves against herbivores. But this is not the only reason to study these emissions from plants. The study described in the published article in Appendix F was related to the possibility of using plants to clean contaminated environment - **phytoremediation**.

Phytoremediation is a relatively new and promising technology. It represents a set of methods that uses plants with associated soil microorganisms to remove toxic substances from the environment or to prevent their further spread [221]. Currently, phytoremediation is used to eliminate many classes of contaminants including petroleum hydrocarbons [222], chlorinated solvents, pesticides, explosives [223-226], heavy metals [227-230] and radionuclides. Now, new sources of contamination such as various pharmaceuticals, perfumes, detergents and flame retardants are also being considered. Plants have developed many mechanisms during their evolution to remove the contamination of soil by inorganic and organic compounds completely naturally. They can be used in highly contaminated areas as well as in the slightly contaminated areas or as a further treatment after the use of other physicochemical methods. The phytoremediation technology can be also considered for the prevention of wind or water erosion and landfill recultivation [231].

Such plant activity (phytoremediation) includes degradation, adsorption, accumulation and **phytovolatilization** of compounds or promoting the activity of soil micro flora in the rhizosphere. This was demonstrated, for example, in the research on poplar trees, where the process of phytovolatilization is an effective mechanism in remediation of methyl tertiary butyl ether, MTBE [232]. However, the potential of microbial degradation of MTBE in the rhizosphere is an additional relevant step in the entire remediation process [233]. Note that the rhizosphere has a very close relationship with the root system of plants. It is a key resource for the storage of organic and mineral substances, which are collectively known as the root exudates. They promote the growth of soil micro flora and affect the composition of the soil surrounding the plants. They represent a diverse group of compounds including sugars, amino acids, organic acids, fatty acids and enzymes. The first mention of plant root exudates appeared in the early 20th century [234-236]. Over time, however, the methodology used to investigate this has improved and the individual components can now be identified [237-240]. The diversity of these compounds found in root exudates is discussed in many publications [241, 242].

Phytoremediation is a passive method of decontamination based on the natural ability of vegetation to use nutrients that are transported from the soil and water through the root system. It is faster than natural attenuation. It is an *in situ* method; the decontamination can be performed at the site of the pollution; the soil stays in place and the use of heavy machinery is not necessary. The method is not expensive and it is effectively powered by solar energy. Application of plants in contaminated areas does not harm the surroundings; it has an esthetical benefit, and thus is highly acceptable to the public. The applicability of phytoremediation techniques is limited by the low tolerance of plants; each plant is not able to tolerate high concentrations of some contaminants. Also, the transport of contaminants from the roots to the parts of the plants above ground is sometimes not efficient. Plants that are suitable for remediation are often of small size. The optimal plant used for phytoremediation must have characteristics including resistance to stressful environmental conditions; tolerance to the climate of contaminated areas, rapid growth, large amount of biomass and high absorption capacity for contaminants - to be a hyper-accumulator [243]. Thus, the interest is currently focused on genetic engineering that allows translocation and transfer of any of these genes into candidate plants for improved phytoremediation traits [244]. The contaminated plant waste must be further treated, either by controlled

incineration or composting. Phytoremediation is a long process that is slower than conventional physical-chemical methods [245].

The present study was mainly focused on **phytovolatilization**, the process where plants take up contaminants which are water soluble and release them into the atmosphere in the same way as they transpire water [246]. As mentioned earlier, this project began with the study of volatiles naturally released by plants during their development or as a defence against predators (Appendix A). The phytovolatilization project is concerned with the conversion of inorganic form of selenium into volatile organic forms (e.g. dimethylselenide) by plants.

5.5.1 Phytovolatilization of selenium

Objectives

The aim of this study was to develop a method for the real time quantification of volatile forms of selenium (Se) which are formed during the process of phytovolatilization (Figure 5.19). Some plant species are known to be Se accumulators; they are growing on seleniferous soils and are thus tolerant to high concentrations of Se; on the other hand most plants are Se non-accumulators [247].

It has been shown previously that Se protects plants from herbivores [248-251]. The protection is based on the toxicity of selenium. Selenium is an essential nutrient in physiology, but becomes toxic at elevated concentrations due to its chemical similarity to sulphur. Se replaces sulphur in proteins and some other compounds important to all living organisms. It has become an element of global environmental and health concern because of its toxicity to organisms and the extensive use in industrial activities. Removal of Se-containing toxins from contaminated water and soil using physical, chemical, and engineering techniques is quite complicated and expensive [252], but it can effectively be achieved by phytoremediation techniques that include the already mentioned phytovolatilization [230, 253]. The main forms of Se in soils or water are inorganic water soluble selenate (SeO_4^{2-}) or selenite (SeO_3^{2-}) ions. The ions are assimilated using sulphur transporters and enzymes and transformed into volatile forms, including dimethylselenide, $(\text{CH}_3)_2\text{Se}$, and dimethyldiselenide, $(\text{CH}_3)_2\text{Se}_2$ [254]. Much of the research in this area is not only related to bioremediation of selenium polluted soil, but also to the importance of plants as a nutritional source of Se in the human diet

[255]. Note that, for example, in the Czech Republic there is a recognised deficiency of selenium in agricultural produce.

The Se accumulator plants *Brassica juncea* have been used in many studies of selenium speciation [256, 257]. In the present study, the maize plant (*Zea mays*) cultivated with an enhanced supply of Se nutrients was used. This plant was chosen due to its high water uptake per day. Our exploratory experiments with *Brassica juncea* were not successful. Finally the use of *Capsidum annuum L.* (pepper) was also tested. Thus, the SIFT-MS experiments involved an ion chemistry study of $(\text{CH}_3)_2\text{Se}$ and other possible volatile forms of selenium (H_2Se , $(\text{CH}_3)_2\text{Se}_2$ and CH_4Se).

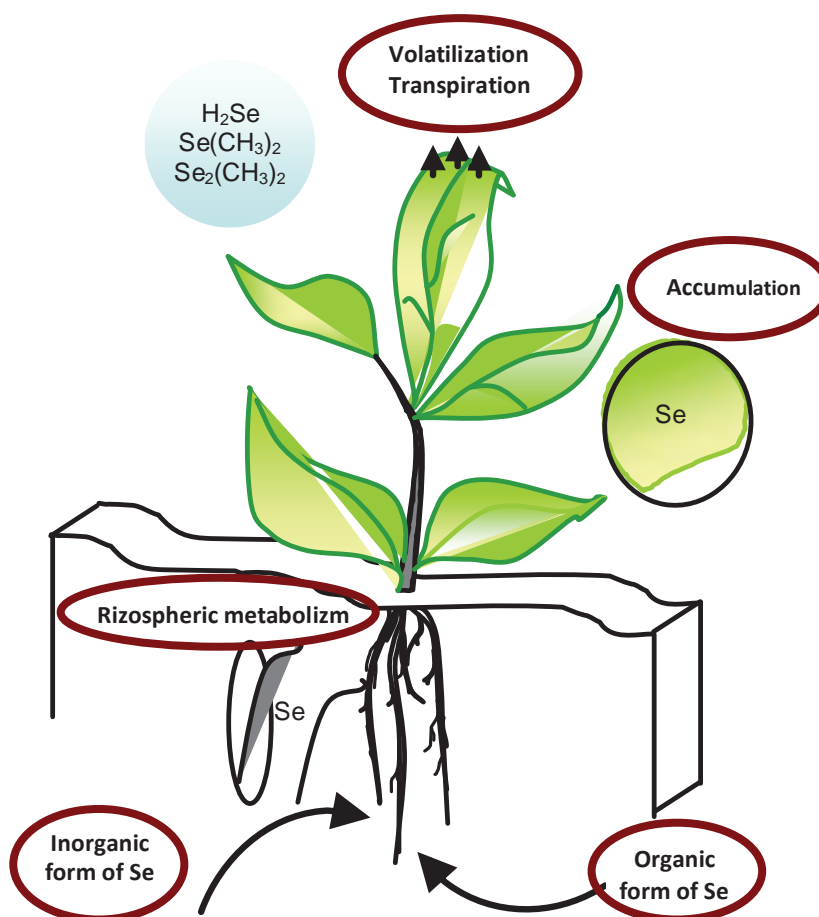


Figure 5.19 The scheme of selenium (Se) uptake, transport, accumulation in the root and to the shoots and transpiration of volatile forms.

Materials and methods

The ion chemistry study of $(\text{CH}_3)_2\text{Se}$

The vapour of dimethyl selenide (purchased from Sigma Aldrich) was introduced into the SIFT-MS instrument at a variable flow rate controlled by a needle valve and monitored by a flow-meter (Voegtlin, Aesch, Switzerland). The primary product branching ratios of the reaction of H_3O^+ , NO^+ and $\text{O}_2^{+\bullet}$ were determined and the reaction rate constants required for the absolute quantification of this compound in air were estimated by the procedure reported in Section 5.1 and so need not be discussed in detail here. The rate constants and product ion branching ratios for the other compounds involved in this study (H_2Se , CH_3SeH , $(\text{CH}_3)_2\text{Se}_2$) were obtained on the basis of the thermochemical calculations of exothermicities of possible reaction channels [258] by calculations of the collisional rate constants for the exothermic proton transfer reactions of H_3O^+ (k_c) according to Su and Chesnavich [177] using the dipole moments and polarisabilities of these molecules.

Zea mays

The seeds of *Zea mays* were cultivated with an enhanced supply of Se nutrients in Petri dishes filled up with cotton-wool soaked with 5 mL of the different solutions of inorganic forms of Se used as a germinating medium. Five different concentrations (0.2, 2.0, 10.0, 20.0 and 200 μM in aqueous solution) of selenium salts (sodium selenate, A, and sodium selenite, B) were thus prepared. After two days, the maize seedlings (Figure 5.20) grew to a length of about 3 cm and the characteristic garlic odour of $(\text{CH}_3)_2\text{Se}$ became noticeable. The headspace above the covered cultivating Petri dishes was analyzed using SIFT-MS in real time. $(\text{CH}_3)_2\text{Se}$ was monitored in the multi ion monitoring (MIM) mode and the absolute concentration was obtained. In order to identify other possible Se volatile forms, full scan mass spectra were acquired.



Figure 5.20 The seedlings of *Zea mays* inside the Petri dishes.

Capsidum annuum L.

Three plants of *Capsidum annuum L.* (pepper) of 20 cm in size were grown for 10 days in 1mM of sodium selenite salt hydroponic medium in an enclosed apparatus. The headspace was monitored in the MIM mode and also in the full scan mode. After 10 days the plants were harvested and the content of selenium was determined in digested samples by atomic absorption spectroscopy, AAS with the hydride generation technique (HGAAS). The measurement was carried out at the Czech University of Life Sciences Prague in cooperation with Ing. Daniela Miholová from the Faculty of Agrobiological Sciences, Food and Natural Resources. The sample preparation was time consuming by following procedure:

Fresh plant samples were finely ground, dried by the lyophilisation in LYOVAG GT 2 (Leybold-Heraeus, Germany), and then digested in an acid solution using microwave heating by MWS instrument (Berghof Products + Instruments, Germany). 150-200 mg of the sample was then weighted into the Teflon digestion vessel DAP-60S and 2 mL of nitric acid 65 %, p.a. ISO (Merck) and 3 mL H₂O₂ 30 %, Trace Select (Fluka) were added. The mixture was shaken carefully and after half-an-hour the vessel was closed and heated in the microwave oven. The samples proceeded for 1 hour in the temperature range 100-190°C. The digest obtained was transferred into a 50 mL silica beaker and evaporated to wet residue, then diluted with a minimum amount of 10 % hydrochloric acid prepared from HCl 37 %, p.a. + (Analytika, CR) and deionised water

(Barnstead). Formic acid 98 %, p.a. (Sigma-Aldrich) in a volume of 1 mL was added for the reduction of nitrogen oxides from the reaction mixture. To reduce all selenium compounds in the digest to Se^{IV} , 5 mL of hydrochloric acid diluted with deionised water 1:1 (V/V) was added and the solution was heated at 90°C for half-an-hour. Then digests were transferred to probes and adjusted with 10 % HCl to 12 mL.

The concentration of selenium in the digests of plants were measured by the HGAAS technique using a Varian AA 280Z (Varian, Australia) with a vapour generation accessory VGA-76 and sample preparation system Varian SPS3. Standard solutions ASTASOL (Analytika, CR) of selenium were used in the preparation of a calibration curve for the measurement. Because of the high contents of selenium in the samples, it was necessary to dilute the digests with 10 % HCl before the measurements. Samples of the plants were analyzed in two replicates.

The quality of the analytical data was assessed by simultaneous analysis of two certified materials BCR 402 (White clover) and IAEA 336 (Lichen) (5 % of all the samples). All the data found for CRMs were in the confidence intervals given for the certified content of selenium in these materials, which are 6.45 – 6.95 mg.kg^{-1} for BCR402 and 0.18 – 0.26 mg.kg^{-1} for IAEA 336. The background concentration of Se present in the trace element laboratory was monitored by analysis of 30 % blanks prepared under the same conditions and experimental data were corrected by the mean concentration of analyte in the blanks, and compared with the detection limit (mean +/- 3SD of blanks) which was 0.08 ng.mL^{-1} .

Results and Discussion

Real-time quantification of traces of biogenic volatile selenium compounds in humid air by selected ion flow tube mass spectrometry (see Appendix F)

The ion chemistry study of $(\text{CH}_3)_2\text{Se}$

The ion-molecule reaction of $(\text{CH}_3)_2\text{Se}$ with H_3O^+ produced protonated product ions at m/z 107-109-111-113, these several observed masses being due to the isotopic composition of Se: ^{76}Se (9.02 %), ^{78}Se (23.52 %), ^{80}Se (49.82 %) and ^{82}Se (9.19 %). Note that the isotopic composition is very useful when a complex mixture is analysed, it helps to distinguish overlaps in the spectra.

Table 5.4 Optimized kinetic library entries in the format used in SIFT-MS software

DMSe (H_3O^+)	DMSe 107,109only (H_3O^+)	DMSe (NO^+)	DMSe (O_2^+)
4 precursors	4 precursors	3 precursors	1 precursor
19 2.6e-9 1.0	19 2.6e-9 1.0	30 2.0e-9 1.0	32 2.3e-9 1.0
37 2.0e-9 1.0	37 2.0e-9 1.0	48 1.8e-9 1.0	3 products
55 1.8e-9 1.0	55 1.8e-9 1.0	66 1.7e-9 1.0	106 1.075
73 1.6e-9 1.0	73 1.6e-9 1.0	2 products	108 1.307
3 products	2 products	108 1.307	110 2.0
107 1.075	107 3.0	110 2.0	
109 1.307	109 3.0		
111 2.0			

NO^+ reacts with $(\text{CH}_3)_2\text{Se}$ via charge transfer without any fragmentation producing $(\text{CH}_3)_2\text{Se}^{+\bullet}$ ions at m/z 106, 108, 110 and 112. $\text{O}_2^{+\bullet}$ precursor ions were observed to react with $(\text{CH}_3)_2\text{Se}$ via charge transfer largely producing again $(\text{CH}_3)_2\text{Se}^{+\bullet}$ ions at m/z 106, 108, 110 and 112. The SIFT-MS spectra of a $(\text{CH}_3)_2\text{Se}$ standard are shown in Figure 5.21.

The calculated values of the collisional rate constant (k_c) for the H_3O^+ reaction and the experimentally derived rate constants (k) for the NO^+ and $\text{O}_2^{+\bullet}$ reactions are summarized in Table 5.4 in the format of kinetics library entries together with f_p coefficients. Note the product ions at m/z 107-109-111 (with H_3O^+ precursor) are used in the analyses after multiplying the precursor and product ion count rates by the f_p coefficients. The same was done in case of NO^+ and O_2^+ precursor ions. The ion chemistry of H_2Se , CH_3SeH , $(\text{CH}_3)_2\text{Se}_2$ as the other possible forms of volatile organic selenium is described in detailed in Appendix F.

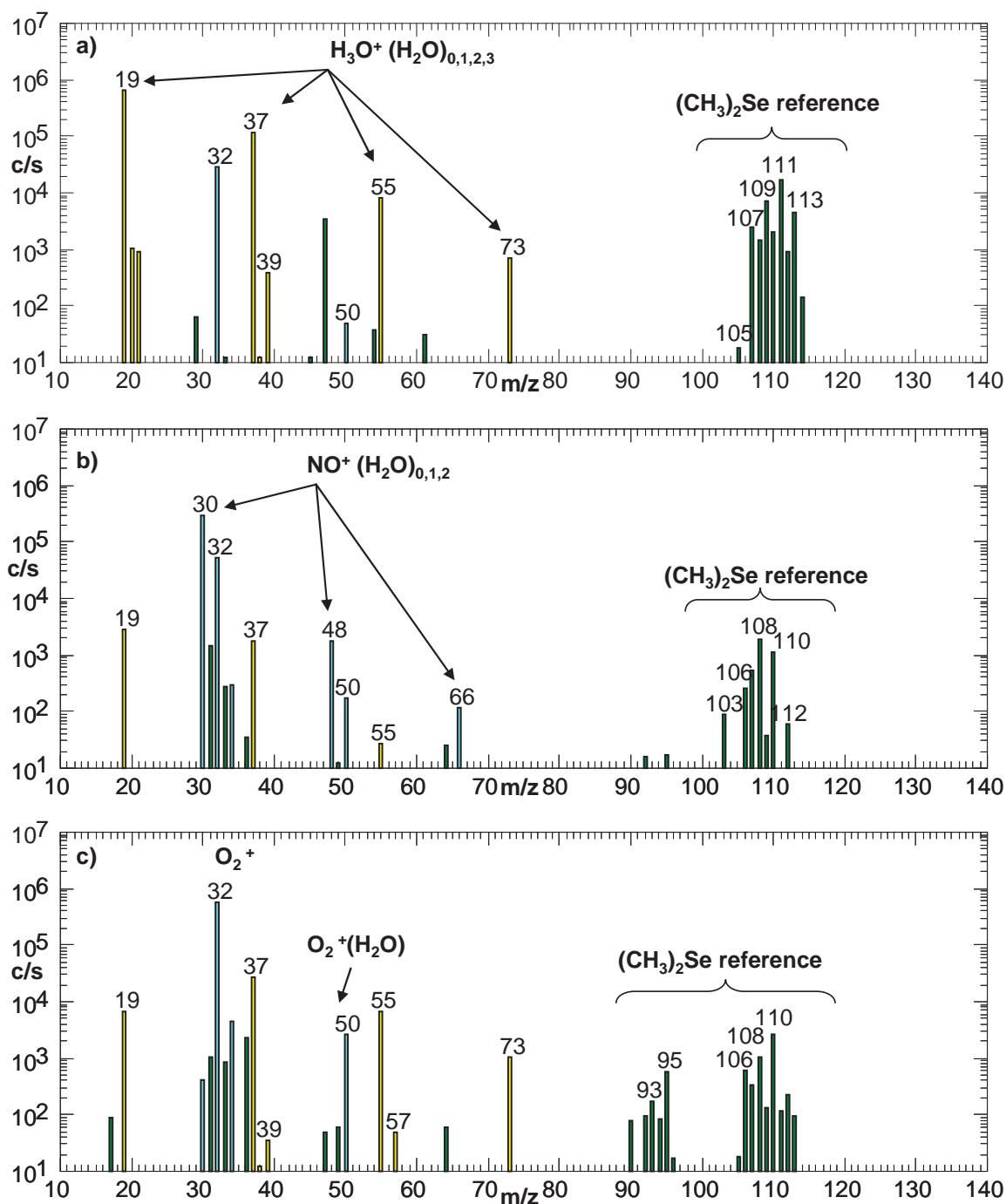


Figure 5.21 The three SIFT-MS spectra obtained as the headspace above dimethyl selenide solution is sampled. The arrows indicate the ions resulting from the reactions of the a) H_3O^+ precursor ions, b) NO^+ precursor ions and c) O_2^+ precursor ions.

Vapours released from seedlings of *Zea mays* enriched with Se salts

$(\text{CH}_3)_2\text{Se}$ was quantified in real time using the MIM mode of SIFT-MS analysis. The kinetics library entries used for quantification were constructed to calculate the absolute concentration of $(\text{CH}_3)_2\text{Se}$ from the ion signals at m/z 107 and 109 multiplied by a coefficient of 3 (corresponding approximately to the contribution of isotopologues

$1/(0.0902 + 0.2352))$ to avoid contribution of the overlapping signal of ethanol at m/z 83. Sample results observed for $(\text{CH}_3)_2\text{Se}$ above cultivations with two different concentrations of two different Se salts are shown in Figure 5.22. This experiment indicated that SIFT-MS quantification of $(\text{CH}_3)_2\text{Se}$ is possible even at absolute humidity of the headspace air $>7\%$ corresponding to saturated water vapour pressure at temperatures in the range of $40\text{--}42\text{ }^\circ\text{C}$.

The full scan spectra confirmed the presence of dimethyl selenide and hydrogen selenide, H_2Se , but did not indicate the presence of any other two possible volatile Se-compounds (methylselenol, CH_3SeH or dimethyl diselenide $(\text{CH}_3)_2\text{Se}_2$). Note, the identification and also quantification of H_2Se are complicated due to the overlaps with the dihydrate of protonated ethanol at m/z 83. However, the presence of other isotopologues allows its detection. Thus, the apparent isotopologue ratios of H_3Se^+ differ from the expected and have to be corrected by subtracting the contributions from ^{13}C isotopologues of $\text{C}_2\text{H}_5\text{OH}_2^+(\text{H}_2\text{O})_2$. Similarly, the observed isotopic ratios for protonated $(\text{CH}_3)_2\text{Se}$ differ somewhat from the expected values, because of the overlaps of the ^{13}C isotopologues of $(\text{C}_2\text{H}_5\text{OH})_2\text{H}^+\text{H}_2\text{O}$ at m/z 111 (see Figure 5.23).

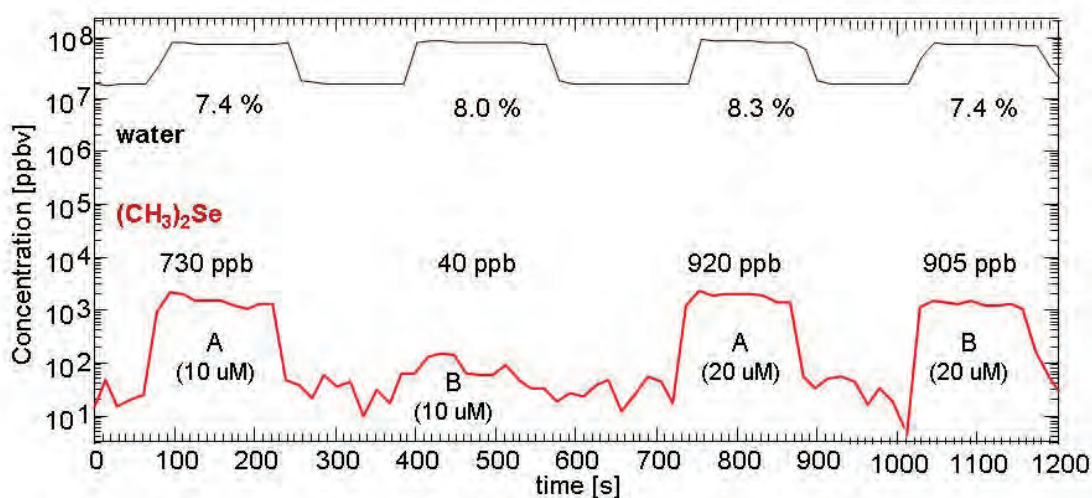


Figure 5.22 Time profile of concentration of $(\text{CH}_3)_2\text{Se}$ obtained using H_3O^+ precursors when the cultivation headspace is sequentially introduced into the SIFT-MS sample inlet from above seeds sprouting in four different media indicated (two different concentrations of sodium selenate, A, and sodium selenite, B).

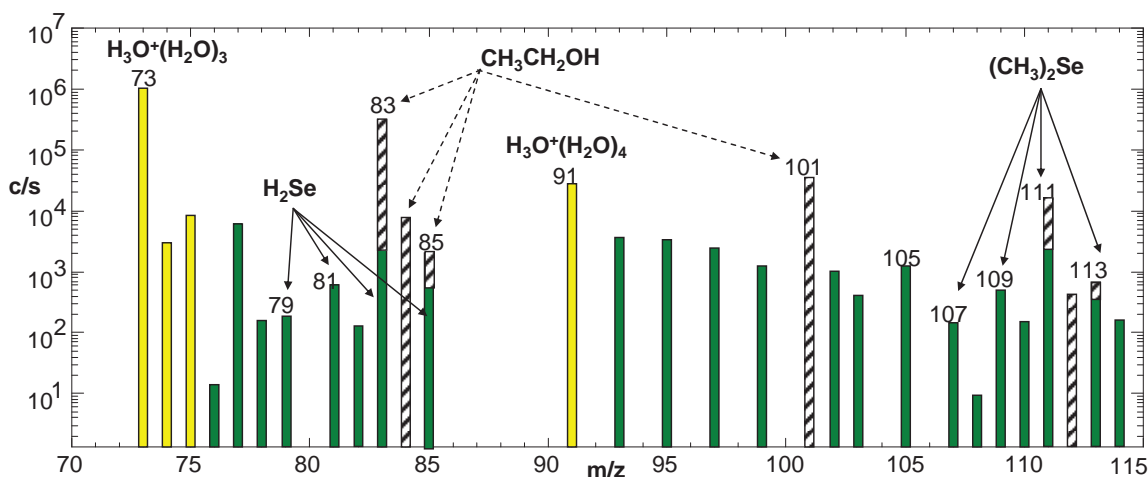


Figure 5.23 SIFT-MS mass spectrum obtained using H_3O^+ precursors while sampling air above maize seedlings cultivated on Se-enriched medium. Note the characteristic product ions of $(\text{CH}_3)_2\text{Se}$ on the m/z 107, 109, 111, 113, and H_2Se in the mass range of m/z 79–85. The contribution of the overlapping ethanol product ions ($\text{C}_2\text{H}_5\text{OH}_2^+(\text{H}_2\text{O})_2$ at m/z 83, ^{13}C isotopologues at m/z 84, ^{18}O at m/z 85, and similarly $(\text{C}_2\text{H}_5\text{OH})_2\text{H}^+\text{H}_2\text{O}$ at m/z 111, 112, and 113) are shown in the spectrum with a hashed pattern.

Vapours released from *Capsidum annuum L.* enriched with Se salts

The headspace of three *Capsidum annuum L.* (pepper) plants was monitored using the MIM mode of SIFT-MS over a period of 10 days. But no volatile forms of Se were observed in the headspace. SIFT-MS is a method of real-time quantification without the need for sample pre-concentration. Thus, parallel SPME/GC/MS qualitative analysis could be carried out. Dimethyl selenide ($(\text{CH}_3)_2\text{Se}$) was identified in the GC-MS data shown in Figure 5.24. The detectable amount of $(\text{CH}_3)_2\text{Se}$ has been observed on the third day and its concentration kept increasing until the eighth day, after which the intensity decreased as the plants were saturated by relatively high amount of inorganic Se in the medium. These plants were also used to analyse the distribution of Se between different parts of their anatomies; the results are given in Table 5.5.

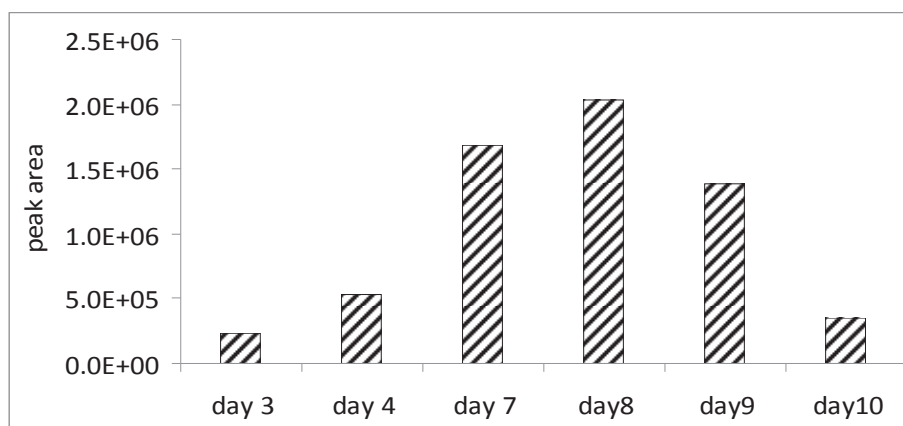


Figure 5.24 Area under the peak of $\text{CH}_3)_2\text{Se}$ expressed in the ion count obtained in SPME/GC-MS analysis of the headspace above *Capsidum annuum L.*

Table 5.5 Se in different parts of the plant

Sample	Mean (mg.kg^{-1} dry weight)	Standard deviation
1 (leafs-lower)	36.75	5.04
2 (stem)	320.6	40.0
3 (leafs-upper)	33.68	1.20
4 (stem)	287.1	37.3
5 (roots)	6568	237

Conclusions

SIFT-MS instrument was used to analyse headspace of *Zea maize* seedlings and *Capsidum annuum* plants cultivated on enriched medium with selenium salts. It has been found that *Capsidum annuum* released small amount of volatile Se (DMSe) that was below the detection limit of SIFT-MS and Se was thus accumulated in the tissues of the plants. The main results is that SIFT-MS is allows **selective** identification and quantification of volatile Se forms such DMSe, H_2Se and DMDS_e.

5.6 Explosives

Objectives

The growing fear of terrorism had led to intensive research all over the world in order to find or develop a reliable, sensitive and accurate method for the early detection of chemical substances that represent a real security threat to society. The group of chemical substances that need to be detected involves explosives, narcotics or biological agents. Special effort has been focused on the detection of trace amounts of explosives and their decomposition products.

The international societies try to join together and fight against this phenomenon. But the solution may come from the science and basic research. The research in Europe suffers from disunity/fragmentation and from a lack of mutual cooperation. This issue has been currently emphasized by the 7th European Community Framework Programme for research and technological development (2007-2013).

In cooperation venture between Explosia a.s in Pardubice (Czech Republic) and the Heyrovský Institute, a research project codename “TANDEM” has been carried out in this field. This project was funded by the Czech Ministry of Trade and Industry. The aim of this research project was to study highly explosives materials and their decomposition products and finally to develop a detection apparatus.

The initial research combined two powerful techniques of Laser Induced Breakdown Spectroscopy, LIBS and Selected Ion Flow tube Mass Spectrometry, SIFT-MS. The combination of these two methods allowed the study and characterization of the products of explosions using microscopic scale laboratory experiments without the need to initiate macroscopic explosions of test charges weighing several grams or more.

The first results obtained were summarized in the diploma thesis (Sovova 2009) and then published in the open literature [259]. This section of this thesis will comment on the more recent results summarized in the publication “Laser Ablation of FOX-7: Proposed Mechanism of Decomposition” (included in Appendix G). Thus, the previously unknown unimolecular decomposition pathway of FOX-7 was investigated. This project finally resulted in the construction of a NQR (nuclear quadrupole resonance) apparatus by Ing. Jiří Kubišta [260].

Methods

The decomposition mechanism of FOX-7 (1,1-diamino-2,2-dinitroethylene), a member of the new family of potentially threatening explosive materials, which has the same molecular stoichiometry as the well-known RDX (1,3,5-trinitro-2-oxo-1,3,5-triazacyclo-hexane) and HMX (1,3,5,7-tetranitro-1,3,5,7-tetraazacyclo-octane) explosives, was studied by LIBS/SIFT-MS. Samples of bulk explosive FOX 7 were prepared in the form of tablets by compressing its powder using a standard press in order to avoid emissions originating from the metal target supporting the sample. The unique experimental set-up is schematically illustrated by the diagram in Figure 5.25.

An ArF excimer laser was used to generate the laser pulses (193 nm, 30 μ s pulse width, 200 mJ). The radiation pulse passed through focusing lenses (15 cm focal length) and interacted with the sample located on the metal target. This experiment was performed in an evacuated ablation cell. The optic fibre delivers the emitted radiation to a UV-VIS spectrometer with an ICCD detector. The ICCD began to collect the spectra 1840 ns after initiation of the plasma. Simultaneously, the gaseous emissions were analyzed using SIFT-MS. The stable gaseous products were introduced via a heated calibrated capillary directly into the SIFT-MS instrument. Ten laser pulses were chosen each with the duration of 10 s allowing monitoring of time profiles of concentrations of the products of combustion using SIFT-MS. The SIFT-MS sampling capillary was placed at a distance of 2 cm from the surface of the sample. Full scan mass spectra were obtained using all three precursor ions in the mass region 10-240 m/z . The MIM mode was used to investigate time profiles of the concentrations of selected molecular species.

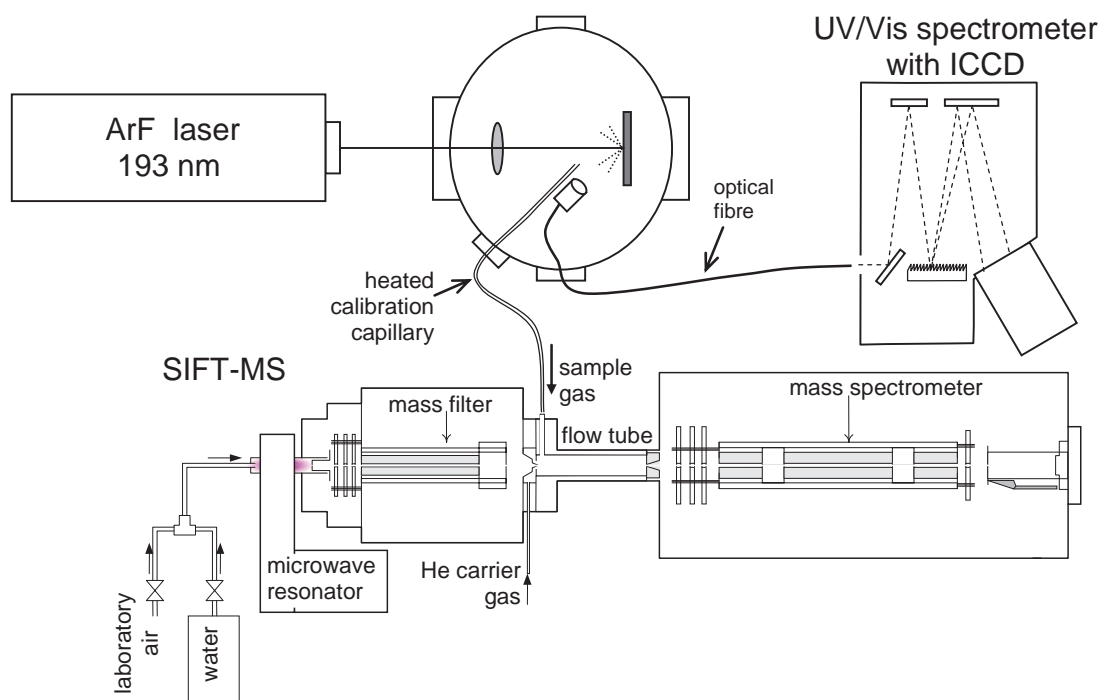


Figure 5.25 Schematic diagram of the LIBS/SIFT-MS experimental apparatus.

Results and discussion

Laser Ablation of FOX-7: Proposed Mechanism of Decomposition (Appendix G)

My contribution to this work encompassed the analysis of SIFT-MS spectra (examples given in Figure 5.26) resulting from the real-time analyses of gases released into the vacuum chamber.

The common combustion stable products namely: NO, NO₂, HCN, HONO, HCHO, CH₃CH₂OH, and C₂H₂ were analysed using SIFT-MS. A reaction scheme for the decomposition of FOX-7 was constructed on the basis of the results and it is presented in the manuscript in Appendix G. This reaction scheme thus helps understanding the details of dissociation processes.

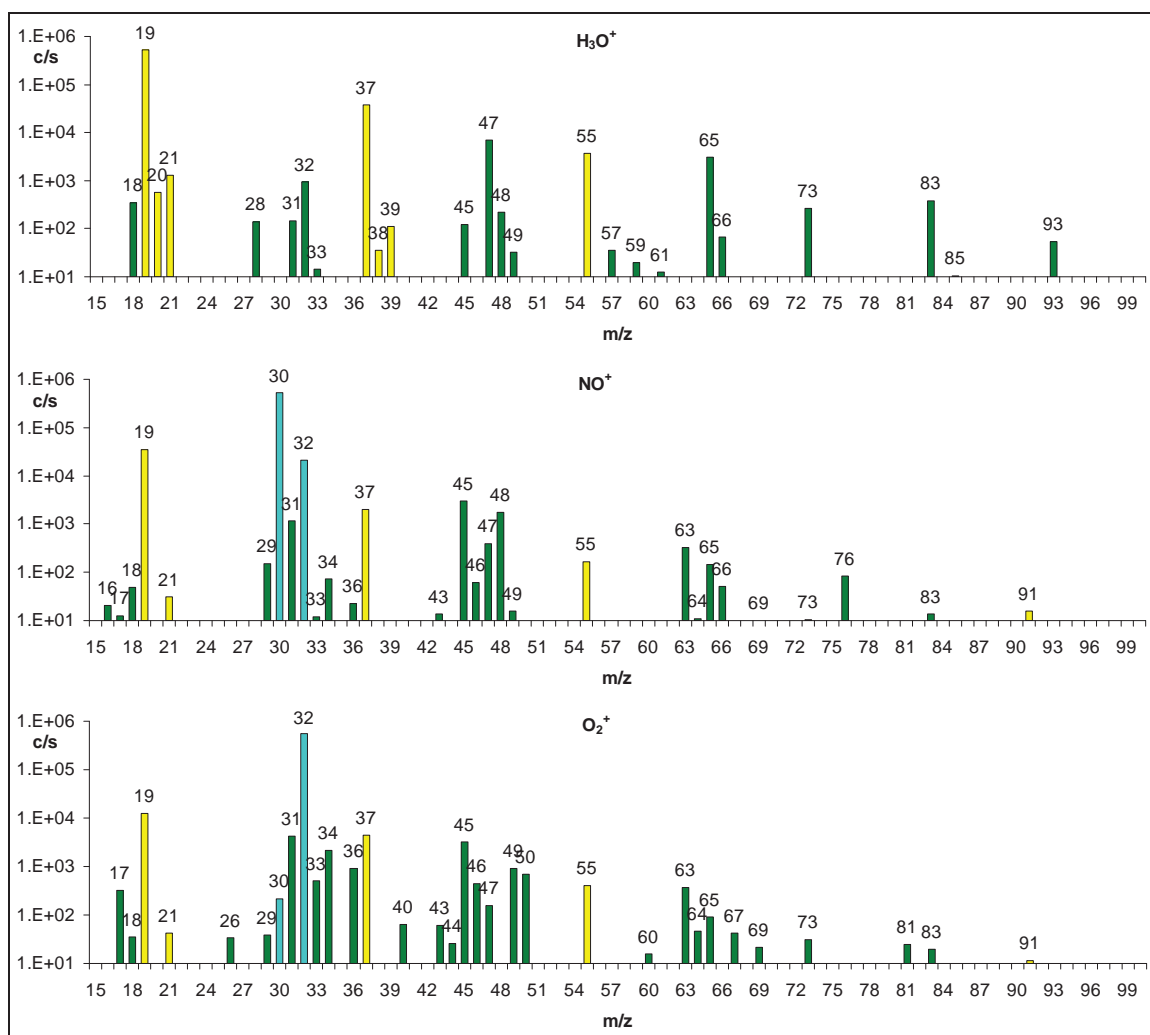


Figure 5.26 SIFT-MS spectra of vapours generated by laser ablation after the reaction with all the three precursor ions H₃O⁺, NO⁺ and O₂⁺.

Conclusions

An understanding of the decomposition mechanism is an important step in the evaluation of the properties of a new type of explosive, FOX 7. The combination of LIBS and SIFT-MS represents a powerful tool for the analysis of explosive decomposition products. The relevance of the topic is obvious; the published paper has already been cited four times according to the Web of Science (without self-citations). These results were referred to by Gottfried *et al.* [261, 262], who used spectroscopic techniques of laser induced breakdown spectroscopy (LIBS) to study explosive residues, and by Cai *et al.* [263] who have very recently described the effect of an ordered space structure on explosive properties of FOX-7 nanocrystals.

6 Summary and concluding remarks

This thesis summarises my research in a variety of subjects related to SIFT-MS from fundamental ion chemistry, via development of analytical methods to their use in interdisciplinary areas of research including microbiology, plant physiology, explosives and medical diagnostics. In the population dynamics study I have also touched upon advanced statistical analyses of data obtained using SIFT-MS.

There are several outcomes of my work:

1. I have obtained kinetic data for ion-molecule reaction of group of esters and hexanol isomers. The rate constants and product ion branching ratio were published in peer reviewed journals for almost 40 reactions (Appendices A and B). The methodology for optimization of kinetics library entries avoiding cross sensitivity was formulated and in detail described in Appendix A.
2. A new method for selective monitoring of volatile selenium forms such as dimethylselenide, dimethyldiselenide, hydrogen selenide and methyl selenol was described (Appendix F).
3. The ion chemistry of pentane and methyl thiocyanate relevant for the real time monitoring of these two biomarkers of inflammatory bowel disease and cystic fibrosis in human breath was investigated (Appendices C and D).
4. Results of a pilot study of population dynamics of three different bacterial species that has been carried out non-destructively and quantitatively in real time (Appendix E).
5. A reaction scheme for the decomposition of FOX-7 has been proposed on the basis of SIFT-MS analyses of fumes (Appendix G).

These results will hopefully be useful for other researchers working in the individual areas of science where SIFT-MS analyses of volatile compounds helps to understand biological or chemical processes.

References

- [1] K. Goodner, R. Rouseff, Practical analysis of flavor and fragrance materials, Wiley-Blackwell, 2011.
- [2] A. Herrmann, The chemistry and biology of volatiles, Wiley Online Library, 2010.
- [3] A. Amann, D. Smith, Volatile Biomarkers: Non-Invasive Diagnosis in Physiology and Medicine in, Elsevier, Oxford UK, 2013.
- [4] K. Demeestere, J. Dewulf, B. De Witte, H. Van Langenhove, Sample preparation for the analysis of volatile organic compounds in air and water matrices, *J. Chromatogr. A*, 1153 (2007) 130-144.
- [5] J. Koziel, M.Y. Jia, J. Pawliszyn, Air sampling with porous solid-phase microextraction fibers, *Anal. Chem.*, 72 (2000) 5178-5186.
- [6] V. Ruzsanyi, J.I. Baumbach, S. Sielemann, P. Litterst, M. Westhoff, L. Freitag, Detection of human metabolites using multi-capillary columns coupled to ion mobility spectrometers, *J. Chromatogr. A*, 1084 (2005) 145-151.
- [7] M. Junger, W. Vautz, M. Kuhns, L. Hofmann, S. Ulbricht, J.I. Baumbach, M. Quintel, T. Perl, Ion mobility spectrometry for microbial volatile organic compounds: a new identification tool for human pathogenic bacteria, *Appl. Microbiol. Biotechnol.*, 93 (2012) 2603-2614.
- [8] H.H. Mantsch, D. Naumann, Terahertz spectroscopy: The renaissance of far infrared spectroscopy, *Journal of Molecular Structure*, 964 (2010) 1-4.
- [9] J. Griffiths, A brief history of mass spectrometry, *Anal. Chem.*, 80 (2008) 5678-5683.
- [10] K.D. Bartle, P. Myers, History of gas chromatography, *TrAC Trends in Analytical Chemistry*, 21 (2002) 547-557.
- [11] M. Ligor, T. Ligor, A. Bajtarevic, C. Ager, M. Pienz, M. Klieber, H. Denz, M. Fiegl, W. Hilbe, W. Weiss, P. Lukas, H. Jamnig, M. Hackl, B. Buszewski, W. Miekisch, J. Schubert, A. Amann, Determination of volatile organic compounds in exhaled breath of patients with lung cancer using solid phase microextraction and gas chromatography mass spectrometry, *Clinical Chemistry and Laboratory Medicine*, 47 (2009) 550-560.
- [12] E. Matisova, M. Dömötörová, Fast gas chromatography and its use in trace analysis, *J. Chromatogr. A*, 1000 (2003) 199-221.
- [13] M.S. Klee, L.M. Blumberg, Theoretical and practical aspects of fast gas chromatography and method translation, *Journal of chromatographic science*, 40 (2002) 234-247.
- [14] W. Filipiak, A. Sponring, A. Filipiak, C. Ager, J. Schubert, W. Miekisch, A. Amann, J. Troppmair, TD-GC-MS analysis of volatile metabolites of human lung cancer and normal cells in vitro, *Cancer Epidemiology Biomarkers & Prevention*, 19 (2010) 182-195.
- [15] V.T. Virkki, R.A. Ketola, M. Ojala, T. Kotiaho, V. Komppa, A. Grove, S. Facchetti, On-site environmental analysis by membrane inlet mass spectrometry, *Anal. Chem.*, 67 (1995) 1421-1425.
- [16] A. Taylor, R. Linforth, B. Harvey, A. Blake, Atmospheric pressure chemical ionisation mass spectrometry for in vivo analysis of volatile flavour release, *Food Chemistry*, 71 (2000) 327-338.
- [17] F.M. Benoit, W. Davidson, A. Lovett, S. Nacson, A. Ngo, Breath analysis by atmospheric pressure ionization mass spectrometry, *Anal. Chem.*, 55 (1983) 805-807.

- [18] B. Thomson, W. Davidson, A. Lovett, Applications of a versatile technique for trace analysis: atmospheric pressure negative chemical ionization, *Environ. Health Perspect.*, 36 (1980) 77.
- [19] I. Délérís, A. Saint - Eve, E. Sémon, H. Guillemin, E. Guichard, I. Souchon, J.L. Le Quéré, Comparison of direct mass spectrometry methods for the on - line analysis of volatile compounds in foods, *J. Mass Spectrom.*, 48 (2013) 594-607.
- [20] L. Zhu, G. Gamez, H.W. Chen, H.X. Huang, K. Chingin, R. Zenobi, Real - time, on - line monitoring of organic chemical reactions using extractive electrospray ionization tandem mass spectrometry, *Rapid Commun. Mass Spectrom.*, 22 (2008) 2993-2998.
- [21] J.J. Zhu, H.D. Bean, Y.M. Kuo, J.E. Hill, Fast Detection of Volatile Organic Compounds from Bacterial Cultures by Secondary Electrospray Ionization-Mass Spectrometry, *Journal of Clinical Microbiology*, 48 (2010) 4426-4431.
- [22] A. Amann, The State of Breath Analysis: Achievements and Challenges, Consequences for Applications, in: CONFERENCE SERIES, 2013, pp. 20.
- [23] E. Ferguson, F. Fehsenfeld, A. Schmeltekopf, Ion-molecule reaction rates measured in a discharge afterglow, *Advances in Chemistry Series*, (1969) 83-91.
- [24] W. Lindinger, A. Hansel, A. Jordan, On-line monitoring of volatile organic compounds at pptv levels by means of proton-transfer-reaction mass spectrometry (PTR-MS) medical applications, food control and environmental research, *Int. J. Mass Spectrom. Ion Process.*, 173 (1998) 191-241.
- [25] W. Lindinger, A. Jordan, Proton-transfer-reaction mass spectrometry (PTR-MS): on-line monitoring of volatile organic compounds at pptv levels, *Chem. Soc. Rev.*, 27 (1998) 347-375.
- [26] A. Hansel, A. Jordan, R. Holzinger, P. Prazeller, W. Vogel, W. Lindinger, Proton transfer reaction mass spectrometry: on-line trace gas analysis at the ppb level, *Int. J. Mass Spectrom. Ion Process.*, 149 (1995) 609-619.
- [27] L. Cappellin, E. Aprea, P.M. GRANITTO, A. Romano, F. Gasperi, F. Biasioli, Chemometrics and direct injection analysis of volatile compounds by PTR-TOF-MS: a tool for metabolomic investigations, in: Pulkrabova, J.; Tomaniova, M.; Nielsen, M.; Hajslova, J.(editors), *Ist European workshop on ambient mass spectrometry and related mass spectrometry-based techniques in food/natural products control: safety, authenticity, forensics, metabolomics: June 18-20, 2012, Prague, Czech Republic, CZ, 2012.*
- [28] A. Jordan, S. Haidacher, G. Hanel, E. Hartungen, J. Herbig, L. Märk, R. Schotchkowsky, H. Seehauser, P. Sulzer, T. Märk, An online ultra-high sensitivity Proton-transfer-reaction mass-spectrometer combined with switchable reagent ion capability (PTR+ SRI- MS), *Int. J. Mass Spectrom.*, 286 (2009) 32-38.
- [29] A. Edtbauer, E. Hartungen, A. Jordan, P. Sulzer, S. Jürschik, S. Feil, G. Hanel, S. Jaksch, L. Märk, T.D. Märk, From Proton-Transfer-Reaction Mass Spectrometry (PTR-MS) to Universal Trace Gas Analysis with Selective-Reagent-Ionization Mass Spectrometry (SRI-MS) in Kr+ mode, in: CONFERENCE SERIES, 2013, pp. 76.
- [30] W. Lindinger, A. Hansel, A. Jordan, On-line monitoring of volatile organic compounds at pptv levels by means of proton-transfer-reaction mass spectrometry (PTR-MS) - Medical applications, food control and environmental research, *Int. J. Mass Spectrom.*, 173 (1998) 191-241.
- [31] J. Herbig, M. Muller, S. Schallhart, T. Titzmann, M. Graus, A. Hansel, On-line breath analysis with PTR-TOF, *J. Breath Res.*, 3 (2009).
- [32] P. Španěl, D. Smith, Progress in SIFT-MS: Breath analysis and other applications, *Mass Spectrometry Reviews*, 30 (2011) 236-267.

- [33] N. Adams, D. Smith, The selected ion flow tube (SIFT); a technique for studying ion-neutral reactions, *Int. J. Mass Spectrom. Ion Phys.*, 21 (1976) 349-359.
- [34] C.H. DePuy, V.M. Bierbaum, Gas-phase reactions of organic anions as studied by the flowing afterglow technique, *Accounts Chem. Res.*, 14 (1981) 146-153.
- [35] D. Smith, N. Adams, Recent advances in flow tubes: Measurement of ion-molecule rate coefficients and product distribution, *Gas phase ion chemistry*, 1 (1979) 1-44.
- [36] D. Smith, N. Adams, The selected ion flow tube (SIFT): studies of ion-neutral reactions, *Adv. Atom. Mol. Phys.*, 24 (1987) 1-49.
- [37] D. Smith, N.G. Adams, W. Lindinger, Reactions of the HS ions ($n=0$ to 3) with several molecular gases at thermal energies, *The Journal of Chemical Physics*, 75 (1981) 3365.
- [38] D. Smith, P. Španěl, Selected ion flow tube mass spectrometry (SIFT-MS) for on-line trace gas analysis, *Mass Spectrom. Rev.*, 24 (2005) 661-700.
- [39] N.G. Adams, D. Smith, Selected ion flow tube (SIFT) - technique for studying ion-neutral reactions, *Int. J. Mass Spectrom. Ion Process.*, 21 (1976) 349-359.
- [40] D. Smith, P. Španěl, Application of ion chemistry and the SIFT technique to the quantitative analysis of trace gases in air and on breath, *International Reviews in Physical Chemistry*, 15 (1996) 231-271.
- [41] P. Španěl, D. Smith, A selected ion flow tube study of the reactions of NO^+ and O_2^+ ions with some organic molecules: The potential for trace gas analysis, *J. Chem. Phys.*, 104 (1996) 7.
- [42] D. Smith, P. Španěl, Ions in the terrestrial atmosphere and in interstellar clouds, *Mass Spectrom. Rev.*, 14 (1995) 255-278.
- [43] P. Španěl, K. Dryahina, D. Smith, Microwave plasma ion sources for selected ion flow tube mass spectrometry: Optimizing their performance and detection limits for trace gas analysis, *International Journal of Mass Spectrometry*, 267 (2007) 117-124.
- [44] D. Smith, A. Pysanenko, P. Španěl, Ionic diffusion and mass discrimination effects in the new generation of short flow tube SIFT-MS instruments, *International Journal of Mass Spectrometry*, 281 (2009) 15-23.
- [45] P. Španěl, D. Smith, Advances in on-line absolute trace gas analysis by SIFT-MS, *Current Analytical Chemistry*, 9 (2013) 525-539.
- [46] P. Španěl, K. Dryahina, D. Smith, A general method for the calculation of absolute trace gas concentrations in air and breath from selected ion flow tube mass spectrometry data, *Int. J. Mass Spectrom.*, 249 (2006) 230-239.
- [47] P. Španěl, D. Smith, SIFT studies of the reactions of H_3O^+ , NO^+ and O_2^+ with a series of alcohols, *Int. J. Mass Spectrom.*, 167 (1997) 375-388.
- [48] P. Španěl, Y.F. Ji, D. Smith, SIFT studies of the reactions of H_3O^+ , NO^+ and O_2^+ with a series of aldehydes and ketones, *Int. J. Mass Spectrom.*, 165 (1997) 25-37.
- [49] P. Španěl, J.M. Van Doren, D. Smith, A selected ion flow tube study of the reactions of H_3O^+ , NO^+ , and O_2^+ with saturated and unsaturated aldehydes and subsequent hydration of the product ions, *Int. J. Mass Spectrom.*, 213 (2002) 163-176.
- [50] P. Španěl, D. Smith, SIFT studies of the reactions of H_3O^+ , NO^+ and O_2^+ with a series of volatile carboxylic acids and esters, *Int. J. Mass Spectrom.*, 172 (1998) 137-147.
- [51] P. Španěl, D. Smith, Selected ion flow tube studies of the reactions of H_3O^+ , NO^+ , and O_2^+ with several aromatic and aliphatic hydrocarbons, *International Journal of Mass Spectrometry*, 181 (1998) 1-10.
- [52] N. Schoon, C. Amelynck, L. Vereecken, E. Arijs, A selected ion flow tube study of the reactions of H_3O^+ , NO^+ and O_2^+ with a series of monoterpenes, *International Journal of Mass Spectrometry*, 229 (2003) 231-240.

- [53] T.S. Wang, P. Španěl, D. Smith, Selected ion flow tube, SIFT, studies of the reactions of H_3O^+ , NO^+ and O_2^+ with eleven $\text{C}_{10}\text{H}_{16}$ monoterpenes, *Int. J. Mass Spectrom.*, 228 (2003) 117-126.
- [54] P. Španěl, D. Smith, Selected ion flow tube studies of the reactions of H_3O^+ , NO^+ , and O_2^+ with some organosulphur molecules, *International Journal of Mass Spectrometry*, 176 (1998) 167-176.
- [55] P. Španěl, T. Wang, D. Smith, A selected ion flow tube, SIFT, study of the reactions of H_3O^+ , NO^+ and O_2^+ ions with a series of diols, *Int. J. Mass Spectrom.*, 218 (2002) 227-236.
- [56] K. Dryahina, M. Polášek, P. Španěl, A selected ion flow tube, SIFT, study of the ion chemistry of H_3O^+ , NO^+ and O_2^+ ions with several nitroalkanes in the presence of water vapour, *International Journal of Mass Spectrometry*, 239 (2004) 57-65.
- [57] P. Španěl, D. Smith, Selected ion flow tube studies of the reactions of H_3O^+ , NO^+ , and O_2^+ with several amines and some other nitrogen-containing molecules, *International Journal of Mass Spectrometry*, 176 (1998) 203-211.
- [58] P. Španěl, D. Smith, Reactions of hydrated hydronium ions and hydrated hydroxide ions with some hydrocarbons and oxygen-bearing organic molecules, *The Journal of Physical Chemistry*, 99 (1995) 15551-15556.
- [59] P. Španěl, D. Smith, Influence of water vapour on selected ion flow tube mass spectrometric analyses of trace gases in humid air and breath, *Rapid Commun. Mass Spectrom.*, 14 (2000) 1898-1906.
- [60] P. Španěl, D. Smith, A selected ion flow tube study of the reactions of NO^+ and O_2^+ ions with some organic molecules: The potential for trace gas analysis of air, *J. Chem. Phys.*, 104 (1996) 1893-1899.
- [61] P. Španěl, D. Smith, Quantification of trace levels of the potential cancer biomarkers formaldehyde, acetaldehyde and propanol in breath by SIFT-MS, *J. Breath Res.*, 2 (2008) 046003.
- [62] D. Smith, T.W. Chippendale, P. Španěl, Minimising the Effects of Isobaric Product Ions in SIFT-MS Quantification of Acetaldehyde, Dimethyl Sulphide and Carbon Dioxide, *Current Analytical Chemistry*, (submitted 2013) 8.
- [63] P. Španěl, S. Davies, D. Smith, Quantification of ammonia in human breath by the selected ion flow tube analytical method using H_3O^+ and O_2^+ precursor ions, *Rapid Commun. Mass Spectrom.*, 12 (1998) 763-766.
- [64] K. Dryahina, D. Smith, P. Španěl, Quantification of methane in humid air and exhaled breath using selected ion flow tube mass spectrometry, *Rapid Commun. Mass Spectrom.*, 24 (2010) 1296-1304.
- [65] S. Davies, P. Španěl, D. Smith, A new 'online' method to measure increased exhaled isoprene in end-stage renal failure, *Nephrol. Dial. Transplant.*, 16 (2001) 836-839.
- [66] P. Španěl, D. Smith, Influence of water vapour on selected ion flow tube mass spectrometric analyses of trace gases in humid air and breath, *Rapid Commun. Mass Spectrom.*, 14 (2000) 1898-1906.
- [67] J. Čepl, I. Pátková, A. Blahušková, F. Cvrčková, A. Markoš, Patterning of mutually interacting bacterial bodies: close contacts and airborne signals, *Bmc Microbiology*, 10 (2010).
- [68] S.P. Bernier, S. Létoffé, M. Delepierre, J.M. Ghigo, Biogenic ammonia modifies antibiotic resistance at a distance in physically separated bacteria, *Molecular microbiology*, 81 (2011) 705-716.

- [69] K.-s. Kim, S. Lee, C.-M. Ryu, Interspecific bacterial sensing through airborne signals modulates locomotion and drug resistance, *Nature communications*, 4 (2013) 1809.
- [70] C. Scholler, S. Molin, K. Wilkins, Volatile metabolites from some gram-negative bacteria, *Chemosphere*, 35 (1997) 1487-1495.
- [71] E.V. Bowman, L.R. Freeman, D.W. Later, M.L. Lee, Comparison of volatiles produced by selected pseudomonads on chicken skin, *Journal of Food Science*, 48 (1983) 1358-1359.
- [72] S. Schulz, J.S. Dickschat, Bacterial volatiles: the smell of small organisms, *Natural Product Reports*, 24 (2007) 814-842.
- [73] M. Kai, M. Haustein, F. Molina, A. Petri, B. Scholz, B. Piechulla, Bacterial volatiles and their action potential, *Appl. Microbiol. Biotechnol.*, 81 (2009) 1001-1012.
- [74] V. Shestivska, A. Nemeč, P. Dřevínek, K. Sovová, K. Dryahina, P. Španěl, Quantification of methyl thiocyanate in the headspace of *Pseudomonas aeruginosa* cultures and in the breath of cystic fibrosis patients by selected ion flow tube mass spectrometry, *Rapid Commun. Mass Spectrom.*, 25 (2011) 2459-2467.
- [75] V. Shestivska, P. Španěl, K. Dryahina, K. Sovová, D. Smith, M. Musilek, A. Nemeč, Variability in the concentrations of volatile metabolites emitted by genotypically different strains of *Pseudomonas aeruginosa*, *J. Appl. Microbiol.*, 113 (2012) 701-713.
- [76] T.W.E. Chippendale, P. Španěl, D. Smith, Time-resolved selected ion flow tube mass spectrometric quantification of the volatile compounds generated by *E. coli* JM109 cultured in two different media, *Rapid Commun. Mass Spectrom.*, 25 (2011) 2163-2172.
- [77] <http://www.mrc.ac.uk/Fundingopportunities/Calls/Biomarkers/MRC004512>, last accessed on 26.6. 2013.
- [78] M. Kumar, S.K. Sarin, Biomarkers of diseases in medicine, *Current Trends of Science Platinum Jubilee Special*, Indian Academy of Sciences, Bangalore, India, (2009) 403-417.
- [79] C.W. Turck, *Biomarkers for psychiatric disorders*, Springer, 2008.
- [80] W. Filipiak, A. Sponring, M.M. Baur, A. Filipiak, C. Ager, H. Wiesenhofer, M. Nagl, J. Troppmair, A. Amann, Molecular analysis of volatile metabolites released specifically by *Staphylococcus aureus* and *Pseudomonas aeruginosa*, *Bmc Microbiology*, 12 (2012).
- [81] J.J. Zhu, H.D. Bean, M.J. Wargo, L.W. Leclair, J.E. Hill, Detecting bacterial lung infections: in vivo evaluation of in vitro volatile fingerprints, *J. Breath Res.*, 7 (2013).
- [82] S. Mann, Über den Geruchstoff von *Pseudomonas aeruginosa*, *Archiv Fur Mikrobiologie*, 54 (1966) 184-190.
- [83] A.J. Scott-Thomas, M. Syhre, P.K. Pattemore, M. Epton, R. Laing, J. Pearson, S.T. Chambers, 2-Aminoacetophenone as a potential breath biomarker for *Pseudomonas aeruginosa* in the cystic fibrosis lung, *Bmc Pulmonary Medicine*, 10 (2010) 56.
- [84] C.D. Cox, J. Parker, Use of 2-aminoacetophenone production of *Pseudomonas aeruginosa*, *Journal of Clinical Microbiology*, 9 (1979) 479-484.
- [85] J.N. Labows, K.J. McGinley, G.F. Webster, J.J. Leyden, Headspace analysis of volatile metabolites of *Pseudomonas-aeruginosa* and related species by gass chromatography-mass spectrometry, *Journal of Clinical Microbiology*, 12 (1980) 521-526.
- [86] A. Scott-Thomas, J. Pearson, S. Chambers, Potential sources of 2-aminoacetophenone to confound the *Pseudomonas aeruginosa* breath test, including analysis of a food challenge study, *J. Breath Res.*, 5 (2011).

- [87] B. Enderby, D. Smith, W. Carroll, W. Lenney, Hydrogen Cyanide as a Biomarker for *Pseudomonas Aeruginosa* in the Breath of Children With Cystic Fibrosis, *Pediatr. Pulmonol.*, 44 (2009) 142-147.
- [88] F.J. Gilchrist, R.J. Bright-Thomas, A.M. Jones, D. Smith, P. Španěl, A.K. Webb, W. Lenney, Hydrogen cyanide concentrations in the breath of adult cystic fibrosis patients with and without *Pseudomonas aeruginosa* infection, *J. Breath Res.*, 7 (2013) 026010.
- [89] W. Lenney, F.J. Gilchrist, *Pseudomonas aeruginosa* and cyanide production, *European Respiratory Journal*, 37 (2011) 482-483.
- [90] W. Filipiak, A. Sponring, M.M. Baur, C. Ager, A. Filipiak, H. Wiesenhofer, M. Nagl, J. Troppmair, A. Amann, Characterization of volatile metabolites taken up by or released from *Streptococcus pneumoniae* and *Haemophilus influenzae* by using GC-MS, *Microbiology-(UK)*, 158 (2012) 3044-3053.
- [91] R.A. Allardyce, V.S. Langford, A.L. Hill, D.R. Murdoch, Detection of volatile metabolites produced by bacterial growth in blood culture media by selected ion flow tube mass spectrometry (SIFT-MS), *J. Microbiol. Methods*, 65 (2006) 361-365.
- [92] R. Portner, S. Nagel-Heyer, C. Goepfert, P. Adamietz, N.M. Meenen, Bioreactor design for tissue engineering, *Journal of Bioscience and Bioengineering*, 100 (2005) 235-245.
- [93] V. Havlicek, K. Lemr, K.A. Schug, Current Trends in Microbial Diagnostics Based on Mass Spectrometry, *Anal. Chem.*, 85 (2013) 790-797.
- [94] B. Kerr, M.A. Riley, M.W. Feldman, B.J.M. Bohannan, Local dispersal promotes biodiversity in a real-life game of rock-paper-scissors, *Nature*, 418 (2002) 171-174.
- [95] M. Juhas, L. Eberl, B. Tümmler, Quorum sensing: the power of cooperation in the world of *Pseudomonas*, *Environmental microbiology*, 7 (2005) 459-471.
- [96] E.B. Jacob, I. Becker, Y. Shapira, H. Levine, Bacterial linguistic communication and social intelligence, *TRENDS in Microbiology*, 12 (2004) 366-372.
- [97] E. Ben-Jacob, D. S Coffey, H. Levine, Bacterial survival strategies suggest rethinking cancer cooperativity, *TRENDS in Microbiology*, (2012).
- [98] I. Pátková, J. Čepl, T. Rieger, A. Blahušková, Z. Neubauer, A. Markoš, Developmental plasticity of bacterial colonies and consortia in germ-free and gnotobiotic settings, *Bmc Microbiology*, 12 (2012) 178.
- [99] T. Rieger, Z. Neubauer, A. Blahuskova, F. Cvrčková, A. Markos, Bacterial body plans: colony ontogeny in *Serratia marcescens*, *Communicative & integrative biology*, 1 (2008) 78-87.
- [100] J.T. Knudsen, L. Tollsten, L.G. Bergström, Floral scents—a checklist of volatile compounds isolated by head-space techniques, *Phytochemistry*, 33 (1993) 253-280.
- [101] F.B. Abeles, P.W. Morgan, M.E. Saltveit Jr, *Ethylene in plant biology*, Access Online via Elsevier, 1992.
- [102] P.W. Paré, J.H. Tumlinson, Plant volatiles as a defense against insect herbivores, *Plant Physiology*, 121 (1999) 325-332.
- [103] M. Dicke, J. Bruin, Chemical information transfer between plants:: back to the future, *Biochemical Systematics and Ecology*, 29 (2001) 981-994.
- [104] S. Heuskin, F.J. Verheggen, E. Haubruge, J.-P. Wathelet, G. Lognay, The use of semiochemical slow-release devices in integrated pest management strategies, *Biotechnol. Agron. Soc. Environ*, 15 (2011) 459-470.
- [105] A. Das, S.-H. Lee, T.K. Hyun, S.-W. Kim, J.-Y. Kim, Plant volatiles as method of communication, *Plant biotechnology reports*, 7 (2013) 9-26.
- [106] Z.-G. Yan, C.-Z. Wang, Wound-induced green leaf volatiles cause the release of acetylated derivatives and a terpenoid in maize, *Phytochemistry*, 67 (2006) 34-42.

- [107] J.G. de Boer, C.A. Hordijk, M.A. Posthumus, M. Dicke, Prey and non-prey arthropods sharing a host plant: effects on induced volatile emission and predator attraction, *Journal of Chemical Ecology*, 34 (2008) 281-290.
- [108] T. Hirao, A. Okazawa, K. Harada, A. Kobayashi, T. Muranaka, K. Hirata, Green leaf volatiles enhance methyl jasmonate response in *Arabidopsis*, *Journal of Bioscience and Bioengineering*, (2012).
- [109] E. Gallego Piñol, A. Gelabert, F.J. Roca Mussons, F. Perales, X. Guardino, Identification of volatile organic compounds (VOC) emitted from three European orchid species with different pollination strategies: two deceptive orchids (*Himantoglossum robertianum* and *Ophrys apifera*) and a rewarding (*Gymnadenia conopsea*), (2012).
- [110] S. Oluwafemi, M. Birkett, J. Caulfield, J. Pickett, Variability of volatile organic compounds emitted by seedlings of seven African maize varieties when infested by adult *Cicadulina storeyi* China leafhopper vectors of maize streak virus, *African Crop Science Journal*, 20 (2012) 117-124.
- [111] J. Linz, A. Baschwitz, A. Strutz, H.K. Dweck, S. Sachse, B.S. Hansson, M.C. Stensmyr, Host plant-driven sensory specialization in *Drosophila erecta*, *Proceedings of the Royal Society B: Biological Sciences*, 280 (2013).
- [112] R.A. Levin, R.A. Raguso, L.A. McDade, Fragrance chemistry and pollinator affinities in *Nyctaginaceae*, *Phytochemistry*, 58 (2001) 429-440.
- [113] I. Guterman, T. Masci, X. Chen, F. Negre, E. Pichersky, N. Dudareva, D. Weiss, A. Vainstein, Generation of phenylpropanoid pathway-derived volatiles in transgenic plants: rose alcohol acetyltransferase produces phenylethyl acetate and benzyl acetate in *petunia* flowers, *Plant molecular biology*, 60 (2006) 555-563.
- [114] H. Taki, H. Makihara, T. Matsumura, M. Hasegawa, T. Matsuura, H. Tanaka, S.i. Makino, K. Okabe, Evaluation of secondary forests as alternative habitats to primary forests for flower-visiting insects, *Journal of Insect Conservation*, (2013) 1-8.
- [115] J.-i. Horiuchi, D.V. Badri, B.A. Kimball, F. Negre, N. Dudareva, M.W. Paschke, J.M. Vivanco, The floral volatile, methyl benzoate, from snapdragon (*Antirrhinum majus*) triggers phytotoxic effects in *Arabidopsis thaliana*, *Planta*, 226 (2007) 1-10.
- [116] W. Kegge, R. Pierik, Biogenic volatile organic compounds and plant competition, *Trends in plant science*, 15 (2010) 126-132.
- [117] E. Pichersky, J. Gershenzon, The formation and function of plant volatiles: perfumes for pollinator attraction and defense, *Current opinion in plant biology*, 5 (2002) 237-243.
- [118] M.C. Wildermuth, Variations on a theme: synthesis and modification of plant benzoic acids, *Current opinion in plant biology*, 9 (2006) 288-296.
- [119] J.G. De Boer, M. Dicke, The role of methyl salicylate in prey searching behavior of the predatory mite *Phytoseiulus persimilis*, *Journal of Chemical Ecology*, 30 (2004) 255-271.
- [120] R.A. Robergs, D. Dwyer, T. Astorino, Recommendations for improved data processing from expired gas analysis indirect calorimetry, *Sports Medicine*, 40 (2010) 95-111.
- [121] D.A. Lindberg, Hydrogen Breath Testing in Adults: What Is It and Why Is It Performed?, *Gastroenterology Nursing*, 33 (2010) 8.
- [122] P. Španel, D. Smith, Volatile compounds in health and disease, *Current Opinion in Clinical Nutrition & Metabolic Care*, 14 (2011) 455-460.
- [123] S.F. Solga, M. Mudalel, L.A. Spacek, R. Lewicki, F. Tittel, C. Loccioni, A. Russo, T.H. Risby, Factors influencing breath ammonia determination, *J. Breath Res.*, 7 (2013) 037101.

- [124] P. Španěl, K. Dryahina, D. Smith, The concentration distributions of some metabolites in the exhaled breath of young adults, *J. Breath Res.*, 1 (2007) 026001.
- [125] E.E. Owen, R.R. Robinson, Amino acid extraction and ammonia metabolism by the human kidney during the prolonged administration of ammonium chloride, *Journal of Clinical Investigation*, 42 (1963) 263.
- [126] C. Turner, B. Parekh, C. Walton, P. Španěl, D. Smith, M. Evans, An exploratory comparative study of volatile compounds in exhaled breath and emitted by skin using selected ion flow tube mass spectrometry, *Rapid communications in mass spectrometry*, 22 (2008) 526-532.
- [127] F.M. Schmidt, O. Vaittinen, M. Metsala, M. Lehto, C. Forsblom, P.H. Groop, L. Halonen, Ammonia in breath and emitted from skin, *J. Breath Res.*, 7 (2013).
- [128] P. Španěl, C. Turner, T.S. Wang, R. Bloor, D. Smith, Generation of volatile compounds on mouth exposure to urea and sucrose: implications for exhaled breath analysis, *Physiol. Meas.*, 27 (2006) N7-N17.
- [129] T.S. Wang, A. Pysanenko, K. Dryahina, P. Španěl, D. Smith, Analysis of breath, exhaled via the mouth and nose, and the air in the oral cavity, *J. Breath Res.*, 2 (2008).
- [130] D. Smith, T.S. Wang, A. Pysanenko, P. Španěl, A selected ion flow tube mass spectrometry study of ammonia in mouth- and nose-exhaled breath and in the oral cavity, *Rapid Commun. Mass Spectrom.*, 22 (2008) 783-789.
- [131] P.R. Boshier, N. Marczin, G.B. Hanna, Repeatability of the Measurement of Exhaled Volatile Metabolites Using Selected Ion Flow Tube Mass Spectrometry, *J. Am. Soc. Mass Spectrom.*, 21 (2010) 1070-1074.
- [132] D. Smith, P. Španěl, The challenge of breath analysis for clinical diagnosis and therapeutic monitoring, *Analyst*, 132 (2007) 390-396.
- [133] A. Kotani, Y. Wakabayashi, M. Kohama, F. Kusu, Determination of Ammonia in Exhaled Breath by Flow Injection Analysis with Electrochemical Detection, *Electrochemistry*, 80 (2012) 340-344.
- [134] F.K. Tittel, R.F. Curl, L. Dong, R. Lewicki, Infrared Semiconductor laser based trace gas sensor Technologies: Recent Advances and Applications, in: F. Baldini, J. Homola, R.A. Lieberman, K. Kalli (Eds.) *Optical Sensors 2011 and Photonic Crystal Fibers V*, 2011.
- [135] T. Hibbard, K. Crowley, A.J. Killard, Direct measurement of ammonia in simulated human breath using an inkjet-printed polyaniline nanoparticle sensor, *Anal. Chim. Acta*, 779 (2013) 56-63.
- [136] L.R. Narasimhan, W. Goodman, C.K.N. Patel, Correlation of breath ammonia with blood urea nitrogen and creatinine during hemodialysis, *Proceedings of the National Academy of Sciences of the United States of America*, 98 (2001) 4617-4621.
- [137] G. Neri, A. Lacquaniti, G. Rizzo, N. Donato, M. Latino, M. Buemi, Real-time monitoring of breath ammonia during haemodialysis: use of ion mobility spectrometry (IMS) and cavity ring-down spectroscopy (CRDS) techniques, *Nephrol. Dial. Transplant.*, 27 (2012) 2945-2952.
- [138] C. Turner, P. Španěl, D. Smith, A longitudinal study of ammonia, acetone and propanol in the exhaled breath of 30 subjects using selected ion flow tube mass spectrometry, SIFT-MS, *Physiol. Meas.*, 27 (2006) 321-337.
- [139] P. Španěl, K. Dryahina, D. Smith, Acetone, ammonia and hydrogen cyanide in exhaled breath of several volunteers aged 4-83 years, *J. Breath Res.*, 1 (2007).
- [140] L. Laffel, Ketone bodies: a review of physiology, pathophysiology and application of monitoring to diabetes, *Diabetes/metabolism research and reviews*, 15 (1999) 412-426.

- [141] M.P. Kalapos, On the mammalian acetone metabolism: from chemistry to clinical implications, *Biochimica et Biophysica Acta (BBA)-General Subjects*, 1621 (2003) 122-139.
- [142] A. Manolis, The Diagnostic Potential of Breath Analysis, *Clinical Chemistry*, 29 (1983) 5-15.
- [143] A.D. Worrall, J.A. Bernstein, A.P. Angelopoulos, Portable method of measuring gaseous acetone concentrations, *Talanta*, 112 (2013) 26-30.
- [144] J. Shin, S.J. Choi, I. Lee, D.Y. Youn, C.O. Park, J.H. Lee, H.L. Tuller, I.D. Kim, Thin-Wall Assembled SnO₂ Fibers Functionalized by Catalytic Pt Nanoparticles and their Superior Exhaled-Breath-Sensing Properties for the Diagnosis of Diabetes, *Advanced Functional Materials*, 23 (2013) 2357-2367.
- [145] T.I. Nasution, I. Nainggolan, S.D. Hutagalung, K.R. Ahmad, Z.A. Ahmad, The sensing mechanism and detection of low concentration acetone using chitosan-based sensors, *Sensors and Actuators B-Chemical*, 177 (2013) 522-528.
- [146] M. Righettoni, A. Tricoli, S. Gass, A. Schmid, A. Amann, S.E. Pratsinis, Breath acetone monitoring by portable Si:WO₃ gas sensors, *Anal. Chim. Acta*, 738 (2012) 69-75.
- [147] G.F. Meng, Q. Xiang, Q.Y. Pan, J.Q. Xu, The Selective Acetone Detection Based on Fe₃O₄ Doped WO₃ Nanorods, *Sensor Letters*, 9 (2011) 128-131.
- [148] P. Španěl, K. Dryahina, A. Rejšková, T.W. Chippendale, D. Smith, Breath acetone concentration; biological variability and the influence of diet, *Physiol. Meas.*, 32 (2011) N23.
- [149] W. Carroll, W. Lenney, T.S. Wang, P. Španěl, A. Alcock, D. Smith, Detection of volatile compounds emitted by *Pseudomonas aeruginosa* using selected ion flow tube mass spectrometry, *Pediatr. Pulmonol.*, 39 (2005) 452-456.
- [150] F.J. Gilchrist, A. Alcock, J. Belcher, M. Brady, A. Jones, D. Smith, P. Španěl, K. Webb, W. Lenney, Variation in hydrogen cyanide production between different strains of *Pseudomonas aeruginosa*, *European Respiratory Journal*, 38 (2011) 409-414.
- [151] F.J. Gilchrist, C. Razavi, A.K. Webb, A.M. Jones, P. Španěl, D. Smith, W. Lenney, An investigation of suitable bag materials for the collection and storage of breath samples containing hydrogen cyanide, *J. Breath Res.*, 6 (2012) 036004.
- [152] J. Dummer, M. Storer, S. Sturney, A. Scott-Thomas, S. Chambers, M. Swanney, M. Epton, Quantification of hydrogen cyanide (HCN) in breath using selected ion flow tube mass spectrometry-HCN is not a biomarker of *Pseudomonas* in chronic suppurative lung disease, *J. Breath Res.*, 7 (2013).
- [153] C. Turner, P. Španěl, D. Smith, A longitudinal study of methanol in the exhaled breath of 30 healthy volunteers using selected ion flow tube mass spectrometry, SIFT-MS, *Physiological Measurement*, 27 (2006) 637.
- [154] W. Lindinger, J. Taucher, A. Jordan, A. Hansel, W. Vogel, Endogenous production of methanol after the consumption of fruit, *Alcoholism: Clinical and Experimental Research*, 21 (1997) 939-943.
- [155] R.J. Siragusa, J.J. Cerda, M. Baig, C. Burgin, F. Robbins, Methanol production from the degradation of pectin by human colonic bacteria, *The American journal of clinical nutrition*, 47 (1988) 848-851.
- [156] K. Rycerz, J.E. Jaworska-Adamu, Review paper Effects of aspartame metabolites on astrocytes and neurons, *Folia Neuropathol*, 51 (2013) 10-17.
- [157] H.H. Butchko, W.W. Stargel, C.P. Comer, D.A. Mayhew, C. Benninger, G.L. Blackburn, L.M.J. de Sonnevile, R.S. Geha, Z. Hertelendy, A. Koestner, A.S. Leon, G.U. Liepa, K.E. McMartin, C.L. Mendenhall, I.C. Munro, E.J. Novotny, A.G. Renwick, S.S. Schiffman, D.L. Schomer, B.A. Shaywitz, P.A. Spiers, T.R. Tephly, J.A.

- Thomas, F.K. Trefz, Aspartame: Review of safety, *Regulatory Toxicology and Pharmacology*, 35 (2002) S1-S93.
- [158] P. Španěl, K. Dryahina, D. Smith, A quantitative study of the influence of inhaled compounds on their concentrations in exhaled breath, *J. Breath Res.*, 7 (2013) 017106.
- [159] J. Huang, S. Kumar, N. Abbassi-Ghadi, P. Španěl, D. Smith, G.B. Hanna, Selected Ion Flow Tube Mass Spectrometry Analysis of Volatile Metabolites in Urine Headspace for the Profiling of Gastro-Esophageal Cancer, *Anal. Chem.*, 85 (2013) 3409-3416.
- [160] A.M. Diskin, P. Španěl, D. Smith, Time variation of ammonia, acetone, isoprene and ethanol in breath: a quantitative SIFT-MS study over 30 days, *Physiological Measurement*, 24 (2003) 107.
- [161] B.G. Stone, T.J. Besse, W.C. Duane, C.D. Evans, E.G. DeMaster, Effect of regulating cholesterol biosynthesis on breath isoprene excretion in men, *Lipids*, 28 (1993) 705-708.
- [162] D. Smith, P. Španěl, B. Enderby, W. Lenney, C. Turner, S.J. Davies, Isoprene levels in the exhaled breath of 200 healthy pupils within the age range 7–18 years studied using SIFT-MS, *J. Breath Res.*, 4 (2010) 017101.
- [163] C. Turner, P. Španěl, D. Smith, A longitudinal study of breath isoprene in healthy volunteers using selected ion flow tube mass spectrometry (SIFT-MS), *Physiological Measurement*, 27 (2006) 13.
- [164] J. King, A. Kupferthaler, K. Unterkofler, H. Koc, S. Teschl, G. Teschl, W. Miekisch, J. Schubert, H. Hinterhuber, A. Amann, Isoprene and acetone concentration profiles during exercise on an ergometer, *J. Breath Res.*, 3 (2009) 027006.
- [165] A. Jordan, A. Hansel, R. Holzinger, W. Lindinger, Acetonitrile and benzene in the breath of smokers and non-smokers investigated by proton transfer reaction mass spectrometry (PTR-MS), *Int. J. Mass Spectrom. Ion Process.*, 148 (1995) L1-L3.
- [166] S.M. Abbott, J.B. Elder, P. Španěl, D. Smith, Quantification of acetonitrile in exhaled breath and urinary headspace using selected ion flow tube mass spectrometry, *International Journal of Mass Spectrometry*, 228 (2003) 655-665.
- [167] K. Sovová, K. Dryahina, P. Španěl, Selected ion flow tube (SIFT) studies of the reactions of H_3O^+ , NO^+ and O_2^+ with six volatile phytogetic esters, *Int. J. Mass Spectrom.*, 300 (2011) 31-38.
- [168] D. Smith, K. Sovová, P. Španěl, A selected ion flow tube study of the reactions of H_3O^+ , NO^+ and O_2^+ with seven isomers of hexanol in support of SIFT-MS, *Int. J. Mass Spectrom.*, 319 (2012) 25-30.
- [169] P.W. Pare, J.H. Tumlinson, Plant volatiles as a defense against insect herbivores, *Plant Physiology*, 121 (1999) 325-331.
- [170] R.N. Kigathi, W.W. Weisser, D. Veit, J. Gershenzon, S.B. Unsicker, Plants Suppress Their Emission of Volatiles When Growing with Conspecifics, *Journal of Chemical Ecology*, 39 (2013) 537-545.
- [171] W.G.M. P.J. Linstrom, NIST Chemistry WebBook, NIST Standard Reference Database Number 69, in: National Institute of Standards and Technology, Gaithersburg, 2011.
- [172] R. Weast, *CRC Handbook of Chemistry & Physics*. 66th, CRC, Boca Raton, Florida.
- [173] K.J. Miller, J.A. Savchik, New empirical-method to calculate average molecular polarisabilities, *J. Am. Chem. Soc.*, 101 (1979) 7206-7213.
- [174] D. Smith, K. Sovova, P. Spanel, A selected ion flow tube study of the reactions of H_3O^+ , NO^+ and O_2^+ with seven isomers of hexanol in support of SIFT-MS, *International Journal of Mass Spectrometry*, 319 (2012) 25-30.

- [175] V. Anicich, An Index of the Literature for Bimolecular Gas Phase Cation-Molecule Reaction Kinetics, JPL Publication 03-19, National Aeronautics and Space Administration, Jet Propulsion Laboratory, California Institute of Technology, Pasadena, California, 2003.
- [176] G. Bouchoux, J.Y. Salpin, D. Leblanc, A relationship between the kinetics and thermochemistry of proton transfer reactions in the gas phase, *Int. J. Mass Spectrom. Ion Process.*, 153 (1996) 37-48.
- [177] T. Su, W.J. Chesnavich, Parametization of the ion-polar molecule collision rate-constant by trajectory calculations, *Journal of Chemical Physics*, 76 (1982) 5183-5185.
- [178] D. Smith, A. Pysanenko, P. Španěl, Ionic diffusion and mass discrimination effects in the new generation of short flow tube SIFT-MS instruments, *International Journal of Mass Spectrometry*, 281 (2009) 15-23.
- [179] P.J. Linstrom, W.G. Mallard, NIST Chemistry WebBook, NIST Standard Reference Database Number 69, in, National Institute of Standards and Technology, Gaithersburg, 2010.
- [180] P. Španěl, D. Smith, SIFT studies of the reactions of H_3O^+ , NO^+ and O_2^+ with a series of alcohols, *International journal of mass spectrometry and ion processes*, 167 (1997) 375-388.
- [181] D. Smith, P. Španěl, Ambient analysis of trace compounds in gaseous media by SIFT-MS, *Analyst*, 136 (2011) 2009-2032.
- [182] J.B. Kirsner, Inflammatory bowel disease Part I: Nature and pathogenesis, *Disease-a-Month*, 37 (1991) 610-666.
- [183] S.B. Hanauer, Inflammatory bowel disease: epidemiology, pathogenesis, and therapeutic opportunities, *Inflammatory bowel diseases*, 12 (2006) S3-S9.
- [184] R. Xavier, D. Podolsky, Unravelling the pathogenesis of inflammatory bowel disease, *Nature*, 448 (2007) 427-434.
- [185] W. Strober, I. Fuss, P. Mannon, The fundamental basis of inflammatory bowel disease, *Journal of Clinical Investigation*, 117 (2007) 514-521.
- [186] A. Krishnan, J.R. Korzenik, Inflammatory bowel disease and environmental influences, *Gastroenterology Clinics of North America*, 31 (2002) 21-39.
- [187] J. Cosnes, Tobacco and IBD: relevance in the understanding of disease mechanisms and clinical practice, *Best practice & research Clinical gastroenterology*, 18 (2004) 481-496.
- [188] J. Kokoszka, R.L. Nelson, W.I. Swedler, M. John Skosey, H. Abcarian, Determination of inflammatory bowel disease activity by breath pentane analysis, *Dis. Colon Rectum*, 36 (1993) 597-601.
- [189] M.A. Pelli, G. Trovarelli, E. Capodicasa, G.E. De Medio, M. Gabrio Bassotti, Breath alkanes determination in ulcerative colitis and Crohn's disease, *Dis. Colon Rectum*, 42 (1999) 71-76.
- [190] B.E. Wendland, E. Aghdassi, C. Tam, J. Carrier, A.H. Steinhart, S.L. Wolman, D. Baron, J.P. Allard, Lipid peroxidation and plasma antioxidant micronutrients in Crohn disease, *The American journal of clinical nutrition*, 74 (2001) 259-264.
- [191] G. Spiteller, Peroxidation of linoleic acid and its relation to aging and age dependent diseases, *Mechanisms of ageing and development*, 122 (2001) 617-657.
- [192] P. Španěl, D. Smith, A selected ion flow tube study of the reactions of NO^+ and O_2^+ ions with some organic molecules: The potential for trace gas analysis of air, *Journal of Chemical Physics*, 104 (1996) 1893-1899.
- [193] P. Španěl, D. Smith, SIFT studies of the reactions of H_3O^+ , NO^+ and O_2^+ with several aromatic and aliphatic hydrocarbons, *Int. J. Mass Spectrom.*, 181 (1998) 1-10.

- [194] K. Sovová, K. Dryahina, P. Španěl, Selected ion flow tube (SIFT) studies of the reactions of H_3O^+ , NO^+ and O_2^+ with six volatile phytogetic esters, *Int. J. Mass Spectrom.*, 300 (2011) 31-38.
- [195] <http://www.who.int/genomics/public/geneticdiseases/en/index2.html#CF>, last accessed on 17.7. 2012.
- [196] J.R. Riordan, J.M. Rommens, B. Kerem, N. Alon, R. Rozmahel, Z. Grzelczak, J. Zielenski, S. Lok, N. Plavsic, J.L. Chou, Identification of the cystic fibrosis gene: cloning and characterization of complementary DNA, *Science*, 245 (1989) 1066-1073.
- [197] P.M. Quinton, Cystic fibrosis: lessons from the sweat gland, *Physiology*, 22 (2007) 212-225.
- [198] B.W. Ramsey, S. Banks-Schlegel, F.J. Accurso, R.C. Boucher, G.R. Cutting, J.F. Engelhardt, W.B. Guggino, C.L. Karp, M.R. Knowles, J.K. Kolls, Future Directions in Early Cystic Fibrosis Lung Disease Research, *Am. J. Respir. Crit. Care Med.*, (2012).
- [199] <http://www.clinicians.co.nz/cystic-fibrosis/>, last accessed on 9.9. 2013.
- [200] P.K. Singh, A.L. Schaefer, M.R. Parsek, T.O. Moninger, M.J. Welsh, E. Greenberg, Quorum-sensing signals indicate that cystic fibrosis lungs are infected with bacterial biofilms, *Nature*, 407 (2000) 762-764.
- [201] P.O.F.P. EXACERBATIONS, Cystic fibrosis pulmonary exacerbations, *The Journal of pediatrics*, 148 (2006) 259-264.
- [202] C. Stover, X. Pham, A. Erwin, S. Mizoguchi, P. Warrener, M. Hickey, F. Brinkman, W. Hufnagle, D. Kowalik, M. Lagrou, Complete genome sequence of *Pseudomonas aeruginosa* PAO1, an opportunistic pathogen, *Nature*, 406 (2000) 959-964.
- [203] J.R.W. Govan, V. Deretic, Microbial pathogenesis in cystic fibrosis: Mucoid *Pseudomonas aeruginosa* and *Burkholderia cepacia*, *Microbiological Reviews*, 60 (1996) 539-+.
- [204] D. Tubbs, W. Lenney, P. Alcock, C.A. Campbell, J. Gray, C. Pantin, *Pseudomonas aeruginosa* in cystic fibrosis: cross-infection and the need for segregation, *Respiratory Medicine*, 95 (2001) 147-152.
- [205] M. Rosenfeld, J. Emerson, F. Accurso, D. Armstrong, R. Castile, K. Grimwood, P. Hiatt, K. McCoy, S. McNamara, B. Ramsey, Diagnostic accuracy of oropharyngeal cultures in infants and young children with cystic fibrosis, *Pediatr. Pulmonol.*, 28 (1999) 321-328.
- [206] S. Maiya, M. Desai, A. Baruah, P. Weller, J. Clarke, J. Gray, Cough plate versus cough swab in patients with cystic fibrosis; a pilot study, *Archives of disease in childhood*, 89 (2004) 577-579.
- [207] J. Govan, V. Deretic, Microbial pathogenesis in cystic fibrosis: mucoid *Pseudomonas aeruginosa* and *Burkholderia cepacia*, *Microbiological Reviews*, 60 (1996) 539-574.
- [208] W. Carroll, W. Lenney, T. Wang, P. Španěl, A. Alcock, D. Smith, Detection of volatile compounds emitted by *Pseudomonas aeruginosa* using selected ion flow tube mass spectrometry, *Pediatr. Pulmonol.*, 39 (2005) 452-456.
- [209] F.J. Gilchrist, A. Alcock, J. Belcher, M. Brady, A. Jones, D. Smith, P. Španěl, K. Webb, W. Lenney, Variation in hydrogen cyanide production between different strains of *Pseudomonas aeruginosa*, *European Respiratory Journal*, 38 (2011) 409-414.
- [210] C.M. Robroeks, J.J.B.N. Van Berkel, J.W. Dallinga, Q. Jöbsis, L.J.I. Zimmermann, H.J.E. Hendriks, M.F.M. Wouters, C.P.M. Van Der Grinten, K.D.G. Van De Kant, F.J. Van Schooten, Metabolomics of volatile organic compounds in cystic fibrosis patients and controls, *Pediatric Research*, 68 (2010) 75-80.

- [211] P. Španel, D. Smith, Volatile compounds in health and disease, *Current Opinion in Clinical Nutrition & Metabolic Care*, 14 (2011) 455.
- [212] R. Cipollone, M.G. Bigotti, E. Frangipani, P. Ascenzi, P. Visca, Characterization of a rhodanese from the cyanogenic bacterium *Pseudomonas aeruginosa*, *Biochemical and Biophysical Research Communications*, 325 (2004) 85-90.
- [213] W.H. Ewing, B.R. Davis, M.A. Fife, E.F. Lessel, Biochemical characterization of *Serratia-lique-faciens* (Grimes and Hennerty) BASCOMB and AL (formerly *Enterobacter-liquefaciens*) and *Serratia-Rubidaea* (STAPP) COMB NOV and designation of type and neotype strains, *International Journal of Systematic Bacteriology*, 23 (1973) 217-225.
- [214] G. Szabo, G. Fath, Evolutionary games on graphs, *Physics Reports-Review Section of Physics Letters*, 446 (2007) 97-216.
- [215] S.A. West, A.S. Griffin, A. Gardner, S.P. Diggle, Social evolution theory for microorganisms, *Nature Reviews Microbiology*, 4 (2006) 597-607.
- [216] G.J. Velicer, Social strife in the microbial world, *TRENDS in Microbiology*, 11 (2003) 330-337.
- [217] J.W. Park, H. Min, Y.P. Kim, H.K. Shon, J. Kim, D.W. Moon, T.G. Lee, Multivariate analysis of ToF-SIMS data for biological applications, *Surface and Interface Analysis*, 41 (2009) 694-703.
- [218] I.T. Jolliffe, Principal component analysis, in, Springer-Verlag, New York, 1986.
- [219] M. Bunge, N. Araghipour, T. Mikoviny, J. Dunkl, R. Schnitzhofer, A. Hansel, F. Schinner, A. Wisthaler, R. Margesin, T.D. Mark, On-line monitoring of microbial volatile metabolites by proton transfer reaction-mass spectrometry, *Appl. Environ. Microbiol.*, 74 (2008) 2179-2186.
- [220] J.W. Gardner, Detection of vapors and odors from a multisensor array using pattern-recognition.1.Principal Component and Cluster-Analysis, *Sensors and Actuators B-Chemical*, 4 (1991) 109-115.
- [221] T. Macek, J. Rezek, B. Vrchotova, K. Beranova, O. Uhlik, J. Najmanova, M. Novakova, Z. Chrastilova, P. Kotrba, K. Demnerova, M. Mackova, *Phytoremediation, Listy Cukrovarnicke a Reparske*, 123 (2007) 312-314.
- [222] C.W. Arnold, D.G. Parfitt, M. Kaltreider, Phytovolatilization of oxygenated gasoline-impacted groundwater at an underground storage tank site via conifers, *International Journal of Phytoremediation*, 9 (2007) 53-69.
- [223] O.V. Singh, R.K. Jain, Phytoremediation of toxic aromatic pollutants from soil, *Appl. Microbiol. Biotechnol.*, 63 (2003) 128-135.
- [224] E.L. Rylott, A. Lorenz, N.C. Bruce, Biodegradation and biotransformation of explosives, *Current Opinion in Biotechnology*, 22 (2011) 434-440.
- [225] J.D. Rodgers, N.J. Bunce, Treatment methods for the remediation of nitroaromatic explosives, *Water Research*, 35 (2001) 2101-2111.
- [226] B. Zhu, R.H. Peng, X.Y. Fu, X.F. Jin, W. Zhao, J. Xu, H.J. Han, J.J. Gao, Z.S. Xu, L. Bian, Q.H. Yao, Enhanced Transformation of TNT by *Arabidopsis* Plants Expressing an Old Yellow Enzyme, *Plos One*, 7 (2012).
- [227] A.C.P. Heaton, C.L. Rugh, N.J. Wang, R.B. Meagher, Phytoremediation of mercury- and methylmercury-polluted soils using genetically engineered plants, *Journal of Soil Contamination*, 7 (1998) 497-509.
- [228] R.L. Chaney, M. Malik, Y.M. Li, S.L. Brown, E.P. Brewer, J.S. Angle, A.J.M. Baker, Phytoremediation of soil metals, *Current Opinion in Biotechnology*, 8 (1997) 279-284.

- [229] S.P. Cheng, Heavy metals in plants and phytoremediation - A state-of-the-art report with special reference to literature published in Chinese journals, *Environmental Science and Pollution Research*, 10 (2003) 335-340.
- [230] D.L. LeDuc, N. Terry, Phytoremediation of toxic trace elements in soil and water, *Journal of Industrial Microbiology & Biotechnology*, 32 (2005) 514-520.
- [231] <http://www.phytosanitary.org/projekty/2004/vvf-13-04.pdf>, last accessed on 30.9.2011.
- [232] E. Rubin, A. Ramaswami, The potential for phytoremediation of MTBE, *Water Research*, 35 (2001) 1348-1353.
- [233] A. Ramaswami, E. Rubin, S. Bonola, Non-significance of rhizosphere degradation during phytoremediation of MTBE, *International Journal of Phytoremediation*, 5 (2003) 315-331.
- [234] B.H. Cranner, Zur Biochemie and Physiologie der granzschichten lebender Pflanzenzellen, *Meldinger Norg. Landbrukhoiskole*, 5 (1922) 1-55.
- [235] S.J. Grayston, D. Vaughan, D. Jones, Rhizosphere carbon flow in trees, in comparison with annual plants: The importance of root exudation and its impact on microbial activity and nutrient availability, *Applied Soil Ecology*, 5 (1997) 29-56.
- [236] L. Knudson, The secretion of invertase by plant roots, *American Journal of Botany*, 7 (1920) 371-379.
- [237] N.C. Uren, H.M. Reisenaner, The role of root exudates in nutrient acquisition, in: P.B. Tinker, A. Lanchli (Eds.) *Advances in Plant Nutrition*, Praeger, New York, 1988, pp. 79-114.
- [238] D.L. Jones, P.R. Darrah, Amino-acid influx at the soil-root interface of Zea-mays L and its implications in the rhizosphere, *Plant and Soil*, 163 (1994) 1-12.
- [239] I. Krafczyk, G. Trolldenier, H. Beringer, Soluble root exudates of maize - influence of potassium supply and rhizosphere microorganisms, *Soil Biology & Biochemistry*, 16 (1984) 315-322.
- [240] P. Sundin, A. Valeur, S. Olsson, G. Odham, Interactions between bacteria-feeding nematodes and bacteria in the rape rhizosphere - effects on root exudation and distribution of bacteria, *Fems Microbiology Ecology*, 73 (1990) 13-22.
- [241] J.M. Lynch, J.M. Whipps, Substrate flow in the rhizosphere, *Plant and Soil*, 129 (1990) 1-10.
- [242] A.D. Rovira, Plant root exudates, *Botanical Review*, 35 (1969) 35-57.
- [243] N. Verbruggen, C. Hermans, H. Schat, Molecular mechanisms of metal hyperaccumulation in plants, *New Phytol.*, 181 (2009) 759-776.
- [244] S. Eapen, S.F. D'Souza, Prospects of genetic engineering of plants for phytoremediation of toxic metals, *Biotechnol. Adv.*, 23 (2005) 97-114.
- [245] P. Kučerová, M. Macková, T. Macek, Perspektivy fytoemediace při odstraňování organických polutantů a xenobiotik z životního prostředí, *Chemické listy*, 93 (1999) 19-26.
- [246] A. Bhandari, Environmental, W.R.I.E. Council, W.R.I.R.T.f. Soils, G.T. Committee, *Remediation Technologies for Soils and Groundwater*, American Society of Civil Engineers, 2007.
- [247] N. Terry, A.M. Zayed, M.P. de Souza, A.S. Tarun, Selenium in higher plants, *Annual Review of Plant Physiology and Plant Molecular Biology*, 51 (2000) 401-432.
- [248] J.L. Freeman, S.D. Lindblom, C.F. Quinn, S. Fakra, M.A. Marcus, E.A.H. Pilon-Smits, Selenium accumulation protects plants from herbivory by Orthoptera via toxicity and deterrence, *New Phytol.*, 175 (2007) 490-500.
- [249] B. Hanson, G.F. Garifullina, S.D. Lindblom, A. Wangeline, A. Ackley, K. Kramer, A.P. Norton, C.B. Lawrence, E.A.H. Pilon-Smits, Selenium accumulation

- protects *Brassica juncea* from invertebrate herbivory and fungal infection, *New Phytol.*, 159 (2003) 461-469.
- [250] C.F. Quinn, J.L. Freeman, M.L. Galeas, E.M. Klamper, E.A.H. Pilon-Smits, The role of selenium in protecting plants against prairie dog herbivory: implications for the evolution of selenium hyperaccumulation, *Oecologia*, 155 (2008) 267-275.
- [251] A.F. El Mehdawi, C.F. Quinn, E.A.H. Pilon-Smitst, Selenium Hyperaccumulators Facilitate Selenium-Tolerant Neighbors via Phytoenrichment and Reduced Herbivory, *Current Biology*, 21 (2011) 1440-1449.
- [252] X.Z. Yu, J.D. Gu, Differences in uptake and translocation of selenate and selenite by the weeping willow and hybrid willow, *Environmental Science and Pollution Research*, 15 (2008) 499-508.
- [253] Z.Q. Lin, R.S. Schemenauer, V. Cervinka, A. Zayed, A. Lee, N. Terry, Selenium volatilization from a soil-plant system for the remediation of contaminated water and soil in the San Joaquin Valley, *Journal of Environmental Quality*, 29 (2000) 1048-1056.
- [254] M.P. de Souza, C.M. Lytle, M.M. Mulholland, M.L. Otte, N. Terry, Selenium assimilation and volatilization from dimethylselenoniopropionate by Indian mustard, *Plant Physiology*, 122 (2000) 1281-1288.
- [255] M. Kieliszek, S. Blazejak, Selenium: Significance, and outlook for supplementation, *Nutrition*, 29 (2013) 713-718.
- [256] M. Montes-Bayon, M.J.D. Molet, E.B. Gonzalez, A. Sanz-Medel, Evaluation of different sample extraction strategies for selenium determination in selenium-enriched plants (*Allium sativum* and *Brassica juncea*) and Se speciation by HPLC-ICP-MS, *Talanta*, 68 (2006) 1287-1293.
- [257] M. Montes-Bayon, E.G. Yanes, C.P. de Leon, K. Jayasimhulu, A. Stalcup, J. Shann, J.A. Caruso, Initial studies of selenium speciation in *Brassica juncea* by LC with ICPMS and ES-MS detection: an approach for phytoremediation studies, *Anal. Chem.*, 74 (2002) 107-113.
- [258] K.M. Ervin, Experimental techniques in gas-phase ion thermochemistry, *Chem. Rev.*, 101 (2001) 391-444.
- [259] K. Sovová, K. Dryahina, P. Španěl, M. Kyncl, S. Civiš, A study of the composition of the products of laser-induced breakdown of hexogen, octogen, pentrite and trinitrotoluene using selected ion flow tube mass spectrometry and UV-Vis spectrometry, *Analyst*, 135 (2010) 1106-1114.
- [260] J. Kubišta, M. Civiš, P. Španěl, S. Civiš, Combining Fourier transform nuclear quadrupole resonance (FT-NQR) spectroscopy and mass spectrometry (MS) to study the electronic structure of titanocene dichlorides, *Analyst*, 137 (2012) 1338-1342.
- [261] J.L. Gottfried, Laser-induced plasma chemistry of the explosive RDX with various metallic nanoparticles, *Applied Optics*, 51 (2012) B13-B21.
- [262] J.L. Gottfried, Influence of metal substrates on the detection of explosive residues with laser-induced breakdown spectroscopy, *Applied Optics*, 52 (2013) B10-B19.
- [263] H. Cai, L. Tian, B. Huang, G. Yang, D. Guan, H. Huang, 1, 1-Diamino-2, 2-dinitroethene (FOX-7) nanocrystals embedded in mesoporous carbon FDU-15, *Microporous and Mesoporous Materials*, (2012).

Appendix A, Sovová *et al.* Int. J. Mass. Spectrom. 300 (2011)

31

Selected ion flow tube, SIFT, studies of the reactions of H_3O^+ , NO^+ and $\text{O}_2^{+\bullet}$ with six volatile phytogetic esters

Kristýna Sovová^{a,b}, Kseniya Dryahina^a, Patrik Španěl^{a,*}

^a*J. Heyrovský Institute of Physical Chemistry of Science, Academy of Science of the Czech Republic Dolejškova 3, 18223 Prague 8, Czech Republic*

^b*Department of Physical and Macromolecular Chemistry, Faculty of Science, Charles University, Albertov 2030, 128 40 Prague 2, Czech Republic*



Selected ion flow tube (SIFT) studies of the reactions of H_3O^+ , NO^+ and $\text{O}_2^{+\bullet}$ with six volatile phytogetic esters

Kristýna Sovová^{a,b}, Kseniya Dryahina^a, Patrik Španěl^{a,*}

^a J. Heyrovský Institute of Physical Chemistry of Science, Academy of Science of the Czech Republic, Dolejškova 3, 18223 Prague 8, Czech Republic

^b Department of Physical and Macromolecular Chemistry, Faculty of Science, Charles University, Albertov 2030, 12840 Prague 2, Czech Republic

ARTICLE INFO

Article history:

Received 25 October 2010

Received in revised form

29 November 2010

Accepted 30 November 2010

Available online 7 December 2010

Keywords:

SIFT-MS

Ion–molecule reactions

Plant esters

Proton transfer

Charge transfer

Adduct ion formation

ABSTRACT

The selected ion flow tube (SIFT) was used to study the reactions of the three SIFT-MS precursor ions H_3O^+ , NO^+ and $\text{O}_2^{+\bullet}$ with six phytogetic esters: hexyl acetate, phenethyl acetate, benzyl acetate, methyl salicylate, methyl benzoate and benzyl benzoate. These compounds are emitted into the atmosphere by various species of plants and play a role in communication between individual plants and also amongst different species. Thus, it is necessary to know the rate constants and branching ratios of the different ion products of these reactions for identification and quantification by SIFT-MS. The results of this study show that the reactions of H_3O^+ with the esters proceed via proton transfer, which is non-dissociative for methyl salicylate, entirely dissociative for benzyl benzoate and partly dissociative for the remaining four esters. All protonated esters readily associate with water molecules with the notable exception of methyl salicylate. All six NO^+ reactions result in formation of adduct ions in parallel with charge transfer or with reactions leading to fragment ions. All six $\text{O}_2^{+\bullet}$ reactions proceed by charge transfer with the production of one or two major fragment ions; the parent molecular radical cation is formed in three reactions only. Kinetic library entries allowing unambiguous quantification of the six esters by SIFT-MS are presented together with their experimental validation.

© 2010 Elsevier B.V. All rights reserved.

1. Introduction

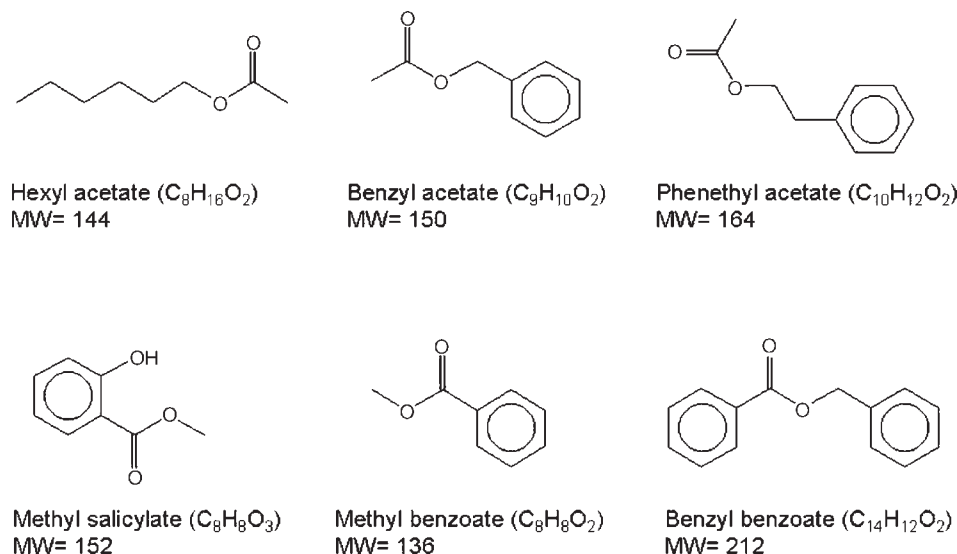
The phytogetic volatile organic compounds (VOCs) are generally small molecules that play an important role in various aspects of plant physiology including growth, development and communication between individual plants and also amongst different species. Some VOCs are released by plants continuously under normal physiological conditions, these include ethylene, isoprene, terpenes, sesquiterpenes [1] methanol [2] and some esters including benzyl acetate, phenethyl acetate, methyl benzoate and benzyl benzoate [3]. However, plants may respond to damage or externally induced stress by releasing specific types of molecules exemplified by hexyl acetate [4], and methyl salicylate that is known to be released by plants in response to damage caused by herbivores [5] and actually acts as an elicitor of foraging predatory mites [6]. The objective of the present study is to obtain kinetic data on ion molecule reactions of the six esters shown in Scheme 1 with the three commonly used SIFT-MS precursor (reagent) ions H_3O^+ , NO^+ and $\text{O}_2^{+\bullet}$.

The ion chemistry of these SIFT-MS precursor ions with these esters has not been previously studied except for methyl salicylate which has been studied by Iachetta et al. [8]. The earliest SIFT studies were concerned with a series of simpler esters [9]. SIFT-MS has been successfully used for measurements of the concentrations of some flavourant biogenic monoterpenes and sesquiterpenes emitted by vegetation such as myrcene, ocimene, α - and β -pinene, α - and γ -terpinene, 2- and 3-carene, *R*- and *S*-limonene and camphene [10,11]. In those studies it was observed that the H_3O^+ reactions with the monoterpenes (M), proceeded via proton transfer and result in formation of the protonated molecules MH^+ at an m/z value of 137 and partly of a fragment ion at an m/z of 81. The NO^+ reactions proceeded via charge transfer resulting mainly in the ionized monoterpenes $\text{C}_{10}\text{H}_{16}^+$ [10]. Thus, using H_3O^+ and NO^+ , SIFT-MS can be used to measure the total collective concentration of these terpenes in air. Their reactions with $\text{O}_2^{+\bullet}$ result in greater amount of fragments.

VOC emissions from plants, after extraction, can be very effectively studied using the well proven separation methods of gas and liquid chromatography [12,13]. The main shortcoming of these methods is that they cannot provide real time quantification, which is the main practical advantage of the SIFT-MS method. Proton-transfer reaction mass spectrometry, PTR-MS, which is in some aspects similar to SIFT-MS, is also capable of quantification of VOCs

* Corresponding author. Tel.: +420 2 6605 2112; fax: +420 2 8658 2307.

E-mail addresses: spanel@seznam.cz, patrik.spanel@jh-inst.cas.cz (P. Španěl).



Scheme 1. Chemical structures (according to [7]), summary formulas and molecular weights of the six studied phytogetic esters.

in real time [14] and has been used to analyse ethyl and methyl esters in the headspace of water and water/ethanol solutions [15]. PTR-MS has been also used to quantify total collective amounts of mono- and sesquiterpenes both in laboratory studies and in VOC emissions by trees [16,17].

One of the important objectives of the research of VOCs released by plants relates to the capability of various types of plants to clean up contaminated soil and water in the so-called phytoremediation process. One variant of this is phytovolatilization where plants take up contaminants from water or soil and release them into the atmosphere. The question is whether or not the final gaseous products resulting from phytovolatilization cause any secondary pollution of the environment. Thus, the present ion chemistry study involving plant VOCs will facilitate differentiation between the natural (baseline) plant volatiles and the possible additional volatile products resulting from the process of phytovolatilization.

2. Experimental methods

The SIFT technique [18] has been described many times for determination of the rate constants (often called rate coefficients in the field of ion chemistry) and ion product distributions of the reaction of H₃O⁺, NO⁺ and O₂⁺ with organic compounds [8–11,18,19]. Thus, only the specific detail of the present experimental procedure, are outlined below.

2.1. Determination of the branching ratios and the rate constants of ion-molecule reactions

In order to determine the product ions and their branching ratios, a sample mixture of dry air and a trace amount (typically less than 10 ppm) of vapour of a compound of interest (one of the six esters purchased from Sigma–Aldrich with stated purity of >99%) was introduced into the SIFT instrument (*Profile 3* SIFT-MS manufactured by Instrument Science Limited, Crewe, UK) via a heated calibrated capillary and full scan mass spectra were acquired whilst each of the three selected precursor ions were alternately injected into the helium carrier gas. The *m/z* mass spectral range was chosen as 10–250 covering the molecular weights of the six chosen esters and allowing for possible formation of adduct ions. For each precursor ion, five mass spectra were obtained with a total integration time of 60 s. The major ion products were identified and their count rates were precisely determined in separate experiments using the

multi-ion monitoring (MIM) mode [18]. In order to determine the primary product branching ratios of the reactions, it is required to plot the percentages of the individual product ions on a linear scale as a function of the sample mixture flow rate determined accordingly to the exponential reduction of the precursor ion count rate (see such a plot for hexyl acetate in Fig. 1). By extrapolating to zero flow (i.e., estimating the limit at zero sample concentration) the true primary branching ratios, excluding any secondary reactions can be obtained. Only product ions with resulting branching ratio greater than 5% are reported.

It is well established that proton transfer reactions of H₃O⁺ proceed at the collisional rate as described by the collisional rate coefficient *k_c* when these reactions are exothermic by more than 40 kJ/mol [20]. Thus, the rate constants for the reactions of H₃O⁺ were calculated as collisional (*k_c*) according to Su and Chesnavich [21] using the dipole moment and polarisability data from [22–25]. The rate constants for the reactions with NO⁺ and O₂⁺ (*k*) were then derived from their experimentally derived decay rates relatively to that for the H₃O⁺ reaction [26] by injecting all three precursors simultaneously and allowing them to react with the sample introduced at varied concentrations. The count rates of H₃O⁺, NO⁺ and

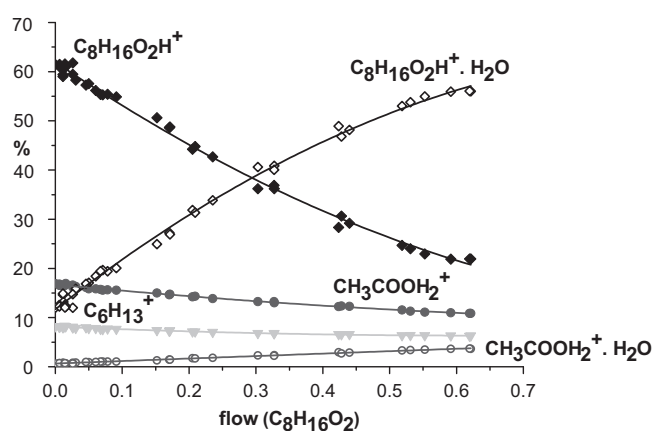


Fig. 1. A plot of percentages of individual product ions as a function of the flow rate of a mixture containing trace amount of hexyl acetate in humid air introduced into SIFT when H₃O⁺ precursor ions are injected. The primary product branching ratios are obtained by extrapolating the lines to zero flow. Note that the sample flow rate is in relative units when flow = 1 corresponds to the e-fold reduction of the count rate of H₃O⁺ due to the reaction with the studied compound.

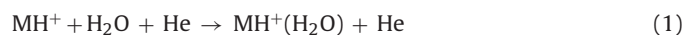
O_2^{+*} were plotted on a semi-logarithmic scale as functions of the sample flow rate and the rate constants (k) for the NO^+ and O_2^{+*} reactions were determined from the relative slopes of these plots.

2.2. Kinetics of the ion chemistry involving water molecules: determination of three-body association rate constants

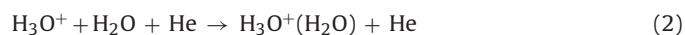
The reactions of most molecules M with H_3O^+ precursor ions generally result in the formation of nascent MH^+ ions. In the presence of water molecules, the H_3O^+ ions are partially converted to hydrated hydronium ions $H_3O^+(H_2O)_{1,2,3}$. These cluster ions can act as additional precursors and produce additional ion products like $MH^+(H_2O)_{1,2,3}$ via ligand switching reactions. The MH^+ product ions of proton transfer can also directly associate with H_2O similarly forming ions $MH^+(H_2O)_{1,2,3}$. Thus, the ion chemistry, which is important for real time and accurate quantification by SIFT-MS, is influenced by the presence of water vapour and it is necessary to account for this [27].

In SIFT-MS measurements using H_3O^+ precursor ions it is usually the case that both MH^+ and its hydrates $MH^+(H_2O)_{1,2,3}$ are formed. The ratio of the count rates of these ions change with the sample flow rate and the sample humidity and by recording these relative count rates the efficiency of clustering as a fundamental parameter, related to elementary rate constants, can be obtained. The objective of this section is to indicate the kinetic principles and the procedure adopted to analyse the experimental data.

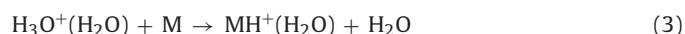
Three-body rate constants for the association reactions of MH^+ ions with H_2O molecules in helium, k_{MH^+} describe the rate of hydration of the protonated molecules in the gas phase:



In order to obtain these rate constants experimentally it is important to consider the role of $H_3O^+(H_2O)$ ions formed in the following three-body reaction described by the rate constant $k_{H_3O^+}$



The three body-rate constant for reaction (2) has been previously determined to be $k_{H_3O^+} = 6 \times 10^{-28} \text{ cm}^6 \text{ s}^{-1}$ [27]. The cluster ions formed in reaction (2) contribute to the formation of $MH^+(H_2O)$ ions via ligand switching with M :



So these hydrated protonated molecules $MH^+(H_2O)$ can be produced by two parallel routes, viz reactions (1) and (3). The separate contribution of reaction (3) can be quantified by a parameter S_{eff} representing the contribution of the switching reactions to their formation taken relatively to the formation of hydrated hydronium ions [27]:

$$S_{eff} = \frac{\ln([MH^+] + [MH^+(H_2O)_{1,2,3}]_s/[MH^+])}{\ln([H_3O^+]_0/[H_3O^+])} \quad (4)$$

Here, $[MH^+]$ and $[H_3O^+]$ (or [19]) are the count rates of MH^+ and H_3O^+ ions detected by the downstream mass spectrometer, tacitly assumed to be proportional to the concentrations of the ions at the end of the flow tube. $[H_3O^+]_0$ is the count rate observed in the absence of water vapour, which is also equivalent to the sum of count rates of $H_3O^+(H_2O)_{0,1,2,3}$. The subscript s denotes the theoretical count rates of the $MH^+(H_2O)_{1,2,3}$ ions formed in switching reactions only, as calculated from the linearised kinetic equation (see [27]):

$$[MH^+(H_2O)_{1,2,3}]_s = [M]t \left([37] \frac{k_{37}}{2} + [55] \frac{k_{55}}{2} + [73] \frac{k_{73}}{2} \right) \quad (5)$$

where t is reaction time, k_{37} , k_{55} and k_{73} are the rate constants for the switching reactions of the respective hydrated hydronium ions with M and [37], [55], and [73] are the actual count rates of the

$H_3O^+(H_2O)_{1,2,3}$ ions as observed in the experiments. The divisors 2 in Eq. (5) describe the fact that due to their continuous formation in the flow tube [27], reaction times of the $H_3O^+(H_2O)_{1,2,3}$ ions are approximately half the reaction time of H_3O^+ . Thus:

$$S_{eff} = \frac{\ln(1 + ([M]t([37](k_{37}/2) + [55](k_{55}/2) + [73](k_{73}/2))/([M]t \cdot [19]k_{19}))}{\ln(1 + (([37] + [55] + [73])/[19]))} \quad (6)$$

By simplification of this expression the S_{eff} parameter can be calculated from the known rate constants and the experimental data as follows:

$$S_{eff} = \frac{\ln(1 + (([37](k_{37}/2) + [55](k_{55}/2) + [73](k_{73}/2))/([19]k_{19}))}{\ln(1 + (([37] + [55] + [73])/[19]))} \quad (7)$$

Similarly, the total contribution of both parallel routes of formation of the protonated hydrated ions, i.e., via the association reaction (1) and via the above switching reactions relative to that for the reaction of H_3O^+ with H_2O , can be described by a coefficient A_{eff} :

$$A_{eff} = \frac{2 \ln([MH^+] + [MH^+(H_2O)_{1,2,3}]_A)/([MH^+])}{\ln([H_3O^+]_0/[H_3O^+])} \quad (8)$$

Again, the subscript 0 indicates the respective ion count rate in the absence of water vapour in the helium carrier gas. Thus, the $[MH^+]_0$ can be acquired during analysis as the sum of the $[MH^+]$ and $[MH^+(H_2O)_n]$ count rates (same as the procedure to determine $[H_3O^+]_0$). The factor 2 in Eq. (8) is again a compensation of the reaction time for continuously formed MH^+ ions, which is half of that for H_3O^+ . Because A_{eff} is expressed in the terms of ion count rates only, it can be directly obtained from the experimental data such as mass spectra. An important test is that the experimental value of A_{eff} is invariant with $[M]$ and also invariant with $[H_2O]$. The value of A_{eff} has a very simple interpretation as it describes how much faster clustering of MH^+ is compared to clustering of H_3O^+ . Mathematically A_{eff} so defined and expressed by Eq. (8) agrees with A_{eff} as used in [27] however the verbal definition of A_{eff} in the previous paper [27] was not strictly speaking correct because it incorrectly neglected the contribution of switching.

Now the true contribution of association without switching is simply described as $A_{eff} - S_{eff}$ and the value of three-body association rate constant can be calculated as:

$$k_{MH^+} = (A_{eff} - S_{eff}) \cdot k_{H_3O^+} \quad (9)$$

So k_{MH^+} obtained from Eq. (9) is a fundamental three body association rate constant anchored to the known value of $k_{H_3O^+}$. Numerical examples of calculations of A_{eff} and S_{eff} are given in Appendix A.

3. Results and discussion

3.1. Rate constants for the H_3O^+ , NO^+ and O_2^{+*} reactions

The calculated rate constants, k_c , for the reactions of H_3O^+ with the esters and the experimentally determined rate constants, k , for the NO^+ and O_2^{+*} are summarized in Table 1. As can be seen, all experimental rate constants are within the experimental uncertainty $\pm 20\%$ equivalent to the theoretical collisional k_c values. The only exceptions are benzyl acetate where the NO^+ reaction proceeds only at 60% of k_c and methyl benzoate for which O_2^{+*} reaction apparently proceeds faster than k_c . A possible explanation for this is that the H_3O^+ rate constant is slower than k_c by about 20% or that the Su and Chesnavich theory is not precise for interactions of ions with geometrically large molecules. Unfortunately the current experimental method does not allow absolute determinations of the concentrations of volatile compounds such as methyl benzoate to accuracy better than 20%.

Table 1
Rate constants for the reactions of H₃O⁺, NO⁺ and O₂^{•+} with the six esters indicated, given in the units of 10⁻⁹ cm³ s⁻¹. Also given are the molecular weights (MW), polarisabilities, α, and the dipole moments, μ_r, of these esters.

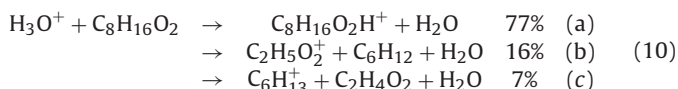
	Molecule	MW	α (10 ⁻²⁴ cm ³) ^a	μ _r (D) ^a	H ₃ O ⁺ [k _c]	NO ⁺ k [k _c]	O ₂ ^{•+} k [k _c]
Hexyl acetate	C ₈ H ₁₆ O ₂	144	16.20	1.86	[3.2]	2.6 [2.6]	2.3 [2.6]
Benzyl acetate	C ₉ H ₁₀ O ₂	150	16.90	2.00	[3.4]	1.9 [2.8]	2.5 [2.7]
Phenethyl acetate	C ₁₀ H ₁₂ O ₂	164	18.56	2.04	[3.5]	2.9 [2.8]	3.0 [2.8]
Methyl salicylate	C ₈ H ₈ O ₃	152	15.82	2.53	[3.8]	3.2 [3.1]	3.5 [3.0]
Methyl benzoate	C ₈ H ₈ O ₂	136	15.07	2.01	[3.3]	2.4 [2.7]	3.5 [2.7]
Benzyl benzoate	C ₁₄ H ₁₂ O ₂	212	24.78	2.08	[3.7]	2.5 [3.1]	2.8 [3.0]

^a Values of α and μ_r are taken from the literature [22–25].

3.2. Ion products of the H₃O⁺ reactions

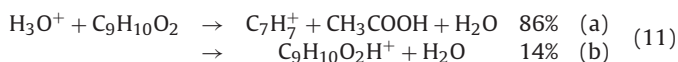
The reactions of five of the six esters with H₃O⁺ proceed via the formation of a protonated molecule, MH⁺, which is the only ion product for the methyl salicylate reaction (in agreement with the previous study [8]) and the major ion product for the hexyl acetate and methyl benzoate. Benzyl benzoate reaction is an exception to this rule as it results only in formation of fragment product ions.

Partial fragmentation of the nascent MH⁺ ions occurs in the hexyl acetate reaction leading to the formation of C₂H₅O₂⁺ (*m/z* 61) and C₆H₁₃⁺ (*m/z* 85):



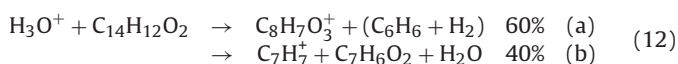
Note the likely release of a hexene molecule in reaction (10b) and an acetic acid molecule in reaction (10c).

The major product ion of benzyl acetate is C₇H₇⁺ (*m/z* 91):



The C₇H₇⁺ fragment is usually observed for electron ionisation (EI) mass spectra of aromatic compounds and is called the tropylium ion [28]. It is a heptagonal and planar, cyclic ion with 6 π-electrons. Note the parallel release of an acetic acid molecule. The minority product (11b) is the protonated parent molecule MH⁺.

The tropylium ion is also formed in the benzyl benzoate reaction. Note that MH⁺ is not produced at observable intensity in this reaction, which leads to two ion products with *m/z* identical to the products of the benzyl acetate reaction (*m/z* 151 and *m/z* 91). However the most plausible structure of the *m/z* 151 ion is C₈H₇O₃⁺ implying that the water molecule from H₃O⁺ is incorporated into the ion product:



Note that formation of C₉H₁₁O₂⁺ ion after proton transfer would require a very unlikely neutral product C₅H₂.

The H₃O⁺ reaction with phenethyl acetate produces the C₈H₉⁺ ion (80%) and, again, an acetic acid molecule and the protonated

molecular ion C₁₀H₁₂O₂H⁺ (20%).

The rate constants of the three-body association reactions of the MH⁺ ions with water molecules (1), as determined according Section 2.2 (see also examples in Appendix A) are given in Table 2. The three protonated acetates form water clusters very efficiently (*A_{eff}* 6.6–21; note that *A_{eff}* for protonated acetone is 3.1), the *k_{MH+}* being fastest for hexyl acetate, presumably because of the aliphatic chain has many vibrational degrees of freedom. Protonated methyl benzoate and the *m/z* product of the benzyl benzoate reaction (C₈H₇O₃⁺) associate relatively slowly (*A_{eff}* 2.2 to 2.6) even though the proton affinity of methyl benzoate is very similar to that of hexyl acetate and thus any difference cannot be simply related to the energetics of a proton bound structures. A possible explanation why association of the protonated benzoates is slower than association of protonated acetates can be that it is due to steric hindrance when the charge is located in the inner parts of the ion and not on an accessible functional group, but this would have to be substantiated by quantum chemical modelling. Protonated methyl salicylate represents a very unusual exception in that, according to the value of *k_{MH+}*, this ion does not associate with H₂O (see also the mass spectrum in Fig. 2 demonstrating the absence of an association product). Note that the PA of methyl salicylate is somewhat greater than that of the other esters; however, the difference is only 5–10 kJ/mol, but still much greater than the PA of H₂O at 690 kJ/mol. Again, we can only hypothesise that the reason for this observed anomaly is steric hindrance and that the charge is not located on an accessible functional group.

3.3. Ion products of the NO⁺ reactions

The reactions of NO⁺ with the esters proceed via three-body association reactions forming M·NO⁺ adduct ions or via charge transfer that in some cases results in fragmentation products [18]. The reaction with methyl salicylate proceeds as simple non-dissociative charge transfer in agreement with the previous study [8]. The benzyl benzoate reaction leads to several fragment ions including the tropylium ion. The reaction of NO⁺ with hexyl acetate is an example of straightforward simple three-body association:

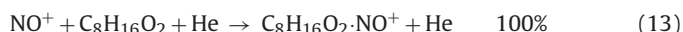


Table 2
Kinetic data for the formation of hydrates of the protonated esters indicated, as formed by ligand switching and three-body association.

Compound	P.A. (kJ/mol) ^a	<i>S_{eff}</i> ^b	<i>A_{eff}</i> ^c	<i>k_{MH+}</i> (10 ⁻²⁷ cm ⁶ s ⁻¹) ^d
Hexyl acetate	845	0.4	21.0	12.4
Benzyl acetate	n.a.	0.4	10.7	6.2
Phenethyl acetate	n.a.	0.4	6.6	3.7
Methyl salicylate	855	0.4	0.3	<0.1
Methyl benzoate	850	0.4	2.6	1.3
C ₈ H ₇ O ₃ ^{•+} ^e	n.a.	0.4	2.2	1.1

^a Proton affinities as taken from [7] are given where available; n.a. means that the P.A. is not known.

^b Ligand switching efficiencies calculated from Eq. (7).

^c Association efficiencies obtained from experimental data using Eq. (8).

^d Three body association rate constants calculated from Eq. (9).

^e Protonated benzyl benzoate was not observed, reported values refer to the fragment ion indicated.

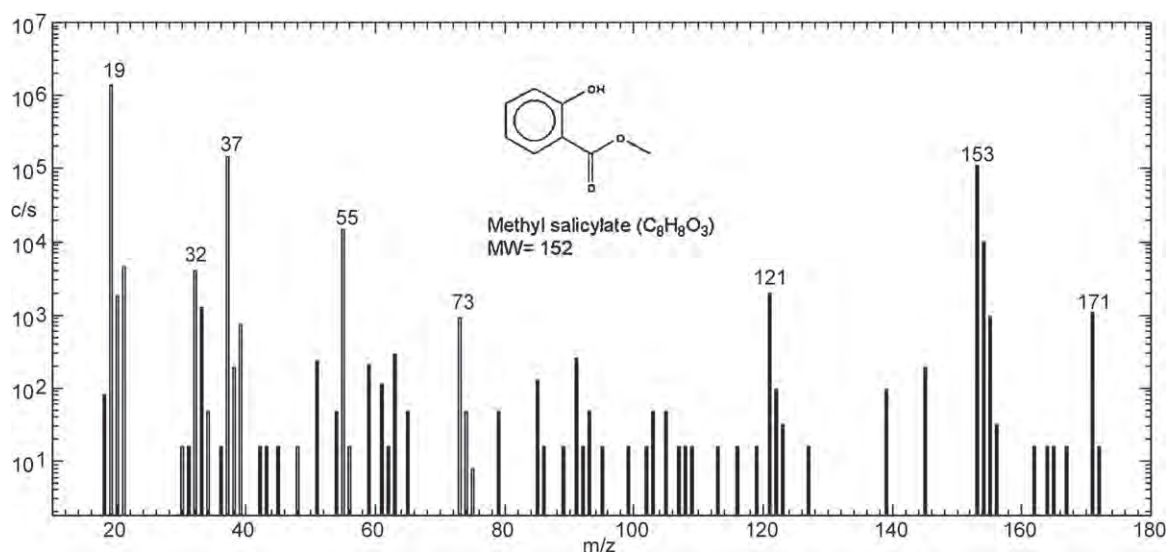
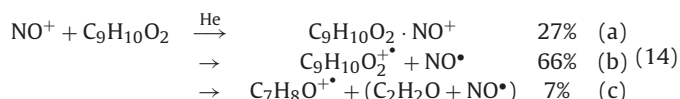


Fig. 2. The SIFT-MS spectrum obtained using the H_3O^+ precursor ions when methyl salicylate is introduced into the helium carrier gas; ion count rates are given on semi-logarithmic scale as a function of m/z . Note the characteristic ion products at m/z 121, 153 and the relatively small peak of the hydrated protonated parent molecule at m/z 171 that originates entirely from ligand switching reactions involving the hydrated hydronium ions at m/z 37, 55 and 73.

The benzyl acetate reaction:

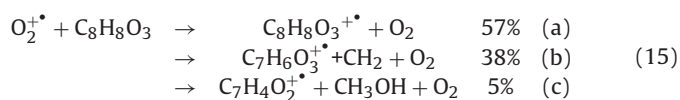


is an example of the three-body association reaction occurring in parallel with charge transfer producing the parent radical cation $\text{M}^+\cdot$. Unfortunately no values of ionisation potentials are available in the current literature for any of the six esters. However, on the basis of the present data we can conclude, that the ionisation potentials of benzyl acetate and methyl salicylate are less than ionisation potential of NO, 9.25 eV, because otherwise charge transfer would be endothermic and could not occur at room temperature.

The minor channel (14c) can be seen as a dissociative charge transfer or as a transfer of $\text{C}_2\text{H}_2\text{O}^-$ ion forming a neutral product $\text{C}_7\text{H}_2\text{ONO} \cdot$.

3.4. Ion products of the $\text{O}_2^+\cdot$ reactions

Reactions with the $\text{O}_2^+\cdot$ precursor ion mostly proceed either via non-dissociative charge transfer producing the parent radical cation $\text{M}^+\cdot$ or via dissociative charge transfer reactions resulting in several fragment ions [18]. The methyl salicylate reactions exemplifies both of these processes:



Note that our experimental data indicate that two fragment ions are produced (15b) and (15c) in addition to non-dissociative charge transfer that was previously reported by Iachetta et al. [8] to be the only reaction channel. It is worthy of note that all products of the $\text{O}_2^+\cdot$ reactions given in Table 3 are also present on the EI spectra [7] with the exception of benzyl benzoate, which on reaction with $\text{O}_2^+\cdot$ forms fragments that are not seen on EI spectra.

3.5. Avoiding m/z overlaps and optimised kinetic library entries for SIFT-MS

The SIFT-MS method of determination of absolute concentrations in real time is based on obtaining the ratio of the sum of several

product ion count rates to the sum of the precursor ion count rates weighted by their reaction rate constants. Additional coefficients can be also applied to account for special circumstances such as overlaps of contributions from different characteristic ions at the same m/z value [29]. In analysis, these calculations are carried out by the SIFT-MS analytic software on-line taking the rate constants and other coefficients from the kinetic library [29]. Our objective was to construct entries for this kinetics library (i.e., define the sets of m/z values of product ions needed for quantification of the six esters together with the appropriate rate constants and with coefficients to be applied in order to minimise cross sensitivity between different compounds. These library entries will thus allow selective measurement of the concentrations of these six esters.

In the course of this work we initially simply chose to sum the count rates of all product ions of the H_3O^+ reactions given in Table 3 together with their hydrates. This was done by listing the product ions in the kinetic library with all f_p coefficients (used to multiply the corresponding ion count rates) set as 1.0. Validations of this initial kinetic library using reference mixtures of the six esters in air at approximately 10 ppm concentrations indicated m/z overlaps between hexyl acetate and phenethyl acetate and then amongst the group of benzoates (see Fig. 3a). Only methyl salicylate was quantified without any signs of overlap. The m/z overlaps between hexyl acetate and phenethyl acetate was caused due to the m/z 61 and 79 ions. The product branching ratios of m/z 61 and its hydrate 79 was less than 5% for phenethyl acetate (and this it does not even appear in Table 3) and 16% for hexyl acetate (see Table 3). To avoid this overlap problem we have excluded these m/z values from the final kinetic library entry (given in Table 4) for phenethyl acetate. Other overlaps amongst benzoates were caused by the same m/z values of the ion products of the benzyl acetate and benzyl benzoate reactions (91, 151, and 169). The methyl benzoate reaction leads to a small m/z 91 product (less than 2%) and thus we excluded this product ion from the methyl benzoate entry.

Somewhat more challenging was to resolve the m/z overlaps between benzyl acetate and benzyl benzoate. The three main ion products (including one hydrate) of the reactions of these two esters are the same (m/z 91, 151 and 169); however the percentages of product branching ratios are significantly different (Table 3). Thus, we have exploited this difference in order to distinguish these

Table 3

The product ions and the corresponding branching ratios for the reactions of H₃O⁺, NO⁺ and O₂⁺⁺ with the six esters in helium carrier gas at 300 K.

Compound	MW	Formula	H ₃ O ⁺	<i>m/z</i> ^a	NO ⁺	<i>m/z</i>	O ₂ ⁺⁺	<i>m/z</i> ^a	
Hexyl acetate	144	C ₈ H ₁₆ O ₂	77% C ₈ H ₁₆ O ₂ H ⁺	145	(163)	100% C ₈ H ₁₆ O ₂ NO ⁺	174	73% C ₆ H ₁₂ O ₃ ⁺⁺	84
			16% CH ₃ COOH ₂ ⁺	61	(79)			27% C ₂ H ₅ O ₂ ⁺	61
			7% C ₆ H ₁₃ ⁺	85					(79)
Benzyl acetate	150	C ₉ H ₁₀ O ₂	86% C ₇ H ₇ ⁺	91	(169)	66% C ₉ H ₁₀ O ₂ ⁺⁺	150	88% C ₇ H ₈ O ⁺⁺	108
			14% C ₉ H ₁₀ O ₂ H ⁺	151		27% C ₉ H ₁₀ O ₂ NO ⁺	180	12% C ₉ H ₁₀ O ₂ ⁺⁺	150
						7% C ₇ H ₈ O ⁺⁺	108		
Phenethyl acetate	164	C ₁₀ H ₁₂ O ₂	80% C ₈ H ₉ ⁺	105	(183)	84% C ₈ H ₈ ⁺⁺	104	100% C ₈ H ₈ ⁺⁺	104
			20% C ₁₀ H ₁₂ O ₂ H ⁺	165		16% C ₁₀ H ₁₂ O ₂ NO ⁺	194		
Methyl salicylate	152	C ₈ H ₈ O ₃	100% C ₈ H ₈ O ₃ H ⁺	153	(171)	100% C ₈ H ₈ O ₃ ⁺⁺	152	57% C ₈ H ₈ O ₃ ⁺⁺	152
Methyl benzoate	136	C ₈ H ₈ O ₂	93% C ₈ H ₈ O ₂ H ⁺	137	(155)	41% C ₈ H ₉ ⁺	105	38% C ₇ H ₆ O ₃ ⁺⁺	138
			7% C ₈ H ₉ ⁺	105		53% C ₈ H ₈ O ₂ NO ⁺	166	5% C ₇ H ₄ O ₂ ⁺⁺	120
						6% C ₈ H ₈ O ₂ ⁺⁺	136	62% C ₈ H ₈ O ₂ ⁺⁺	136
Benzyl benzoate	212	C ₁₄ H ₁₂ O ₂	60% C ₈ H ₇ O ₃ ⁺	151	(169)	45% C ₉ H ₁₀ O ₂ NO ⁺	180	46% C ₇ H ₈ O ⁺⁺	108
			40% C ₇ H ₇ ⁺	91		25% C ₇ H ₇ O ⁺	107	23% C ₇ H ₆ O ₂ ⁺⁺	122
						18% C ₇ H ₅ O ⁺	105	10% C ₉ H ₁₀ O ₂ ⁺⁺	150
						12% C ₇ H ₇ ⁺	91	16% C ₆ H ₇ ⁺	79

^a *m/z* of the primary products with branching ratios >5% only are given (*m/z* of hydrated product ions are given in parentheses).

two compounds. The main idea in constructing the final kinetic library entries for these compounds is to find linear combinations of ion product count rates that would allow selective quantification of different compounds. Note that for this purpose the ion count

rates of hydrated ions (when these are formed) should be added to the ion count rates of the corresponding primary product ions in order to ensure that the results will be valid for any concentration of H₂O in sample. Such linear combination can be found by the

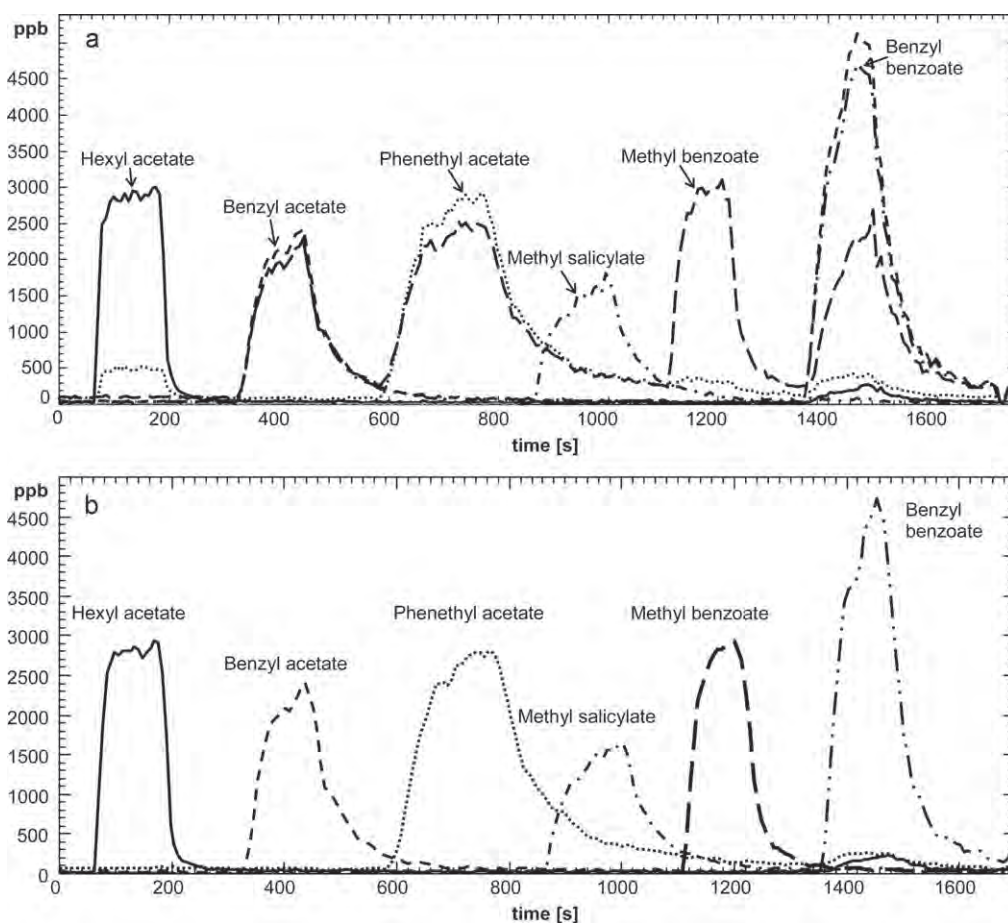


Fig. 3. (a) Time profile of the concentration of the six esters calculated (in ppb) simply from the sum of the characteristic product ions in a validation experiment when diluted samples of reference compounds are introduced sequentially. Note that overlaps between *m/z* values of products cause cross-sensitivity between hexyl acetate and phenethyl acetate and amongst the group of benzoates. (b) The same raw experimental data evaluated using the optimised kinetic library as given in Table 4; note that cross sensitivity has been dramatically reduced.

Table 4

SIFT-MS kinetics library in the format required by the SIFT-MS software for on-line calculations of the concentrations of the six esters, optimised for minimum cross sensitivity (see the text for further discussion).

Hexyl acetate (H ₃ O ⁺)			Phenethyl acetate (H ₃ O ⁺)			Methyl salicylate (H ₃ O ⁺)			Methyl benzoate (H ₃ O ⁺)			Benzyl benzoate (H ₃ O ⁺)					
4 Precursors			4 Precursors			4 Precursors			4 Precursors			4 Precursors					
19	3.2e-9	1.0	19	3.5e-9	1.0	19	3.8e-9	1.0	19	3.3e-9	1.0	19	3.7e-9	1.0			
37	2.4e-9	1.0	37	2.6e-9	1.0	37	2.9e-9	1.0	37	2.5e-9	1.0	37	2.8e-9	1.0			
55	2.1e-9	1.0	55	2.2e-9	1.0	55	2.5e-9	1.0	55	2.2e-9	1.0	55	2.4e-9	1.0			
73	1.9e-9	1.0	73	2.0e-9	1.0	73	2.2e-9	1.0	73	2.0e-9	1.0	73	2.1e-9	1.0			
Hexyl acetate (H ₃ O ⁺)			Benzyl acetate (H ₃ O ⁺)			Phenethyl acetate (H ₃ O ⁺)			Methyl salicylate (H ₃ O ⁺)			Methyl benzoate (H ₃ O ⁺)			Benzyl benzoate (H ₃ O ⁺)		
5 Products			3 Products			6 Products			3 Products			3 Products			3 Products		
61	1.0		91	1.38		105	1.088		121	1.077		137	1.236		91	-0.30	
79	1.0		151	-0.86		137	-0.06		153	1.088		155	1.088		151	1.96	
85	1.066		169	-0.86		155	-0.06		171	1.088		153	-0.16		169	1.96	
145	1.088					163	-0.01										
163	1.088					165	1.1										
						183	1.1										

simple solution of a set of the linear equations:

$$\begin{aligned} A &= f_A [91]_A + g_A [151 + 169]_A \quad (\text{a}) \\ B &= f_B [91]_B + g_B [151 + 169]_B \quad (\text{b}) \end{aligned} \quad (16)$$

Here A represents the linear combination used to quantify benzyl acetate and B represents the linear combination to quantify benzyl benzoate. The square brackets indicate the product ion count rates registered when the compound indicated by subscripts A (benzyl acetate) and B (benzyl benzoate) is introduced into SIFT-MS. The constraints on the coefficients f and g (treated as the unknowns in the set of equations) are given by the requirement of calculating zero concentration of A when only B is introduced and vice versa:

$$\begin{aligned} 0 &= f_A [91]_B + g_A [151 + 169]_B \quad (\text{a}) \\ 0 &= f_B [91]_A + g_B [151 + 169]_A \quad (\text{b}) \end{aligned} \quad (17)$$

Now it is possible to calculate f and g coefficients from the experimental data of ion count rates using the pure compounds. For the case of benzyl acetate and benzyl benzoate the results are: $f_A = 1.38$, $g_A = -0.86$, $f_B = -0.30$ and $g_B = 1.96$. Details of calculation for these two compounds are given in Appendix B. Similar experiments and calculations were used to resolve other m/z overlaps. The final kinetics library entries as given in Table 4 were then used to calculate concentrations of all these six esters in the H₃O⁺ validation experiment and, as can be seen in Fig. 3b, cross sensitivity has been successfully minimised using this kinetic library. Finally, it is worthy of a note that the m/z 91 product of benzyl acetate overlaps with the H₃O⁺(H₂O)₄ water cluster and thus NO⁺ that leads to m/z 150 and 180 characteristic product ions is a more suitable precursor ion for this compound, however m/z 180 is a main product of benzyl benzoate and thus only m/z 150 should be used with an appropriate coefficient.

4. Concluding remarks

The data obtained in this study allow SIFT-MS analyses of phyto-genic esters in the presence of water vapour. On the basis of these data it is now possible to use SIFT-MS to study ester emissions from plants and possibly also from other organisms such as bacteria. The combination of the three different precursor ions used for SIFT-MS provides a tool to diminish ambiguity and to positive identify the esters in mixtures of volatile compounds in air. Protonated esters have a propensity to form cluster ions with water molecules and the rate constants for such reactions have been also obtained in this study. As a practical outcome, in addition to fundamental ion kinetics data, SIFT-MS kinetic library entries have been constructed

that allow selective quantification of these esters in spite of some overlaps between the m/z values of characteristic product ions.

Acknowledgements

We thank Violetta Shestivska for introducing us to the field of phytoremediation and her help with some of the present experiments, to Ondřej Zemek for providing reference samples of the esters and to David Smith for his careful reading and editing of the manuscript. We gratefully acknowledge financial support by the Grant Agency of the Czech Republic (projects number 202/09/0800 and 203/09/0256) and by Grant Agency of Charles University (project GAUK 32010).

Appendix A. Numerical examples of the calculations of the parameters S_{eff} , A_{eff} and k_{MH^+} for hexyl acetate and methyl salicylate

The experimental precursor and product ion count rates (corrected for mass discrimination and differential diffusion) for H₃O⁺ reactions of hexyl acetate and methyl salicylate are given in Table A.1. The data were acquired in the MIM mode, as described in Section 2.1. The symbols k_{19} , k_{37} , k_{55} and k_{73} indicate the rate constants for the proton transfer reaction and for the switching reactions of the respective hydrated hydronium ions with M and are calculated according Su and Chesnavich [21]. Square brackets [19], [37], [55], and [73] indicate the actual count rates of the H₃O⁺(H₂O)_{1,2,3} ions and [MH⁺] and [MH⁺(H₂O)] are the actual count rates of the protonated molecule of a sample and its hydrate.

Assigning these numerical values for hexyl acetate to Eq. (7) gives the value $S_{eff} = 0.4$. Using the values from Table A.1 in Eq. (8) gives.

$$A_{eff} = \frac{2 \ln(\frac{[198802 + 337378]_0}{[198802]})}{\ln(\frac{[1108200 + 96514 + 12455 + 1018]_0}{[1108200]})} = 21.0 \quad (\text{A.1})$$

Finally combining these two numbers with the known rate constant gives $k_{MH^+} = (21.0 - 0.4) \cdot 6.0 \cdot 10^{-28} = 12.4 \cdot 10^{-27} \text{ cm}^6 \text{ s}^{-1}$.

Analogical calculation for methyl salicylate provides according to Eq. (7) the same result for $S_{eff} = 0.4$ however the value of A_{eff} according to Eq. (8) is much smaller:

$$A_{eff} = \frac{2 \ln(\frac{[135510 + 2029]_0}{[135510]})}{\ln(\frac{[1856555 + 177350 + 14608 + 703]_0}{[1856555]})} = 0.3 \quad (\text{A.2})$$

The fact that A_{eff} is very close to S_{eff} (actually somewhat smaller in this example) means that within the experimental error association does not measurably contribute to the formation of the hydrated protonated ions.

Table A.1
Experimental count rates and rate constants used in this example.

M	c/s				k (10 ⁻⁹ cm ³ s ⁻¹)					c/s[MH ⁺ (H ₂ O)]
	[19]	[37]	[55]	[73]	k ₁₉	k ₃₇	k ₅₅	k ₇₃	[MH ⁺]	
Hexyl acetate	1108200	96514	12455	1018	3.2	2.4	2.1	1.9	198802	337379
Methyl salicylate	1856555	177350	14608	733	3.8	2.9	2.5	2.2	135510	2029

Appendix B. Numerical examples illustrating optimisation of the kinetic library entries for minimisation of the effect of overlaps.

This appendix illustrate the numerical calculations used in obtaining the *f_p* coefficients for benzyl acetate and benzyl benzoate accounting for the overlaps of the ion products at *m/z* 91, 151 and 169 according to the procedure explained in Section 3.5. The experimental count rates (in *c/s* after correction for mass discrimination and differential diffusion) were obtained when benzyl acetate (symbol A) was introduced as [91]_A = 8606, [151]_A = 609, [169]_A = 746 and when benzyl benzoate (symbol B) was introduced as [91]_B = 8822, [151]_B = 11088, [169]_B = 3318.

The solution to a set of linear equations (17a) and (17b) for these count rates is

$$f_A = -g_A \frac{[151 + 169]_B}{[91]_B} = -g_A \cdot 1.63 \tag{B.1}$$

$$f_B = -g_B \frac{[151 + 169]_A}{[91]_A} = -g_B \cdot 0.157 \tag{B.2}$$

The coefficients *g_A*, *g_B*, *f_A* and *f_B* can now be calculated by solving the following set of equations obtained from (16a) and (16b):

$$9961 = -g_A \cdot 12698 \tag{B.3}$$

$$23228 = -g_B \cdot 13017 \tag{B.4}$$

as *f_A* = 1.28, *g_A* = -0.78, *f_B* = -0.28, *g_B* = 1.78.

Finally in order to produce practically applicable accurate kinetics library it is important to account for the isotopic abundance of ¹³C by multiplying these coefficient by 1.077 for *m/z* 91 and 1.099 for *m/z* 151 and 169.

References

[1] J. Peñuelas, J. Llusià, *Biologia Plantarum* 41 (1998) 139–143.
 [2] R. Fall, A.A. Benson, *Trends in Plant Science* 1 (1996) 296–301.
 [3] G. König, M. Brunda, *Atmospheric Environment* 29 (1995) 861–874.

[4] R. Fall, T. Karl, A. Hansel, A. Jordan, W. Lindinger, *Journal of Geophysical Research-Atmospheres* 104 (1999) 15963–15974.
 [5] M.R. Kant, P.M. Bleeker, M. Van Wijk, R.C. Schuurink, M.A. Haring, *Plant volatiles in defence*, in: *Plant Innate Immunity*, 2009, pp. 613–666.
 [6] J.G. De Boer, M.A. Posthumus, M. Dicke, *Journal of Chemical Ecology* 30 (2004) 2215–2230.
 [7] P.J. Linstrom, W.G. Mallard, NIST Chemistry WebBook, NIST Standard Reference Database Number 69, National Institute of Standards and Technology, Gaithersburg, 2010.
 [8] L. Iachetta, L. Malek, B.M. Ross, *Rapid Communications in Mass Spectrometry* 24 (2010) 815–822.
 [9] P. Španěl, D. Smith, *International Journal of Mass Spectrometry* 172 (1998) 137–147.
 [10] N. Schoon, C. Amelynck, L. Vereecken, E. Arijs, *International Journal of Mass Spectrometry* 229 (2003) 231–240.
 [11] T.S. Wang, P. Španěl, D. Smith, *International Journal of Mass Spectrometry* 228 (2003) 117–126.
 [12] U.S.R. Rose, A. Manukian, R.R. Heath, J.H. Tumlinson, *Plant Physiology* 111 (1996) 487–495.
 [13] L. Tollsten, P.M. Muller, *Phytochemistry* 43 (1996) 759–762.
 [14] W. Lindinger, A. Hansel, A. Jordan, *Chemical Society Reviews* 27 (1998) 347–354.
 [15] E. Aprea, F. Biasioli, T.D. Mark, F. Gasperi, *International Journal of Mass Spectrometry* 262 (2007) 114–121.
 [16] M. Demarcke, C. Amelynck, N. Schoon, F. Dhooghe, H. Van Langenhove, J. Dewulf, *International Journal of Mass Spectrometry* 279 (2009) 156–162.
 [17] E. Joo, J. Dewulf, M. Demarcke, C. Amelynck, N. Schoon, J.F. Muller, M. Simpraga, K. Steppe, H. Van Langenhove, *International Journal of Mass Spectrometry* 291 (2010) 90–95.
 [18] D. Smith, P. Španěl, *Mass Spectrometry Reviews* 24 (2005) 661–700.
 [19] K. Dryahina, M. Polášek, P. Španěl, *International Journal of Mass Spectrometry* 239 (2004) 57–65.
 [20] G. Bouchoux, J.Y. Salpin, D. Leblanc, *International Journal of Mass Spectrometry and Ion Processes* 153 (1996) 37–48.
 [21] T. Su, W.J. Chesnavich, *Journal of Chemical Physics* 76 (1982) 5183–5185.
 [22] G.P. Johari, *Digest of Literature on Dielectrics*, National Academy of Sciences, Washington, DC, 1977.
 [23] C.S. Copeland, M.W. Rigg, *Journal of American Chemical Society* 73 (1951) 5.
 [24] <http://www.thegoodscentscompany.com/>, last accessed on October 2010.
 [25] R. Weast, *CRC Handbook of Chemistry & Physics*. 66th ed., CRC, Boca Raton, FL, 1988.
 [26] D. Smith, A. Pysanenko, P. Španěl, *International Journal of Mass Spectrometry* 281 (2009) 15–23.
 [27] P. Španěl, D. Smith, *Rapid Communications in Mass Spectrometry* 14 (2000) 1898–1906.
 [28] W.V. Doering, L.H. Knox, *J. Am. Chem. Soc.* 76 (1954) 3203–3206.
 [29] P. Španěl, K. Dryahina, D. Smith, *International Journal of Mass Spectrometry* 249 (2006) 230–239.

**Appendix B, Smith *et al.* Int. J. Mass. Spectrom. 319-320
(2012) 25**

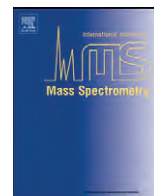
A selected ion flow tube study of the reactions of H_3O^+ , NO^+ and $\text{O}_2^{+\bullet}$ with seven isomers of hexanol in support of SIFT-MS

David Smith^a, Kristýna Sovová^{b,c}, Patrik Španěl^{a,b*}

^a*Institute for Science and Technology in Medicine, School of Medicine, Keele University, Thornburrow Drive, Hartshill, Stoke-on-Trent ST4 7QB, UK*

^b*J. Heyrovský Institute of Physical Chemistry, Academy of Sciences of the Czech Republic, Dolejškova 3, 182 23, Prague 8, Czech Republic*

^c*Department of Physical and Macromolecular Chemistry, Faculty of Science, Charles University, Albertov 2030, 128 40 Prague 2, Czech Republic*



A selected ion flow tube study of the reactions of H_3O^+ , NO^+ and $\text{O}_2^{+\bullet}$ with seven isomers of hexanol in support of SIFT-MS

David Smith^a, Kristýna Sovová^{b,c}, Patrik Španěl^{a,b,*}

^a Institute for Science and Technology in Medicine, School of Medicine, Keele University, Thornburrow Drive, Hartshill, Stoke-on-Trent ST4 7QB, UK

^b J. Heyrovský Institute of Physical Chemistry, Academy of Sciences of the Czech Republic, Dolejškova 3, 182 23, Prague 8, Czech Republic

^c Department of Physical and Macromolecular Chemistry, Faculty of Science, Charles University, Albertov 2030, 128 40, Prague 2, Czech Republic

ARTICLE INFO

Article history:

Received 14 March 2012

Received in revised form 29 March 2012

Accepted 29 March 2012

Available online 6 April 2012

Keywords:

Selected ion flow tube mass spectrometry

Ion molecule reaction

Proton transfer

Hydride ion transfer

Volatile organic compound

Chemical ionisation

ABSTRACT

A selected ion flow tube, SIFT, study has been carried out of the reactions of H_3O^+ , NO^+ and $\text{O}_2^{+\bullet}$ with seven structural isomers of hexanol with the common molecular formula $\text{C}_6\text{H}_{14}\text{O}$ and molecular weight 102 that are commonly met in food science studies. The main objective is to provide the kinetic data, i.e., the rate constants and the product ion branching ratios to be included in the SIFT-MS kinetics database that would allow the separate identification and quantification of these compounds. The specific compounds involved are the primary alcohols 1-hexanol, $\text{CH}_3(\text{CH}_2)_5\text{OH}$; 2-ethyl-1-butanol, $(\text{C}_2\text{H}_5)_2\text{CHCH}_2\text{OH}$; 4-methyl-1-pentanol, $(\text{CH}_3)_2\text{CH}(\text{CH}_2)_3\text{OH}$; secondary alcohols 2-hexanol, $\text{CH}_3(\text{CH}_2)_3\text{CH}(\text{OH})\text{CH}_3$; 4-methyl-2-pentanol, $(\text{CH}_3)_2\text{CHCH}_2\text{CH}(\text{OH})\text{CH}_3$; 3-hexanol, $\text{CH}_3(\text{CH}_2)_2\text{CH}(\text{OH})\text{CH}_2\text{CH}_3$ and a tertiary alcohol 3-methyl-3-pentanol, $(\text{CH}_3\text{CH}_2)_2\text{C}(\text{CH}_3)\text{OH}$. The reactions of H_3O^+ proceed via dissociative proton transfer invariably producing $\text{C}_6\text{H}_{13}^+$ hydrocarbon ions (m/z 85). The reactions of NO^+ proceed predominantly via hydride ion transfer producing $\text{C}_6\text{H}_{13}\text{O}^+$ ions (m/z 101) for the primary and secondary hexanols, with a minor fragmentation channel for the primary hexanols, when a H_2O molecule is lost from the major product ion resulting in $\text{C}_6\text{H}_{11}^+$ ions (m/z 83), and a minor channel representing the process of hydroxide ion transfer producing $\text{C}_6\text{H}_{13}^+$ ions (m/z 85) for secondary alcohols. The latter reaction is also the dominant process for the tertiary alcohol. $\text{O}_2^{+\bullet}$ reacts by dissociative charge transfer in all reactions resulting in multiple product ions analogous to electron ionization. The differences in product ion branching ratios and fragmentation patterns can thus assist SIFT-MS identification of the different hexanol isomers in cases when they are not present in complex mixtures.

© 2012 Elsevier B.V. All rights reserved.

1. Introduction

Volatile alcohols are ubiquitous in nature and must be expected to be detected when studying the volatile organic compounds, VOCs, released by plants and animals, cell and bacterial cultures and natural foods and food products, often termed biogenic VOCs or BVOCs [1]. Selected ion flow tube mass spectrometry, SIFT-MS [2,3], has been developed for the study of such systems, with special attention being given to the real time analysis of exhaled breath [4] in which the three simplest aliphatic alcohols methanol, ethanol and propanol are readily detected unambiguously [5], except to say that a challenge is constantly met, i.e., distinguishing between isomeric forms of VOCs, already demonstrated by 1-propanol and 2-propanol [6,7]. Some progress in isomeric detection can be made by analysis gaseous samples using the three different precursor ions H_3O^+ , NO^+ and $\text{O}_2^{+\bullet}$, which are available for SIFT-MS

analyses, by virtue of the fact that different product ions sometimes result in the reactions of these precursor ions with the different isomers of specific compounds [8,9]. This important point will be discussed more thoroughly later in this paper in relation to the present study. However, it is clear that the numbers of possible isomeric forms of a compound increases as the (constant) molecular weight of the compound increases and then using SIFT-MS the challenge becomes increasingly difficult. Then it usually becomes necessary to exploit gas chromatography, GC, to identify isomeric forms in complex mixtures. We have previously shown how 1-propanol and 2-propanol can be separated and quantified using a combination of GC and SIFT-MS [10].

The stimulus for the present study came from the observation that an alcohol of molecular weight 102 g/mol was present in the VOCs emitted by a bacterial culture and it is easy to see that such an alcohol can have several isomeric forms with the same molecular formula $\text{C}_6\text{H}_{14}\text{O}$. Polyatomic alcohols are very common in nature and have an inevitable place in everyday life. It is thus desirable that they can be analyzed by SIFT-MS. This requires a study of the kinetics of their reactions with the precursor ions

* Corresponding author.

E-mail address: patrik.spanel@jh-inst.cas.cz (P. Španěl).

used in SIFT-MS, as mentioned above, and the appropriate rate constants and product ions for the reactions included in the analytical kinetics library [11]; such studies will need to be carried out as and when required. However, the list of isomeric forms can be very long and we have limited the present kinetics study to seven alcohols with the common molecular formula $C_6H_{14}O$, as given above, these being 1-, 2-, 3-hexanol; 3-methyl-3-pentanol; 4-methyl-1-pentanol; 4-methyl-2-pentanol and 2-ethyl-1-butanol. The ultimate aim of this study is to be able to identify and analyze these compounds using SIFT-MS and to develop a method to obtain their absolute concentration in real time.

The alcohols chosen for this study are not arbitrarily chosen; they are mostly of biogenic origin. 2-Ethyl-1-butanol is a member of the fragrance group of branched chain saturated alcohols that are used in cosmetics and also in non-cosmetics products such as household cleaners [12]. It is also known in the field of food science as an oxidation product of cheese components released following light exposure [13]. 4-Methyl-1-pentanol is released from crushed transgenic tobacco leaves by expressing *Aspergillus niger* [14] and together with 4-methyl-2-pentanol and 1-hexanol contributes to wine flavour [15]. Their known occurrences are summarized in Table 1.

Hence, the rate constants and the product ion distributions of the reactions of these seven chosen alcohols with H_3O^+ , NO^+ and O_2^{+*} have been studied primarily to explore this ion chemistry and to investigate the feasibility of using the kinetic information to construct database entries for their quantification using SIFT-MS. It is now well understood that quantification of compounds, M, in humid samples by SIFT-MS must involve hydrated precursor ions, e.g., $H_3O^+(H_2O)_{1,2,3}$ and $NO^+(H_2O)_{1,2}$, and hydrated product ions, e.g., $MH^+(H_2O)_{1,2}$ and $[M-H]^+(H_2O)_{1,2}$, that inevitably form, if accurate concentration of M is to be obtained [2,30]. These hydrates, often termed cluster ions, can be formed via three-body reactions and ligand switching reactions, and we have also determined the three-body rate constants for some of these reactions.

2. Experimental

The conventional way to study the kinetics of ion-molecule reactions at thermal energies and to provide the required rate constants (often termed rate coefficients) and product ion for use in SIFT-MS analyses is by using the selected ion flow tube technique as described previously [2,31]. The SIFT technique has been used to study numerous ion-molecule reactions in several laboratories around the world, especially recently to study the reactions of H_3O^+ , NO^+ and O_2^{+*} with many types of organic compounds [2,8,32–35]. Current SIFT-MS instruments can readily be used for this purpose, as described previously [7,36,37], and so only the specific detail of the present experimental procedure are outlined below.

2.1. Determination of the branching ratios and the rate constants for the bimolecular reactions of H_3O^+ , NO^+ and O_2^{+*} with the alcohols $C_6H_{14}O$

In order to determine the product ions and their branching ratios of these reactions, the headspace of weak aqueous solutions of each alcohol (purchased from Sigma–Aldrich, 97–99% purity) were prepared at 20 °C and then the humid headspace was introduced into a Profile 3 SIFT-MS instrument (Instrument Science Limited, Crewe, UK) via a heated calibrated capillary and full scan mass spectra were acquired whilst each of the three selected precursor ions were alternately injected into the helium carrier gas in the reactor flow tube. The range of mass-to-charge ratio (m/z) was chosen as 10–160, which covered all m/z values of the expected primary product ions and any adduct (hydrated) ions that might form. For each precursor

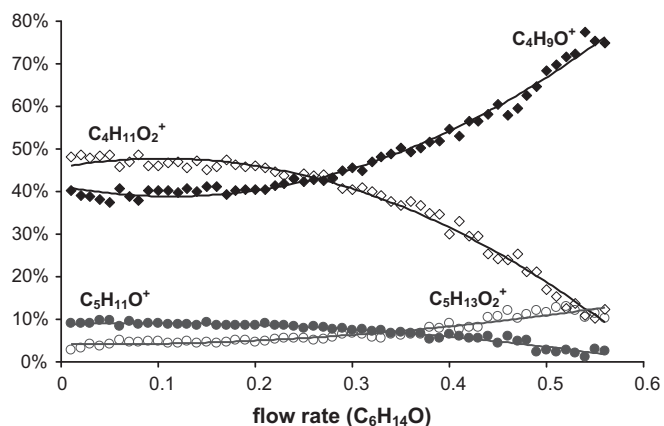


Fig. 1. Percentages of the primary ion product count rates for the reaction of O_2^{+*} with 3-methyl-3-pentanol as a function of the flow rate of the air/alcohol vapour mixture. The flow rate is in relative units corresponding to the rate of loss of the precursor ion count rate $\ln(I_0/I)$.

ion, five mass spectra were obtained each with a total integration time of 60 s. The major ion product ions of each reaction were identified and their count rates were precisely determined in separate experiments using the multi-ion monitoring, MIM, mode [2]. In order to determine the primary ion product branching ratios of the reactions, it is necessary to plot the percentages of the individual product ions on a linear scale as a function of the sample mixture (headspace) flow rate. This flow rate was measured by a flow meter (manufactured by Voegtlin, Aesch, Switzerland) and regulated by a Swagelok needle valve. An example of these plots is shown in Fig. 1). By extrapolating to zero sample gas/vapour flow rate (i.e., estimating the percentage at zero sample concentration) the true primary branching ratios, excluding any secondary reactions, can be obtained. The flow rate of hexanol vapour which is proportional to concentration of $C_6H_{14}O$ molecules in He carrier gas, can be most conveniently expressed in dimensionless units of the logarithm of the reduction of the precursor ion signal $\ln(I_0/I)$. Only product ions with a resulting branching ratio greater than 3% are reported in this paper.

It is well established that proton transfer reactions of H_3O^+ proceed at the collisional rate, as described by the collisional rate constant k_c , when these reactions are exothermic by more than 40 kJ/mol [38]. Thus, the k_c for the reactions of H_3O^+ were calculated according to Su and Chesnavich [39] using their dipole moments [40] and polarisabilities calculated according to [41] (see Table 2). The rate constants for the reactions with NO^+ and O_2^{+*} (k) were then derived from their experimentally-derived decay rates relatively to that for the H_3O^+ reaction [42] by injecting all three precursors simultaneously and allowing them to react with the sample introduced at varied concentrations. The count rates of H_3O^+ , NO^+ and O_2^{+*} were plotted on a semi-logarithmic scale as functions of the sample flow rate and the k values for the NO^+ and O_2^{+*} reactions were determined from the relative slopes of these plots [5]. The collisional rate constants for the NO^+ and O_2^{+*} reactions were also calculated according to [39]; they differ from the corresponding k_c for the H_3O^+ reactions only by virtue of the larger reduced mass of the NO^+/M and O_2^{+*}/M systems as compared to that for the H_3O^+/M system.

In a later section we discuss the termolecular reactions of some of the product ions of the above reactions, focusing on the ion products $[M-H]^+$ of the NO^+ reactions following a similar procedure we adopted to determine the three-body rate constants for the reactions of protonated molecules MH^+ formed in the reactions of H_3O^+ with M, as described in detail in our previous publications [30,36,43].

Table 1

Biological relevance and occurrence of the hexanol isomers indicated with source references.

Hexanol isomers	Component of volatile emissions of ^a :
1-Hexanol	wine [15]
2-Ethyl-1-butanol	fragrance; cleaning liquids [12]; cheese oxidation product [13]
4-Methyl-1-pentanol	tobacco tissues [14]; wine [15]
2-Hexanol	caja-umbu (Spondias sp.) fruits [16]; tomato [17]; olive oil [18]
4-Methyl-2-pentanol	wine [19]; beer [20]; grapefruit [21]; turbot fish [22]
3-Hexanol	turbot fish [22]; tomato [23,24]; wine [25]; bell peppers [26]; honey [27]; umbu fruits [28]
3-Methyl-3-pentanol	porcine subcutaneous fat [29]

^a References are given to original literature reporting detection of these hexanol isomers in foods and products.

3. Results

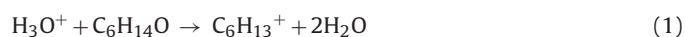
3.1. Bimolecular reactions

3.1.1. Bimolecular rate constants

Given the similarities of the dipole moments and polarisabilities of the seven hexanol isomers included in this study it is no surprise that the calculated values for the collisional rate constants, k_c , of their proton transfer reactions with H_3O^+ are very similar, as can be seen in Table 2. Similarly, the experimentally derived relative rate constants for the corresponding NO^+ and $\text{O}_2^{+\bullet}$ reactions, k , are also at their respective collisional values, the latter being calculated from the k_c for the H_3O^+ reactions and the reduced masses of the NO^+/M and O_2^+/M systems [39]. Actually, it is apparent that the k values are generally a little greater than their collisional values, but these differences are within the bounds of error in this overall procedure. However, this must reflect in the uncertainties in the quantification of these alcohols by SIFT-MS.

3.1.2. Primary ion products of the H_3O^+ reactions

Much previous work has shown that the simplest two aliphatic alcohols methanol and ethanol react with H_3O^+ to produce only the protonated alcohol, MH^+ [5]. If this remained as the only product when analyzing these alcohols in humid samples such as exhaled breath, then analysis of these compounds by SIFT-MS would be simple. However, it has to be appreciated that the MH^+ ions also form hydrates at the high number densities of H_2O molecules present and these hydrates have to be included in SIFT-MS quantification. As mentioned above, we consider hydration reactions later in this paper (Section 3.2). For higher order alcohols, including the isomers of propanol, MH^+ is no longer the major product and it is seen that H_2O elimination from the $[\text{MH}^+]^*$ excited nascent product ion occurs producing $[\text{M}-\text{OH}]^+$ hydrocarbon ions [5]. For the reactions of the hexanol isomers included in this study the only primary ion product appears at m/z 85 which is $\text{C}_6\text{H}_{13}^+$ due to the elimination of water after the formation of protonated nascent $[\text{MH}^+]$ ion, thus:



We have observed previously (see for example [5,7]) that hydrocarbon ions do not associate with H_2O molecules under SIFT-MS conditions (helium pressure about 1 Torr; room temperature) and

this was again the situation for the all the isomeric forms of the $\text{C}_6\text{H}_{13}^+$ produced in these reactions. However, ion products of the form $\text{C}_6\text{H}_{15}\text{O}^+\text{H}_2\text{O}$ at m/z 121 were clearly seen for humid air/alcohol samples and this is attributed to ligand switching reactions of the alcohol concerned with the hydrated hydronium ions $\text{H}_3\text{O}^+(\text{H}_2\text{O})_{1,2,3}$ that are inevitably formed when using H_3O^+ ions to analyze humid samples [30,44]. Even though the $\text{C}_6\text{H}_{15}\text{O}^+\text{H}_2\text{O}$ ions do not result directly from the reactions of H_3O^+ precursor ions, they must be included for accurate quantification of the alcohol by SIFT-MS [11].

3.1.3. Primary ion products of the NO^+ reactions

Hydride ion (H^-) transfer occurs as the major reaction pathway in the reactions of NO^+ with most primary and secondary alcohols, including these hexanol isomers, thus forming $\text{C}_6\text{H}_{13}\text{O}^+$ ions at m/z 101. Consideration of the energetics of such processes indicates that the hydrogen atom involved in the transfer is not that of the OH group, but is removed from the alpha C atom forming cations that can be seen formally as protonated aldehydes for the reactions of primary alcohols and as protonated ketones for the reactions of the secondary alcohols. The only exception to this is the tertiary alcohol 3-methyl-3-pentanol that does not form this product ion (because the alpha C atom does not bind to any H). Rather, one primary ion product at m/z 85 results, involving the elimination of an OH group from the nascent $[\text{NO}^+\text{C}_6\text{H}_{14}\text{O}]^*$, thus forming the $\text{C}_6\text{H}_{13}^+$ ion and a neutral nitrous acid molecule HONO, thus:



The reactions of the primary alcohols, 1-hexanol; 2-ethyl-1-butanol and 4-methyl-1-pentanol, result in two product ions, the major product ion at m/z 101 resulting from H^- transfer (Reaction (3a)) and a minor product ion at m/z 83 by which, additionally, an H_2O molecule is eliminated from the nascent, unstable intermediate complex ion, thus:



The reactions of the secondary alcohols, 2-hexanol; 4-methyl-2-pentanol and 3-hexanol, also result in two product ions, the major product ion again being at m/z 101 as in Reaction (3a), but in this case a minor product ion is at m/z 85, which is the $\text{C}_6\text{H}_{13}^+$

Table 2

The collisional rate constants, k_c , for the reactions with the various isomers of hexanol, given in square brackets, are calculated using the parameterization given by Su and Chesnavich [39] using the estimated polarisabilities, α , and the dipole moments, μ_r , of these hexanols. The k values for the NO^+ and $\text{O}_2^{+\bullet}$ reactions have been determined experimentally; see the text. Both k and k_c are given in units of $10^{-9} \text{ cm}^3 \text{ s}^{-1}$.

Compound	Linear formula	α (10^{-24} cm^3)	μ_r (D)	H_3O^+ [k_c]	$\text{NO}^+ k$ [k_c]	$\text{O}_2^{+\bullet} k$ [k_c]
1-Hexanol	$\text{CH}_3(\text{CH}_2)_5\text{OH}$	12.5	1.6	[2.9]	2.8 [2.4]	2.2 [2.3]
2-Ethyl-1-butanol	$(\text{C}_2\text{H}_5)_2\text{CHCH}_2\text{OH}$	12.5	1.6	[2.9]	2.7 [2.4]	2.0 [2.3]
4-Methyl-1-pentanol	$(\text{CH}_3)_2\text{CH}(\text{CH}_2)_3\text{OH}$	12.5	1.6	[2.9]	2.7 [2.4]	2.3 [2.3]
2-Hexanol	$\text{CH}_3(\text{CH}_2)_3\text{CH}(\text{OH})\text{CH}_3$	12.5	1.5	[2.8]	2.6 [2.3]	2.3 [2.3]
4-Methyl-2-pentanol	$(\text{CH}_3)_2\text{CHCH}_2\text{CH}(\text{OH})\text{CH}_3$	12.5	1.7	[3.0]	2.8 [2.5]	2.5 [2.4]
3-Hexanol	$\text{CH}_3(\text{CH}_2)_2\text{CH}(\text{OH})\text{CH}_2\text{CH}_3$	12.5	1.5	[2.8]	2.8 [2.3]	2.7 [2.3]
3-Methyl-3-pentanol	$(\text{CH}_3\text{CH}_2)_2\text{C}(\text{CH}_3)\text{OH}$	12.5	1.7	[3.0]	2.6 [2.5]	2.3 [2.4]

Table 3
Percentages, %, of each of the product ions formed in the reactions of H_3O^+ , NO^+ and $\text{O}_2^{+\bullet}$ with the seven structural isomers of hexanol with the common molecular formula $\text{C}_6\text{H}_{14}\text{O}$ and molecular weight 102. Note in the H_3O^+ reactions that the same product ion $\text{C}_6\text{H}_{13}^+$ at a mass-charge-ratio, m/z , 85 is formed for all isomers, but it is not implied that these product ions have the same structure. Also given are the m/z values of the hydrated forms of the product ions observed; it is seen that mono-, di- and trihydrates are variously seen. Note that the hydrocarbon ions $\text{C}_6\text{H}_{13}^+$ formed in the H_3O^+ reactions are not observed to form hydrates under SIFT-MS conditions.

Compound	H_3O^+	m/z	NO^+	m/z	Hydrates m/z	O_2^+	m/z	Hydrates m/z
<i>Primary</i>								
1-Hexanol	100% $\text{C}_6\text{H}_{13}^+$	85	96% $\text{C}_6\text{H}_{13}\text{O}^+$ 4% $\text{C}_6\text{H}_{11}^+$	101 83	(119, 137, 155)	45% $\text{C}_6\text{H}_{12}^{+\bullet}$ 42% $\text{C}_4\text{H}_8^{+\bullet}$ 13% C_5H_9^+	84 56 69	
2-Ethyl-1-butanol	100% $\text{C}_6\text{H}_{13}^+$	85	96% $\text{C}_6\text{H}_{13}\text{O}^+$ 4% $\text{C}_6\text{H}_{11}^+$	101 83	(119, 137)	32% $\text{C}_6\text{H}_{12}^{+\bullet}$ 31% $\text{C}_5\text{H}_{10}^{+\bullet}$ 27% $\text{C}_5\text{H}_{11}^+$ 5% $\text{C}_4\text{H}_8^{+\bullet}$ 5% C_5H_9^+	84 70 71 56 69	
4-Methyl-1-pentanol	100% $\text{C}_6\text{H}_{13}^+$	85	92% $\text{C}_6\text{H}_{13}\text{O}^+$ 8% $\text{C}_6\text{H}_{11}^+$	101 83	(119, 137, 155)	70% $\text{C}_4\text{H}_8^{+\bullet}$ 14% C_5H_9^+ 14% $\text{C}_6\text{H}_{12}^{+\bullet}$	56 69 84	
<i>Secondary</i>								
2-Hexanol	100% $\text{C}_6\text{H}_{13}^+$	85	95% $\text{C}_6\text{H}_{13}\text{O}^+$ 5% $\text{C}_6\text{H}_{13}^+$	101 85	(119)	67% $\text{C}_2\text{H}_5\text{O}^+$ 14% $\text{C}_6\text{H}_{12}^{+\bullet}$ 13% $\text{C}_5\text{H}_{11}\text{O}^+$ 6% C_5H_9^+	45 84 87 69	(63) (105)
4-Methyl-2-pentanol	100% $\text{C}_6\text{H}_{13}^+$	85	94% $\text{C}_6\text{H}_{13}\text{O}^+$ 6% $\text{C}_6\text{H}_{13}^+$	101 85	(119, 137)	57% $\text{C}_2\text{H}_5\text{O}^+$ 17% $\text{C}_6\text{H}_{12}^{+\bullet}$ 15% $\text{C}_5\text{H}_{11}\text{O}^+$ 11% C_5H_9^+	45 84 87 69	(63) (105)
3-Hexanol	100% $\text{C}_6\text{H}_{13}^+$	85	95% $\text{C}_6\text{H}_{13}\text{O}^+$ 5% $\text{C}_6\text{H}_{13}^+$	101 85	(119)	60% $\text{C}_4\text{H}_9\text{O}^+$ 40% $\text{C}_3\text{H}_7\text{O}^+$	73 59	(91, 109) (77)
<i>Tertiary</i>								
3-Methyl-3-pentanol	100% $\text{C}_6\text{H}_{13}^+$	85	100% $\text{C}_6\text{H}_{13}^+$	85		87% $\text{C}_4\text{H}_9\text{O}^+$ 13% $\text{C}_5\text{H}_{11}\text{O}^+$	73 87	(91) (105)

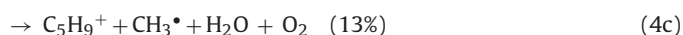
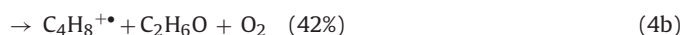
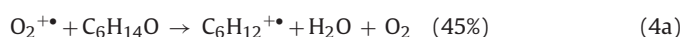
hydrocarbon ion, and a neutral product HONO molecule is released as indicated for Reaction (2). All these results are summarised in Table 3.

These data for hexanol isomers, in accordance with previous studies [5], has indicated that SIFT-MS analyses using NO^+ precursor ions can, in principle, distinguish between primary, secondary or tertiary alcohols. However, in practice this may not be always straightforward because some of the characteristic product ions originate from minor (<10%) channels and their ion count rate will not be precisely determined when analysing trace amounts of isomers of hexanol.

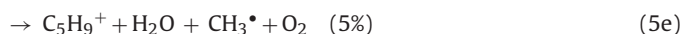
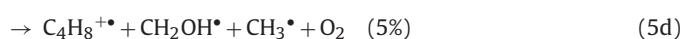
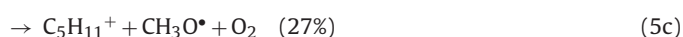
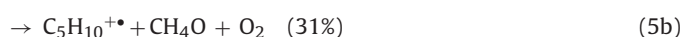
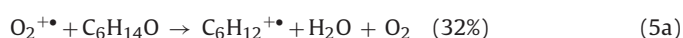
3.1.4. Primary ion products of the $\text{O}_2^{+\bullet}$ reactions

The reaction between $\text{O}_2^{+\bullet}$ and all seven alcohols proceed via dissociative charge transfer and result in several fragment ions, at least 2 and in one reaction 5 product ions (see Table 3). The observed product ion spectra were compared with the analogous electron ionisation, EI, spectra obtained from the NIST database.

The most abundant ions on the EI spectrum of 1-hexanol are at m/z values of 56, 43, 31 and 27. Detailed inspection of the $\text{O}_2^{+\bullet}$ SIFT-MS spectrum reveals three major product ions at m/z 84, 56 and 69, formed thus:

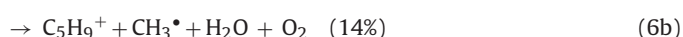
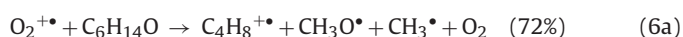


The reaction of $\text{O}_2^{+\bullet}$ with 2-ethyl-1-butanol proceeds results in five fragment ions at m/z values of 56, 69, 70, 71 and 84 as can be seen here:

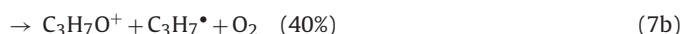


The EI spectrum indicates the most abundant ion peak to be at m/z 43, which represents less than 1% in these SIFT-MS thermal energy reactions, presumably because the ionisation/ground state recombination energy of O_2 molecules (12.06 eV) ensures that less energy is imparted to the $[\text{C}_6\text{H}_{14}\text{O}]^{+\bullet}$ excited ion, thus minimizing fragmentation.

The SIFT-MS spectrum obtained for the 4-methyl-1-pentanol reaction more closely mirrors the corresponding EI spectrum. The major fragment ion is at m/z 56, followed by an ion at m/z 69. The $\text{O}_2^{+\bullet}$ reaction proceeds thus:



The 3-hexanol and 3-methyl-3-pentanol are the simplest of these $\text{O}_2^{+\bullet}$ reactions in that only two product ions are observed, as exemplified by the 3-hexanol reaction:



Note that a neutral hydrocarbon radical is also generated in both channels. For more details see Table 3. Whilst these products and their distributions are complex and variable, they might be used to facilitate SIFT-MS identification of some of these hexanol isomers, but again in mixtures of these compounds this will be very challenging.

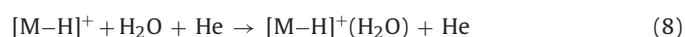
3.2. Kinetics of the ion chemistry involving water molecules: determination of three-body association rate constants

It is important to recognise when using NO^+ precursor ions to analyse humid samples that a fraction of them directly associate with H_2O molecules forming hydrated nitrosonium ions,

$\text{NO}^+(\text{H}_2\text{O})_{1,2}$ [45]. These hydrates must be considered as precursor ions in SIFT-MS analyses, because they can produce additional ion products of the kind $[\text{M}+\text{NO}]^+$ via ligand switching reactions [46]; however, significant fractions of these were not observed in the product ion spectra in the present experiments. As seen above and in Table 3, the reactions of NO^+ precursor ions with all but one of the hexanol isomers, M, result in the formation of $[\text{M}-\text{H}]^+$ or, more specifically, $\text{C}_6\text{H}_{13}\text{O}^+$ ions. It was observed in the presence of water molecules that these product cations associated with H_2O molecules to form the adduct ions $[\text{M}-\text{H}]^+(\text{H}_2\text{O})_{1,2,3}$. The m/z values of the hydrates seen in these experiments are also given in Table 3; variously, the mono-, di- and trihydrates are seen. Thus, the ion chemistry, which is important for real time and accurate quantification by SIFT-MS, is influenced by the presence of water vapour and it is necessary to account for this [30].

In SIFT-MS measurements of humid samples using H_3O^+ precursor ions it is usually the case that both $\text{MH}^+(\text{H}_2\text{O})_{1,2,3}$ and $\text{H}_3\text{O}^+(\text{H}_2\text{O})_{1,2,3}$ hydrates are formed. The ratio of the count rates of these various ions change with the sample flow rate and the sample humidity and by recording these relative count rates the efficiency of hydration as a fundamental parameter, described by elementary rate constants, can be obtained. We routinely exploit the formation of the H_3O^+ hydrates to great effect in SIFT-MS to determine the humidity of the sample being analysed [30,36]. The objective of this section is to indicate the kinetic principles and the procedure adopted to analyse the experimental data when $[\text{M}-\text{H}]^+$ hydrate ions are formed.

Three-body rate constants for the association reactions of $[\text{M}-\text{H}]^+$ ions with H_2O molecules in helium, $k_{\text{M}-\text{H}^+}$, describe the rate of hydration of the protonated molecules in the gas phase. Formation of the monohydrate proceeds thus:



The formation rate of these monohydrated ions relative to that for the reaction of H_3O^+ with H_2O (rate constant, $k_{\text{H}_3\text{O}^+}$) and to the significantly slower association reaction of NO^+ with H_2O (rate constant k_{NO^+}), both of which have been thoroughly studied [47], can be described by a constant A_{eff} . The value of this constant can be obtained from experimental data by relating the conversion rate of $[\text{M}-\text{H}]^+$ to the hydrates to the conversion rate of NO^+ to its hydrates:

$$A_{\text{eff}} = \frac{2 \ln([\text{M}-\text{H}]_0/[\text{M}-\text{H}^+])}{\ln([\text{H}_3\text{O}^+]_0/[\text{H}_3\text{O}^+])} = \frac{2 \ln([\text{M}-\text{H}]_0/[\text{M}-\text{H}^+])}{(k_{\text{H}_3\text{O}^+}/k_{\text{NO}^+}) \ln([\text{NO}^+]_0/[\text{NO}^+])} \quad (9)$$

The subscript 0 indicates the respective ion count rate in the absence of water vapour in the helium carrier gas. The value of A_{eff} has a very simple interpretation, as it describes how much faster clustering of $[\text{M}-\text{H}]^+$ is compared to clustering of H_3O^+ , and the value of three-body association rate constant can be calculated as: $k_{\text{M}-\text{H}^+}$

$$k_{\text{M}-\text{H}^+} = A_{\text{eff}} \cdot k_{\text{H}_3\text{O}^+} = A_{\text{eff}} \cdot \frac{k_{\text{H}_3\text{O}^+}}{k_{\text{NO}^+}} k_{\text{NO}^+} \quad (10)$$

So $k_{\text{M}-\text{H}^+}$ obtained from Eq. (10) is a fundamental three-body association rate constant anchored to the known values of $k_{\text{H}_3\text{O}^+}$ ($6.0 \times 10^{-28} \text{ cm}^6 \text{ s}^{-1}$) [30,36] and k_{NO^+} ($5.0 \times 10^{-29} \text{ cm}^6 \text{ s}^{-1}$) determined experimentally under the actual conditions of this study. The values of $k_{\text{M}-\text{H}^+}$ so obtained for the $[\text{M}-\text{H}]^+$ ions formed from six hexanol isomers are given in Table 4. Note that the association efficiencies range from 2.8 to 21.3. The fastest association is observed for the ions derived from the primary alcohols and slowest association for the secondary alcohols. Especially slow association is

Table 4

Kinetics of the association reactions of the $\text{C}_6\text{H}_{13}\text{O}^+$ ($[\text{M}-\text{H}]^+$) ions produced in the NO^+ ion reactions with the hexanol isomers listed. See the text for the meanings of A_{eff} and $k_{[\text{M}-\text{H}]^+}$.

Compound	Reaction	A_{eff}	$k_{[\text{M}-\text{H}]^+}$ ($10^{-27} \text{ cm}^6 \text{ s}^{-1}$)
1-Hexanol	$[\text{M}-\text{H}]^+ + \text{H}_2\text{O} + \text{He}$	21.3	13.0
2-Ethyl-1-butanol	$[\text{M}-\text{H}]^+ + \text{H}_2\text{O} + \text{He}$	16.5	9.9
4-Methyl-1-pentanol	$[\text{M}-\text{H}]^+ + \text{H}_2\text{O} + \text{He}$	13.6	8.1
2-Hexanol	$[\text{M}-\text{H}]^+ + \text{H}_2\text{O} + \text{He}$	2.8	1.7
4-Methyl-2-pentanol	$[\text{M}-\text{H}]^+ + \text{H}_2\text{O} + \text{He}$	11.8	7.1
3-Hexanol	$[\text{M}-\text{H}]^+ + \text{H}_2\text{O} + \text{He}$	10.0	5.8

seen for the product $\text{C}_6\text{H}_{13}\text{O}^+$ ion formed in the 2-hexanol reaction. Note that an $[\text{M}-\text{H}]^+$ ion is not formed for the tertiary alcohol at all; rather, a hydrocarbon ion $\text{C}_6\text{H}_{13}^+$ is formed. It is observed that the hydrocarbon product ions $\text{C}_6\text{H}_{13}^+$ do not associate with H_2O molecules in agreement with previous SIFT-MS observations [2].

It is worthy of note that the protonated aldehydes, $\text{C}_5\text{H}_{11}\text{O}^+$ and $\text{C}_7\text{H}_{15}\text{O}^+$, associate with H_2O with rate constants 10 and 12 in the units of $10^{-27} \text{ cm}^6 \text{ s}^{-1}$ [43], which is comparable with the present results. Protonated hexanone, however, was seen to associate with $k = 9.5 \times 10^{-27} \text{ cm}^6 \text{ s}^{-1}$ [48], which is significantly faster than the present result for the (presumed ketone ion) corresponding product of hydride ion transfer from 2-hexanol, as mentioned above.

4. Concluding remarks

Major objectives of this study on seven isomeric forms of hexanol were: to investigate the prospect of separately identifying by SIFT studies the different hexanol isomers, M, exploiting the three available precursor ions for chemical ionisation and the various characteristic product ions that result from these reactions; then to provide the essential kinetic data for their analysis using SIFT-MS. The H_3O^+ reactions produce only $\text{C}_6\text{H}_{13}^+$ primary product ions at the same m/z value in all cases, which is the result of loss of an H_2O molecule from the protonated $\text{C}_6\text{H}_{15}\text{O}^+$ nascent product ions. The NO^+ reactions produce $[\text{M}-\text{H}]^+$ primary product ions at the same m/z value, except for one isomer 3-methyl-3-pentanol. Thus, separation of the isomers using these precursor ions is not possible. However, global analysis of the isomers when more than one is present in a mixture can be carried out with reasonable accuracy, because the rate constants for the reactions of the various isomers with H_3O^+ and NO^+ are essentially the same (see Table 2), so both ions can be used simultaneously for their analysis by SIFT-MS. However, it is important to realize that primary ion products of the NO^+ reactions associate in three-body reactions with the H_2O molecules present in humid samples to be analyzed and these hydrates have to be included as product ions for accurate analyses to be achieved. A determination of the three-body rate constants, $k_{[\text{M}-\text{H}]^+}$, can give some help in identifying the isomer that is present, because these rate constants are different (see Table 4), but this can only be helpful when a single isomer is present. Similarly, the varying product ion percentages in the $\text{O}_2^{+\bullet}$ reactions offer some support to isomer identification, but the complexity of the product distributions diminishes their value to this pursuit. Nevertheless the data presented in this study will allow absolute quantification of the total concentration of all hexanol isomers, because it is shown that the differences between individual rate constants (Table 2) of their reactions with H_3O^+ are less than 3%, with NO^+ less than 4%, and with $\text{O}_2^{+\bullet}$ less than 10%.

Acknowledgements

We gratefully partial acknowledge financial support by the Grant Agency of the Czech Republic (project number 203/09/0256)

and by Grant Agency of Charles University (project GAUK 32010). We are also grateful to the reviewers for their comments and suggestions for revisions.

References

- [1] D. Smith, P. Španěl, Direct, rapid quantitative analyses of BVOCs using SIFT-MS and PTR-MS obviating sample collection, *Trends in Analytical Chemistry* 30 (2011) 945–959.
- [2] D. Smith, P. Španěl, Selected ion flow tube mass spectrometry (SIFT-MS) for on-line trace gas analysis, *Mass Spectrometry Reviews* 24 (2005) 661–700.
- [3] P. Španěl, D. Smith, Selected ion flow tube-mass spectrometry: detection and real-time monitoring of flavours released by food products, *Rapid Communications in Mass Spectrometry* 13 (1999) 585–596.
- [4] P. Španěl, D. Smith, Progress in SIFT-MS: breath analysis and other applications, *Mass Spectrometry Reviews* 30 (2011) 236–267.
- [5] P. Španěl, D. Smith, SIFT studies of the reactions of H_3O^+ , NO^+ and O_2^+ with a series of alcohols, *International Journal of Mass Spectrometry* 167 (1997) 375–388.
- [6] T.S. Wang, W. Carroll, W. Lenny, P. Boit, D. Smith, The analysis of 1-propanol and 2-propanol in humid air samples using selected ion flow tube mass spectrometry, *Rapid Communications in Mass Spectrometry* 20 (2006) 125–130.
- [7] A. Pysanenko, P. Španěl, D. Smith, Analysis of the isobaric compounds propanol, acetic acid and methyl formate in humid air and breath by selected ion flow tube mass spectrometry, SIFT-MS, *International Journal of Mass Spectrometry* 285 (2009) 42–48.
- [8] T.S. Wang, P. Španěl, D. Smith, Selected ion flow tube, SIFT, studies of the reactions of H_3O^+ , NO^+ and O_2^+ with eleven $\text{C}_{10}\text{H}_{16}$ monoterpenes, *International Journal of Mass Spectrometry* 228 (2003) 117–126.
- [9] P. Španěl, D. Smith, Selected ion flow tube studies of the reactions of H_3O^+ , NO^+ , and O_2^+ with eleven amine structural isomers of $\text{C}_5\text{H}_{13}\text{N}$, *International Journal of Mass Spectrometry* 187 (1999) 139–147.
- [10] J. Kubista, P. Španěl, K. Dryahina, C. Workman, D. Smith, Combined use of gas chromatography and selected ion flow tube mass spectrometry for absolute trace gas quantification, *Rapid Communications in Mass Spectrometry* 20 (2006) 563–567.
- [11] P. Španěl, K. Dryahina, D. Smith, A general method for the calculation of absolute trace gas concentrations in air and breath from selected ion flow tube mass spectrometry data, *International Journal of Mass Spectrometry* 249 (2006) 230–239.
- [12] D. McGinty, C.S. Letizia, A.M. Api, Fragrance material review on 2-ethyl-1-butanol, *Food and Chemical Toxicology* 48 (2010) S85–S88.
- [13] M. Juric, G. Bertelson, G. Mortenson, M.A. Petersen, Light-induced colour and aroma changes in sliced, modified atmosphere packaged semi-hard cheeses, *International Dairy Journal* 13 (2003) 239–249.
- [14] S. Wei, I. Marton, M. Dekel, D. Shalitin, E. Lewinsohn, B.A. Bravo, O. Shoseyov, Manipulating volatile emission in tobacco leaves by expressing *Aspergillus niger* beta-glucosidase in different subcellular compartments, *Plant Biotechnology Journal* 2 (2004) 341–350.
- [15] I. Moret, A. Gambaro, Trend analysis in selection of aroma components as variables for chemometric studies of typical wines, *Annali di Chimica* 86 (1996) 309–318.
- [16] N. Narain, M.D. Galvao, M.S. Madruga, Volatile compounds captured through purge and trap technique in caja-umbu (*Spondias* sp.) fruits during maturation, *Food Chemistry* 102 (2007) 726–731.
- [17] E.A. Baldwin, J.W. Scott, M.A. Einstein, T.M.M. Malundo, B.T. Carr, R.L. Shewfelt, K.S. Tandon, Relationship between sensory and instrumental analysis for tomato flavor, *Journal of the American Society for Horticultural Science* 123 (1998) 906–915.
- [18] A.K. Kiritsakis, Flavor components of olive oil – a review, *Journal of the American Oil Chemists Society* 75 (1998) 673–681.
- [19] L. Rebiere, A.C. Clark, L.M. Schmidtke, P.D. Prenzler, G.R. Scollary, A robust method for quantification of volatile compounds within and between vintages using headspace-solid-phase micro-extraction coupled with GC-MS – application on Semillon wines, *Analytica Chimica Acta* 660 (2010) 149–157.
- [20] M.M. Liu, Z.R. Zeng, B. Xiong, Preparation of novel solid-phase microextraction fibers by sol-gel technology for headspace solid-phase microextraction-gas chromatographic analysis of aroma compounds in beer, *Journal of Chromatography A* 1065 (2005) 287–299.
- [21] J.M. Lin, R.L. Rouseff, S. Barros, M. Haim, Aroma composition changes in early season grapefruit juice produced from thermal concentration, *Journal of Agricultural and Food Chemistry* 50 (2002) 813–819.
- [22] C. Prost, T. Serot, M. Demainay, Identification of the most potent odors in wild and farmed cooked turbot (*Scophthalmus maximus* L), *Journal of Agricultural and Food Chemistry* 46 (1998) 3214–3219.
- [23] A. Alonso, L. Vazquez-Araujo, S. Garcia-Martinez, J.J. Ruiz, A.A. Carbonell-Barrachina, Volatile compounds of traditional and virus-resistant breeding lines of Muchamiel tomatoes, *European Food Research and Technology* 230 (2009) 315–323.
- [24] H.Y. Gao, B.Z. Zhu, H.L. Zhu, Y.L. Zhang, Y.H. Xie, Y.C. Li, Y.B. Luo, Effect of suppression of ethylene biosynthesis on flavor products in tomato fruits, *Russian Journal of Plant Physiology* 54 (2007) 80–88.
- [25] V. Ferreira, R. Lopez, J.F. Cacho, Quantitative determination of the odorants of young red wines from different grape varieties, *Journal of the Science of Food and Agriculture* 80 (2000) 1659–1667.
- [26] P.A. Luning, D. Yuksel, R.V. deVries, J.P. Roozen, Aroma changes in fresh bell peppers (*Capsicum annuum*) after hot-air drying, *Journal of Food Science* 60 (1995) 1269–1276.
- [27] A. Bouseta, V. Scheirman, S. Collin, Flavor and free amino acid composition of lavender and eucalyptus honeys, *Journal of Food Science* 61 (1996) 683–687.
- [28] M.D. Galvao, N. Narain, M.D.P. dos Santos, M.L. Nunes, Volatile compounds and descriptive odor attributes in umbu (*Spondias tuberosa*) fruits during maturation, *Food Research International* 44 (2011) 1919–1926.
- [29] M. Narvaez-Rivas, F. Pablos, J.M. Jurado, M. Leon-Camacho, Authentication of fattening diet of Iberian pigs according to their volatile compounds profile from raw subcutaneous fat, *Analytical and Bioanalytical Chemistry* 399 (2011) 2115–2122.
- [30] P. Španěl, D. Smith, Influence of water vapour on selected ion flow tube mass spectrometric analyses of trace gases in humid air and breath, *Rapid Communications in Mass Spectrometry* 14 (2000) 1898–1906.
- [31] D. Smith, N. Adams, The selected ion flow tube (SIFT): studies of ion-neutral reactions, *Advances in Atomic and Molecular Physics* 24 (1988) 1–49.
- [32] K. Dryahina, M. Poláček, P. Španěl, A selected ion flow tube, SIFT, study of the ion chemistry of H_3O^+ , NO^+ and O_2^+ ions with several nitroalkanes in the presence of water vapour, *International Journal of Mass Spectrometry* 239 (2004) 57–65.
- [33] L. Iachetta, L. Malek, B.M. Ross, The reactions of H_3O^+ , NO^+ and O_2^+ with several flavourant esters studied using selected ion flow tube mass spectrometry, *Rapid Communications in Mass Spectrometry* 24 (2010) 815–822.
- [34] N. Schoon, C. Amelynck, L. Vereecken, E. Arijs, A selected ion flow tube study of the reactions of H_3O^+ , NO^+ and O_2^+ with a series of monoterpenes, *International Journal of Mass Spectrometry* 229 (2003) 231–240.
- [35] P. Španěl, D. Smith, SIFT studies of the reactions of H_3O^+ , NO^+ and O_2^+ with a series of volatile carboxylic acids and esters, *International Journal of Mass Spectrometry* 172 (1998) 137–147.
- [36] K. Sovová, K. Dryahina, P. Španěl, Selected ion flow tube (SIFT) studies of the reactions of H_3O^+ , NO^+ and O_2^+ with six volatile phytochemical esters, *International Journal of Mass Spectrometry* 300 (2011) 31–38.
- [37] K. Dryahina, B.K.C. de Miranda, P. Španěl, J. Zabka, C. Alcaraz, Z. Herman, Selected ion flow tube study of ion molecule reactions of $\text{N}^+(\text{?P})$ and Kr^+ with C_3 hydrocarbons propane, propene, and propyne, *Journal of Physical Chemistry A* 115 (2011) 7310–7315.
- [38] G. Bouchoux, J.Y. Salpin, D. Leblanc, A relationship between the kinetics and thermochemistry of proton transfer reactions in the gas phase, *International Journal of Mass Spectrometry and Ion Processes* 153 (1996) 37–48.
- [39] T. Su, W.J. Chesnavich, Parametization of the ion-polar molecule collision rate-constant by trajectory calculations, *Journal of Chemical Physics* 76 (1982) 5183–5185.
- [40] C.L. Yaws, *Thermophysical Properties of Chemicals and Hydrocarbons*, William Andrew Inc., New York, 2008.
- [41] K.J. Miller, J.A. Savchik, New empirical-method to calculate average molecular polarisabilities, *Journal of the American Chemical Society* 101 (1979) 7206–7213.
- [42] D. Smith, A. Pysanenko, P. Španěl, Ionic diffusion and mass discrimination effects in the new generation of short flow tube SIFT-MS instruments, *International Journal of Mass Spectrometry* 281 (2009) 15–23.
- [43] P. Španěl, J.M. Van Doren, D. Smith, A selected ion flow tube study of the reactions of H_3O^+ , NO^+ , and O_2^+ with saturated and unsaturated aldehydes and subsequent hydration of the product ions, *International Journal of Mass Spectrometry* 123 (2002) 163–176.
- [44] P. Španěl, D. Smith, Reactions of hydrated hydronium ions and hydrated hydroxide ions, with some hydrocarbons and oxygen-bearing organic-molecules, *Journal of Physical Chemistry* 99 (1995) 15551–15556.
- [45] P. Španěl, D. Smith, Influence of weakly bound adduct ions on breath trace gas analysis by selected ion flow tube mass spectrometry (SIFT-MS), *International Journal of Mass Spectrometry* 280 (2009) 128–135.
- [46] D. Smith, A.M. Diskin, Y.F. Ji, P. Španěl, Concurrent use of H_3O^+ , NO^+ , and O_2^+ precursor ions for the detection and quantification of diverse trace gases in the presence of air and breath by selected ion-flow tube mass spectrometry, *International Journal of Mass Spectrometry* 209 (2001) 81–97.
- [47] Y. Ikezoe, S. Matsuoka, M. Takebe, A. Viggiano, Gas Phase Ion-Molecule Reaction Rate Constants Through 1986, Maruzen, Tokyo, 1987.
- [48] D. Smith, T.S. Wang, P. Španěl, Analysis of ketones by selected ion flow tube mass spectrometry, *Rapid Communications in Mass Spectrometry* 17 (2003) 2655–2660.

Appendix C, Dryahina *et al.* Rapid Commun. Mass Spectrom.
27 (2013) 1983

Quantification of pentane in exhaled breath, a biomarker of bowel disease,
using selected ion flow tube mass spectrometry

Kseniya Dryahina^a, Patrik Španěl^{a,d}, Veronika Pospíšilová^{a,b}, Kristýna Sovová^{a,b}, Luděk
Hrdlička^c, Naděžda Machková^c, Milan Lukáš^c David Smith^d

^a*J. Heyrovský Institute of Physical Chemistry, Academy of Sciences of the Czech
Republic, Dolejškova 3, 182 23, Prague 8, Czech Republic*

^b*Department of Physical and Macromolecular Chemistry, Faculty of Science, Charles
University, Albertov 2030, 128 40 Prague 2, Czech Republic*

^b*Clinical and Research Centre for Inflammatory Diseases, ISCARE Lighthouse,
Jankovcova 1569/2c, 170 04 Prague 7, Czech Republic*

^d*Institute for Science and Technology in Medicine, School of Medicine, Keele
University, Thornburrow Drive, Hartshill, Stoke-on-Trent ST4 7QB, UK*

Rapid Commun. Mass Spectrom. 2013, 27, 1983–1992
(wileyonlinelibrary.com) DOI: 10.1002/rcm.6660

Quantification of pentane in exhaled breath, a potential biomarker of bowel disease, using selected ion flow tube mass spectrometry

Kseniya Dryahina¹, Patrik Španěl^{1*}, Veronika Pospíšilová^{1,2}, Kristýna Sovová^{1,2},
Luděk Hrdlička³, Naděžda Machková³, Milan Lukáš³ and David Smith⁴

¹J. Heyrovský Institute of Physical Chemistry, Academy of Sciences of the Czech Republic, Dolejškova 3, 182 23 Prague 8, Czech Republic

²Faculty of Science, Charles University, Albertov 2030, 128 40 Prague 2, Czech Republic

³IBD Clinical and Research Centre, ISCARE a.s., Jankovcova 1569/2c, 170 00 Prague 7, 1st Faculty of Medicine, Charles University in Prague, Czech Republic

⁴Institute for Science and Technology in Medicine, School of Medicine, Keele University, Thornburrow Drive, Hartshill, Stoke-on-Trent ST4 7QB, UK

RATIONALE: Inflammatory bowel disease has a relatively large incidence in modern populations and the current diagnostic methods are either invasive or have limited sensitivity or specificity. Thus, there is a need for new non-invasive methods for its diagnosis and therapeutic monitoring, and breath analysis represents a promising direction in this area of research. Specifically, a method is needed for the absolute quantification of pentane in human breath.

METHODS: Selected ion flow tube mass spectrometry (SIFT-MS) has been used to study the kinetics of the O_2^+ reaction with pentane. Product ions at m/z 42 and 72 were chosen as characteristic ions useful for the quantification of pentane and the reactivity of these ions with water vapour was characterized. A pilot study has been carried out of pentane in the exhaled breath of patients with Crohn's disease (CD) and ulcerative colitis (UC) and of healthy volunteers.

RESULTS: Accurate data on the kinetics of the gas phase reaction of the O_2^+ ions with pentane have been obtained: rate coefficient $8 \times 10^{-10} \text{ cm}^3 \text{ s}^{-1}$ ($\pm 5\%$) and branching ratios into the following product ions $C_5H_{12}^+$ (m/z 72, 31%); $C_4H_9^+$ (m/z 57, 8%); $C_3H_7^+$ (m/z 43, 40%), $C_3H_6^+$ (m/z 42, 21%). A method of calculation of absolute pentane concentration in exhaled breath was formulated using the count rates of the ions at m/z 32, 42, 55 and 72. Pentane was found to be significantly elevated in the breath of both the CD (mean 114 ppbv) and the UC patients (mean 84 ppbv) relative to the healthy controls (mean 40 ppbv).

CONCLUSIONS: SIFT-MS can be used to quantify pentane in human breath in real time avoiding sample storage. This method of analysis can ultimately form the basis of non-invasive screening of inflammatory processes, including inflammatory bowel disease. Copyright © 2013 John Wiley & Sons, Ltd.

The analysis of exhaled breath is potentially a non-invasive contributor to clinical diagnosis and therapeutic monitoring.^[1–3] There have been remarkable advances in breath analysis techniques, not least in the improvements and developments of new analytical methodologies. Of note are the new techniques by which on-line, real-time analyses of exhaled breath can be realized obviating sample collection; these include selected ion flow tube mass spectrometry (SIFT-MS)^[4,5] and proton transfer mass spectrometry (PTR-MS),^[6,7] the special features and advantages of which for breath analysis have recently been compared and contrasted.^[8] By exploiting these methods, many trace compounds have been quantified in exhaled breath,^[3,9] and the reference ranges for several of them have been established

for cohorts of healthy people, notably using SIFT-MS.^[10–14] The large majority of these compounds can be classified as volatile organic compounds (VOCs) prevalent amongst which are homologous series of alcohols, aldehydes, ketones and long-chain and branched-chain hydrocarbons. Many studies have been carried out that focus on associating these compounds with established disease conditions such as cancer^[15] and diabetes.^[1–3] However, a major challenge that has to be met is that most of the breath VOCs, so far recognised to relate to disease, are present at very low concentrations, typically at the parts-per-billion by volume (ppbv), and lower. It is because of this that techniques that collect and concentrate the trace VOCs in breath samples prior to analysis, such as the gas chromatography/mass spectrometry methods associated with solid-state microextraction (SPME/GC/MS)^[16] and automated thermal desorption (TD/GC/MS),^[17] have had most success in detecting disease biomarkers in breath.^[2,15] However, real-time, on-line analysis involving accurate quantification remains an important objective in breath analysis, and the above collection techniques fall short in this regard, whereas SIFT-MS fulfils these objectives even though

* Correspondence to: P. Španěl, J. Heyrovský Institute of Physical Chemistry, Academy of Sciences of the Czech Republic, Dolejškova 3, 182 23 Prague 8, Czech Republic. E-mail: spanel@jh-inst.cas.cz

it does not yet have sufficient sensitivity to accurately quantify breath compounds present below ppbv concentrations. Fortunately, there is still much that can be done of good physiological and clinical value in the direct, on-line quantification of breath VOCs present at ppbv levels and above.^[5,18] It must be stressed that to achieve accurate quantification by SIFT-MS it is essential to characterise the kinetics of the ion chemical reactions (i.e. the rate coefficients and characteristic ion products) that underpin this analytical method.^[5,19] This has required continuous and wide-ranging studies of the kinetics of the reactions of the reagent ions H_3O^+ , O_2^+ and NO^+ with the trace compounds that need to be quantified in exhaled breath and other gaseous media.^[19,20] Whilst the ion chemistry of most of such compounds does not offer difficult experimental challenges, analyses of some compounds required focused studies, the results of which have been reported in the series of papers published in this journal. These compounds include hydrogen cyanide,^[21] hydrogen sulphide,^[22] formaldehyde^[23] and methane.^[24]

Recently, interest in real-time quantification of pentane in exhaled human breath using SIFT-MS has grown,^[25] since this is considered to be a valuable biomarker of oxidative stress, lipid peroxidation and inflammation in the body, including inflammatory bowel disease. (Note that according to the current IUPAC nomenclature, 'pentane' is the unbranched isomer, n-pentane.) In this paper, we first briefly discuss the production of pentane by lipid peroxidation and its appearance in exhaled human breath, which is the major focus of the present study. This is followed by a detailed report of a study of the kinetics of the reaction of the SIFT-MS O_2^+ reagent ions with pentane, description of the concomitant new method for the accurate quantification of pentane, and the construction of the kinetics library entry for its analysis in humid air and exhaled breath. Finally, the results of a pilot study are presented of the analysis of the exhaled breath of a cohort of patients suffering from two types of inflammatory bowel disease (IBD), viz. Crohn's disease (CD) and ulcerative colitis (UC), which demonstrate the viability of SIFT-MS analysis of breath pentane with indications of the potential of this to the diagnosis and subsequent treatment of these IBD conditions.

Pentane in exhaled breath; production by lipid peroxidation

Pentane has been known to be present in exhaled human breath for some years. Early GC studies sometimes confused this compound with isoprene that is present in exhaled breath in similar concentrations, but this was resolved by more careful GC separation methods.^[26] The reports from previous studies provide a very wide range of pentane concentrations: from 0.57 ± 0.3 nmol/L (13 ppbv)^[26] to 4 ± 0.5 nmol/L (90 ppbv)^[27,28] for healthy control subjects; 8.4 ± 2.9 nmol/L (190 ppbv) for acute asthma,^[28] 6.1 ± 1.2 nmol/L (140 ppbv) in the exhaled breath of patients with obstructive sleep apnea,^[27] as measured by GC/MS; 0.6 nmol/L (14 ppbv) for patients with non-small-cell lung cancer compared with 0.3 nmol/L (7 ppbv) for a healthy group measured by a combination of solid-phase microextraction with GC/MS, i.e. SPME/GC/MS,^[29] and about 1 ppbv for unmedicated patients with schizophrenia measured using thermal desorption coupled with GC/MS, i.e. TD/GC/MS.^[25] In another study, the alveolar gradient^[30] measured by TD/GC/MS was

increased in acutely psychotic schizophrenic patients by $+0.048$ nmol/L (+1 ppbv) compared with a control group; however, the laboratory background concentration in the inhaled air was greater than the concentration of pentane in the exhaled breath of the control group. The lack of consistency in the absolute values of concentrations of exhaled pentane explains the growing interest in an absolute direct method of its analysis in breath.

It is now understood that pentane production is the result of lipid peroxidation, which is associated with inflammatory processes (see below). Lipid peroxidation is a mechanism, which can be initiated by the oxygen activated radical species OH^\bullet . The initiation step is a hydrogen atom abstraction from a polyunsaturated fatty acid (LH, see Fig. 1) leading to a carbon-centred radical (L^\bullet), which, after reaction with oxygen, forms a peroxide radical (LOO^\bullet).^[31,32] This peroxide radical is able to abstract a hydrogen atom from another LH molecule (reinitiation) leading to the formation of a hydroperoxide (LOOH). In the presence of iron (Fe), LOOH is converted into an alkoxy radical. In the case of linoleic acid,^[33] this alkoxy radical is degraded into the pentanyl radical, which abstracts a hydrogen atom producing pentane, C_5H_{12} .

Pentane excretion in breath has been previously used as an index of lipid peroxidation based on the premise that this hydrocarbon is not metabolized. However, it is now known that pentane is metabolized by the liver in animals into 2-pentanol^[34,35] and that concentration of exhaled pentane is affected both by its production and by its metabolic loss.^[36]

Inflammatory bowel disease

It is the association of systemic pentane production with inflammatory processes that has revealed the need to investigate the possibility of SIFT-MS accurate quantification of pentane in breath, and especially because it is cited in previous work^[37,38] as a possible biomarker of inflammatory bowel disease (IBD), which is a serious health problem in modern society.

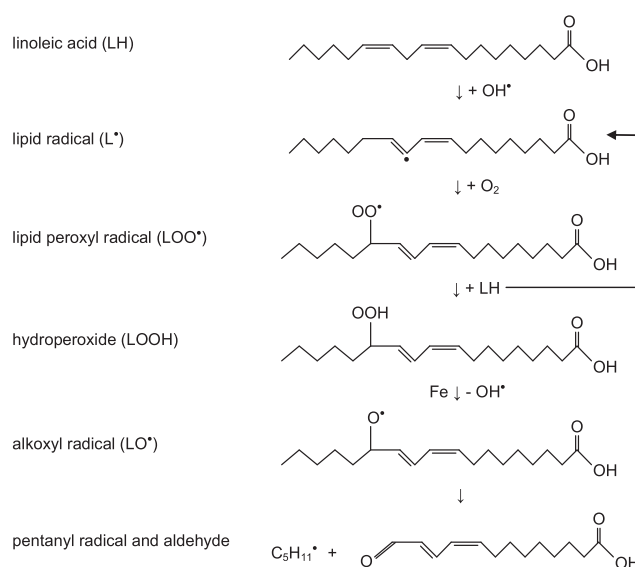


Figure 1. Scheme of the radical chemistry by which pentane is produced (compiled from information in Spittler^[32] and Rosa *et al.*^[33]).

Ulcerative colitis (UC) and Crohn's disease (CD) are types of chronic inflammatory bowel disease affecting the intestinal tract. The aetiology and pathogenesis of these autoimmune diseases still have not been entirely elucidated, but the roles of genetics, immune aberrations and bowel flora are unquestionable. Both UC and CD can seriously diminish the quality of life, lead to a shorter life expectancy and thus have significant negative socioeconomic consequences. They affect primarily young patients aged from 20 to 30 years. The estimated prevalence in the Czech population is about 0.3%, but accurate epidemiological data are not available.

Although UC and CD are similar diseases, the differences between them are crucial for correct diagnosis and optimal choice of treatment. In CD the location of the inflammation may occur anywhere along the digestive tract from the mouth to the anus, most usually in the last segment of the small intestine – the terminal ileum. In UC the large intestine (colon) is typically the only site that is affected. Another difference is in the depth of penetration of inflammation within an intestinal wall – UC is a disease of the mucosa only, whereas CD may affect the entire bowel wall. Many symptoms of UC and CD are similar (abdominal pain, diarrhea, weight loss), but there are some subtle differences. UC patients tend to have pain in the lower left part of the abdomen, while CD patients commonly (but not always) experience pain in the lower right abdomen. With UC, bleeding from the rectum during bowel movements is very common, but such bleeding is less common in patients with CD.^[39] In both diseases, severe extra-intestinal manifestations (arthritis, skin and ocular inflammation, thrombo-embolic complications or liver abnormalities) may occur.^[40] It is worthy of note that fecal volatile organic metabolites were recently identified, using SPME/GC/MS, that are characteristic of UC and CD.^[41]

Current treatments for IBD (pharmacological and surgical) can ameliorate symptoms, but there is no curative therapy available to date. Endoscopy (ileocoloscopy, enteroscopy and gastroscopy) and CT and MRI imaging and sonography are currently used to aid diagnosis of IBD and to differentially diagnose specific diseases. It is essential to monitor the activity of IBD using specialised clinical indices (Mayo index,^[42] Crohn's disease activity index – CDAI^[39]) or repeated endoscopic and imaging examinations, or to use biochemical analyses (serum C-reactive protein-CRP, faecal calprotectin) to adjust therapy, and accordingly plan the clinical follow-up. All currently used tests have some limitations, including low sensitivity (CRP, X-ray) and/or low specificity (CRP, calprotectin, imaging), and some of them bring discomfort or risk to the patient (endoscopy, X-ray). Thus, there is a need for new non-invasive methods for the diagnosis and therapeutic monitoring of IBD.

As outlined previously, IBD results in localised oxidative stress in the intestinal wall that causes degradation of cellular membranes by lipid peroxidation. Volatile organic compounds, including alkanes, produced by this process are transported by the blood stream into the lungs and thus appear in the exhaled breath. A previous study in CD^[43] indicated that breath pentane output in CD patients (7.5 ± 1 pmol/kg/min) was significantly ($p < 0.025$) greater than in control subjects (5 ± 0.5 pmol/kg/min). Whilst breath analysis cannot replace the conventional diagnostic methods (endoscopy with histopathology, CT and MRI studies, blood and faecal

biomarkers), which provide the detailed pathology and differentiate between the different forms of IBD, it does have the advantage that it is non-invasive and can, perhaps, be used as a monitor of the exacerbation and the effectiveness of treatment in diminishing the inflammation. This is the major motivation for developing the SIFT-MS method of pentane quantification and for the subsequent preliminary studies of pentane in the exhaled breath of healthy volunteers and patients suffering from IBD, as described in this paper.

Background on pentane ion chemistry relevant to SIFT-MS

In SIFT-MS there are just three reagent ionic species available for trace gas analysis, viz. H_3O^+ and NO^+ , which are those most commonly used, and O_2^+ , which is only rarely used when H_3O^+ and NO^+ do not react under SIFT-MS conditions with the particular gas/VOC to be analysed, as is the case for pentane,^[44] the focus of this paper. Since it has been reported that pentane reacts with H_3O^+ only by slow three body association and the $\text{H}_3\text{O}^+\text{M}$ product ions undergo rapid ligand switching with water molecules forming a water cluster,^[44,45] and NO^+ does not react with pentane at a measurable rate, they are not suitable for pentane analysis. Thus, O_2^+ reagent ions are the only option for pentane analysis in SIFT-MS, but this is not straightforward, because previous work has indicated that multiple product ions result from the O_2^+ /pentane reaction^[44,46] and no information has yet been obtained concerning their secondary reactions with the water molecules that are so abundant in exhaled breath samples. Whilst the basic kinetics of the reactions of O_2^+ with pentane have been studied previously using the SIFT technique,^[44–46] these data have not been utilized in SIFT-MS because of the uncertainties in the accurate value of the rate coefficient and the overlaps of the characteristic product ions with other isobaric product ions commonly present in the O_2^+ SIFT-MS spectra.^[47] It is imperative to establish accurate rate coefficients and product ion branching ratio for the analytical O_2^+ /pentane reaction, to fully understand any secondary ion chemistry and thus to choose appropriate characteristic ions if accurate quantification of pentane in exhaled breath is to be achieved. Thus, we have carried out a detailed study to provide these data, which is described below.

EXPERIMENTAL

There are two distinct experimental phases of this study. (i) A detailed study of the kinetics of reaction of the SIFT-MS O_2^+ reagent ions with pentane in order to establish the accurate rate coefficient for the reaction and the precise branching ratio of the product ions and to investigate their secondary reactions with water vapour. Hence, a kinetics library entry that formalizes pentane quantification using SIFT-MS was obtained. (ii) Pilot breath analyses testing the use of this SIFT-MS method to analyse pentane in the exhaled breath of healthy people and of patients suffering from CD and UC.

The kinetics of the reaction of O_2^+ with pentane and the influence of water vapour

The previous work performed using the traditional SIFT method to determine the rate coefficients^[48] involved indirect

measurement of the flow rate of pentane gas^[49] using an MKS flow meter and a 'gas correction factor'. In the present work, two independent absolute approaches to creating known dilute concentrations of pentane in air were followed.

First, sequential dilution of pentane gas in which 200 μL of liquid pentane (cooled down to -4°C) was injected into a 2 L glass vessel filled by synthetic air at atmospheric pressure and allowed to fully evaporate and equilibrate. Then 2 mL of this gas mixture was injected into a second 2 L vessel again filled by synthetic air and the concentration of pentane vapour was calculated volumetrically.

Secondly, known pentane mixtures were created using the permeation tube method, as described for the previously reported SIFT-MS validations for several VOCs.^[50] The permeation device was constructed in the form of a small glass vial containing pentane closed by a Nalophan film (the permeation membrane) to provide a stable concentration of pentane vapour in a continuous flow of 25 mL/min of synthetic air. The pentane permeation rate, q_d , was calculated from the change in weight of the vial pentane source over 3 h of operation. The pentane concentration, C , was then calculated as:

$$C = \frac{q_d}{Q} \cdot \frac{22.4 \text{ L/mol}}{M} \quad (1)$$

where Q is the flow rate of air through the permeation device and M is the molar mass of pentane.

The kinetics of the O_2^+ /pentane reaction were studied using the *Profile 3* SIFT-MS instrument (Instrument Science Ltd, Crewe, UK) in the SIFT mode, as described previously.^[51–53] O_2^+ reagent ions were prepared in a microwave discharge through a mixture of air and water vapour, filtered using an injection mass filter, and injected into the flow tube (5 cm length, 1 cm diameter) into helium carrier gas (1 Torr pressure, 300 K temperature). Known flow rates of the prepared pentane/air mixtures were introduced into the helium carrier gas via a heated calibrated capillary. Precise determination of the product ion branching ratios was carried out by sequentially decreasing the pentane concentration using an in-line metering valve and extrapolating the product ion count rates obtained by the downstream mass spectrometer to zero flow in order to exclude the influence of any secondary reactions.^[48]

In order to investigate the influence of water vapour on the analytical product ions, liquid water was injected into the pentane/air mixture in the glass bottle to elevate its humidity and the vessel was heated to 40°C to reach a humidity corresponding to exhaled breath. The pentane concentration, as calculated from the ratio of the product ion count rates to the O_2^+ precursor ion count rates,^[20] was recorded and compared with the expected value as measured in the absence of water vapour. The kinetics library entry was then optimized to suppress the effect of water vapour on the count rates of characteristic product ions using the approach described in Dryahina *et al.*^[24]

Breath analysis

Approval for the study was obtained from the Ethics Committee of Iscare I.V.F. a.s (Prague, Czech Republic). Breath analysis studies involving the patients were performed at the IBD Centre of Iscare, which focuses on

diagnoses and treatment of patients with CD and UC. The data for the healthy control group were obtained at the J. Heyrovsky Institute of Physical Chemistry, Prague (JHI). The diagnosis of Crohn's disease and ulcerative colitis in the selected cohort of patients was established according to the ECCO guidelines.^[39] Patients and healthy volunteers provided informed consent before providing the breath samples. The breath analyses were performed using a *Profile 3* SIFT-MS instrument, which was located in the clinic to directly analyse patients' breath and at the JHI to directly analyse the breath of the healthy volunteers. Real-time sampling of three successive exhalations and inhalations via the mouth by each volunteer was performed using a disposable mouthpiece.^[4,54] A constant flow rate of sample (25 mL/min) was introduced via a heated (70°C) PEEK capillary into the SIFT-MS flow tube. The local ambient air was analysed during the inhalation phases, as indicated in Fig. 2.

The numbers of healthy volunteers and patients with CD and UC (Male, M, and female, F), together with the age ranges and also the status of the diseases, are given in Table 1. Note the large number of healthy volunteers and that these data were obtained in a single day, which shows the very rapid data acquisition allowed by on-line analyses of exhaled breath by SIFT-MS (see also Dryahina *et al.*^[55]).

RESULTS AND DISCUSSION

Ion chemistry of pentane

In agreement with previous work, it was observed that pentane does not react at a significant rate with H_3O^+ or NO^+ under the thermalised conditions (300 K) of SIFT-MS, but it does react with O_2^+ . The first SIFT study of this reaction was carried out in 1996 as part of the early exploration of the usefulness of the NO^+ and O_2^+ reagent ions for trace gas analysis.^[46] Thus, the rate coefficient for the O_2^+ /pentane reaction was measured as $8 \times 10^{-10} \text{ cm}^3 \text{ s}^{-1}$ at 300 K compared with the collisional rate coefficient of $1.6 \times 10^{-9} \text{ cm}^3 \text{ s}^{-1}$. This 300 K value is adopted in this study and, as we show later, it is confirmed by the present experimental validation using standard mixtures. This previous determination^[42] was achieved using a mass flow meter and a tabulated gas correction factor to measure the flow rate of pentane vapour into the helium carrier gas. In a subsequent 1998 SIFT study, the rate coefficient for this reaction was assumed to be equal to the calculated theoretical collisional rate coefficient.^[44] In both these SIFT studies the ion product ratios were also reported and there are significant differences between the reported values from the two studies. Also, no attempt was previously made to investigate the influence of water vapour on the ion products. This is an unacceptable situation given the current desire to use accurate rate coefficients and product ion distributions that will provide accurate analyses of exhaled breath pentane. Thus, the major objective of this part of the present study was to determine accurate product ion branching ratios, to check the rate coefficient for the reaction, and to select suitable characteristic product ions for the accurate analysis of breath pentane by SIFT-MS.

The first stage of this procedure was to introduce into the helium carrier gas sufficient pentane to reduce the precursor O_2^+ ion count rate only slightly (no more than a few %) and

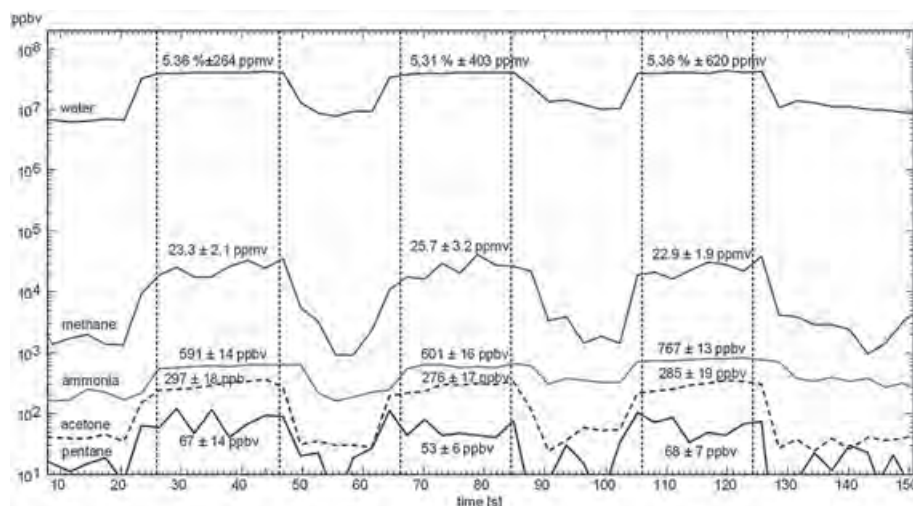
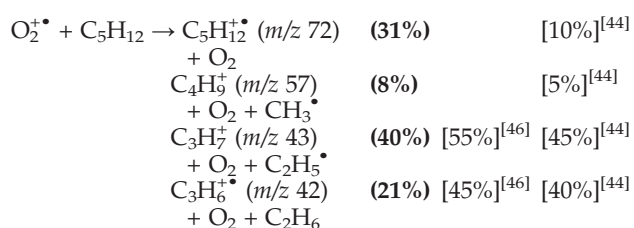


Figure 2. Typical data obtained by SIFT-MS for the on-line analysis of three sequential inhalations and exhalations by a single IBD patient indicating concentrations of water vapour (in %),^[56] methane (ppmv),^[24] ammonia (ppbv) and pentane (ppbv). Mean concentrations of particular metabolites are obtained by numerical integration within intervals demarcated by the vertical dashed lines.

Table 1. Characteristics of the study group

Diagnose	Number	Age range (years)	Active/remission
healthy controls	140 (69M and 71F)	16–68	–
Crohn's disease, CD	20 (10M and 10F)	21–66	9/11
ulcerative colitis, UC	28 (13M and 15F)	18–53	14/14

to operate the analytical mass spectrometer in the full scan mode^[20] in order to identify the ion products of the reaction. Four distinct product ions appeared; the percentage product distributions are given in bold and those for the previous studies^[40,42] are given in square brackets:



The next phase of the present study was to investigate the variation of the count rates of these four product ions as the pentane flow into the helium was varied using the SIFT-MS instrument in the multiple ion monitoring mode.^[19] The true primary product ion branching ratio is obtained at the limit of zero pentane flow at which secondary reactions of these primary ions with pentane are eliminated. Thus, the percentage product ion distribution arrived at is given in bold in parentheses in the equation above. The failure to recognize the significant product ion at m/z 72 in the previous study^[42] was possibly due to the inadequate resolution of the analytical mass spectrometer and the overlap of this product ion with the ubiquitous $\text{H}_3\text{O}^+(\text{H}_2\text{O})_3$ ion at m/z 73 that is present in SIFT-MS spectra even when using O_2^+ precursor ions.^[47] However, what is most important now is that the

ion product distributions determined in this study have been obtained with much greater precision than was possible previously. Equally important is that this branching ratio has been obtained under conditions closely equivalent to those under which the pentane analysis is carried out using the same SIFT/SIFT-MS instrument.

Choice of characteristic product ion for the SIFT-MS quantification of pentane

In principle, for accurate SIFT-MS analyses, all the product ions of the utilized analytical reaction should be included,^[20] but in practice this is sometimes not possible due to the overlap of product ions of the reactions of other trace gases present in real samples such as breath, as mentioned previously. It is then necessary to recognize these potential overlaps and use only those product ions that are unambiguously identified while accounting for the omission of the overlapping product ions in the final quantifications. This is the situation for the O_2^+ /pentane reaction indicated above; it is not possible to use the m/z 43 ion in the analysis because an isobaric m/z 43 ion is a common fragment of the reactions of ketones with O_2^+ , especially for acetone that is always present at significant concentrations (typically greater than pentane) in exhaled breath.^[4] This ion must therefore be excluded from the pentane analysis. The product ion at m/z 57 must also be excluded because it is isobaric with the ^{18}O isotopologue of the $\text{H}_3\text{O}^+(\text{H}_2\text{O})_2$ ion that is always present in SIFT-MS spectra.^[47]

Thus, we are left with the product ions at m/z 42 and 72 for the analysis of pentane using O_2^+ reagent ions.

Influence of water vapour on the count rates of the product ions at m/z 42 and 72

It is essential to investigate if the analytical product ions react with the water molecules that are abundant in the exhaled breath samples to be analysed. This was achieved as described above. The absolute humidity of the sample was determined in the now familiar and routine way by determining the relative count rates of the reagent ions and their hydrates in SIFT-MS, as has been reported in detail in previous publications.^[20,56] Data obtained over an absolute humidity range for the pentane/air/water vapour mixture are given in Fig. 3. In Fig. 3(a) it can be seen that the chosen m/z 42 analytical product ion ($C_3H_6^+$) reacts only slowly with H_2O molecules, whereas the reaction of the chosen m/z 72 analytical product ion ($C_5H_{12}^+$) is faster. The percentage product distributions and the variation with humidity of the sample are shown in Fig. 3(b).

Plots are shown in Fig. 4(a) of the pentane concentration, as calculated using each of the m/z 42 and 72 product ions separately and also using the sum of the count rates of these two product ions by adopting a rate coefficient $8 \times 10^{-10} \text{ cm}^3 \text{ s}^{-1}$,^[46] as a function of the sample humidity. Clearly, the fractions of these ions must be increased to account for the fractions of the unused ions at m/z 43 and 57 to obtain accurate analyses. These corrections can be seen as the factors of 4 and 2 associated with each ion seen in the library entries given in Table 2. As can be seen, the apparent pentane

concentration varies only slowly with humidity when using the m/z 42 product ion only, but markedly reduces with humidity when using the m/z 72 product ion only.

Clearly, compensation is required for the influence of humidity in the SIFT-MS analysis of pentane. This can be achieved by including the $H_3O^+(H_2O)_2$ m/z 55 ion, formed by a sequence of reactions of O_2^+ with water vapour,^[47] into the calculation of concentration of pentane molecules in the flow tube $[M]$ as:

$$[M] = \frac{1 f_{p1}[42] + f_{p2}[72]}{kt_r [32] - f_{i2}[55]} \quad (2)$$

where k is the rate coefficient for the reaction of O_2^+ with pentane, t_r is the reaction time,^[20] the numbers in square brackets indicate the count rates of ions at the specific m/z (32, 42, 55 and 72), and f_{p1} , f_{p2} , f_{i2} are coefficients obtained by the least-squares fitting of the values calculated using Eqn. (2) from the experimentally determined count rates to the expected constant humidity independent concentration $[M]$. Fitting of the data from Fig. 4(a) thus results in values $f_{p1} = f_{p2} = 2$ and $f_{i2} = 5$ and the results of calculation using these coefficients are included in Fig. 4(b). Thus, a kinetics library entry in the format used in Profile 3 SIFT-MS software^[52] can be constructed as indicated in Table 2. A discussion of the construction of such kinetics library entries is given in recent publications.^[24,52,57]

Using this library entry and exploiting both m/z 42 and 72 product ions, the plot of pentane concentration with and without compensation for the humidity is shown in Fig. 4(b).

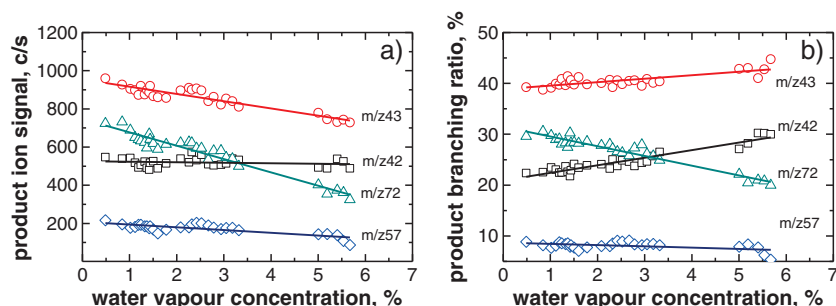


Figure 3. (a) Influence of absolute humidity on the count rates of product ions of O_2^+ reaction with pentane. (b) The variation of the percentage product distributions with humidity of the sample.

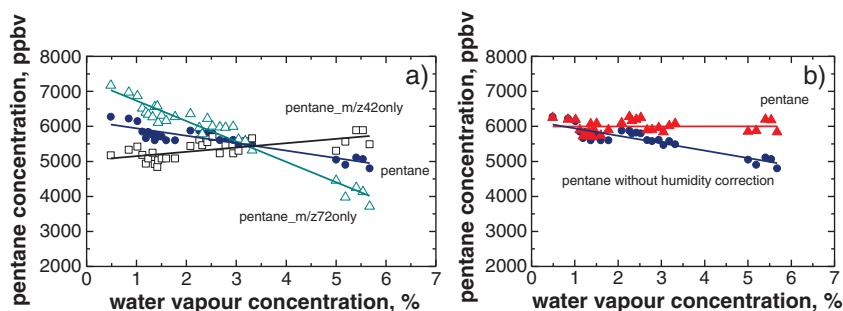


Figure 4. (a) Concentrations of pentane calculated using three kinetics library entries indicated (m/z 42 only, m/z 72 only, and a sum of both, pentane) without correction for humidity. (b) Concentrations of pentane calculated from the sum of both m/z 42 and m/z 72 with and without correction for humidity.

Table 2. SIFT-MS kinetics library entries for the determination of the concentrations of pentane in humid samples using O_2^+ reagent ions

pentane (without humidity correction)	pentane (m/z 42 only)	pentane (m/z 72 only)	pentane (with humidity correction)
1 precursor 32 0.8e-9 1.0	1 precursors 32 0.8e-9 1.0	1 precursors 32 0.8e-9 1.0	2 precursors 32 0.8e-9 1.0
2 products 42 2.0 72 2.0	1 product 42 4.0	1 product 72 4.0	55 0.8e-9 -5.0 2 products 42 2.0 72 2.0

The variation in the derived compensated pentane concentration with humidity is only about 10% over the complete absolute humidity range up to that appropriate for exhaled breath of 6%, which, even if ignored, would be quite acceptable for breath analysis studies given such small variations would normally be subsumed by biological variability. Nevertheless, it is our aim to quantify breath metabolites as accurately as possible to eliminate any uncertainties and to provide the facility to study small changes such as diurnal variations.

Results of validation of the rate coefficient using standard mixtures of pentane in air

As described in the Experimental section, standard mixtures of pentane in dry air were prepared using known amounts of liquid pentane dispersed into a known volume of air and also using the permeation tube method. These mixtures were then analysed using the kinetics library entry for pentane given above using a rate coefficient of $8 \times 10^{-10} \text{ cm}^3 \text{ s}^{-1}$. The results are summarized in Table 3.

As can be seen, there is excellent agreement between the expected pentane concentration and that measured with SIFT-MS using both methods of preparation of the pentane/air mixtures. This provides evidence that the rate coefficient for the O_2^+ /pentane reaction is $8 \times 10^{-10} \text{ cm}^3 \text{ s}^{-1}$ with a relative error less than $\pm 5\%$ (in agreement with Španěl and Smith^[46] but with better accuracy) and the characteristic product ions are properly representative of pentane. It is thus now possible to measure the concentration of breath pentane with confidence given also that proper compensation has been made for the presence of water vapour.

Analysis of pentane in exhaled breath

The details of these measurements and of the cohorts of healthy volunteers and patients with IBD were described previously. A summary of the data obtained that include the numbers of persons in each volunteer cohort (count), with the gender split for the healthy cohort, and the summary statistics is given in Table 4.

Note that the mean values and the median values are both given. The similarity of these mean and median values implies that the population distribution for breath pentane is reasonably close to normal. There are sufficient numbers in the healthy cohort to construct the distribution and this can be seen in Fig. 5. Note that there is a small but apparently significant difference between breath pentane for male and female healthy controls ($p < 10^{-3}$). A similar but not significant difference was observed between the male and female patients ($p = 0.2$). The difference between breath pentane for healthy persons and the patients with IBD is, however, clear and quite stark, especially for the patients with CD, as can be seen in Table 4 and the statistical evaluation. This is the important result of these studies, as it offers a non-invasive monitor of these IBD conditions, which has value to clinicians involved in their treatment.

These differences are well illustrated by the box-and-whisker plots shown in Fig. 6 for the three identifiable cohorts – healthy, patients with CD, patients with UC. The breath concentration of pentane thus seems to be relevant for IBD diagnostics. This is reinforced by the receiver operating curve (ROC, see Fig. 7) for diagnostic sensitivity and specificity of pentane concentration as a biomarker of IBD. The area under the curve (AUC) is 0.927 and the pentane threshold concentration corresponding to the maximal Youden index (0.70) is 53 ppbv.

Table 3. Expected concentrations of pentane in prepared standard mixtures in parts-per-million by volume, ppmv, and the results of their quantitative SIFT-MS analyses using Eqn. (2) and a rate coefficient $8 \times 10^{-10} \text{ cm}^3 \text{ s}^{-1}$

Method	Comments	Expected, ppmv	Obtained, ppmv
mixture I	200 μL of liquid pentane into a 2 L	19441	-----*
mixture II	1 mL of mixture I into a 2 L of dry air	9.72	10.15
permeation	Permeation rate 847ng/min, with air flow 25 mL/min	10.51	10.73

*Concentration too large for quantification by SIFT-MS.

Table 4. Summary statistics: average, median, standard deviation (S.D.) and inter-quartile concentration ranges, all in parts-per-billion by volume, ppbv, in exhaled breath

Studied group	Count	Pentane, ppbv				p
		mean	median	S.D.	quartile	
healthy	140	40	38	17	27 – 52	
male	69	45	43	16	33 – 56	$\sim 10^{-3*}$
female	71	35	30	16	24 – 43	
Crohn's disease	20	114	113	46	73 – 142	$< 10^{-7**}$
Ulcerative colitis	28	84	73	28	57 – 96	$< 10^{-7**}$

*p value characterizing the significance of the difference between male and female groups calculated by the t-test
 **p value characterizing the significance of the difference between IBD (both CD and UC) and healthy groups calculated by the t-test

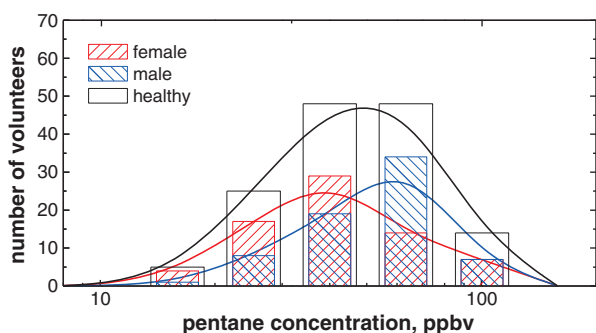


Figure 5. Population distributions of breath pentane (concentration in parts-per-billion by volume, ppbv) in the exhaled breath of 140 healthy controls.

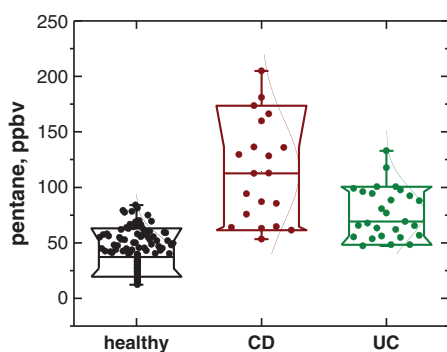


Figure 6. Box-and-whisker plots for the breath pentane concentrations in parts-per-billion by volume, ppbv, for the three cohorts – healthy, patients with CD and patients with UC. The boxes range from 10th to 90th percentiles with the narrower part indicating 25th and 75th percentiles and the near-centre horizontal lines indicate medians. The whiskers indicate the ranges (min to max) and the curves outline the fitted normal distributions.

The pentane concentrations observed in the breath of patients with CD were significantly different from those in UC patients ($p = 0.0058$). However, the sensitivity and specificity of pentane concentration as a biomarker to distinguish these two patient groups were low ($AUC = 0.68$,

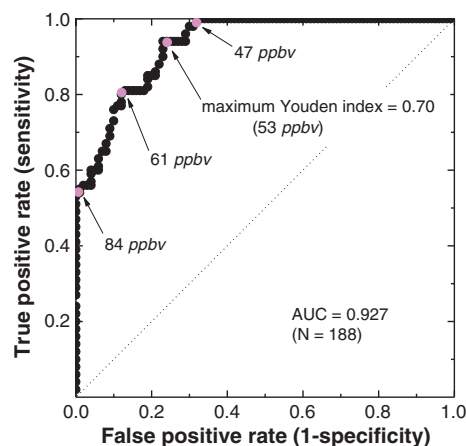


Figure 7. The exhaled breath concentration of pentane turns out to be significant for IBD diagnostics. This Receiver Operating Curve (ROC) demonstrates the relevance of pentane as a predictor of IBD. The area under the curve (AUC) is 0.927 and the pentane concentration corresponding to a maximal Youden index (0.70) is 53 ppbv.

Youden index = 0.42). A major motivation for this study was to investigate if there was any quantitative relation of the breath pentane concentration with the inflammation activity. However, possibly due to the small cohort sizes, no significant difference was seen between patients classed as active or remission ($p = 0.93$ for CD and $p = 0.46$ for UC).

CONCLUDING REMARKS

We have taken great care to ensure that the quantification of pentane in exhaled breath by SIFT-MS is as accurate as currently be achieved, because of the potential importance of such measurements in medicine. This has been achieved by detailed and careful studies of the ion chemistry that underpins pentane measurements by SIFT-MS in dry and especially in humid air, the latter being of particular importance due to the high humidity of exhaled breath. The SIFT-MS analyses have been checked and validated by the use of prepared standard mixtures of pentane.

Having this analytical tool for breath pentane quantification, we have carried out a pilot study of the exhaled breath of cohorts of patients suffering from two forms of inflammatory bowel disease (IBD), viz. Crohn's disease (CD) and ulcerative colitis (UC), with the necessary parallel cohort of healthy volunteers. The results reveal that breath pentane, as measured in single exhalations in real time without sample collection or storage, is significantly elevated in the breath of both CD patients and UC patients relative to the healthy controls, being at a somewhat lower mean concentration in UC than CD breath, with statistical analysis indicating that these elevations in the patients' breath are significant. The mean/median values for breath pentane in ppbv are: Healthy (40, 38), CD patients (114, 113), UC patients (84, 73), which establish the benchmark values for these cohorts.

These breath pentane values are similar to those values obtained in some previous studies of healthy populations (13 to 90 ppbv)^[26–28] and patients with other clinical conditions (140 to 190 ppbv).^[27,28] However, these values and those determined in the present study do not overlap with the very low concentrations reported for breath pentane in patients with acutely psychotic conditions and parallel healthy volunteers (1 ppbv)^[30] as obtained using TD/GC/MS.

The value of the present SIFT-MS measurements of exhaled breath pentane is that they were obtained on-line and in real time in single breath exhalations and so data acquisition is very fast and reliable, because sample collection is avoided with all the potential complications that entails. Thus, rapid measurement of pentane concentration in breath of patients can be carried out in the clinic with neither pain nor long waiting periods for the patients. Further extensive studies of breath pentane and other trace metabolites, including aldehydes, (also possible biomarkers of oxidative stress^[58]) in exhaled breath using SIFT-MS are now possible as a contribution and support to clinical diagnosis and therapeutic monitoring.

REFERENCES

- [1] A. Amann, D. Smith. *Breath Analysis for Clinical Diagnosis and Therapeutic Monitoring*. World Scientific, Singapore, 2005.
- [2] A. Amann, D. Smith. *Volatile Biomarkers: Non-Invasive Diagnosis in Physiology and Medicine*. Elsevier, 2013.
- [3] T. H. Risby, S. F. Solga. Current status of clinical breath analysis. *Appl. Phys. B –Lasers and Optics* 2006, 85, 421.
- [4] P. Španěl, D. Smith. Progress in SIFT-MS; breath analysis and other applications. *Mass Spectrom. Rev.* 2011, 30, 236.
- [5] D. Smith, P. Španěl. Selected ion flow tube mass spectrometry (SIFT-MS) for on-line trace gas analysis. *Mass Spectrom. Rev.* 2005, 24, 661.
- [6] K. Schwarz, W. Filipiak, A. Amann. Determining concentration patterns of volatile compounds in exhaled breath by PTR-MS. *J. Breath Res.* 2009, 3, 027002.
- [7] J. King, P. Mochalski, A. Kupferthaler, K. Unterkofler, H. Koc, W. Filipiak, S. Teschl, H. Hinterhuber, A. Amann. Dynamic profiles of volatile organic compounds in exhaled breath as determined by a coupled PTR-MS/GC-MS study. *Physiological Measurement* 2010, 31, 1169.
- [8] D. Smith, P. Španěl. Direct, rapid quantitative analyses of BVOCs using SIFT-MS and PTR-MS obviating sample collection. *TRAC – Trends Anal. Chem.* 2011, 30, 945.
- [9] P. Španěl, D. Smith. Volatile compounds in health and disease. *Curr. Opin. Clin. Nutr. Metab. Care* 2011, 14, 455.
- [10] D. Smith, C. Turner, P. Španěl. Volatile metabolites in the exhaled breath of healthy volunteers: their levels and distributions. *J. Breath Res.* 2007, 1, 014004.
- [11] C. Turner, P. Španěl, D. Smith. A longitudinal study of ammonia, acetone and propanol in the exhaled breath of 30 subjects using selected ion flow tube mass spectrometry, SIFT-MS. *Physiological Measurement* 2006, 27, 321.
- [12] C. Turner, P. Španěl, D. Smith. A longitudinal study of breath isoprene in healthy volunteers using selected ion flow tube mass spectrometry (SIFT-MS). *Physiological Measurement* 2006, 27, 13.
- [13] C. Turner, P. Španěl, D. Smith. A longitudinal study of ethanol and acetaldehyde in the exhaled breath of healthy volunteers using selected-ion flow-tube mass spectrometry. *Rapid Commun. Mass Spectrom.* 2006, 20, 61.
- [14] C. Turner, P. Španěl, D. Smith. A longitudinal study of methanol in the exhaled breath of 30 healthy volunteers using selected ion flow tube mass spectrometry, SIFT-MS. *Physiological Measurement* 2006, 27, 637.
- [15] I. Horvath, Z. Lazar, N. Gyulai, M. Kollai, G. Losonczy. Exhaled biomarkers in lung cancer. *Eur. Respir. J.* 2009, 34, 261.
- [16] W. Filipiak, V. Ruzsanyi, P. Mochalski, A. Filipiak, A. Bajtarevic, C. Ager, H. Denz, W. Hilbe, H. Jamnig, M. Hackl, A. Dzien, A. Amann. Dependence of exhaled breath composition on exogenous factors, smoking habits and exposure to air pollutants. *J. Breath Res.* 2012, 6, 036008.
- [17] B. Wzorek, P. Mochalski, I. Sliwka, A. Amann. Application of GC-MS with a SPME and thermal desorption technique for determination of dimethylamine and trimethylamine in gaseous samples for medical diagnostic purposes. *J. Breath Res.* 2010, 4, 026002.
- [18] P. Španěl, D. Smith. Progress in SIFT-MS: breath analysis and other applications. *Mass Spectrom. Rev.* 2011, 30, 236.
- [19] D. Smith, P. Španěl. Ambient analysis of trace compounds in gaseous media by SIFT-MS. *Analyst* 2011, 136, 2009.
- [20] P. Španěl, K. Dryahina, D. Smith. A general method for the calculation of absolute trace gas concentrations in air and breath from selected ion flow tube mass spectrometry data. *Int. J. Mass Spectrom.* 2006, 249, 230.
- [21] P. Španěl, T. S. Wang, D. Smith. Quantification of hydrogen cyanide in humid air by selected ion flow tube mass spectrometry. *Rapid Commun. Mass Spectrom.* 2004, 18, 1869.
- [22] P. Španěl, D. Smith. Quantification of hydrogen sulphide in humid air by selected ion flow tube mass spectrometry. *Rapid Commun. Mass Spectrom.* 2000, 14, 1136.
- [23] P. Španěl, D. Smith, T. A. Holland, W. Al Singary, J. B. Elder. Analysis of formaldehyde in the headspace of urine from bladder and prostate cancer patients using selected ion flow tube mass spectrometry. *Rapid Commun. Mass Spectrom.* 1999, 13, 1354.
- [24] K. Dryahina, D. Smith, P. Španěl. Quantification of methane in humid air and exhaled breath using selected ion flow tube mass spectrometry. *Rapid Commun. Mass Spectrom.* 2010, 24, 1296.
- [25] B. Ross, S. Shah, M. Peet. Increased breath ethane and pentane concentrations in currently unmedicated patients with schizophrenia. *Open J. Psychiatry* 2011, 1, 1.
- [26] S. Mendis, P. A. Sobotka, D. E. Euler. Pentane and isoprene in expired air from humans - gas-chromatographic analysis of single-breath. *Clin. Chem.* 1994, 40, 1485.
- [27] C. O. Olopade, J. A. Christon, M. Zakkar, C. W. Hua, W. I. Swedler, P. A. Scheff, I. Rubinstein. Exhaled pentane and nitric oxide levels in patients with obstructive sleep apnea. *Chest* 1997, 111, 1500.
- [28] C. O. Olopade, M. Zakkar, W. I. Swedler, I. Rubinstein. Exhaled pentane levels in acute asthma. *Chest* 1997, 111, 862.

- [29] D. Poli, P. Carbognani, M. Corradi, M. Goldoni, O. Acampa, B. Balbi, L. Bianchi, M. Rusca, A. Mutti. Exhaled volatile organic compounds in patients with non-small cell lung cancer: cross sectional and nested short-term follow-up study. *Respir. Res.* **2005**, *6*, 71.
- [30] M. Phillips, M. Sabas, J. Greenberg. Increased pentane and carbon-disulfide in the breath of patients with schizophrenia. *J. Clin. Pathol.* **1993**, *46*, 861.
- [31] A. Vangossum, J. Decuyper. Breath alkanes as an index of lipid-peroxidation. *Eur. Respir. J.* **1989**, *2*, 787.
- [32] G. Spiteller. Peroxidation of linoleic acid and its relation to aging and age dependent diseases. *Mechanisms Ageing Develop.* **2001**, *122*, 617.
- [33] A. Rosa, G. Appendino, M. P. Melis, M. Deiana, A. Atzeri, I. Alessandra, A. Minassi, M. A. Dessi. Protective effect and relation structure-activity of nonivamide and iododerivatives in several models of lipid oxidation. *Chemico-Biological Interactions* **2009**, *180*, 183.
- [34] J.-K. Kim, H.-W. Cho, J.-H. Han, S.-B. Lee, Y.-H. Chung, K.-T. Rim, J.-S. Yang. Subchronic Inhalation Toxicity Study of n-pentane in Rats. *Saf. Health Work* **2012**, *3*, 224.
- [35] U. Frommer, V. Ullrich, H. Stauding. Hydroxylation of aliphatic compounds by liver microsomes. 1. Distribution pattern of isomeric alcohols. *Hoppe-Seylers Zeitschrift fur Physiologische Chemie* **1970**, *351*, 903.
- [36] S. R. B. Allerheiligen, T. M. Ludden, R. F. Burk. The pharmacokinetics of pentane, a by-product of lipid-peroxidation. *Drug Metabo. Dispos.* **1987**, *15*, 794.
- [37] J. Kokoszka, R. L. Nelson, W. I. Swedler, J. Skosey, H. Abcarian. Determination of inflammatory bowel-disease activity by breath pentane analysis. *Diseases of the Colon & Rectum* **1993**, *36*, 597.
- [38] S. Sedghi, A. Keshavarzian, M. Klamut, D. Eiznhamer, E. J. Zarling. Elevated breath ethane levels in active ulcerative-colitis – evidence for excessive lipid-peroxidation. *Am. J. Gastroenterol.* **1994**, *89*, 2217.
- [39] G. Van Assche, A. Dignass, J. Panes, L. Beaugerie, J. Karagiannis, M. Allez, T. Ochsenkuhn, T. Orchard, G. Rogler, E. Louis, L. Kupcinkas, G. Mantzaris, S. Travis, E. Stange, Ecco. The second European evidence-based consensus on the diagnosis and management of Crohn's disease: Definitions and diagnosis. *J. Crohns & Colitis* **2010**, *4*, 7.
- [40] M. Lukas, M. Bortlik, Z. Maratka. What is the origin of ulcerative colitis? Still more questions than answers. *Postgrad. Med. J.* **2006**, *82*, 620.
- [41] I. Ahmed, R. Greenwood, B. D. Costello, N. M. Ratcliffe, C. S. Probert. An investigation of fecal volatile organic metabolites in irritable bowel syndrome. *Plos One* **2013**, *8*, 13.
- [42] G. D'Haens, W. J. Sandborn, B. G. Feagan, K. Geboes, S. B. Hanauer, E. J. Irvine, M. Lemann, P. Marteau, P. Rutgeerts, J. Scholmerich, L. R. Sutherland. A review of activity indices and efficacy end points for clinical trials of medical therapy in adults with ulcerative colitis. *Gastroenterology* **2007**, *132*, 763.
- [43] B. E. Wendland, E. Aghdassi, C. Tam, J. Carrier, A. H. Steinhart, S. L. Wolman, D. Baron, J. P. Allard. Lipid peroxidation and plasma antioxidant micronutrients in Crohn disease. *Am. J. Clin. Nutr.* **2001**, *74*, 259.
- [44] P. Španěl, D. Smith. Selected ion flow tube studies of the reactions of H_3O^+ , NO^+ , and O_2^+ with several aromatic and aliphatic hydrocarbons. *Int. J. Mass Spectrom.* **1998**, *181*, 1.
- [45] G. J. Francis, P. F. Wilson, D. B. Milligan, V. S. Langford, M. T. McEwan. GeoVOC: A SIFT-MS method for the analysis of small linear hydrocarbons of relevance to oil exploration. *Int. J. Mass Spectrom.* **2007**, *268*, 38.
- [46] P. Španěl, D. Smith. A selected ion flow tube study of the reactions of NO^+ and O_2^+ ions with some organic molecules: The potential for trace gas analysis of air. *J. Chem. Phys.* **1996**, *104*, 1893.
- [47] P. Španěl, D. Smith. Influence of weakly bound adduct ions on breath trace gas analysis by selected ion flow tube mass spectrometry (SIFT-MS). *Int. J. Mass Spectrom.* **2009**, *280*, 128.
- [48] N. G. Adams, D. Smith. Selected ion flow tube (SIFT) – technique for studying ion-neutral reactions. *Int. J. Mass Spectrom. Ion Processes* **1976**, *21*, 349.
- [49] P. Španěl, D. Smith. A selected ion flow tube study of the reactions of NO^+ and O_2^+ ions with some organic molecules: The potential for trace gas analysis of air. *J. Chem. Phys.* **1996**, *104*, 1893.
- [50] D. Smith, P. Španěl, J. M. Thompson, B. Rajan, J. Cocker, P. Rolfe. The selected ion flow tube method for workplace analyses of trace gases in air and breath: Its scope, validation, and applications. *Appl. Occupational Environ. Hyg.* **1998**, *13*, 817.
- [51] K. Dryahina, B. K. C. de Miranda, P. Španěl, J. Zabka, C. Alcaraz, Z. Herman. Selected ion flow tube study of ion molecule reactions of $\text{N}^+(\text{P}-3)$ and Kr^+ with C-3 hydrocarbons propane, propene, and propyne. *J. Phys. Chem. A* **2011**, *115*, 7310.
- [52] K. Sovova, K. Dryahina, P. Španěl. Selected ion flow tube (SIFT) studies of the reactions of H_3O^+ , NO^+ and O_2^+ with six volatile phytochemical esters. *Int. J. Mass Spectrom.* **2011**, *300*, 31.
- [53] D. Smith, K. Sovova, P. Španěl. A selected ion flow tube study of the reactions of H_3O^+ , NO^+ and O_2^+ with seven isomers of hexanol in support of SIFT-MS. *Int. J. Mass Spectrom.* **2012**, *319*, 25.
- [54] T. Wang, A. Pysanenko, K. Dryahina, P. Španěl, D. Smith. Analysis of breath, exhaled via the mouth and nose, and the air in the oral cavity. *J. Breath Res.* **2008**, *2*, 037013.
- [55] K. Dryahina, D. Smith, P. Španěl. Quantification of methane in humid air and exhaled breath using selected ion flow tube mass spectrometry. *Rapid Commun. Mass Spectrom.* **2010**, *24*, 1296.
- [56] P. Španěl, D. Smith. On-line measurement of the absolute humidity of air, breath and liquid headspace samples by selected ion flow tube mass spectrometry. *Rapid Commun. Mass Spectrom.* **2001**, *15*, 563.
- [57] P. Španěl, D. Smith. Advances in on-line absolute trace gas analysis by SIFT-MS. *Curr. Anal. Chem.* **2013**, *9*, 525.
- [58] M. Corradi, P. Pignatti, P. Manini, R. Andreoli, M. Goldoni, M. Poppa, G. Moscato, B. Balbi, A. Mutti. Comparison between exhaled and sputum oxidative stress biomarkers in chronic airway inflammation. *Eur. Respir. J.* **2004**, *24*, 1011.

Appendix D, Shestivska *et al.* Rapid Commun. Mass Spectrom. 25 (2011) 2459

Quantification of methyl thiocyanate in the headspace of *Pseudomonas aeruginosa* cultures and in the breath of cystic fibrosis patients by selected ion flow tube mass spectrometry

V. Shestivska^a, P. Španěl^{a,b}, K. Dryahina^a, K. Sovová^{a,c}, D. Smith^b, M. Musílek^d and
A. Nemeč^d

^a*J. Heyrovský Institute of Physical Chemistry, Academy of Sciences of the Czech Republic, Prague, Czech Republic*

^b*Institute for Science and Technology in Medicine, School of Medicine, Keele University, Stoke-on-Trent, UK*

^c*Department of Physical and Macromolecular Chemistry, Faculty of Science, Charles University, Prague, Czech Republic*

^d*Centre of Epidemiology and Microbiology, National Institute of Public Health, Prague, Czech Republic*

Rapid Commun. Mass Spectrom. 2011, 25, 2459–2467
(wileyonlinelibrary.com) DOI: 10.1002/rcm.5146

Quantification of methyl thiocyanate in the headspace of *Pseudomonas aeruginosa* cultures and in the breath of cystic fibrosis patients by selected ion flow tube mass spectrometry

Violetta Shestivska¹, Alexandr Nemeč², Pavel Dřevínek³, Kristýna Sovová^{1,4},
Kseniya Dryahina¹ and Patrik Španěl^{1*}

¹J. Heyrovsky Institute of Physical Chemistry, Academy of Science of the Czech Republic, Dolejškova 3, 18223 Prague 8, Czech Republic

²Centre of Epidemiology and Microbiology, National Institute of Public Health, Srobárova 48, 10042 Prague, Czech Republic

³Department of Paediatrics, 2nd Medical School, Charles University in Prague, V Uvalu 84, 15006 Prague 5, Czech Republic

⁴Department of Physical Macromolecular Chemistry, Faculty of Science, Charles University, Albertov 2030, 12840 Prague 2, Czech Republic

Infection by *Pseudomonas aeruginosa* (PA) is a major cause of morbidity and mortality in patients with cystic fibrosis (CF). Breath analysis could potentially be a useful diagnostic of such infection, and analyses of volatile organic compounds (VOCs) emitted from PA cultures are an important part of the search for volatile breath markers of PA lung infection. Our pilot experiments using solid-phase microextraction, SPME and gas chromatography/mass spectrometric (GC/MS) analyses of volatile compounds produced by PA strains indicated a clear presence of methyl thiocyanate. This provided a motivation to develop a method for real-time online quantification of this compound by selected ion flow tube mass spectrometry, SIFT-MS. The kinetics of reactions of H_3O^+ , NO^+ and O_2^+ with methyl thiocyanate at 300 K were characterized and the characteristic product ions determined (proton transfer for H_3O^+ , rate constant $4.6 \times 10^{-9} \text{ cm}^3 \text{ s}^{-1}$; association for NO^+ , $1.7 \times 10^{-9} \text{ cm}^3 \text{ s}^{-1}$ and nondissociative charge transfer for O_2^+ , $4.3 \times 10^{-9} \text{ cm}^3 \text{ s}^{-1}$). The kinetics library was extended by a new entry for methyl thiocyanate accounting for overlaps with isotopologues of hydrated hydronium ions. Solubility of methyl thiocyanate in water (Henry's law constant) was determined using standard reference solutions and the linearity and limits of detection of both SIFT-MS and SPME-GC/MS methods were characterized. Thirty-six strains of PA with distinct genotype were cultivated under identical conditions and 28 of them (all also producing HCN) were found to release methyl thiocyanate in headspace concentrations greater than 6 parts per billion by volume (ppbv). SIFT-MS was also used to analyze the breath of 28 children with CF and the concentrations of methyl thiocyanate were found to be in the range 2–21 ppbv (median 7 ppbv). Copyright © 2011 John Wiley & Sons, Ltd.

Breath analysis offers great potential as a non-invasive method for diagnosis of lower respiratory tract infections without the need for bronchoscopy or alveolar lavage.^[1] Such a diagnostic tool would be of great value, especially in children with cystic fibrosis (CF), where early detection of respiratory pathogens such as *Pseudomonas aeruginosa* (PA) increases the chance of their eradication in both children and adults.^[2] The reason why a non-invasive breath test would be of a special benefit to children is that they are often unable to reliably expectorate sputum, cultivation of which is the gold standard method for PA diagnosis. Analyses of volatile organic compounds (VOCs) emitted from PA bacterial cultures is a first step in the search for volatile breath markers of lungs infection which can ultimately be used for diagnostics by breath analysis. This approach was evaluated previously by

a proof-of-concept study focusing on HCN.^[3,4] Selected ion flow tube mass spectrometry (SIFT-MS) is primarily used for online quantification of trace gases in human breath^[5,6] and has great potential as a tool for non-invasive physiological monitoring of CF patients.^[2] Recently, HCN was also quantified in human breath using near-infrared cavity ring down spectroscopy (CRDS).^[7] Gas chromatography/mass spectrometry (GC/MS) is a well-established standard technique for analyses of complex mixtures of volatile compounds and it can be used to identify many characteristic compounds released by PA strains. The objective of the present study was to identify biomarkers that would complement already established HCN in the diagnosis of PA infection in CF. The PA population is highly diverse and contains lots of genetically distinct strains although epidemic clones, homogeneous in genotypic and phenotypic properties, may also occur.^[8] As shown previously, phenotypic profiles such as antibiotic resistance in PA strains depend on their genomic types^[9] and it is thus possible that the composition of VOCs may significantly differ in genetically (clonally) distinct PA strains.

* Correspondence to: P. Španěl, J. Heyrovsky Institute of Physical Chemistry, Academy of Science of the Czech Republic, Dolejškova 3, 18223 Prague 8, Czech Republic.
E-mail: spanel@jh-inst.cas.cz

CURRENT KNOWLEDGE AND RESULTS OF PILOT EXPERIMENTS

Hydrogen cyanide in PA

As mentioned earlier, HCN has been previously identified and quantified using SIFT-MS in the headspace of PA cultures^[3] and also in the breath of children with CF.^[2] HCN was also detected in a headspace of alveolar lavage from one PA-positive patient and was absent in samples from PA-negative patients.^[1] These results are in accordance with several other studies carried out using electrochemical methods for analyses of liquid samples (cyanide electrodes), which identified hydrogen cyanide and cyanide in the sputum and bronchoalveolar lavage of large numbers of patients,^[10] even though one recent study of cyanide concentrations in bronchoalveolar lavage suggested that it is not a very specific diagnostic biomarker of PA infection, because it was also observed in significant concentration in non-infected patients.^[11]

The mechanism of biosynthesis of hydrogen cyanide (HCN) or cyanogenesis has been described in only a few bacterial groups, including PA.^[12] However, it is known that the main factors having an effect on cyanogenesis in PA are decreased oxygen concentration and increased bacterial cell density in culture.^[13] PA produces cyanide under microaerobic (<5%) conditions; cyanogenesis is inactivated under atmospheric oxygen concentration or under strict anaerobic conditions.^[14]

This may reflect an evolutionary survival mechanism by which toxic cyanide mediates reduction of density in microbial population under stress conditions.^[15] In relation to laboratory studies of VOCs from bacterial cultures, this implies that microaerobic cultures of PA may produce more HCN than cultures cultivated in aerobic conditions.

Methyl thiocyanate in PA

Cyanide is also toxic for the very bacteria that are producing it. PA avoids cyanide toxicity by a number of adaptive enzymatic pathways. One of the recently described mechanisms of detoxification of HCN by PA is its metabolism into thiocyanate involving the enzyme thiosulphate sulphurtransferase.^[16] Our pilot experiments using GC/MS analyses of volatile compounds produced by PA cultures indicated the prominent presence of methyl thiocyanate (CH_3SCN) based on a match with a mass spectral library^[17] (see Fig. 1). This finding provided the initial impetus for the present study dedicated to accurate quantification of methyl thiocyanate emitted by a range of PA strains and also to investigating the feasibility of its quantification in the exhaled breath of patients using SIFT-MS. Production of methyl thiocyanate by PA has not been described so far to our knowledge, the only relevant mention in the literature being a study of *Arabidopsis* plants where thiocyanate is methylated into methyl thiocyanate.^[18] Previous studies of the headspace of bacterial cultures using SIFT-MS^[3,19,20] identified several VOCs as being produced by PA, including several sulphur compounds (hydrogen sulphide, methanethiol, dimethyl sulphide). However, methyl thiocyanate was not specifically identified. It is worthy of note that identification of methyl thiocyanate by the GC/MS method is readily possible, as was previously demonstrated by the example of cigarette smoke.^[21] However, GC/MS does not allow real-time

accurate quantification of volatile compounds and thus it is desirable to develop a method for SIFT-MS quantification of methyl thiocyanate in the headspace of bacterial cultures of large number of PA strains, as it is reported below.

Henry's law constant for methyl thiocyanate

Henry's law constants related to volatility and solubility of VOCs in water are widely used in chemical and environmental studies. Knowledge of these constants allows the concentrations of VOCs dissolved in water to be related to the concentrations of their vapours in the headspace. Henry's law constants have been determined and converted into a uniform format for more than 500 substances.^[22] Unfortunately, the Henry's law constant for methyl thiocyanate is not known as far as we know. Thus, as a part of the present study, we had to experimentally obtain the Henry's law constant for methyl thiocyanate dissolved in water at two different temperatures.

EXPERIMENTAL

Bacterial strains

A total of 36 strains of PA were included in the present study (see Results and Discussion section). Thirty-three strains (designated NIPH) were selected from a previous study on the genetic diversity of PA strains in the Czech population of CF patients.^[9] These strains were isolated from sputum given by 33 different patients in 2004–2005 and represent different genotypes as defined by AFLP, a high-resolution whole-genome fingerprinting method.^[9] Three additional strains (ANC 3157, ANC 3209, ANC 3488) were selected from another study focused on the population structure of PA isolates from the blood of patients in intensive hospital care.^[23] These three strains represent, three multidrug-resistant epidemic clones widespread in Czech hospitals in 2007. Strain PAO1 was used as the PA reference strain. All strains were stored in glycerol broth at -80°C .

Cultivation and quantification of bacteria

Shaken submersion culture of each strain was performed in 7 mL of Mueller-Hinton Broth (MHB) liquid medium (Oxoid) in a 100 mL hermetically sealed flask. Each culture flask was inoculated with a drop ($\sim 50\ \mu\text{L}$) of cell suspension of standardized turbidity ($\sim 10^8$ colony forming units [CFU] mL^{-1}) prepared in saline from an overnight agar culture. The inoculated flasks were cultivated at 37°C for 20 h using a shaking, thermostatically controlled water bath (IKA HS-B20) at an impeller speed of 160 rpm. The quantity of bacterial growth was assessed both by CFU counting and by measurement of optical density (OD). CFU was assessed by plating serial ten-fold dilutions of the bacterial culture in duplicate on agar plates, which were incubated at 37°C for 20 h. OD was measured in a spectrophotometer at 600 nm using uninoculated MHB as a blank.

Standard solutions

In order to validate the GC/MS identification of methyl thiocyanate and to determine its Henry's law constant using SIFT-MS, an external reference solution was prepared by dissolving

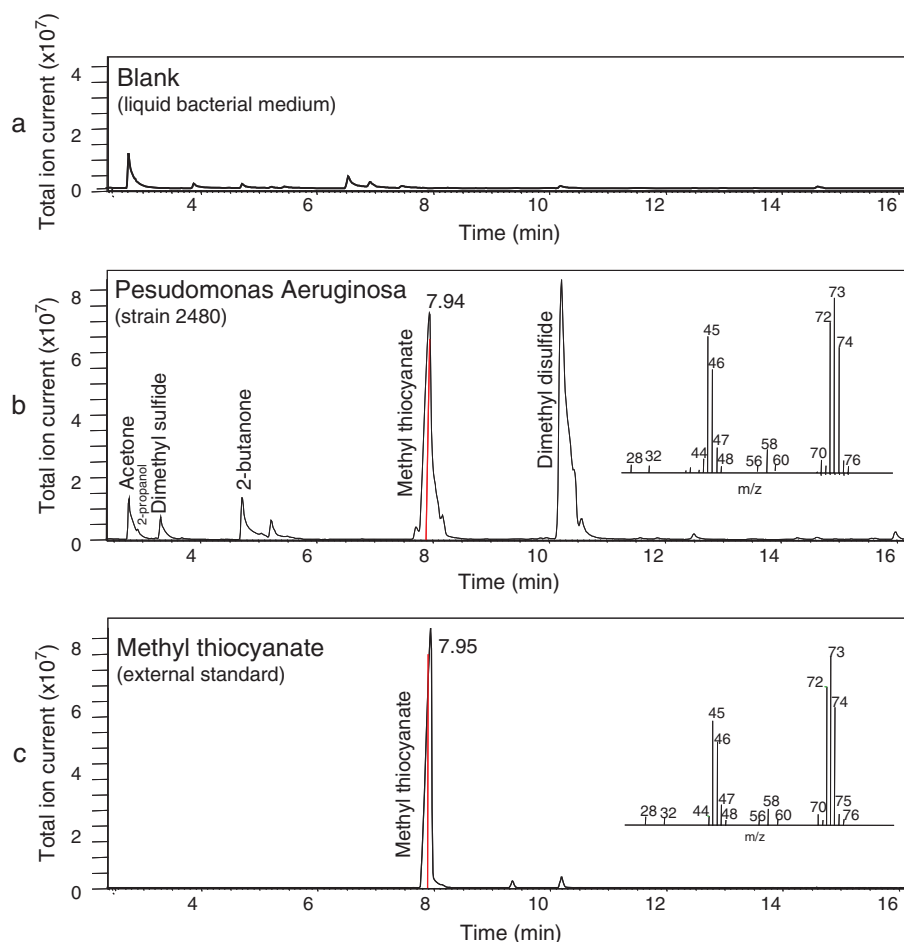


Figure 1. GC/MS analyses of VOCs extracted using SPME from the headspace of (a) a blank sample (liquid MHB medium), (b) identical medium cultivated with a PA strain NIPH 2480 (an electron ionization mass spectrum obtained at elution time of 7.94 min is shown in the inset), and (c) of a reference sample of methyl thiocyanate. Note the absence of this compound in the blank medium and also a good match of the elution time and of the fragmentation pattern between the bacterial culture and external standard.

methyl thiocyanate in the A – identical volume of methanol (1:1); B – 1:100 and this solution was diluted by distilled water (in volume ratios A – 4.2 μ L:500 mL; B – 42 μ L:500 mL) for the Henry's law constant determination (A – 57.3 μ M; B – 1.14 μ M). This was followed by sequential dilutions by a factor of two covering the range from 57.3 μ M down to 0.01 μ M. The methanol (HPLC grade) and methyl thiocyanate (97%) used to prepare these solutions were purchased from Sigma-Aldrich (St. Louis, MO, USA).

SPME sampling protocol from headspace and GC-MS determination method

Whilst the simplest possible sample introduction technique for GC/MS is direct injection, it could not be used in this study because injection of liquid medium itself would damage the column and injection of the gaseous headspace did not provide sufficient sensitivity to detect VOC present at ppbv concentrations. Thus, VOCs were extracted from the headspace of PA cultures using solid-phase microextraction (SPME) by CAR/PDMS-coated fibres (Supelco, Bellefonte, PA, USA) for a period of 30 min at a temperature of 37 °C following

previous equilibration for 30 min without sampling. After adsorption, the SPME fibres were directly inserted into an injector of a GC/MS instrument (FOCUS GC with SSL, ITQ 700 ion trap mass spectrometer using electron ionization) held at 210 °C. GC conditions were the following: splitless injection, He carrier gas at 1 mL/min, GC oven temperature program 38 °C (hold 3 min) 4 °C/min ramp up to 100 °C, 30 °C/min to 210 °C and a final hold 5 min (total run time 28 min). A GC/MS capillary column TR-1 (fused 100% dimethyl polysiloxane, 30 m \times 0.25 mm i.d. \times 1.0 μ m film) was used. Electron ionization at 70 eV was used to generate ions analyzed by the ion trap operating in the scan mode (m/z 15–400, scan rate 1 scan/s). Peak identification was based on mass spectral interpretation and on comparisons with the NIST 2.0 library. The identity of the methyl thiocyanate elution peak was verified using the external reference mentioned above, that confirmed both elution time and ion fragmentation pattern. Coefficient of variation (c.v.) of integrated ion signals obtained for repeated sampling of methyl thiocyanate standard solution in water was 6%, reproducibility of methyl thiocyanate quantification in the head space of PA cultures was significantly poorer, c.v. = 20%.

SIFT determination of the branching ratios and the rate constants for ion-molecule reactions

The SIFT technique for the determination of the rate constants and ion product distributions of the reaction of H_3O^+ , NO^+ and O_2^+ with organic compounds has been described in detail previously^[5] and used many times including a recent study reported in RCM.^[24] Thus, only the specific details of the present experimental procedure are outlined here. In order to determine the product ions and their branching ratios, a sample mixture of dry air and a trace amount (typically less than 10 ppm) of methyl thiocyanate vapour was introduced into the SIFT-MS instrument (*Profile 3*, manufactured by Instrument Science Ltd., Crewe, UK) via a heated calibrated capillary and full scan mass spectra were acquired whilst each of the three selected precursor ions were alternately injected into the helium carrier gas. The m/z mass spectral range was chosen as m/z 10–150 covering the molecular weight of the compound and allowing for possible formation of adduct ions. For each precursor ion, five mass spectra were obtained each with an integration time of 60 s. The major ion products were identified and their count rates determined. The rate constant for the reaction of H_3O^+ with methyl thiocyanate was calculated using the parameterized trajectory theory^[25] and the rate constants for the reactions of NO^+ and O_2^+ were determined from the relative rates of reactions, a procedure described by Španěl and Smith^[26] and subsequently used in many studies including those described by Iachetta *et al.*^[24] and Sovová *et al.*^[27] The three-body association rate constant for the reaction of protonated methyl thiocyanate with H_2O was also determined according to the procedure described in Sovová *et al.*^[27]

SIFT-MS determination of Henry's law constant

The SIFT-MS method for absolute quantification of volatile compounds in humid air has been described in detail previously.^[5,28] It exploits chemical ionization using selected precursor ions, which are injected into helium carrier gas in a flow tube. The flow speed of the ion swarm/helium carrier gas defines the reaction time of the precursor ions with the trace compounds present in an analyte mixture (sample) that is introduced at a known flow rate into the helium. Precursor ions H_3O^+ , NO^+ , and O_2^+ are used, because they do not react with the major components of air, but selectively ionize only the trace gases and volatile compounds present in the air sample being analyzed producing characteristic product ions. Quantitative analysis is achieved by measuring the ratio of the product ion count rates to the precursor ion count rates using the known rate constant for the reaction, known reaction time and known dilution of the sample in the helium carrier gas.^[28] In the present study, a standard solution of identical volumes of methanol and methyl thiocyanate at concentrations in water of 98.3 μM and 57.3 μM respectively was used in a series of sequential dilutions down to 0.4 and 0.2 μM . Vapour concentrations of both methanol and methyl thiocyanate were determined using SIFT-MS as the headspace was sampled at three different temperatures of 293, 301, 309 K. The solubilities (Henry's law constants) were calculated from the slopes of regression lines of plots of headspace concentrations as a function of the molar strength of the solution.

SIFT-MS analyses of methyl thiocyanate in the culture headspace and in breath

In SIFT-MS a chosen precursor ion (H_3O^+ , NO^+) is selected by a quadrupole mass filter from a mixture of ions generated in a microwave discharge and injected into fast-flowing helium carrier gas. The chosen precursor ion is used to ionize the trace gases in the headspace of a sample that is introduced at a known flow rate into the carrier gas downstream of the ion injection point. The reactions between the precursor ions and the trace compounds in the sample result in characteristic product ions that identify the compounds and their count rates allow quantification.^[6]

For the present study, the same SIFT-MS *Profile 3* instrument was used as for the rate constant measurements described above. The kinetic library was extended by a new entry for methyl thiocyanate (see Table 1) based on the results of the present ion chemistry study. Only H_3O^+ precursor ions were used to directly quantify HCN and methyl thiocyanate released into the headspace (HS) above the bacterial cultures. The full scan mode was used in the range from m/z 10–200 and four scans each of duration of 1 min were acquired. A pause of at least 1 min was left between any two samples in order to minimize cross-contamination due to the surface adsorption on the sampling tubing. Each strain was cultivated under identical conditions in duplicate vials and each sample was analyzed separately. Finally, the concentrations of HCN and methyl thiocyanate were calculated for the entire data set of 36 strains. The coefficient of variation (c.v.) obtained for repeated sampling of methyl thiocyanate standard solution using an identical method was 2%; reproducibility of methyl thiocyanate quantification in the headspace of PA cultures was at a c.v. <15% when the concentration was >3 ppbv.

Breath analysis was carried out at the CF Centre at the Teaching hospital in Motol (Prague). In total, 28 patients were recruited for the breath analysis study that was approved by the local ethics committee. Parents of all the patients gave informed consent to the children's inclusion in the study.

Table 1. Kinetics library entry in the format required for the SIFT-MS software^[27,28]

Methyl_thiocyanate(H_3O^+)

4 precursors ^a	<i>k</i>	<i>f</i>
19	4.6E-09	0.60
37	3.6E-09	0.50
55	3.2E-09	1.00
73	2.9E-09	1.70
4 products ^b		<i>f</i>
91		-0.004
92		1.2
110		1
128		1.2

^aEach row of the precursors section contains the m/z value of each ion, the rate constant for its reaction with methyl thiocyanate and finally the *f* coefficient multiplying the ion count rate.

^bEach row of the products section gives the m/z value of each product ion followed by the *f* coefficient used to multiply its count rate. The negative value accounts for the overlap of the isotopologues of $\text{H}_3\text{O}^+(\text{H}_2\text{O})_4$ at m/z 92.^[28]

Disposable bacterial filters were used instead of the cardboard mouthpieces to prevent risk of cross-infection. The seats and the parts of equipment that were in any contact with the patients were disinfected with bleach following each sampling. Each patient was asked to provide three exhalations which were analyzed by SIFT-MS using the H_3O^+ precursor ion in the multiple ion monitoring mode^[6] and the mean values of the three analyses were recorded. Raw data files were archived. The breath of 28 patients (7 males and 21 females within the age range from 5 to 21 years) was analyzed; the infection status in this cohort at the time of sampling was: 9 PA positive patients (diagnosed by culture or by species-specific PCR) and 19 negative patients (negative by both methods). Note that only 5 out of 9 positive patients were known to be chronically infected at the time of breath analysis whilst the remaining 13 of 19 currently negative patients had infection reported previously in their medical history. In addition to patients, the breath of 9 healthy children in age range from 9 to 11 years was analyzed using the same protocol.

RESULTS AND DISCUSSION

Kinetics of reactions of H_3O^+ , NO^+ and O_2^+ with methyl thiocyanate

The primary ion chemistry involved in SIFT-MS quantification of methyl thiocyanate is relatively simple: H_3O^+ reacts only by proton transfer giving a primary product ion at m/z 74 CH_3SCNH^+ . This protonated molecule associates to form hydrates at m/z 92, 110, 128. The association efficiency, A_{eff} , describing the relative rate constant for three-body association of CH_3SCNH^+ with H_2O molecules with respect to the rate constant of association of H_3O^+ with H_2O , is 1.6 and thus the three-body rate constant for this reaction is $6.1 \times 10^{-28} \text{ cm}^6 \text{ s}^{-1}$ (a relatively small value in comparison with larger organic molecules like esters^[27]). The rate constant for the formation of CH_3SCNH^+ by proton transfer from H_3O^+ to CH_3SCN is $4.6 \times 10^{-9} \text{ cm}^3 \text{ s}^{-1}$ according to the calculation using the parameterized trajectory theory^[25] and the known polarizability and dipole moment of CH_3SCN ($\alpha = 7.62 \times 10^{-24} \text{ cm}^3$ and $\mu = 3.56 \text{ D}$, respectively). When using H_3O^+ for SIFT-MS analysis of methyl thiocyanate it is important to account for the overlap of the product ions with the ^{17}O and D isotopologues of the hydrated hydronium ions. This can be achieved on the Profile 3 SIFT-MS data analysis software by including negative coefficients as given in Table 1. Note that such subtraction at m/z 74 leads to a decrease in the precision and thus the kinetics library was optimized using the method described by Sovová *et al.*^[27] so that only hydrated products at m/z 92, 110 and 128 are used in the analyses after multiplying the precursor and product ion count rates by coefficients, f , given as the last entries in each row of the kinetics library entry (Table 1). NO^+ reacts by three-body association only forming the adduct ion $\text{CH}_3\text{SCNNO}^+$ at m/z 103, the effective two-body rate constant for this reaction (proceeding at 1.3 mbar of He pressure) is $1.7 \times 10^{-9} \text{ cm}^3 \text{ s}^{-1}$, which is slower than the collisional rate constant $4.4 \times 10^{-9} \text{ cm}^3 \text{ s}^{-1}$. The O_2^+ charge transfer reaction forms the radical cation $\text{CH}_3\text{SCN}^{\bullet+}$ only, and proceeds rapidly with a rate constant equal to the collisional rate constant of $4.3 \times 10^{-9} \text{ cm}^3 \text{ s}^{-1}$. The primary product ion overlaps with the $\text{H}_3\text{O}^+(\text{H}_2\text{O})_3$ ion and thus cannot be

used for analyses in humid air. Uncertainties in the absolute values of the determined rate constants are better than $\pm 20\%$, as is typical for SIFT measurements.^[5]

Henry's law constant for methyl thiocyanate

The results of this measurement relate the headspace vapour concentrations to the liquid solution concentrations. Note that the standard methyl thiocyanate solution was prepared in methanol because of its known poor solubility in water. The standard solution used for the solubility measurement thus included two substances (same initial volumes of liquid methanol and methyl thiocyanate) with known concentrations. The results of the measurements of the solubility of methyl thiocyanate were 94 nM/ppbv at 293 K, 71 nM/ppbv at 301 K and 54 nM/ppbv at 309 K. By fitting the plot of the logarithm of these values against $1/T$ the following values were obtained: solubility at 298 K, $k_{\text{H}_0} = 79 \text{ nM/ppbv}$ (units identical to M/atm) and enthalpy of solution, 377 J/mol (slope 3136 K). Note that the corresponding parallel result for methanol $k_{\text{H}_0} = 210 \text{ nM/ppbv}$ agrees well with the literature values (140 to 230) M/atm.^[22] The agreement for methanol thus increased confidence in this original measurement for methyl thiocyanate.

Characterization of GC/MS and SIFT-MS analyses using standard reference solutions of methyl thiocyanate in water

In order to quantitatively interpret the GC/MS analyses of bacterial culture headspace, calibration was achieved by observing the dependence of the integrated ion count of the methyl thiocyanate elution peak of the on the vapour concentration of methyl thiocyanate using standard mixtures and using parallel SIFT-MS measurements. Headspace analyses of the CH_3SCN methanol/water solution in the concentration range from 9 nM to 57.3 μM indicated that the lower limit of detection (LOD) for SPME/GC/MS was 18 nM concentration in the liquid, and higher limit of detection (HLD) given by linearity between concentration and ion current peak area was observed at about 14 μM (see the nonlinearity of the response presumably caused by saturation of the SPME fibre surface plotted in Fig. 2). The reproducibility of SPME-GC/MS analyses in the absence of other VOCs is described by a c.v. of 6%. For SIFT-MS real-time sampling in the MIM mode (1 min integration time) the LOD was 140 nM and HLD 49 μM corresponding to the headspace vapour concentration limits of LOD 8 ppbv and HLD 5 ppmv. The LOD value was not limited by the detectable product ion count rate, but rather by the background signal present in the absence of sample. The reproducibility of SIFT-MS quantification of methyl thiocyanate in the headspace of standard solutions is described by a c.v. of 2%.

Methyl thiocyanate in the PA culture headspace

The GC/MS data resulting from analyses of SPME-extracted headspace of 36 genetically diverse strains of PA indicate the presence of several VOCs (including acetone, 2-propanol, dimethyl sulphide, etc.) in all samples. The presence of methyl thiocyanate was confirmed by both elution time and the ion fragmentation mass spectrum. The chromatograms obtained for headspace analyses of a sterile liquid medium, an example strain PA and a reference standard solution of 0.9 μM methyl thiocyanate are shown in Fig. 1. The elution

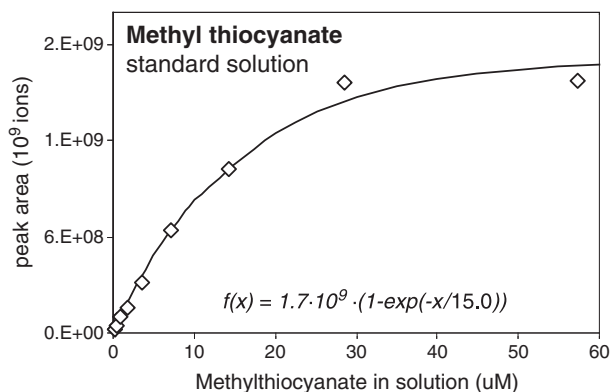


Figure 2. Area under the methyl thiocyanate GC/MS peaks obtained after SPME sampling of the headspace of reference standard aqueous solutions plotted as a function of the liquid concentrations. The solid line is a fit corresponding to saturation kinetics according to the equation given in the figure.

time of the peak observed in the headspace of the PA cultures and the fragmentation pattern were confirmed to be in agreement with the reference standard sample.

The results of quantitative analyses of the headspace of 36 PA strains and of the blank medium are summarized in Table 2 giving both GC/MS and SIFT-MS analyses of methyl thiocyanate and also SIFT-MS analyses of HCN. Production of HCN by PA cultures has been observed several times previously^[3,4] and it is thus a proposed biomarker for infection caused by these bacteria. Note, however, that using SPME and GC/MS we were unable to detect HCN and thus only SIFT-MS results are presented in Table 2. It is seen that all PA strains produce HCN at measurable concentrations, but it is important to note that the control medium sample also released HCN at 20 ppbv, and four strains actually produced less HCN than was released from the control medium. It is also interesting to note that one recent study of cyanide concentrations in the liquid from bronchoalveolar lavage is not a very specific diagnostic biomarker of PA infection, because it was also observed in significant concentration in non-infected patients.^[11] This provides additional motivation for identifying an additional biomarker of PA infection other than HCN.

The relative concentrations of methyl thiocyanate obtained using GC/MS and SIFT-MS in percentages, %, of the concentration obtained for strain NIPH 2471 are plotted in Fig. 3. Note that the blank sample of sterile medium that underwent the same cultivation protocol as the PA cultures does not contain any detectable methyl thiocyanate (SIFT-MS measurement indicates a baseline value of 3 ppbv that is below the experimentally determined LOD and probably caused by background in the laboratory air and on the surfaces of the sampling tubing). Note that eleven strains (NIPH 2415, NIPH 2427, NIPH 2433, NIPH 2454, NIPH 2472, NIPH 2473, NIPH 2496, NIPH 2498, ANC 3209) did not release sufficient amounts of methyl thiocyanate that would be detectable by the SPME-GC/MS technique. However, SIFT-MS provided concentrations above its LOD for all but eight strains (observed concentrations in the headspace of these eight strains were less than 6 ppbv). This means that in practical use with a headspace rich in several VOCs, SPME/GC/MS has actually a poorer detection sensitivity than SIFT-MS, an

Table 2. Headspace analyses of 36 different PA strains using GC/MS and SIFT-MS. In the SPME-GC/MS column the ion current peak area for methyl thiocyanate is normalized to that for the strain NIPH 2471 ($1.18\text{E}+09$ ion counts taken as a 100%)

Strain No	Methylthiocyanate (SPME-GC/MS) peak area %	Methylthiocyanate SIFT-MS ppbv	HCN SIFT-MS ppbv
Blank	-	3	20
NIPH 2414	1	31	654
NIPH 2415	-	8	17
NIPH 2418	1	16	317
NIPH 2421	-	20	3849
NIPH 2423	9	58	7604
NIPH 2425	32	182	2367
NIPH 2427	0.3	2	6925
NIPH 2430	68.7	887	5912
NIPH 2433	0.3	6	1460
NIPH 2440	1	17	5110
NIPH 2443	3	32	5506
NIPH 2449	0.2	15	5521
NIPH 2451	12	67	2257
NIPH 2452	-	11	1282
NIPH 2454	-	2	12
NIPH 2455	-	12	48
NIPH 2457	0.6	9	5998
NIPH 2462	-	14	46
NIPH 2463	0.2	12	14
NIPH 2471	100	1784	2763
NIPH 2472	0.1	5	49
NIPH 2473	0.2	6	125
NIPH 2480	58	260	7611
NIPH 2491	60	306	4783
NIPH 2492	-	12	2606
NIPH 2495	2	41	202
NIPH 2496	-	2	2532
NIPH 2498	-	2	6099
NIPH 2502	31	367	1104
NIPH 2507	2	30	488
NIPH 2511	22	61	3502
NIPH 2512	13	256	1658
ANC 3157	-	10	16
ANC 3209	-	3	64
ANC 3488	18	313	4752
PAO13888	8	83	5339

unexpected result in the light of the experimental results using standard mixtures mentioned earlier. This could possibly be explained as a result of saturation of the SPME fibre by other VOCs present in the matrix.^[29,30]

Worthy of note is that previously published AFLP fingerprinting data do not suggest that the strains included in the present study are genetically more similar to each other than to the other strains or that the genotypes of these strains deviate markedly from those of the other strains.^[9] The noted variations in the methyl thiocyanate production thus seem to reflect the intra-species variability of this property of PA and indicate that this property is not taxonomically and phylogenetically fully conserved.

The cultures of all strains but one (NIPH 2473) yielded an OD above 2.9 and CFU in the range of $1.0\text{--}6.0 \times 10^9$. Strain-to-strain differences in the quantity of the biomass

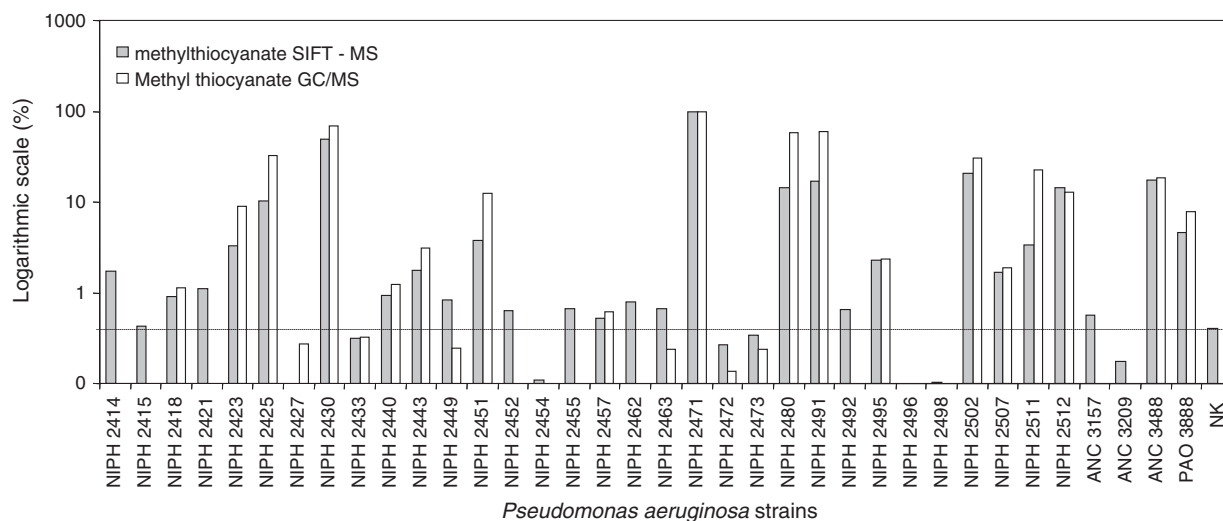


Figure 3. Concentrations of methyl thiocyanate in % relative to a chosen strain NIPH 2471 (taken as 100%) measured in the headspace of 36 PA strains and in the blank medium (NK) using SIFT-MS (shaded bars) and GC/MS (open bars). The horizontal line indicates a level of 3 ppbv as determined by SIFT-MS that is observed for the headspace of blank medium (NK).

or cell counts thus lie in the range less than a half of one order-of-magnitude in nearly all strains and could not substantially influence qualitative production of methyl thiocyanate.

Correlation of the GC/MS peak areas with the SIFT-MS ppbv

Correlation of the GC/MS peak areas with the SIFT-MS ppbv concentrations is plotted in Fig. 4. Note that the correlation is not as good for the headspace of the bacterial culture as it is for the reference standards. This again can be the effect of other VOCs simultaneously extracted by the same SPME fiber. The main difference in the GC/MS and SIFT-MS measurements is in the sample throughput, each

GC/MS measurement took at least 20 min when using SPME whilst SIFT-MS measurements could be done every 2 min (1 min sampling and 1 min pause to minimize memory effects).

Correlation of concentrations of methyl thiocyanate with HCN

Finally, it is interesting to correlate the measured methyl thiocyanate concentrations with the HCN concentrations obtained in parallel. Figure 5 shows a plot of HCN headspace concentrations versus the methyl thiocyanate headspace concentrations for all 36 strains. Note that whilst the linear

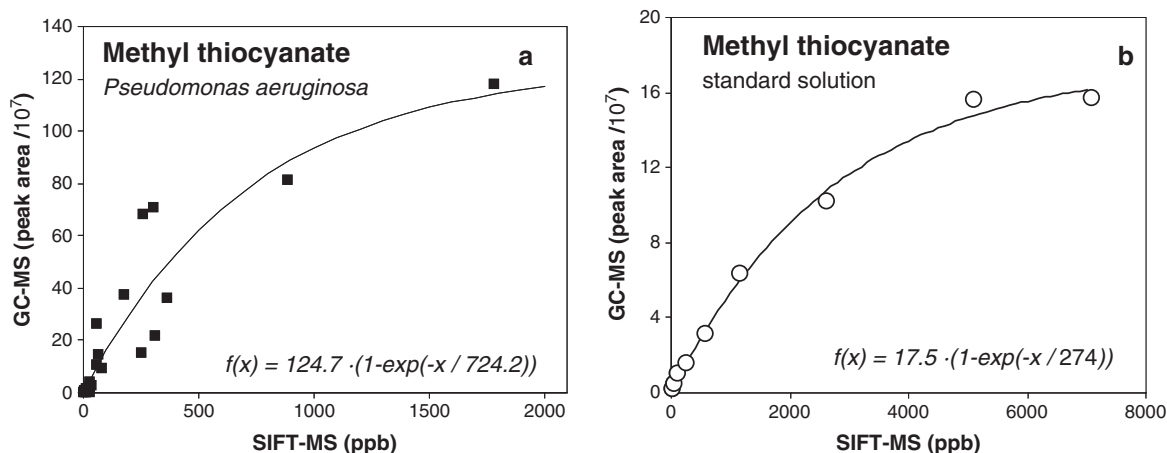


Figure 4. Correlation of GC/MS peak areas corresponding to methyl thiocyanate with its concentration in ppbv determined by SIFT-MS (a) in the headspace of bacterial cultures and (b) in the headspace of reference solutions in methanol and water. Note that at concentrations above 1000 ppbv the GC/MS results show signs of saturation of the SPME fibre. The greater scatter of the bacterial culture results indicates that the presence of other VOCs can seriously influence the accuracy of quantification of methyl thiocyanate by SPME and thus justifying the need for the use of SIFT-MS for its quantitative analyses.

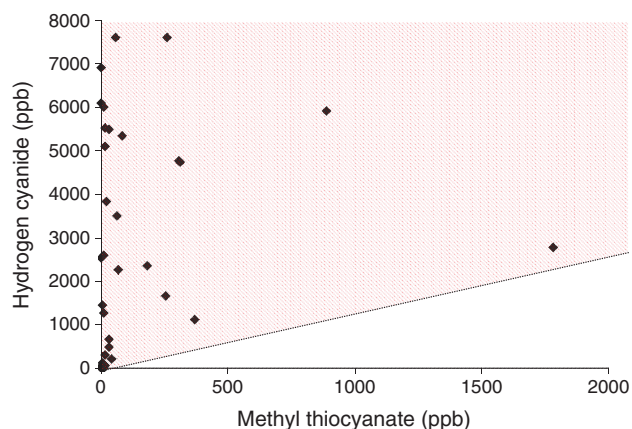


Figure 5. Correlation of the hydrogen cyanide concentrations with the concentrations of methyl thiocyanate, both in ppbv, in the headspace of cultures of different PA strains, as determined by SIFT-MS. Note that the results indicate that production of HCN is a necessary requirement for production of methyl thiocyanate; however, some strains produce relatively large amounts of HCN without producing any methyl thiocyanate.

regression of these two values does not reveal excellent correlation (R^2 is only 0.03), inspection of the data reveals that all points lay in the triangular region above a line indicated in the plot (symbolizing inequality $[\text{HCN}] > 2 [\text{methyl thiocyanate}]$). It thus seems possible that production of HCN is one of several required factors for the production of methyl thiocyanate. This suggestion is based on the fact that all strains which produced methyl thiocyanate also released increased concentration of HCN. There were no strains observed releasing methyl thiocyanate without HCN, but there was a group of strains producing higher concentration of HCN without producing significant amounts (>100 ppbv) of methyl thiocyanate. Thus, we can suggest that HCN is acting as a substrate for methyl thiocyanate production and these two compounds are biochemically associated. For future research it would be interesting to carry out an experiment with different incubation times (for example 24 and 48 h) in order to substantiate the correlation between HCN and methyl thiocyanate.

Breath analysis

Exhaled breath can be easily and non-invasively analysed using the SIFT-MS technique even in young children.^[2] Our interest in this study was focused on quantification of methyl thiocyanate in the exhaled breath of healthy children and CF patients.^[2] Based on the data from the headspace of PA cultures discussed earlier, we have carried out a pilot study to measure the concentrations of methyl thiocyanate directly in breath using SIFT-MS. The concentrations measured in ambient room air that was inhaled by the subjects were up to 2 ppbv; the breath of 9 healthy children were in the range from 5 to 8 ppbv (mean 8 ppbv); in the breath of 19 PA negative CF patients in the range from 2 to 23 ppbv (mean 14 ppbv) and in the breath of 9 PA positive patients in the range from 5 to 28 ppbv (mean 12 ppbv). The differences between the groups were not statistically significant

and a large fraction of measurements gave results below the LOD of 8 ppbv established in the experiments with standard mixtures. No attempt has been made to search for any relation between the breath concentrations and the various bacterial strains isolated from individual patients. It is worthy of note that the bacteria growing in cultures of CF may behave differently to those infecting the airways of CF patients and further detailed research will be required to substantiate the relevance of methyl thiocyanate to the diagnostics of PA infection. The main outcome of this study is thus in establishing the suitability of SIFT-MS for direct breath analysis of this compound and in indicating its typical range of concentrations in breath of healthy children and CF patients. In order to assess the true clinical relevance of methyl thiocyanate as a marker of PA lung infection, it will now be necessary to apply this method to a clinical study with a larger number of patients.

CONCLUSIONS

SPME-GC/MS analyses of bacterial culture headspace indicate that methyl thiocyanate is produced by many PA strains. This observation was confirmed by using reference standards that matched both elution time and fragmentation pattern of the EI mass spectrum. In order to develop the real-time SIFT-MS method of quantification of this compound, its ion chemistry was studied and a kinetics library entry for SIFT-MS analyses was constructed. Rapid SIFT-MS analyses are possible in the range 8–5000 ppbv. The lower limit of detection is, in practice, determined by the baseline level due to contamination of laboratory air and sampling tubing and is significantly worse than the intrinsic statistical LOD of the pulse counting detection in SIFT-MS (<1 ppbv). In our group of 36 PA strains, 28 produced headspace concentrations above the LOD. The remaining eight strains did not produce any measurable methyl thiocyanate even though some of them produced substantial concentrations of HCN. The plausible mechanism of formation of methyl thiocyanate involves detoxification of HCN by PA cells. The pilot study of the exhaled breath of CF patients indicates that concentrations of methyl thiocyanate are in the range up to 28 ppbv and that real-time quantification of this potential infection biomarker is possible using SIFT-MS. Quantification of methyl thiocyanate alone in the headspace of PA cultures and in the breath of patients with CF would be inferior to HCN analyses. However, the combination of these two compounds could form a more robust biomarker or even could have the potential for differential diagnostics of different PA strains.

Acknowledgements

We gratefully acknowledge funding for this study by GACR (Project Nos. 203/09/0256 and 203/09/P172). We are grateful to all the patients participating in the breath analysis study and their parents, to the staff of the CF clinic, especially to the paediatric nurse Katerina Austova for assisting with the patient admissions, and to Martina Maixnerová for her help in cultivating the PA strains. We would also like to thank David Smith for reading and correcting the manuscript.

REFERENCES

- [1] J. Julak, E. Stranska, V. Rosova, H. Geppert, P. Španěl, D. Smith. *J. Microbiol. Methods* **2006**, *65*, 76.
- [2] B. Enderby, D. Smith, W. Carroll, W. Lenney. *Pediat. Pulmonol.* **2009**, *44*, 142.
- [3] W. Carroll, W. Lenney, T. S. Wang, P. Španěl, A. Alcock, D. Smith. *Pediat. Pulmonol.* **2005**, *39*, 452.
- [4] F. J. Gilchrist, A. Alcock, J. Belcher, M. Brady, A. Jones, D. Smith, P. Španěl, K. Webb, W. Lenney. *Eur. Respiratory J.* **2011**, *37*: E pub ahead of print.
- [5] D. Smith, P. Španěl. *Mass Spectrom. Rev.* **2005**, *24*, 661.
- [6] P. Španěl, D. Smith. *Mass Spectrom. Rev.* **2011**, *30*, 236.
- [7] K. Stamy, O. Vaitinen, J. Jaakola, J. Guss, M. Metsala, G. Johanson, L. Halonen. *Biomarkers* **2009**, *14*, 285.
- [8] J. P. Pimay, D. De Vos, C. Cochez, F. Bilocq, A. Vanderkelen, M. Zizi, B. Ghysels, P. Cornelis. *Environ. Microbiol.* **2002**, *4*, 898.
- [9] S. Vosahlikova, P. Drevinek, O. Cinek, P. Pohunek, M. Maixnerova, P. Urbaskova, T. J. K. van den Reijden, L. Dijkshoorn, A. Nemeč. *Res. Microbiol.* **2007**, *158*, 324.
- [10] B. Ryall, J. C. Davies, R. Wilson, A. Shoemark, H. D. Williams. *Eur. Respiratory J.* **2008**, *32*, 740.
- [11] M. D. Stutz, C. L. Gangell, L. J. Berry, L. W. Garratt, B. Sheil, P. D. Sly, C. F. Arest. *Eur. Respiratory J.* **2011**, *37*, 553.
- [12] C. Blumer, D. Haas. *Arch. Microbiol.* **2000**, *173*, 170.
- [13] G. Pessi, D. Haas. *J. Bacteriol.* **2000**, *182*, 6940.
- [14] D. Worlitzsch, R. Tarran, M. Ulrich, U. Schwab, A. Cekici, K. C. Meyer, P. Birrer, G. Bellon, J. Berger, T. Weiss, K. Botzenhart, J. R. Yankaskas, S. Randell, R. C. Boucher, G. Doring. *J. Clin. Invest.* **2002**, *109*, 317.
- [15] P. A. Castric. *Can. J. Microbiol.* **1983**, *29*, 1344.
- [16] R. Cipollone, M. G. Bigotti, E. Frangipani, P. Ascenzi, P. Visca. *Biochem. Biophys. Res. Commun.* **2004**, *325*, 85.
- [17] S. E. Stein. Mass spectra, in *NIST Chemistry WebBook, NIST Standard Reference Database Number 69*, (Eds: J. J. Linstrom, W. G. Mallard), National Institute of Standards and Technology: Gaithersburg, **2010**.
- [18] Y. Nagatoshi, T. Nakamura. *J. Biol. Chem.* **2009**, *284*, 19301.
- [19] A. Pysanenko, P. Španěl, D. Smith. *J. Breath Res.* **2008**, *2*, 046004.
- [20] R. A. Allardyce, V. S. Langford, A. L. Hill, D. R. Murdoch. *J. Microbiol. Methods* **2006**, *65*, 361.
- [21] J.-Z. Dong, S. DeBusk. *Chromatographia* **2010**, *71*, 259.
- [22] R. Sander. *Compilation of Henry's Law Constants for Inorganic and Organic Species of Potential Importance in Environmental Chemistry*. Max-Planck Institute of Chemistry, Air Chemistry Dept, **1999**.
- [23] A. Nemeč, L. Krizova, M. Maixnerova, M. Musilek. *Res. Microbiol.* **2010**, *161*, 234.
- [24] L. Iachetta, L. Malek, B. M. Ross. *Rapid Commun. Mass Spectrom.* **2010**, *24*, 815.
- [25] T. Su, W. J. Chesnavich. *J. Chem. Phys.* **1982**, *76*, 5183.
- [26] P. Španěl, D. Smith. *Int. J. Mass Spectrom.* **1997**, *167*, 375.
- [27] K. Šovová, K. Dryahina, P. Španěl. *Int. J. Mass Spectrom.* **2011**, *300*, 31.
- [28] P. Španěl, K. Dryahina, D. Smith. *Int. J. Mass Spectrom.* **2006**, *249*, 230.
- [29] M. Chai, J. Pawliszyn. *Environ. Sci. Technol.* **1995**, *29*, 693.
- [30] P. A. Martos, J. Pawliszyn. *Anal. Chem.* **1997**, *69*, 206.

Appendix E, Sovová *et al.* Analyst 138 (2013) 4795

Real time monitoring of population dynamics in concurrent bacterial growth using SIFT-MS quantification of volatile metabolites

Kristýna Sovová^{a,b}, Jaroslav Čepl^c, Anton Markoš^c, Patrik Španěl^{a,*}

^a*J. Heyrovský Institute of Physical Chemistry of Science, Academy of Science of the Czech Republic Dolejškova 3, 18223 Prague 8, Czech Republic*

^b*Department of Physical and Macromolecular Chemistry, Faculty of Science, Charles University, Albertov 2030, 128 40 Prague 2, Czech Republic*

^c*Department of philosophy and history of science, Faculty of Science, Charles University in Prague, Viničná 7, 128 44 Prague 2, Czech Republic*

Real time monitoring of population dynamics in concurrent bacterial growth using SIFT-MS quantification of volatile metabolites

Cite this: *Analyst*, 2013, **138**, 4795

Kristýna Sovová,^{ab} Jaroslav Čepl,^c Anton Markoš^c and Patrik Španěl^{*a}

Population dynamics of three different bacterial species, *Serratia rubidaea* (R), *Serratia marcescens* (F) and *Escherichia coli* (Ec), growing in single or mixed populations in liquid media, was monitored by real time headspace quantification of volatile compounds using selected ion flow tube mass spectrometry, SIFT-MS. The three bacterial species interact with each other in a competitive fashion in a way similar to the game “rock-paper-scissors” (R-Ec-F). The concentrations of volatile metabolites (ammonia, ethanol, acetaldehyde, propanol, acetoin, acetone and acetic acid) were measured in the headspace of the individual species and of their mixtures continuously for 24 hour periods. The results demonstrate that dynamics in bacterial cultures can be monitored using SIFT-MS in real time.

Received 8th March 2013

Accepted 24th May 2013

DOI: 10.1039/c3an00472d

www.rsc.org/analyst

Introduction

Bacterial behaviour involves a complex of interactions that allow the individual cells to sense and affect their abiotic and biotic surroundings. This leads to different forms of interaction resembling social behaviour ranging from synergism (cooperation) to antagonism (competition).^{1–3} Interactions between different bacterial species can be studied on solid media,^{4,5} where the bacterial cells can build different types of multicellular structures: monoclonal colonies or multicellular consortia – “chimeras”.⁶ Alternatively, different species of bacteria can live together in a liquid medium and such a suspension represents yet another type of interacting system. The population dynamics of competing/co-habiting species in liquid cultures can be currently observed mainly by taking sample aliquots at selected intervals, inoculating them on the agar plate, culturing for a fixed time and finally counting the individual surviving colony forming units (CFUs). The aim of our present study is to investigate how volatile metabolites could be used to monitor the growth of competing bacterial species in real time without a need to interfere with sampling and culturing.

Bacterial metabolism is known to lead to production of highly diverse multiple volatile organic compounds (VOCs).^{7–9} It was recently suggested that bacteria use airborne volatile organic compounds to sense other bacteria and to change master

regulatory gene activity to adapt.¹⁰ These metabolites are released most vigorously during the proliferation phase of the culture and vary according to the environmental conditions (e.g. composition of media)¹¹ and are specific for bacterial species. Of particular interest is VOC production by pathogenic bacteria. The knowledge of such VOC biomarkers could allow early detection of bacterial infection by non-invasive methods for clinical diagnosis.^{8,11–17} In addition, microbial VOC emissions may also help in distinguishing between different microorganisms.¹⁸ Our hypothesis is that concentrations of VOCs provide information about temporal changes of cell numbers of different clones inhabiting the same niche, like chimeric colonies, biofilms or mixed suspensions. To test this hypothesis we have used selected ion flow tube mass spectrometry, SIFT-MS,¹⁹ to study an *in vitro* model of population dynamics of mixed suspensions of three bacterial species belonging to the enterobacteria family, *Serratia rubidaea* (R – red smooth colonies), *Serratia marcescens* (F – fountain shaped colonies) and *Escherichia coli* (Ec). This bacterial system is well defined and was studied previously;^{4–6} it was also shown that bacteria can display different multicellular forms and their structure and appearance depend on factors like nutrients or the presence/absence of neighbours.⁴ Their concurrent growth in a binary or even ternary system like this can be seen as an analogue of the well known game “rock-paper-scissors” previously studied in the example of three populations of *Escherichia coli*, and provides mechanisms that maintain biodiversity.²⁰ In this game each item is superior to one other, and inferior to the third one, thus forming heterarchy: rock crushes scissors, scissors cut paper, and paper covers rock.²¹ The interactions of our three species on agar plates were previously observed as follows:⁶ The R colony usually overgrows its F partner, chimeric planting of R and F results in a chimeric colony which looks like R with traces of F in the centre. The Ec colony

^aJ. Heyrovský Institute of Physical Chemistry of Science, Academy of Science of the Czech Republic Dolejškova 3, 18223 Prague 8, Czech Republic. E-mail: patrik.spanel@jh-inst.cas.cz

^bDepartment of Physical and Macromolecular Chemistry, Faculty of Science, Charles University, Albertov 2030, 128 40 Prague 2, Czech Republic

^cDepartment of philosophy and history of science, Faculty of Science, Charles University in Prague, Viničná 7, 128 44 Prague 2, Czech Republic

tends to absorb the R colony (but it does not directly become overgrown with Ec, as in the previous case) and the resulting chimera contains a mixture of R and Ec in the middle and solely Ec around. In the last possible setting the F colony has a strong tendency to suppress the growth of its Ec partner, probably due to production of bactericidal compounds, such as marcescin.²² The end point state of F/Ec chimera consists of F cells only and Ec seems to be driven to extinction. In chimera consisting of all three clones F suppresses Ec, subsequently to be overgrown by R.

SIFT-MS, used in the present study, is a direct quantitative mass spectrometric method based on chemical ionization and the principles of fast flowing tubes used to analyse trace gases.^{19,23} SIFT-MS has been used previously in several areas such as breath analysis,^{24–26} food analysis^{27,28} or monitoring of volatile combustion products and engine exhaust gases.^{29,30} SIFT-MS has been also used several times for the detection of volatile compounds released by bacterial and cell cultures^{7–9,31} in order to identify bacterial biomarkers. Thus, SIFT-MS is a promising analytical tool for observation of bacterial population dynamics in real time. In this manuscript we describe preliminary results on the dynamics of mixed bacterial populations growing in suspensions, as revealed by their “breath”, *i.e.* the composition of the gas phase they produce.

Experimental

Bacteria were cultured in 15 mL vials containing 3 mL of Nutrient broth No. 2 (Imuna Pharm a.s.), enriched with glucose (28 mM), NBG for short. The headspace of the liquid culture was sampled directly during this culturing. Three different bacterial strains previously characterised by Rieger *et al.*, 2008,⁵ Čepel *et al.*⁴ and Pátková *et al.*⁶ were used:

S. rubidaea labelled “R” as it forms significant red smooth colonies were obtained from the collection of the Department of Genetics and Microbiology, Faculty of Science, Charles University.

S. marcescens displays centrally organized colonies with cross-shape “resembling a fountain”, thus the label “F”. Strain CNCTS 5965 was obtained from the Czech National Institute of Health.

Escherichia coli (“Ec”) strain 281 was obtained from the collection of the Department of Genetics and Microbiology, Faculty of Science, Charles University.

The SIFT-MS instrument (Profile 3 SIFT-MS manufactured by Instrument Science Limited, Crewe, UK) was used to analyse volatile metabolites from the headspace above growing suspensions of three different strains of bacteria and their binary mixtures. The instrument has been described previously in several papers.^{32,33} Thus, we will just briefly describe the experimental set-up and the sampling arrangement related to the present study. We have used plastic vials of a volume 15 mL containing 3 mL of cultivation medium with suspended bacterial culture. The samples were kept at a temperature of 27 °C in an incubator. The choice of this temperature was critical, because *Serratia* sp. only form the fountain colony shape at this temperature⁴ due to maximised production of prodigiosin.³⁴

The sampling needle connected directly to the SIFT-MS instrument was introduced into the headspace by piercing the vial caps; the headspace was sampled *via* a heated PEEK capillary at a regular flow rate of 20 mL min⁻¹. Thus a total volume of 28 L was sampled over 24 hours and therefore it was necessary to sustain the headspace pressure inside the sampling vial with a second needle continuously introducing air (Fig. 1).

The SIFT-MS instrument was operated in the full scan mode with the scan duration of 120 s in the mass spectral range 10–100 *m/z* and all three precursor ions were cycled. Using this experimental protocol we have analysed time evolution of headspace composition above six different samples: monocultures of R, Ec, F, and binary systems of R/Ec, F/Ec, F/R. Each experiment took 24 hours and typically 273 mass spectra were obtained for each precursor ion in each case. Additionally, concentrations of several compounds (listed in Table 1) were calculated (in parts per billion by volume, ppbv) from the ratios of count rates of characteristic product ions to the count rates of the precursor ion using a library of kinetic data as is usual in SIFT-MS analysis.^{35,36} After 24 h, an aliquot of the liquid culture was inoculated onto agar plates and CFUs were counted. Note that it was not possible to cultivate a reproducible ternary mixture and thus it was not included in the study.

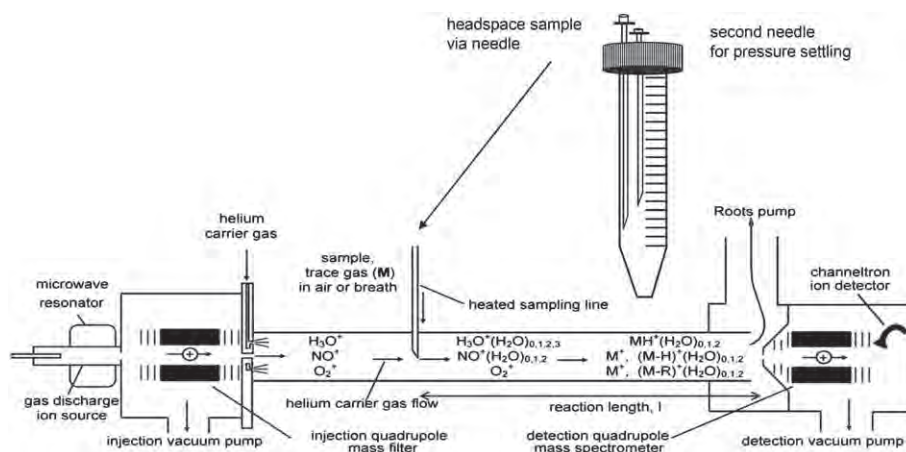


Fig. 1 The SIFT-MS instrument scheme.

Table 1 Concentrations in ppbv of the compounds quantified in the headspace of the nutrient medium and bacterial cultures

Compound	Median [ppbv]		Median (min; max) [ppbv]				
	Medium	R	Ec	F	REc	RF	FEc
Acetaldehyde	210	1796 (3; 3066)	913 (44; 1196)	1002 (29; 1343)	499 (21; 723)	1150 (40; 2125)	1069 (51; 1272)
Acetic acid	2	79 (20; 138)	1050 (45; 1200)	98 (23; 381)	50 (2; 231)	51 (7; 175)	176 (27; 357)
Acetoin	<LOD	559 (0; 825)	5 (0; 21)	56 (1; 103)	23 (1; 46)	215 (0; 708)	110 (3; 174)
Acetone	105	86 (10; 341)	19 (0; 318)	15 (0; 278)	146 (4; 338)	23 (0; 153)	15 (0; 236)
Ammonia	84	179 (39; 688)	36 (0; 368)	30 (0; 663)	77 (17; 402)	167 (32; 470)	68 (7; 232)
Ethanol	69	19 570 (30; 38 305)	16 449 (1016; 27 047)	3245 (245; 4516)	3932 (148; 5326)	13 800 (721; 24 254)	6022 (732; 8179)
Methanol	125	70 (31; 164)	37 (12; 88)	34 (12; 74)	58 (22; 144)	29 (3; 75)	31 (8; 74)
Propanol	<LOD	82 (0; 177)	1327 (61; 3349)	32 (0; 81)	329 (2; 450)	53 (0; 121)	82 (18; 164)

Data on concentrations in ppbv were statistically analyzed using the method of principal component analysis, PCA (software STATISTICA version 10 and R project version 2.14). Combined results obtained for monocultures of R, Ec and F were interpreted as 3 principal components each corresponding to a combination of volatile compounds characteristic for each species. The patterns of concentrations as they developed in the binary culture systems over the course of time were analyzed by PCA separately and the most important 2 principal components were interpreted as corresponding to the two bacterial species competing in the mixture.

Results and discussion

Bacterial growth

Each clone shows a similar growth curve with end of log phase after about 12 hours (Fig. 2a). At the same time, the decrease of VOC concentrations measured by SIFT-MS was observed (see Fig. 3). It may be caused by transition from the logarithmic to stationary phase.

As observed before,⁶ liquid cultures of binary mixtures exhibit somewhat different population dynamics compared to the corresponding cultures on NAG agar. Whilst on agar R limits growth of F by encircling its colony, such spatial limitation does not appear in suspension. The ratio of the end point (after 24 hours) colony forming unit, CFU, counts was observed in the present experiments as $F/R = 108 : 367$ and the R/Ec ratio was $170 : 416$, both are qualitatively in agreement with the previous experiments.⁶ Finally in the F/Ec mixture a complete elimination of Ec and survival of F only was observed which agrees entirely with the previous results. The quantitative growth curves obtained by measurement of optical density (OD) and from the proportions of CFU of the individual strains are also shown in Fig. 2b–d.

SIFT-MS

The sets of the full scan mass spectra (combined peak tables of spectra obtained using all three precursors) for different cultures were normalised to a constant total ion count rate. From the count rates of ions at 90 different m/z for 3 precursor ions (270 values in total) we have excluded precursor ions, their hydrates, ¹³C isotopologues of major product ions and all m/z where the mean signal observed was less than 100 c s^{-1} . Thus 56

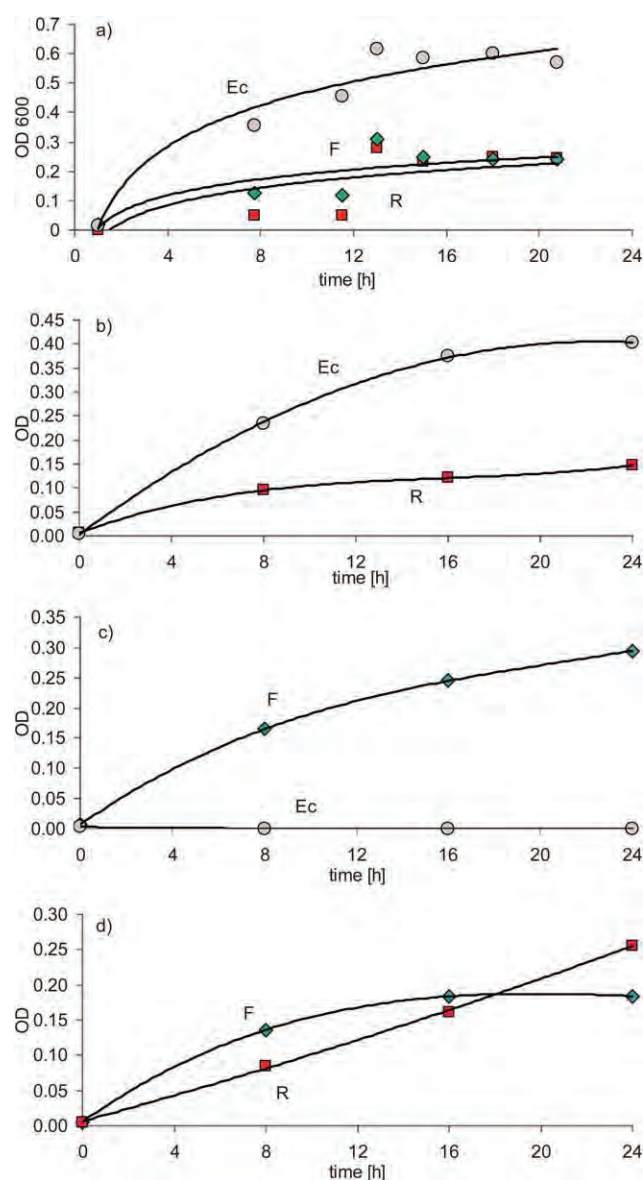


Fig. 2 (a) The growth curves of monocultures F, R and Ec indicating the logarithmic and stationary phases. The data correspond to the maxima of the concentration profiles of selected compounds from Fig. 3. (b–d) Growth curves for components of binary mixtures indicated calculated from total optical densities and proportions of CFU counts.

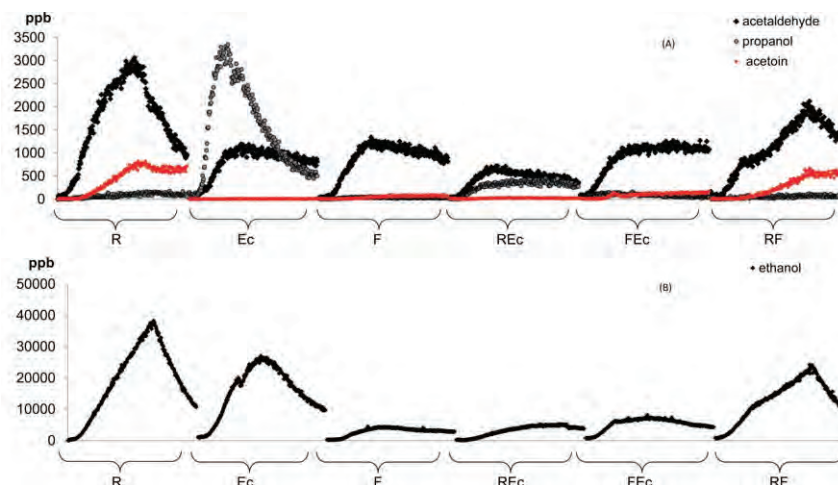


Fig. 3 Concentrations in course of cultivation (in ppbv) of four major volatile compounds: acetaldehyde, propanol and acetoin (A) and ethanol (B) as they are present in all the samples indicated on axes x during 24 hours.

characteristic combinations of precursor ion type and product ion m/z were included in the matrix (273 rows and 56 columns) to be processed by PCA.

The data sets obtained for the monocultures F, R and Ec were combined into a large matrix of 819 cases (rows) and 56 variables (columns). The rows represent signals in counts per second of individual product ions (variables) and the data for the three monocultures were simply ordered into three consecutive blocks (F, R and Ec). The results of PCA analysis of these combined data were obtained from the Statistica software in the form of eigenvectors describing the loadings of individual product ions and the time dependencies of the principal components. The loadings reveal which ion signals that can be related to identified compounds are relevant for each principal component. The first principal component, PC1 (Fig. 4), corresponds to an eigenvector with major loadings from H_3O^+ product ion signals at m/z 18, 36 and 54

resulting from reactions with ammonia; m/z 45, 63, 81 (from H_3O^+) identified as products of acetaldehyde; m/z 89 (H_3O^+) identified as acetoin product ion and m/z 47, 65, 83 corresponding to ethanol. NO^+ and O_2^+ precursors confirm the conclusion from H_3O^+ giving the signal of propanol (NO^+ at m/z 59, 77), ethanol (NO^+ at m/z 45, 63, 79, 81) and ammonia (O_2^+ at m/z 17, 35). Note that m/z 89 was assigned to acetoin on the basis of comparison of the full scan data with product ions discussed in ref. 37 and this was confirmed by SPME GC/MS analyses of headspace. The second principal component, PC2, has major contributions of H_3O^+ product m/z 43 identified with propanol; m/z 61, 79, 97 are additional product ions of propanol, but due to the overlaps with acetic acid (H_3O^+ m/z 61, 79, 97) they were not used for propanol quantification whilst acetic acid was analysed unambiguously using NO^+ at m/z 90.³⁸ The other product ions contributing to PC2 are m/z 59, 77 corresponding to acetone. The third

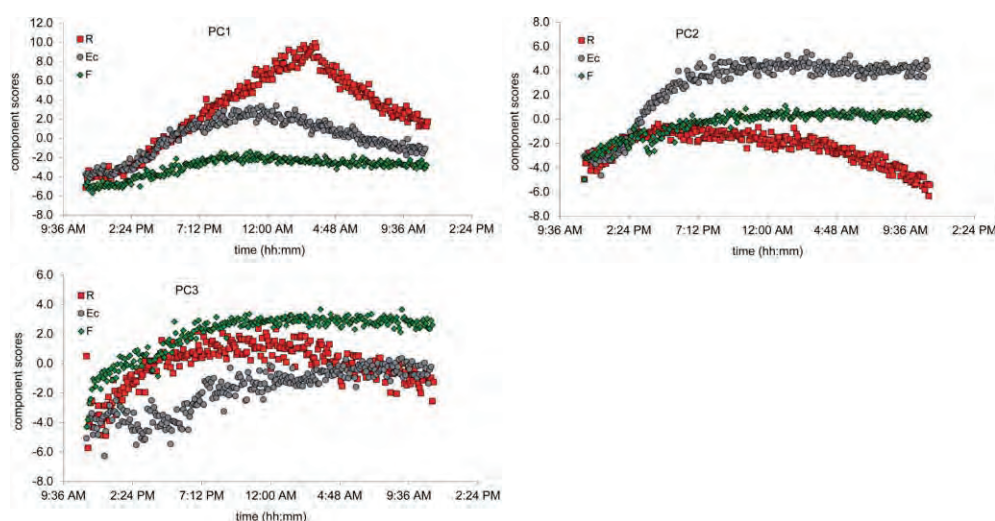


Fig. 4 PCA analysis of the three different monocultures of bacteria. On the axes y are scores of individual components (PC1, PC2 and PC3), on axes x is time dependence evolution. It can be seen that each component is characteristic for one of our bacteria.

principal component, PC3, corresponds to the major characteristic product ion signals of acetaldehyde, ethanol and with some contribution from propanol and acetoin. The curves in Fig. 4 show the time dependences of PC1–PC3 which give the information about VOC's composition of individual monoculture, each component being most prominent for distinct species (PC1 R, PC2 Ec and PC3 F).

The three binary systems were processed separately using the same procedure. The appropriate matrixes now have dimensions (273, 56). The results are shown in Fig. 5. The results can be interpreted as the two principal components corresponding to the two species which are manifested by different combinations of ion signals. For example, in the binary system with R and Ec the two components start to grow in time together and after 8 hours PC2 starts to decrease. Considering the microbiological observations mentioned above PC1 can thus be assigned to Ec that keeps growing and PC2 can be assigned to R that is inhibited in its growth in the later phases of the experiment.

The compounds identified are listed in Table 1 together with their concentrations in ppbv as calculated using the kinetics library. In contrast to Chippendale *et al.*,⁹ who worked with *E. coli* JM109, and to Allardyce *et al.*¹³ who used the strain ATCC 25922, we did not find any sulphur compounds in the headspace. The reason for this can be that different strains of *E. coli* and different nutrient media were used in the present study. The headspace composition of all six studied cultures was qualitatively similar, but concentrations of their components differed quantitatively. The ethanol concentration is highest in cultures containing R. It is a metabolic product of glucose that is present in the nutrient medium (at a concentration of 28 mM). Acetaldehyde correlates very well with ethanol, which may be due to their direct biochemical link. The concentration levels of ammonia are increasing during the experiment in R and decreasing in F and Ec. This decrease can be related to the pH of the medium that starts at the physiological level (7.2–7.4)

at the beginning and gradually decreases and reaches about 5 at the end of the experiment (see Fig. 6). It is interesting to note that ammonia has been shown previously to act as a signalling molecule.³⁹ Propanol (also previously observed¹³) is on average 25 times higher in Ec, compared to the other two monocultures F and R. Thus propanol can be considered as a biomarker indicating the presence of Ec in these systems. Note, however, that even in the absence of "Ec" there is still propanol produced at much lower concentrations. Acetoin (3-hydroxy butanone) at *m/z* 89 is produced in the largest concentration by R and was also detected in the headspace of F in a lower concentration, but not in the headspace of Ec. Thus acetoin in the headspace indicates the presence of R in these experiments. Acetic acid is in our study was only produced by Ec, and it was not detected in the monocultures of the other two bacteria. We do not find any characteristic compound that could act as a unique marker for the monoculture F which produces ethanol and acetaldehyde as its major volatile metabolites. It should also be noted that amounts of released volatiles may depend also on the culturing conditions and nutrients availability, as shown by O'Hara and Mayhew.¹¹ It is interesting to note that concentrations of characteristic VOCs can also increase in binary mixtures in comparison to the monocultures possibly due to inter-species

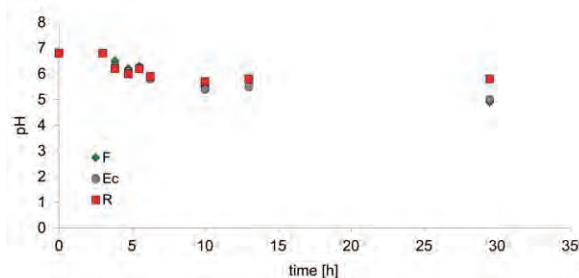


Fig. 6 Evolution of pH in monocultures F, R and Ec over time: its decrease may influence the headspace composition in samples.

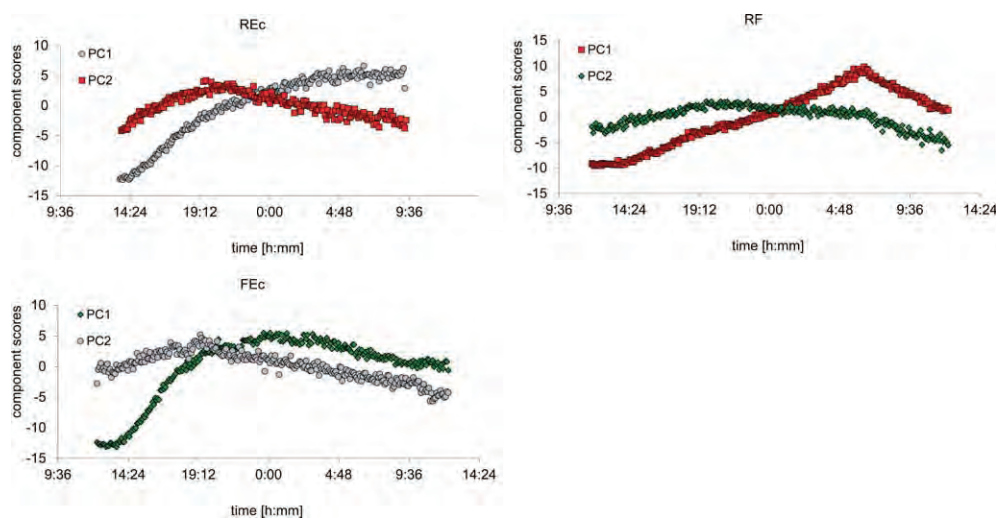


Fig. 5 The time evolution of PCA scores in binary mixtures. In the R/Ec sample PC1 represents the loadings of Ec and PC2 represents the limited growth of R in the mixture.

synergic effects, for example the acetoin concentration in the F/Ec binary system (110 ppb) is higher compared to their monocultures (56 ppb, respectively 5 ppb).

Fig. 3 shows the time changes of concentrations of several selected compounds (acetaldehyde, propanol, acetoin and ethanol) during the 24 hour experiment. The time profile of the curves shows an increase of concentration, as the bacterial cell number in the medium grows. It reaches a maximum, which is specific for each bacterial strain and compound and then the concentration is reduced. In accordance with the growth curves (Fig. 2) this corresponds to the switch from the logarithmic to a stationary phase. The reduction in concentrations may be caused by the loss of volatile compounds due to the sample flow, or they may be consumed by secondary metabolism of bacterial cultures. The binary system represented by R and Ec compared to the corresponding monocultures shows an apparent lack of acetoin, a maximum concentration of only 46 ppbv in comparison with 500 ppbv typical for R after 15 hours. Also the propanol characteristic for Ec (3000 ppbv in the monoculture) is present at a reduced concentration of 450 ppbv. This may indicate that the bacterial composition and the population dynamics resulted in a ratio favouring Ec (in agreement with the microbiologically determined ratio R/Ec = 170 : 416) but in a lower absolute cell number. The OD of the R/Ec binary mixture was observed to be lower than that of the Ec monoculture and higher than OD of the R monoculture. This indicates that the presence of R decreases the rate of growth of Ec and thus the reduction of propanol concentration observed in this binary mixture can be caused by the initial influence of R resulting in a slower growth of Ec regardless of the ultimate victory of Ec in this mixture.

The R/F binary mixture produced time profiles of acetoin, ethanol and acetaldehyde similar to the monoculture of R but in somewhat lower absolute concentrations. The microbiologically determined result for this system is R/F = 108 : 367. Finally, in the binary system of F with Ec, the winner is almost the sole F, Ec usually does not survive. The VOC's composition confirmed the victory of F indicated by the absence of propanol that would be characteristic of Ec.

Conclusions

This study demonstrates that the headspace composition of bacterial samples can be used as a fingerprint typical for a certain species of bacteria and provides quantitative information even in mixtures of two species or strains. This article presents a new method for monitoring of growth dynamics on a specific case of unmixed cultures at 27 °C. The results demonstrate that SIFT-MS can be utilized for monitoring of the bacterial proliferation in real time without interfering with the living organisms. In a system of three different species, two of them can be characterised by unique biomarkers and thus the population dynamics can be studied. Whilst the ultimate result of the population dynamics can be observed by counting surviving CFUs, it is much more instructive to follow them in real time using volatile signatures of the individual clones and therefore suggest a mathematical model of the calculation of

the CFU ratio in a mixture from the VOC's composition. Future work can be extended to include other, more clinically relevant, bacteria growing at conditions closer to physiological.

Acknowledgements

We gratefully acknowledge partial financial support by the Grant Agency of the Czech Republic, project numbers 13-24275S (AM).

Notes and references

- 1 S. A. West, A. S. Griffin, A. Gardner and S. P. Diggle, *Nat. Rev. Microbiol.*, 2006, **4**, 597–607.
- 2 G. J. Velicer, *Trends Microbiol.*, 2003, **11**, 330–337.
- 3 M. R. Parsek and E. P. Greenberg, *Trends Microbiol.*, 2005, **13**, 27–33.
- 4 J. Čepl, I. Pátková, A. Blahušková, F. Cvrčková and A. Markoš, *BMC Microbiol.*, 2010, **10**, 139.
- 5 T. Rieger, Z. Neubauer, A. Blahuskova, F. Cvrčková and A. Markos, *Commun. Integr. Biol.*, 2008, **1**, 78–87.
- 6 I. Pátková, J. Čepl, T. Rieger, A. Blahušková, Z. Neubauer and A. Markoš, *BMC Microbiol.*, 2012, **12**, 178.
- 7 V. Shestivska, A. Nemeč, P. Dřevínek, K. Sovová, K. Dryahina and P. Španěl, *Rapid Commun. Mass Spectrom.*, 2011, **25**, 2459–2467.
- 8 V. Shestivska, P. Španel, K. Dryahina, K. Sovova, D. Smith, M. Musilek and A. Nemeč, *J. Appl. Microbiol.*, 2012, **113**, 701–713.
- 9 T. W. E. Chippendale, P. Španel and D. Smith, *Rapid Commun. Mass Spectrom.*, 2011, **25**, 2163–2172.
- 10 K.-s. Kim, S. Lee and C.-M. Ryu, *Nat. Commun.*, 2013, **4**, 1809.
- 11 M. O'Hara and C. A. Mayhew, *J. Breath Res.*, 2009, **3**, 027001.
- 12 W. Filipiak, A. Sponring, M. M. Baur, A. Filipiak, C. Ager, H. Wiesenhofer, M. Nagl, J. Troppmair and A. Amann, *BMC Microbiol.*, 2012, **12**, 113.
- 13 R. A. Allardyce, V. S. Langford, A. L. Hill and D. R. Murdoch, *J. Microbiol. Methods*, 2006, **65**, 361–365.
- 14 W. Filipiak, A. Sponring, M. M. Baur, C. Ager, A. Filipiak, H. Wiesenhofer, M. Nagl, J. Troppmair and A. Amann, *Microbiology*, 2012, **158**, 3044–3053.
- 15 M. Junger, W. Vautz, M. Kuhns, L. Hofmann, S. Ulbricht, J. I. Baumbach, M. Quintel and T. Perl, *Appl. Microbiol. Biotechnol.*, 2012, **93**, 2603–2614.
- 16 S. Maddula, L. M. Blank, A. Schmid and J. I. Baumbach, *Anal. Bioanal. Chem.*, 2009, **394**, 791–800.
- 17 J. M. Scotter, R. A. Allardyce, V. Langford, A. Hill and D. R. Murdoch, *J. Microbiol. Methods*, 2006, **65**, 628–631.
- 18 M. Bunge, N. Araghipour, T. Mikoviny, J. Dunkl, R. Schnitzhofer, A. Hansel, F. Schinner, A. Wisthaler, R. Margesin and T. D. Mark, *Appl. Environ. Microbiol.*, 2008, **74**, 2179–2186.
- 19 D. Smith and P. Španěl, *Mass Spectrom. Rev.*, 2005, **24**, 661–700.
- 20 B. Kerr, M. A. Riley, M. W. Feldman and B. J. M. Bohannan, *Nature*, 2002, **418**, 171–174.
- 21 G. Szabo and G. Fath, *Phys. Rep.*, 2007, **446**, 97–216.

- 22 A. T. Fuller and J. M. Horton, *J. Gen. Microbiol.*, 1950, **4**, 417–433.
- 23 D. Smith and N. Adams, *Adv. At. Mol. Phys.*, 1988, **24**, 1–49.
- 24 P. Španěl and D. Smith, *Mass Spectrom. Rev.*, 2011, **30**, 236–267.
- 25 P. R. Boshier, J. R. Cushnir, V. Mistry, A. Knaggs, P. Spanel, D. Smith and G. B. Hanna, *Analyst*, 2011, **136**, 3233–3237.
- 26 C. Turner, P. Španěl and D. Smith, *Rapid Commun. Mass Spectrom.*, 2006, **20**, 61–68.
- 27 A. Olivares, K. Dryahina, J. L. Navarro, D. Smith, P. Spanel and M. Flores, *J. Agric. Food Chem.*, 2011, **59**, 1931–1938.
- 28 A. Olivares, K. Dryahina, J. L. Navarro, M. Flores, D. Smith and P. Spanel, *Anal. Chem.*, 2010, **82**, 5819–5829.
- 29 K. Sovová, M. Ferus, I. Matulková, P. Španěl, K. Dryahina, O. Dvořák and S. Civiš, *Mol. Phys.*, 2008, **106**, 1205–1214.
- 30 D. Smith, P. Španěl, D. Dabill, J. Cocker and B. Rajan, *Rapid Commun. Mass Spectrom.*, 2004, **18**, 2830–2838.
- 31 J. Sule-Suso, A. Pysanenko, P. Spanel and D. Smith, *Analyst*, 2009, **134**, 2419–2425.
- 32 P. Španěl and D. Smith, *Mass Spectrom. Rev.*, 2011, **30**, 236–267.
- 33 D. Smith, A. Pysanenko and P. Španěl, *Int. J. Mass Spectrom.*, 2009, **281**, 15–23.
- 34 R. P. Williams, C. L. Gott, S. M. H. Qadri and R. H. Scott, *J. Bacteriol.*, 1971, **106**, 438–443.
- 35 P. Španěl, K. Dryahina and D. Smith, *Int. J. Mass Spectrom.*, 2006, **249**, 230–239.
- 36 D. Smith and P. Španěl, *Analyst*, 2011, **136**, 2009–2032.
- 37 D. Smith, T. W. Chippendale and P. Španěl, *Int. J. Mass Spectrom.*, 2011, **303**, 81–89.
- 38 A. Pysanenko, P. Spanel and D. Smith, *Int. J. Mass Spectrom.*, 2009, **285**, 42–48.
- 39 S. P. Bernier, S. Létoffé, M. Delepierre and J. M. Ghigo, *Mol. Microbiol.*, 2011, **81**, 705–716.

Appendix F, Sovová *et al.* Anal. Chem. 84 (2012) 4979

Real-time quantification of traces of biogenic volatile selenium compounds
in humid air by selected ion flow tube mass spectrometry

Kristýna Sovová^{a,b}, Violetta Shestivska^a, Patrik Španěl^{a,*}.

^a*J. Heyrovský Institute of Physical Chemistry, Academy of Sciences of the Czech
Republic Dolejškova 3, 18223 Prague 8, Czech Republic*

^b*Department of Physical and Macromolecular Chemistry, Faculty of Science, Charles
University, Albertov 2030, 128 40 Prague 2, Czech Republic*

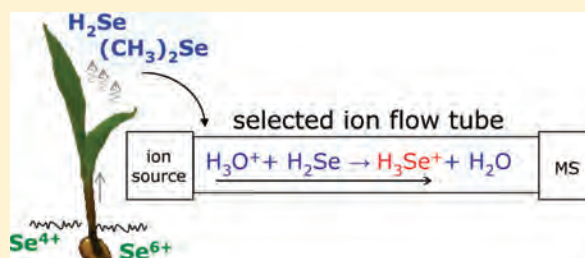
Real-Time Quantification of Traces of Biogenic Volatile Selenium Compounds in Humid Air by Selected Ion Flow Tube Mass Spectrometry

Kristýna Sovová,^{†,‡} Violetta Shestivska,[†] and Patrik Španěl^{*,†}

[†]J. Heyrovský Institute of Physical Chemistry, Academy of Sciences of the Czech Republic, Dolejškova 3, 18223 Prague 8, Czech Republic

[‡]Department of Physical and Macromolecular Chemistry, Faculty of Science, Charles University, Albertov 2030, 128 40 Prague 2, Czech Republic

ABSTRACT: Biological volatilization of selenium, Se, in a contaminated area is an economical and environmentally friendly approach to phytoremediation techniques, but analytical methods for monitoring and studying volatile compounds released in the process of phytovolatilization are currently limited in their performance. Thus, a new method for real time quantification of trace amounts of the vapors of hydrogen selenide (H_2Se), methylselenol (CH_3SeH), dimethylselenide ($(\text{CH}_3)_2\text{Se}$), and dimethyldiselenide ($(\text{CH}_3)_2\text{Se}_2$) present in ambient air adjacent to living plants has been developed. This involves the characterization of the mechanism and kinetics of the reaction of H_3O^+ , NO^+ , and $\text{O}_2^{+\bullet}$ reagent ions with molecules of these compounds and then use of the rate constants so obtained to determine their absolute concentrations in air by selected ion flow tube mass spectrometry, SIFT-MS. The results of experiments demonstrating this method on emissions from maize (*Zea mays*) seedlings cultivated in Se rich medium are also presented.



Selenium (Se) is an essential nutrient in physiology, but this element can become toxic at elevated concentrations due to its chemical similarity to sulfur. This can lead to a nonspecific replacement of sulfur by selenium in proteins and some other compounds important to all living organisms. Se has become an element of global environmental and health concern because of its toxicity to living organisms and the extensive use in industrial activities. Removal of Se containing toxins from contaminated water and soil using physical, chemical, and engineering techniques is quite complicated and expensive,¹ but it can be effectively achieved by phytoremediation techniques that include phytovolatilization,² which is based on the ability of green plants and associated rhizobacteria to take in selenate (SeO_4^{2-}) or selenite (SeO_3^{2-}) ions dissolved in water, to assimilate them using sulfur transporters and enzymes, and to transform them into volatile forms, including dimethylselenide, $(\text{CH}_3)_2\text{Se}$, and dimethyldiselenide, $(\text{CH}_3)_2\text{Se}_2$. Consequently, this process reduces the toxicity of selenium; for example, $(\text{CH}_3)_2\text{Se}$ is more than 500 times less toxic than the inorganic forms of selenium as has been demonstrated in studies on rats.^{3,4} It is now well documented that various plants can volatilize^{5–7} or accumulate^{8,9} selenium, and this opens the way for their practical use in environmental remediation.

Analytical methods currently used to study volatile Se compounds released by plants usually involve quantitative trapping of volatile gases in alkaline peroxide liquid traps¹⁰ followed by Se assays using various techniques including atomic absorption spectroscopy^{10–12} (detection limit, 1.0 mg Se/L)

and the mass spectrometric methods ICPMS, HPLC/MS, GC/MS, GC-ICPMS, or ESI-MS.¹³ Solid-phase microextraction, SPME, has also been used to extract volatile Se compounds directly from air avoiding the use of a liquid trap, when the absolute concentrations of $(\text{CH}_3)_2\text{Se}$ and $(\text{CH}_3)_2\text{Se}_2$ were determined using external standards.¹⁴ Hollow fiber protected liquid-phase microextraction¹⁵ was recently reported as another effective method for direct GC/MS analyses of $(\text{CH}_3)_2\text{Se}$ and $(\text{CH}_3)_2\text{Se}_2$ in air. In our experience,¹⁶ the SPME method can be used for accurate absolute quantification only with some difficulties and we suspect that it does not effectively extract highly volatile H_2Se , which we speculate may also be emitted by plants even though this has not yet been observed.

Methylselenol (CH_3SeH) is another possible volatile form of selenium homologous to H_2Se and $(\text{CH}_3)_2\text{Se}$ that are known to be involved in detoxification of Se in human metabolism.¹⁷ In plants, CH_3SeH is an intermediate metabolite involved in the Se-methionine pathway in the biosynthesis of $(\text{CH}_3)_2\text{Se}$. Other volatile Se compounds, including selenoformaldehyde,¹⁸ H_2CSe , and diallylselenide,¹⁹ $(\text{C}_3\text{H}_5)_2\text{Se}$, are not known to be involved in phytovolatilization, and thus, they are not included formally in this study; however, the mass spectra were inspected in order to check for their possible presence.

Received: March 5, 2012

Accepted: May 2, 2012

Published: May 2, 2012

Table 1. Rate Constants of the Reactions of H_3O^+ , NO^+ , and $\text{O}_2^{+\bullet}$ with the Four Volatile Se-Compounds Indicated, Given in the Units of $10^{-9} \text{ cm}^3\text{s}^{-1}$ ^a

	molecule	MW	α (10^{-24} cm^3) ^b	μ_t (D) ^b	H_3O^+ [k_c]	NO^+ k [k_c]	$\text{O}_2^{+\bullet}$ k [k_c]
	hydrogen selenide	H_2Se	81	3.2	0.63	[1.3]	
	methylselenol	CH_3Se	95	5.1	1.29	[2.1]	
	dimethylselenide	$\text{C}_2\text{H}_6\text{Se}$	109	9.7 ^c	1.32	[2.5]	2.0 [2.1]
	dimethyldiselenide	$\text{C}_2\text{H}_6\text{Se}_2$	188	12.3	1.70	[2.8]	[2.3]

^aThe k_c values in brackets correspond to the collisional rate constant;^{25,26} k is an experimentally derived rate constant as explained in the Experimental Section. Also included are their molecular weights, MW, polarisabilities, α , and dipole moments, μ_t . ^bValues of α and μ_t are taken from refs 33–36 and rounded. ^c α was calculated according Miller and Savchik.³⁷ We had used the value of the atomic hybrid components, τ , for selenium as $4.59 \text{ \AA}^{3/2}$.

Thus, the aim of the present study was to develop a method for real time quantification of several volatile forms of selenium obviating sample collection. The compounds chosen as the volatile forms of Se potentially emitted by plants and included in this study are hydrogen selenide, H_2Se , dimethylselenide, $(\text{CH}_3)_2\text{Se}$, methylselenol, CH_3SeH , and dimethyldiselenide, $(\text{CH}_3)_2\text{Se}_2$.

Selected ion flow tube mass spectrometry, SIFT-MS, has been previously successfully used to quantify other biogenic volatile organic compounds (BVOCs)²⁰ in a range of medical, food science, and security related analyses,²¹ because it allows precise real time quantification of trace volatile compounds in ambient air²⁰ and in exhaled breath.²² SIFT-MS is based on chemical ionization of a continuously flowing air sample diluted in He carrier gas using one of the three precursor ions, H_3O^+ , NO^+ , and $\text{O}_2^{+\bullet}$, reacting selectively with trace gases and vapors during an accurately defined time in a flow tube of a given length. Absolute concentration of reactive compounds present in a sample can be calculated online, in real-time from the ratios of product ion count rates to the precursor ion count rates using known rate constants and the other physical parameters.²³

EXPERIMENTAL SECTION

To obtain the absolute concentration of vapors of volatile compounds in real time using SIFT-MS, it is essential to know the rate constants and the primary ion products of their reactions with the precursor ions used for analysis.²³ These parameters can be obtained experimentally by studying the reactions of the precursor ions with standard mixes of the reference compounds when these are available.²⁴ This was done in the present study for $(\text{CH}_3)_2\text{Se}$. The vapor of this compound (purchased from Sigma Aldrich, purity $\geq 99.0\%$ (GC)) was introduced into the SIFT-MS instrument (*Profile 3*, Instrument Science Limited, Crewe, U.K.) via a heated calibrated capillary, and full scan mass spectra in the range of mass-to-charge ratio m/z 10 to 160 covering the molecular weights were acquired. For each precursor ion, three mass spectra were obtained with a total integration time of 60 s. The major ion products were identified, and their count rates were precisely determined in separate experiments using the multi-ion monitoring, MIM, mode at a variable flow rate controlled by a needle valve and monitored by a flow-meter (manufactured by Voegtlin, Aesch, Switzerland).²⁴ The rate constant for the proton transfer reactions of H_3O^+ is equal to the collisional rate constant k_c because these reactions are exothermic by more than 40 kJ/mol.²⁵ Thus, the rate constants for the reactions of H_3O^+ were calculated as collisional (k_c)²⁶ using the dipole moment and polarizability data (see Table 1). The rate constants for the reactions with NO^+ and $\text{O}_2^{+\bullet}$ (k) were then derived from their

experimental decay rates relatively to that for H_3O^+ by injecting all three precursors simultaneously and allowing them to react with the sample introduced at variable concentrations.²⁴ The count rates of H_3O^+ , NO^+ , and $\text{O}_2^{+\bullet}$ were plotted on a semilogarithmic scale as functions of the sample flow rate and the rate constants (k) for the NO^+ and $\text{O}_2^{+\bullet}$ reactions were determined from the relative slopes of these plots.²⁴

The rate constants and product ions for the other compounds were obtained from thermochemical calculations of exothermicities of possible reaction channels²⁷ and from calculations of the collisional rate constants for the exothermic proton transfer reactions of H_3O^+ (k_c) according to Su and Chesnavich²⁶ using the dipole moments and polarizabilities of the reactant molecules. These rate constants, m/z of the precursor, and product ions are then used in the kinetics library in the format required by the SIFT-MS software for online calculations of the concentrations.²⁴ The kinetics library can be optimized to avoid overlaps (see Results and Discussion) or cross sensitivity.²⁴

The accuracy of the SIFT-MS analysis of volatile Se compounds is influenced by the same factors as previously described for SIFT-MS quantification of other volatile compounds from the ratio of the ion count rates: the reaction time, the rate constant, and the sample flow rate.²³ These parameters are determined for a given instrument with combined accuracy of $\pm 20\%$. Note that concentration of simultaneously quantified water vapor acts as a useful indicator of accuracy of measurement.^{28,29} The precision and reproducibility of the quantification is chiefly given by the counting statistics and is routinely calculated by the data analysis software.²³

Experiments demonstrating the feasibility of SIFT-MS quantification of volatile Se compounds released from maize plants (*Zea mays*) cultivated with an enhanced supply of Se nutrients were carried out by the following protocol: five different concentrations (0.2, 2.0, 10.0, 20.0, and 200 μM in aqueous solution) of selenium salts (sodium selenate, A, and sodium selenite, B) were used as a germinating medium to ascertain whether there is a correlation between the amounts and form of selenium salts and the amounts of volatile selenium compounds released by the seedlings. Ten Petri dishes were filled up with cotton-wool soaked with 5 mL of the different solutions. After 2 days, the maize seedlings grew to a length of about 3 cm and the characteristic garlic odor of $(\text{CH}_3)_2\text{Se}$ became noticeable. The headspace above the covered cultivating Petri dishes was analyzed using SIFT-MS in real time. Each sample was heated for 15 min at the temperature of 40 °C. A heated calibrated capillary was inserted inside the covered dish, and the concentration of $(\text{CH}_3)_2\text{Se}$ was measured using the multi-ion monitoring (MIM) mode;²³ the absolute

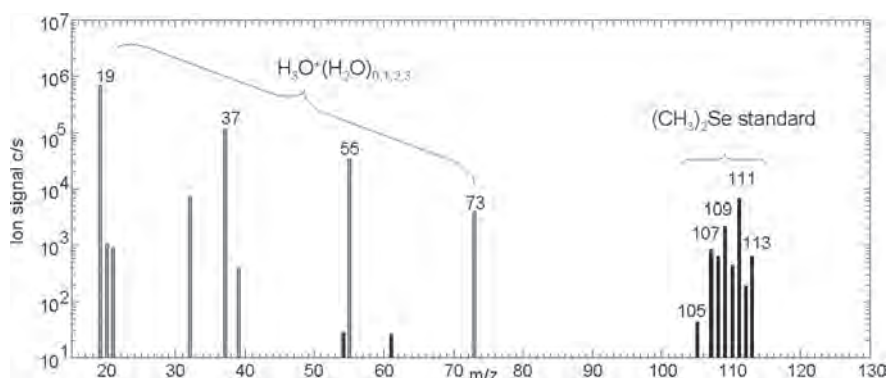


Figure 1. Mass spectrum obtained from the headspace of $(\text{CH}_3)_2\text{Se}$ standard mixture by averaging 12 consequential scans. Signals at m/z 112 and 114 are due to the lower resolution of quadrupole mass spectrometer and due to ^{13}C isotopologues. Minor signal at m/z 50 is $\text{O}_2^+\text{H}_2\text{O}$; 29 m/z 54 and 61 are presumably noise.

concentration was obtained. Thus, the headspace within the covered dish was collected directly, and ambient air was allowed to replace the depleted volume. Background concentrations of volatile Se compounds in the laboratory air were monitored before and after analysis of each sample and compared with the headspace concentrations.

Safety Considerations. The volatile reference reagent, dimethylselenide ($(\text{CH}_3)_2\text{Se}$), is toxic by inhalation, is toxic if swallowed, and causes danger of cumulative effects. This reagent must be handled with caution according to established laboratory safety practices using safety glasses and gloves for personal protection while ensuring good ventilation. Hydrogen selenide (H_2Se) was not used as a reagent, but it is one of the volatile compounds released by plants. H_2Se is also very toxic by inhalation, highly flammable, toxic in contact with skin, and potentially fatal even at low ppm levels. However, in the experiments described in this Article, the concentrations of H_2Se released by plants are seen to be much lower.

RESULTS AND DISCUSSION

Ion Chemistry of $(\text{CH}_3)_2\text{Se}$. The ion chemistry of the three precursor ions (H_3O^+ , NO^+ , and $\text{O}_2^{+\bullet}$) with the standard mixture of $(\text{CH}_3)_2\text{Se}$ was studied experimentally using the well established SIFT method for the determination of ion–molecule kinetics.²⁴ The reaction of H_3O^+ with $(\text{CH}_3)_2\text{Se}$ (Figure 1) produces the protonated ion $(\text{CH}_3)_2\text{SeH}^+$ exclusively, and its four major isotopologues appear at mass-to-charge ratios, m/z , of 107, 108, 109, 111, and 113. This is because selenium has five major stable isotopes: ^{76}Se (9.02%), ^{77}Se (7.63%), ^{78}Se (23.52%), ^{80}Se (49.82%), and ^{82}Se (9.19%) (the sixth isotope ^{74}Se has natural abundance less than 1%). This characteristic isotopic composition is very useful, because it can confirm the presence of Se in volatile compounds released by plants. Note that, unlike many protonated polar compounds, $(\text{CH}_3)_2\text{SeH}^+$ ions do not associate with water molecules forming hydrated ions. This means that the concentration of $(\text{CH}_3)_2\text{Se}$ in the sampled air can be calculated directly from the ratio of the product ion count rates to the precursor ion count rates without the need to consider formation of hydrates.²³

NO^+ and $\text{O}_2^{+\bullet}$ precursor ions were both observed to react with $(\text{CH}_3)_2\text{Se}$ (IE = 8.40 eV) via charge transfer without any fragmentation producing $(\text{CH}_3)_2\text{Se}^{+\bullet}$ at m/z 106, 107, 108, 110, and 112. The calculated values of the collisional rate constant (k_c) for the H_3O^+ reaction and the experimentally

derived rate constants (k) for the NO^+ and $\text{O}_2^{+\bullet}$ reactions are summarized in Table 1.

Ion Chemistry of H_2Se , CH_3SeH , $(\text{CH}_3)_2\text{Se}_2$. Following our previous experience with hydrogen sulfide (H_2S)³⁰ reactions, we presume that H_3O^+ will transfer a proton to H_2Se (proton affinity, PA, 707.8 kJ/mol)³¹ because Se has similar chemical properties to sulfur. Fragmentation after proton transfer cannot occur in this proton transfer reaction because the energy released (calculated as 16.8 kJ/mol from the PA of H_2O of 691 kJ/mol)³¹ is substantially smaller than the strength of the Se–H covalent bond. Thus, a nondissociative proton transfer occurring at the collisional rate²⁵ can be used for absolute quantification of H_2Se . The product ions H_3Se^+ at m/z 79, 81, 83, and 85 are used in the present study; however, there is a potential overlap with the second hydrate of protonated ethanol at m/z 83 and 85. NO^+ cannot react with H_2Se by an exothermic binary reaction because of the value of its ionization energy (IE H_2Se = 9.89 eV) that is larger than recombination energy of NO^+ (RE NO^+ = 9.2 eV). The reaction of $\text{O}_2^{+\bullet}$ is known from previous work³² to form the H_2Se^+ ion product that cannot be used for SIFT-MS analysis because it disappears completely from the flow tube due to its reaction with water to form H_3O^+ .

Methylselenol, CH_3SeH , is expected to have a higher PA than water on the basis of its structure (by analogy with the value of PA of methanethiol, CH_3SH , which is 773.4 kJ/mol), and thus, it will react with H_3O^+ via proton transfer forming $\text{CH}_3\text{SeH}_2^+$ (m/z 93, 95, 97, and 99). The value of the ionization energy of CH_3SeH is not available in the literature, but again by analogy with CH_3SH (IE = 9.44 eV), it is unlikely to react with NO^+ . We can only speculate that methylselenol will react with $\text{O}_2^{+\bullet}$ precursor ion by charge transfer followed by fragmentation. However, as it will be shown later, Se-enriched plants did not produce any methylselenol anyway, because it was not observed on the H_3O^+ SIFT-MS spectra. Similarly, dimethyldiselenide ($\text{C}_2\text{H}_6\text{Se}_2$, IE 8.1 eV) is expected to react with H_3O^+ forming the protonated molecule that would be present at a wide range of isotopologues (significant peaks ranging from m/z 185 to 193 with a characteristic distribution corresponding to two Se atoms). NO^+ and $\text{O}_2^{+\bullet}$ will react with $\text{C}_2\text{H}_6\text{Se}_2$ by charge transfer producing ions in the range from m/z 184 to 192. Again, later it will be shown that these characteristic product ions were not observed in the experiments with plants.

Measurement of Vapor Concentrations of Volatile Se-Compounds Released by Plants. Air above maize seedlings cultivated with an enriched supply of Se was analyzed by SIFT-MS, as described in the Experimental Section. SIFT-MS spectra were acquired while the heated calibrated capillary was inserted into the covered cultivation dishes. The detailed inspection of the full scan mass spectra obtained using H_3O^+ precursors (Figure 2) showed the presence of $(\text{CH}_3)_2\text{Se}$ and H_2Se but did

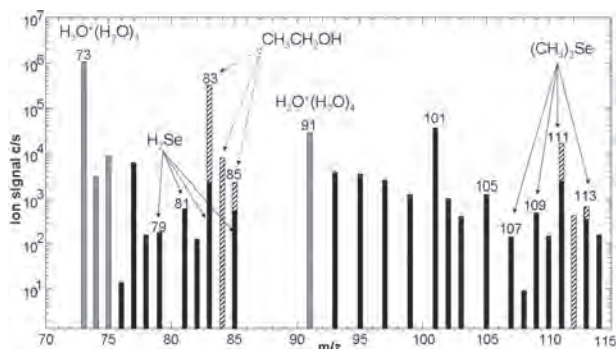


Figure 2. SIFT-MS mass spectrum obtained using H_3O^+ precursors while sampling air above maize seedling cultivated on Se-enriched medium. Note the characteristic product ions of $(\text{CH}_3)_2\text{Se}$ on the m/z 107, 109, 111, 113, and H_2Se in the mass range of m/z 79–85. The contribution of the overlapping ethanol product ions ($\text{C}_2\text{H}_5\text{OH}_2^+(\text{H}_2\text{O})_2$ at m/z 83, ^{13}C isotopologues at m/z 84, ^{18}O at m/z 85, and similarly $(\text{C}_2\text{H}_5\text{OH})_2\text{H}^+\text{H}_2\text{O}$ at m/z 111, 112, and 113) are shown in the spectrum with a dashed pattern.

not indicate the presence of any of the other two possible volatile Se-compounds. Identification and also quantification of H_2Se can be complicated by overlaps with the second hydrate of protonated ethanol.^{38,39} However, presence of other isotopes allows its detection. Thus, the apparent isotopic ratios of H_3Se^+ differ from the expected and have to be corrected by subtracting the contributions from isotopologues of $\text{C}_2\text{H}_5\text{OH}_2^+(\text{H}_2\text{O})_2$. Similarly, the observed isotopic ratios for protonated $(\text{CH}_3)_2\text{Se}$ differ somewhat from the expected values, because of the overlaps of the isotopologues of $(\text{C}_2\text{H}_5\text{OH})_2\text{H}^+\text{H}_2\text{O}$ at m/z 111. The headspace was also analyzed using a standard SPME/GC/MS method (mentioned in the introduction and described in detail in ref 16) to supplement the SIFT-MS results. These analyses confirmed presence of $(\text{CH}_3)_2\text{Se}$; however, as expected, H_2Se was not seen, due to the inability of SPME/GC/MS to detect such highly volatile molecules.

$(\text{CH}_3)_2\text{Se}$ was quantified in real time using the MIM mode for SIFT-MS analysis. The kinetics library used for quantification was thus constructed to calculate the absolute concentration of $(\text{CH}_3)_2\text{Se}$ from the ion signals at m/z 107 and 109 multiplied by a coefficient of 3 (corresponding approximately to the contribution of isotopologues $1/(0.0902 + 0.2352)$) to avoid contribution of the overlapping signal of ethanol. Sample results observed for $(\text{CH}_3)_2\text{Se}$ above cultivations with two different concentrations of two different Se salts are shown in Figure 3. This experiment indicated that SIFT-MS quantification of $(\text{CH}_3)_2\text{Se}$ is possible even at absolute humidity of the headspace air >7% corresponding to saturated water vapor pressure at temperatures in the range of 40–42 °C. The reproducibility of measurement was better than $\pm 3\%$ and was found to be limited by the counting statistics.²⁸

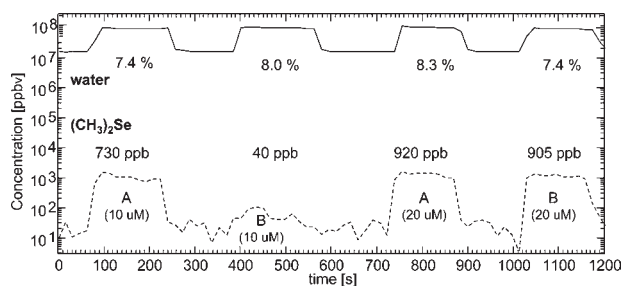


Figure 3. Time profile of concentration of $(\text{CH}_3)_2\text{Se}$ obtained using H_3O^+ precursors when the cultivation headspace is sequentially introduced into the SIFT-MS sample inlet from above seeds sprouting in four different media indicated (two different concentrations of sodium selenate, A, and sodium selenite, B; samples were heated at 40 °C). Concentration of water vapor by volume (absolute humidity calculated from the ion signals of $\text{H}_3\text{O}^+(\text{H}_2\text{O})_{1,2,3}$ ²⁸) is indicated by the solid line; the dashed line corresponds to the concentration of $(\text{CH}_3)_2\text{Se}$.

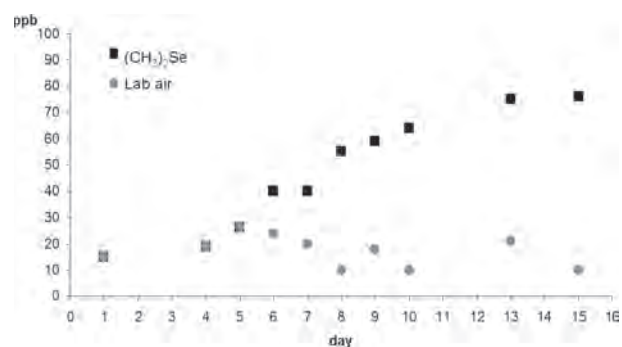


Figure 4. Time profile of the increasing concentration of $(\text{CH}_3)_2\text{Se}$ inside the Petri dish in comparison with the concentration in the background laboratory air.

Note that such reproducibility of quantification is typical for SIFT-MS measurements⁴⁰ of concentrations around 1000 ppb. These results indicate that the released volume of volatile $(\text{CH}_3)_2\text{Se}$ changes with the amounts and type of the selenium salt; however, the exact nature of this relationship, including details of saturation kinetics, will have to be established in more systematic experiments. Another open question is whether the observed $(\text{CH}_3)_2\text{Se}$ and H_2Se originate from the maize seedlings or from the bacterial activity within the growth medium inside the Petri dishes.

In order to demonstrate reproducibility of the quantifications and the ability of SIFT-MS to quantify temporal changes in concentration, we have repeated the analyses using the same seedlings and observed an increase in concentration of $(\text{CH}_3)_2\text{Se}$ in real time during several days of cultivation. The resulting values, together with the concentrations measured in the ambient laboratory air, are plotted in Figure 4. These results conclusively confirm that the observed volatile selenium indeed originates from the prepared samples and not from any pollution from the laboratory air.

CONCLUSIONS

SIFT-MS allows immediate quantification of H_2Se , CH_3SeH , $(\text{CH}_3)_2\text{Se}$, and $(\text{CH}_3)_2\text{Se}_2$ present in humid air based on the values of rate constants obtained in the present study. The study of ion chemistry of $(\text{CH}_3)_2\text{Se}$ provided new experimental

data on the product ions of H_3O^+ , NO^+ , and $\text{O}_2^{+\bullet}$ reactions. The experiments using maize seedlings showed that, from these four compounds, only H_2Se and $(\text{CH}_3)_2\text{Se}$ are produced in measurable concentrations (>1 ppb) in the air adjacent to plants growing in Se-enriched medium. To our knowledge, these were the first online quantitative and selective measurements of concentrations of volatile Se compounds. There were also no indications on the SIFT-MS mass spectra of the presence of selenoformaldehyde, H_2CSe , or diallyl selenide, $(\text{C}_3\text{H}_5)_2\text{Se}$, that were not included formally in the present study. Further experiments now can be done in order to fully utilize the potential of the SIFT-MS analytical method described in this Article. The first questions that need answering is how much volatilization of Se is realized by bacteria in soil or on the plant roots and how much conversion of inorganic Se to organic Se compounds occurs within the plants. In order to answer this question, we intend to perform similar experiments using defined bacterial cultures and to analyze emissions from the plant leaves separately from the soil in which the plants are growing.

AUTHOR INFORMATION

Corresponding Author

*Phone: +420 266 052 112. E-mail: spanel@jh-inst.cas.cz.

Notes

The authors declare no competing financial interest.

ACKNOWLEDGMENTS

We would like to thank Kseniya Dryahina for assistance with some of the SIFT-MS experiments and David Smith for reading and correcting the manuscript. We gratefully acknowledge financial support by the Grant Agency of the Czech Republic (project 203/09/0256) and by Grant Agency of Charles University (project GAUK 32010).

REFERENCES

- (1) Yu, X. Z.; Gu, J. D. *Environ. Sci. Pollut. Res.* **2008**, *15* (6), 499–508.
- (2) Lin, Z. Q.; Schemenauer, R. S.; Cervinka, V.; Zayed, A.; Lee, A.; Terry, N. J. *Environ. Qual.* **2000**, *29* (4), 1048–1056.
- (3) McConnell, K. P.; Portman, O. W. *Proc. Soc. Exp. Biol. Med.* **1952**, *79* (2), 230–231.
- (4) Wilber, C. G. *Clin. Toxicol.* **1980**, *17* (2), 171–230.
- (5) Zayed, A.; Lytle, C. M.; Terry, N. *Planta* **1998**, *206* (2), 284–292.
- (6) Zayed, A. M.; Terry, N. *J. Plant Physiol.* **1992**, *140* (6), 646–652.
- (7) Zayed, A. M.; Terry, N. *J. Plant Physiol.* **1994**, *143* (1), 8–14.
- (8) Di Gregorio, S.; Lampis, S.; Malorgio, F.; Petruzzelli, G.; Pezzarossa, B.; Vallini, G. *Plant Soil* **2006**, *285* (1–2), 233–244.
- (9) de Souza, M. P.; Lytle, C. M.; Mulholland, M. M.; Otte, M. L.; Terry, N. *Plant Physiol.* **2000**, *122* (4), 1281–1288.
- (10) Terry, N.; Carlson, C.; Raab, T. K.; Zayed, A. M. *J. Environ. Qual.* **1992**, *21* (3), 341–344.
- (11) de Souza, M. P.; Pilon-Smits, E. A. H.; Lytle, C. M.; Hwang, S.; Tai, J.; Honma, T. S. U.; Yeh, L.; Terry, N. *Plant Physiol.* **1998**, *117* (4), 1487–1494.
- (12) Pilon-Smits, E. A. H.; de Souza, M. P.; Lytle, C. M.; Shang, C.; Lugo, T.; Terry, N. *J. Exp. Bot.* **1998**, *49* (328), 1889–1892.
- (13) Montes-Bayon, M.; Grant, T. D.; Meija, J.; Caruso, J. A. *J. Anal. At. Spectrom.* **2002**, *17* (9), 1015–1023.
- (14) Meija, J.; Montes-Bayon, M.; Le Duc, D. L.; Terry, N.; Caruso, J. A. *Anal. Chem.* **2002**, *74* (22), 5837–5844.
- (15) Ghasemi, E.; Sillanpaa, M.; Najafi, N. M. *J. Chromatogr., A* **2011**, *1218* (3), 380–386.
- (16) Shestivska, V.; Nemeč, A.; Dřevínek, P.; Sovová, K.; Dryahina, K.; Španěl, P. *Rapid Commun. Mass Spectrom.* **2011**, *25* (17), 2459–2467.
- (17) Rayman, M. P.; Infante, H. G.; Sargent, M. *Br. J. Nutr.* **2008**, *100* (2), 238–253.
- (18) Karpas, Z. *Chem. Phys. Lett.* **1985**, *120* (1), 10.
- (19) Whanger, P. D.; Ip, C.; Polan, C. E.; Uden, P. C.; Welbaum, G. *J. Agric. Food Chem.* **2000**, *48* (11), 5723–5730.
- (20) Smith, D.; Španěl, P. *TrAC Trends Anal. Chem.* **2011**, *30* (7), 945–959.
- (21) Španěl, P.; Smith, D. *Mass Spectrom. Rev.* **2011**, *30* (2), 236–267.
- (22) Boshier, P. R.; Cushnir, J. R.; Mistry, V.; Knaggs, A.; Španěl, P.; Smith, D.; Hanna, G. B. *Analyst* **2011**, *136* (16), 3233–3237.
- (23) Španěl, P.; Dryahina, K.; Smith, D. *Int. J. Mass Spectrom.* **2006**, *249*, 230–239.
- (24) Sovová, K.; Dryahina, K.; Španěl, P. *Int. J. Mass Spectrom.* **2011**, *300* (1), 31–38.
- (25) Bouchoux, G.; Salpin, J. Y.; Leblanc, D. *Int. J. Mass Spectrom. Ion Process* **1996**, *153* (1), 37–48.
- (26) Su, T.; Chesnavich, W. J. *J. Chem. Phys.* **1982**, *76* (10), 5183–5185.
- (27) Ervin, K. M. *Chem. Rev.* **2001**, *101* (2), 391–444.
- (28) Španěl, P.; Smith, D. *Rapid Commun. Mass Spectrom.* **2001**, *15* (8), 563–569.
- (29) Španěl, P.; Smith, D. *Int. J. Mass Spectrom.* **2009**, *280* (1–3), 128–135.
- (30) Španěl, P.; Smith, D. *Rapid Commun. Mass Spectrom.* **2000**, *14* (13), 1136–1140.
- (31) Linstrom, P. J.; Mallard, W. G. *NIST Chemistry WebBook, NIST Standard Reference Database Number 69*; National Institute of Standards and Technology: Gaithersburg, 2011.
- (32) Anicich, V. *An Index of the Literature for Bimolecular Gas Phase Cation-Molecule Reaction Kinetics, JPL Publication 03-19*; National Aeronautics and Space Administration, Jet Propulsion Laboratory, California Institute of Technology: Pasadena, CA, 2003; p 1–1172.
- (33) Mirri, A. M. C. C. P. *J. Chem. Phys.* **1969**, *50*.
- (34) Johari, G. P. *National Research Council Digest of Literature on Dielectrics*; National Academy of Sciences: Washington, D.C., 1977.
- (35) Thoen, K. K.; Beasley, B. J.; Smith, R. L.; Kenttamaa, H. I. *J. Am. Soc. Mass Spectrom.* **1996**, *7* (12), 1245–1250.
- (36) Thomas, C. H. *J. Chem. Phys.* **1973**, *59*, 70.
- (37) Miller, K. J.; Savchik, J. A. *J. Am. Chem. Soc.* **1979**, *101* (24), 7206–7213.
- (38) Dryahina, K.; Pehal, F.; Smith, D.; Španěl, P. *Int. J. Mass Spectrom.* **2009**, *286* (1), 1–6.
- (39) Turner, C.; Španěl, P.; Smith, D. *Rapid Commun. Mass Spectrom.* **2006**, *20* (1), 61–68.
- (40) Boshier, P. R.; Marczin, N.; Hanna, G. B. *J. Am. Soc. Mass Spectrom.* **2010**, *21* (6), 1070–1074.

Appendix G, Civiš *et al.* Anal. Chem. 83 (2011) 1069

Laser Ablation of FOX-7: Proposed Mechanism of Decomposition

Martin Civiš¹, Svatopluk Civiš^{1,*}, Kristýna Sovová¹, Kseniya Dryahina¹, Patrik Španěl¹,
and Martin Kyncl²

¹*J. Heyrovský Institute of Physical Chemistry, Czech Academy of Sciences,
Dolejškova 3, 182 23 Prague 8, Czech Republic*

²*Explosia a.s., Semtín 107, 530 50 Pardubice, Czech Republic*

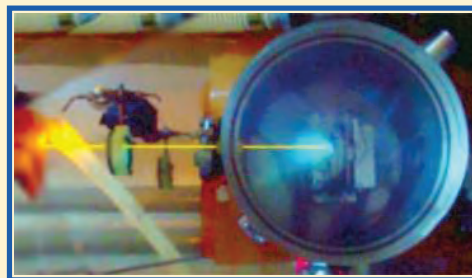
Laser Ablation of FOX-7: Proposed Mechanism of Decomposition

Martin Civiš,[†] Svatopluk Civiš,^{*,†} Kristýna Sovová,[†] Kseniya Dryahina,[†] Patrik Španěl,[†] and Martin Kyncl[‡]

[†]J. Heyrovský Institute of Physical Chemistry, Czech Academy of Sciences, Dolejškova 3, 182 23 Prague 8, Czech Republic

[‡]Explosia a.s., Semtín 107, 530 50 Pardubice, Czech Republic

ABSTRACT: A novel high-energy explosive material, FOX-7 (1,1-diamino-2,2-dinitroethylene), was studied using a combination of laser-induced breakdown spectroscopy (LIBS) and selected ion flow tube mass spectrometry (SIFT-MS). The LIBS technique uses short laser pulses (an ArF excimer laser) as the energy source to convert small quantities of a sample into plasma and to induce the emission of its molecular fragments or atoms. SIFT-MS is a novel method for absolute quantification based on chemical ionization using three reagent ions, with the ability to determine concentrations of trace gases and vapors of volatile organic compounds in real time. SIFT-MS was used to study the release of NO, NO₂, HCN, HONO, HCHO, CH₃CH₂OH, and C₂H₂ after laser ablation of the explosive compound FOX-7 in solid crystalline form. The radiation emitted after excitation was analyzed using a time-resolved UV–vis spectrometer with an ICCD detector. The electronic bands of CN (388 nm), OH (308.4 nm), and NO (237.1 nm) radicals and the atomic lines of C, N, and H were identified.



The fear of terrorism and the need to detect dangerous chemicals in low concentrations have led to an ever-increasing need for reliable, real-time, and sensitive detection of a wide range of substances that represent a security threat to society. The compounds that need to be detected in trace quantities range from explosives to narcotics and chemical or biological agents. Considerable effort has been focused on trace detection of small amounts of explosives and their decomposition products.

One compound from a new family of potentially threatening explosive materials is 1,1-diamino-2,2-dinitroethylene (FOX-7), which has the same molecular stoichiometry as the well-known RDX (1,3,5-trinitro-2-oxo-1,3,5-triazacyclo-hexane) and HMX (1,3,5,7-tetraamino-1,3,5,7-tetraazacyclo-octane) explosives. Methods of laser-induced breakdown spectroscopy (LIBS)¹ and selected ion flow tube mass spectrometry (SIFT-MS)² have been combined in the present study to investigate the decomposition mechanisms that occur during a simulated explosion of a small quantity of the FOX-7 explosive.

Laser-induced breakdown spectroscopy (LIBS) is a spectroscopic analytical method that uses the light emitted from laser-induced microplasma to determine the composition of the sample based on elemental or molecular emission spectra. The specific feature of LIBS is the breakdown of the molecules of the sample, which initiates a rich system of chemical reactions leading to a range of spectroscopically detectable species. LIBS has many practical advantages over the conventional methods of chemical analysis because it operates without the necessity of direct contact, is very sensitive, provides real time results, and in most cases, there is no need for sample preparation. The facility of LIBS for real time and remote sensitive detection of a wide variety of materials makes LIBS an ideal candidate for hazardous material detection.³ LIBS has been used for chemical,^{4,5} biological,^{6–8} and explosive material^{9–12} detection in laboratory and also for remote detection of explosives placed in a vehicle at a distance of

30 m.¹³ The plasma formed during the LIBS analyses leads to formation of stable gaseous compounds that can be the subject of mass spectrometric analyses using sensitive trace gas techniques as SIFT-MS; however, such a combination of the techniques is still in its infancy.

We exploited the combination of these two techniques to solve the very challenging problem of characterizing the products of an explosion using microscopic-scale laboratory experiments without the need to initiate macroscopic explosions of test charges weighing several grams or more. We used LIBS to initiate chemistry-mimicking explosions in microgram quantities of pure explosive compounds and then supplemented time-resolved emission spectroscopy data obtained from SIFT-MS quantifications of the stable gaseous end products of these microscopic explosions. While the detailed mechanism of the processes occurring during LIBS is not still fully described, the time scales observed in the present work (several microseconds) correspond well to typical duration of explosive reactions on the scale of 1 mm. A detailed description of both methods used in combination can be found in our previous paper discussing the results of similar experiments with hexogen, octogen, pentrite, and trinitrotoluene.¹⁴

There have been several studies concerned with quantum chemical calculations used to predict the initial steps of decomposition in solid FOX-7. Unimolecular or intermolecular hydrogen transfer, nitro-nitrite isomerization and C–NO₂ bond dissociation were studied by Dorsett.¹⁵ She found that intermolecular hydrogen transfer results in the production of radical intermediates and water under thermolyzing conditions. Conversely, the dissociation of a C–NO₂ bond requires high energy, suggesting that this reaction is more likely to occur under high

Received: November 3, 2010

Accepted: December 21, 2010

Published: January 12, 2011

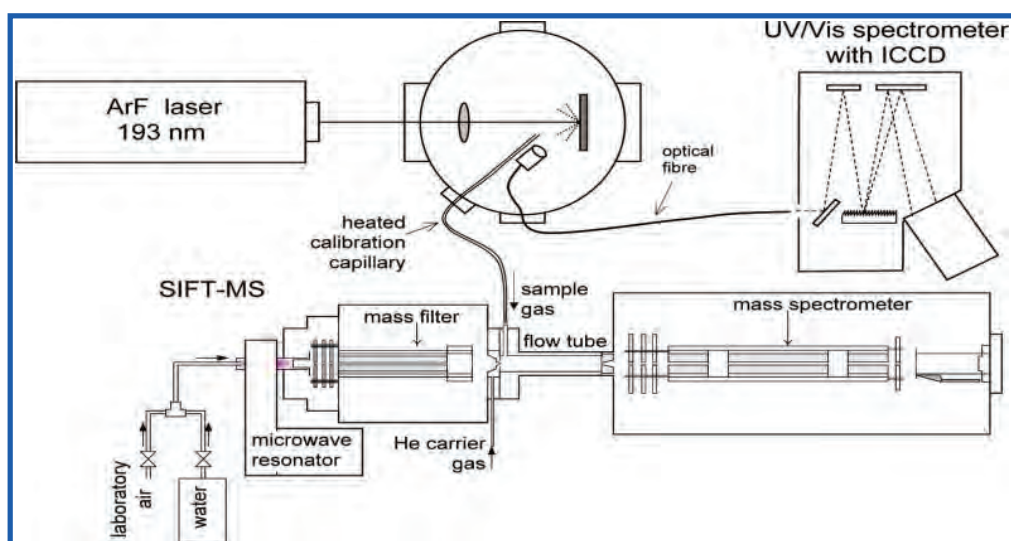


Figure 1. Schematic diagram of the experimental apparatus.

pressure and high temperature conditions typically generated by shock or impact.

The mechanism of FOX-7 decomposition based on functional theory calculation was studied by Gindulyte et al.¹⁶ They found that the FOX-7 decomposition reaction is initiated by a nitro-to-nitrite rearrangement with a calculated energy barrier of approximately 59.1 kcal/mol. They theoretically analyzed the steps in the decomposition process leading to fragments of NO, HONO, CO, NH₂, and HCN and to final products of CO, N₂, H₂O, with an energy release that, on average, can initiate two additional FOX-7 molecular decompositions and thus sustain a chain reaction.

Ion–molecule investigations applying proton-transfer reaction time-of-flight mass spectrometry (PTR-MS-TOF) technology has been used for the detection of trace quantities of solid explosives with very low vapor pressures at room temperature by Mayhew et al.¹⁷ This report illustrated the capability of detecting solid explosives (RDX, TNT, HMX, PETN, and Semtex A) in real time by analyzing the headspace above small quantities of samples. They demonstrated the unambiguous identification of threat agents in complex chemical environments in which multiple threat agents and interferences may be present, thereby eliminating false positives.

Molecules involved in the thermal ignition process of high explosives were studied by the combination of a laser ignition technique (180 W CO₂ laser) with mass spectroscopic analysis by Östmark et al.¹⁸ In the RDX preignition zone, several decomposition intermediates were identified: N₂O, HCN, NO₂, H₂CO, NO, CO₂, and triazine.

Recently, we published a study¹⁴ of four types of explosives, HMX, RDX, PETN and TNT, based on the application of laser-induced breakdown spectroscopy and selected ion flow tube mass spectrometry. Short laser pulses of an ArF excimer laser were used to convert small quantities of samples into plasma to induce emission from their molecular fragments or atoms. SIFT-MS was used for absolute quantification and concentration determination of the volatile organic products in real time.

Objectives of the Study. Objectives of the present study were to identify the atomic and molecular species generated inside a LIBS plume using a combination of the LIBS and

SIFT-MS techniques. Thus, we investigated the so far unknown unimolecular decomposition pathway of FOX-7 into stable end products. Small samples of the explosive were irradiated in argon or air buffer gases, and the generated plasma was investigated to identify transient species and changes in their concentrations in real time by LIBS. The concentrations of stable end product molecules were simultaneously determined by SIFT-MS. The experimental results were interpreted according to a suggested theoretical decomposition reaction scheme of 1,1-diamino-2,2-dinitroethylene based on a density functional theoretical study by Gindulyte et al.¹⁶

EXPERIMENTAL SECTION

LIBS. The experimental setup used in this study was identical to that described in our previous article¹⁴ and is shown schematically in Figure 1.

An ArF excimer laser (193 nm, 20 ns, and 150 mJ) was used to create radiation pulses that were focused using a 15 cm quartz lens onto the surface of a rotating target placed in a vacuum chamber. The radiation emitted from the ablation plume was collected by an optical fiber and was focused onto the entrance slit of a UV–vis spectrometer (MS 257 Oriel) equipped with an intensified ICCD detector. The spectrometer covers a spectral range of 200–1000 nm. Two ruled gratings were interchangeably used in the spectrometer, one for a broad-range preview (150 lines/mm, width of measured spectra = 400 nm) and another to obtain high-resolution spectra (1200 lines/mm, width of measured spectra = 60 nm). The disperse spectrum was detected by an intensified ICCD camera (ICCD; iStar 720, Andor) with a resolution of 0.08 nm/pixel when using the high-resolution grating.

The intensified ICCD camera was synchronized with the laser pulse by using a signal from a photodiode registering the scattered laser pulse radiation. Time-resolved spectra were obtained using different delays between the laser pulse and light acquisition in the ICCD. This delay is given as the time from the beginning of the laser pulse to the point at which the first emission lines appear. A total of 100 repeated laser pulses were used to acquire each of the presented LIBS spectra with a spectral

Table 1. Identification of Molecular Fragments and Their Electronic Transitions along with Atomic Lines and Relative Intensities at Different Times after the Laser Pulse in Argon and Air Atmosphere

name	λ [nm]	band identification ^a	relative intensity in Ar, in air [a.u.] ^b		time of first observation [μ s] ^c
NI	484.7	$2s^2(^3P)3s-2s^2p(^3P)3p$	5 626 500	—	1.2
NI	496.4	$2s^2(^3P)3s-2s^2p(^3P)3p$	4 632 400	—	1.2
NII	500.1	$2s^22p(^2P^o)3p-2s^22p(^2P^o)3d$	4 742 800	452 170	1.2/1.0
CI	505.2	$2s^22p(^2P^o)3s-2s^22p(^2P^o)4p$	3 798 600	—	1.2
CII	514.3	$2s2p(^3P^o)3s-2s2p(^3P^o)3p$	3 278 000	—	1.2
H β	486.1	Balmer series, $E_{exc} = 12.7$ eV, $(2P^o-2D)$	4 044 100	106 230	1.8
CN	385.1	$B^2\Sigma_u^+ - X^2\Sigma_g^+, v' = 4, v'' = 4$	242 270	299 150	1.4
CN	385.4	$B^2\Sigma_u^+ - X^2\Sigma_g^+, v' = 3, v'' = 3$	230 290	275 370	1.4
CN	386.1	$B^2\Sigma_u^+ - X^2\Sigma_g^+, v' = 2, v'' = 2$	251 360	267 140	1.4
CN	387.1	$B^2\Sigma_u^+ - X^2\Sigma_g^+, v' = 1, v'' = 1$	230 290	261 260	1.4
CN	388.2	$B^2\Sigma_u^+ - X^2\Sigma_g^+, v' = 0, v'' = 0$	260 040	260 140	1.4
OH	308.9	$(A^2\Sigma^+ - X^2\Pi)$	2 926 300	297 120	1
NI	279.9	$2s^22p(^2P^o)3p-2s^22p(^2P^o)4d$	3 168 700	—	1.2
CI	247.9	$2s^2p^2-2s^2p(^2P^o)3s$	5 706 100	344 860	1.2/1.3
NO	237.1	$(A^2\Sigma^+ - X^2\Pi), v' = 0, v'' = 1$	—	744 090	1.3
CII	257.5	$3s^23p-3s^2(1S)nd$	—	1 021 200	1.3

^a The bands were assigned according to Pearse and Gaydon,²³ on the basis of our previous work²⁴ and according to Harb et al.^{25 b} The relative intensities are given for both types of atmosphere Ar and air. — means that the line was not observed at sufficient signal-to-noise ratio. ^c Where two values are given, the first one corresponds to Ar atmosphere and the second one corresponds to air.

range of 200–800 nm. This number of repetitions was required to reach a satisfactory signal-to-noise ratio.

The time variations of the intensities of the radiation emitted by the CN and OH species were recorded in the regions of the electronic transition peaks, where the emission intensities are the strongest. The high-resolution grating angle was adjusted in such a way that the studied peak was in the center of the acquired spectral range. The spectra were carefully inspected for the possible presence of atomic lines in the first few nanoseconds after the laser pulse, which would have interfered with the molecular bands of the breakdown products.

SIFT-MS. Selected ion flow tube mass spectrometry, SIFT-MS, is a technique that allows for the quantification of trace amounts of gases and vapors present in air. It is based on chemical ionization using reagent ions, H_3O^+ , O_2^+ , and NO^+ , which do not react with the major components of air but selectively ionize trace amounts of other gases and vapors. Absolute quantification is achieved on the basis of a well-defined reaction time, during which chemical ionization takes place in a helium carrier gas flowing through a flow tube into which the reagent ions are injected and the sample is introduced at a known flow rate. In this study, we used SIFT-MS to quantify the concentrations of stable compounds produced during a LIBS event. Because this technique achieves a real-time analysis of the continuous flow of a sample gas, it is possible to obtain data with a time resolution of 0.5 s. SIFT-MS has previously been used to study trace gases in various biological systems² and gases resulting from controlled combustion.¹⁹

SIFT-MS has been used in combination with LIBS to analyze the stable products produced by explosive chemistry. We note that the vapors of the compounds used in this study were recently detected using proton transfer reaction mass spectrometry PTR-MS.¹⁷ It is also noteworthy that time-of-flight mass spectrometry, TOF MS, has been used previously for analyses of ions generated by LIBS.²⁰

The stable gas products originating from plasma generated by 10 repeated laser pulses were introduced via a heated, calibrated capillary directly into the SIFT-MS (manufactured by Instru-

ment Science Limited, Crewe, U.K.). A total of 10 pulses were chosen, and the duration of the sequence was 10 s, allowing us to monitor the time profiles of the product concentrations. The capillary was placed at a distance of 2 cm from the surface of the sample. Full scan mass spectra were obtained using repeated full scans for all three reagent ions. The concentrations of the main compounds identified on the mass spectra were calculated from the reagent and product ion count rates, the known carrier gas and sample flow rates, and the flow tube pressures, according to the general method for calculating absolute trace gas concentrations in air from selected ion flow tube mass spectrometry data.²¹ The rate coefficients were taken from the kinetic library supplied by the SIFT-MS instrument when available or were estimated theoretically.²² The accuracy of quantification in this complex mixture is estimated to be $\pm 50\%$. The relative precision of the measurement, however, is estimated at $\pm 30\%$. Thus, the results provide approximate information about absolute concentrations of the main components of the degradation products in the gas mixture, even though their interpretation is related to a variable degree of dilution in the atmosphere of the chamber. The multiple ion monitoring mode (MIM) of the SIFT-MS instrument was used to investigate the time profiles of the selected molecular species concentrations.²

Sample Preparation and Experimental Protocol. Samples of bulk explosive FOX-7 were prepared in the form of tablets by compressing powder using a standard press (commonly used in the infrared absorption spectroscopy of powder samples). Bulk (2 mm-thick) samples were used to avoid any emission originating from the metal holder, which complicated the data obtained when thin films of explosive materials were used in our preliminary experiments. Argon at atmospheric pressure was used as the atmosphere surrounding the samples to eliminate interference due to overlapping molecular spectral bands of components of air and also to avoid any secondary chemical reactions with atmospheric oxygen. However, time-resolved studies of the emitted radiation were repeated using an air atmosphere to

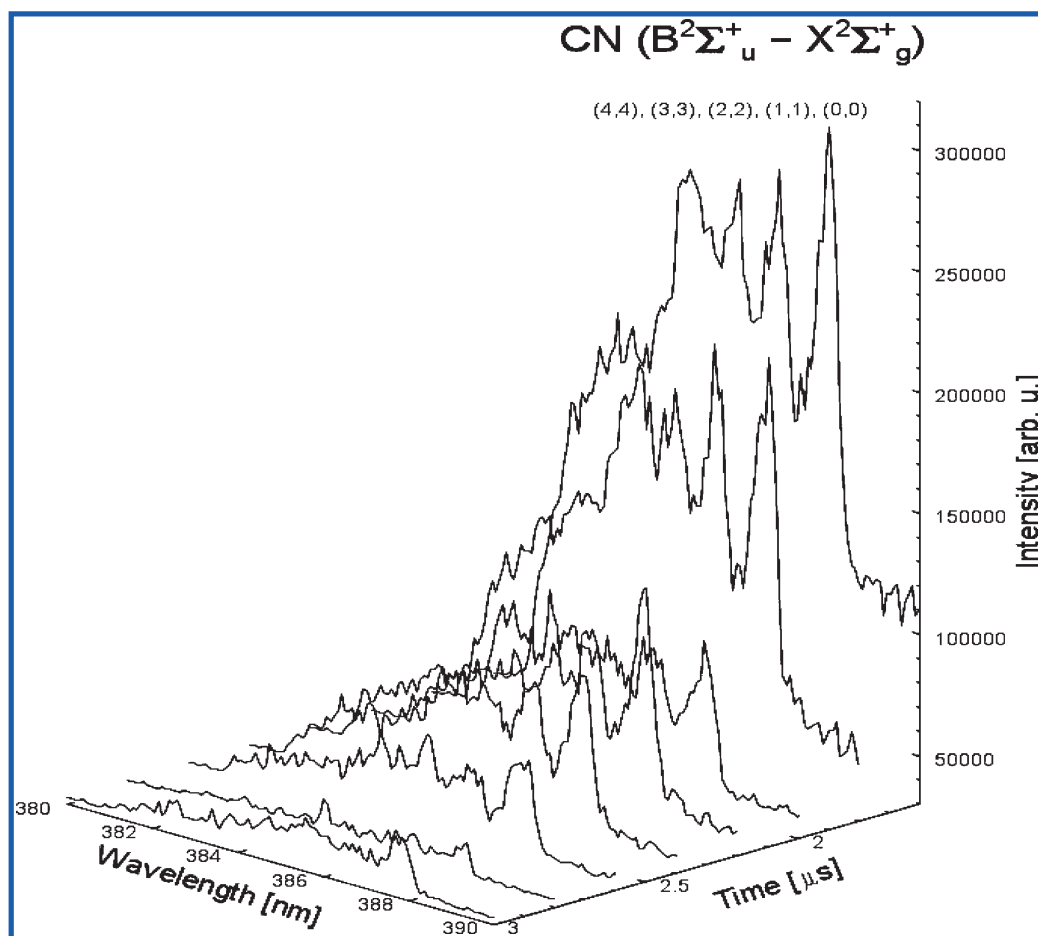


Figure 2. Time-resolved spectra of the CN radical ($B^2\Sigma_u^+ - X^2\Sigma_g^+$) of the FOX-7 sample, measured 1.4–3 μs after the laser pulse in an air atmosphere.

investigate the influence of the atmosphere composition on the lifetimes of the individual species.

Safety Considerations. In the experimental work described in this study, there are two potential safety hazards. One is the use of energetic laser radiation that can be harmful to eyes even when scattered. It is essential that during the operation of the laser, all personnel present in the laboratory wears approved safety glasses and that unexpected entry to the laboratory is prevented. Second hazard is the use of explosive material, FOX-7 is relatively stable, and bulk explosion cannot be triggered by laser pulse shorter than 20 ns (1 ms or more would be potentially dangerous). All regular safety procedures required for safe handling and storage of explosives must be adhered to. The gaseous fumes pumped by a rotary pump must be exhausted in a safe manner outside of the laboratory.

RESULTS AND DISCUSSION

LIBS. Several atomic transitions and molecular electronic bands were observed in the LIBS emission spectra of the FOX-7 explosive. All of the identified lines and bands are listed in Table 1. The spectral intensities were observed at different time delays after the laser pulse. The atomic emission lines were identified as C (247.9 and 505.2 nm), H ($H_\beta = 486.1$ nm), and N (279.9 nm, 496.4 and 484.7 nm). An emission line originating from singly charge carbon atoms, C⁺ was also observed (C II, $\lambda = 257.5$ and 514.3 nm) within the first 1.2 μs in Ar medium and

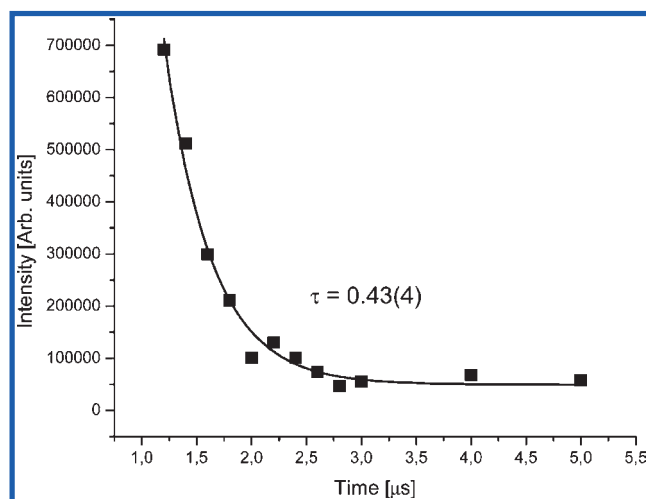


Figure 3. Time-resolved decay of CN ($B^2\Sigma_u^+ - X^2\Sigma_g^+$) in an air atmosphere (FOX-7).

1.3 μs after the laser pulse in air, respectively. Observations of the molecular emission²⁶ corresponded to the transitions of CN and OH radicals.

Time Evolution of CN Emission Spectra. A characteristic CN radical emission band²⁷ was observed in the LIBS spectra in

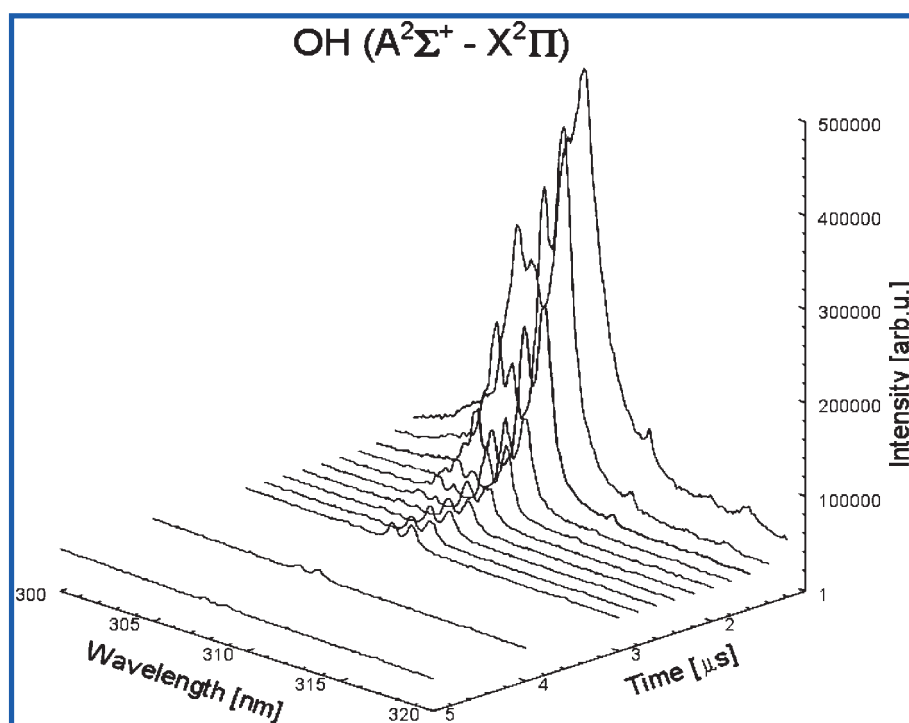


Figure 4. Time-resolved spectrum of the OH radical ($A^2\Sigma^+ - X^2\Pi$) originating from FOX-7 measured in air.

the violet region (Figure 2). This band corresponds to transitions from several vibrational levels from the second excited electronic state to the fundamental electronic state ($B^2\Sigma \rightarrow X^2\Sigma$). The strongest emission was observed at 388.2 nm and corresponds to the (0,0) peak of the $\Delta\nu = 0$ sequence. The time evolution of the CN radical emission intensities was measured in an interval of 1.4–3 μs to quantitatively describe the kinetics of the decay process. Figure 2 depicts the time dependencies of the intensities of the emitted radiation in air.

Time-resolved measurements of small molecular fragments provide information about individual reaction steps, the lifetime of the excited transient species, and their appearance and disappearance in the plasma of a laser ablation plume. The lifetime of the CN radical was measured for the transition at 388.2 nm (see Figure 3). The estimated lifetime of the excited CN radical ($B^2\Sigma_u - X^2\Sigma_g^+$) in air is approximately 0.4 μs . This value is comparable with the lifetimes for CN radicals derived from PETN ($\tau = 0.4 \mu\text{s}$), RDX ($\tau = 0.6 \mu\text{s}$), and HMX ($\tau = 0.5 \mu\text{s}$), with the exception of TNT, for which a lifetime 4 times larger than the CN lifetime ($\tau = 2.3 \mu\text{s}$) has been obtained.¹⁴

OH Emission. Emission from the OH radical was observed at $\lambda = 308.4 \text{ nm}$ and was identified as the (0,0) transition from the first electronic excited state to the ground electronic state ($A^2\Sigma^+ - X^2\Pi$).¹⁴ The time-resolved spectrum measured in the laboratory air atmosphere is depicted in Figure 4.

The OH emission ($A^2\Sigma^+ - X^2\Pi$, (0,0) transition at 308.4 nm) was studied in an atmosphere of air and argon buffer gas. The vibronic bands of the hydroxyl radical appeared in the spectrum 1 μs after the laser pulse and remained detectable for more than 4 μs , both in air and argon medium. Figure 4 shows the time dependence of the OH emission intensities at 308.4 nm obtained at atmospheric pressure in air, while Figure 5 depicts the time dependence of the OH electronic band ($A^2\Sigma^+ - X^2\Pi$) emission intensity. The estimated lifetime is 0.43 μs . This value is

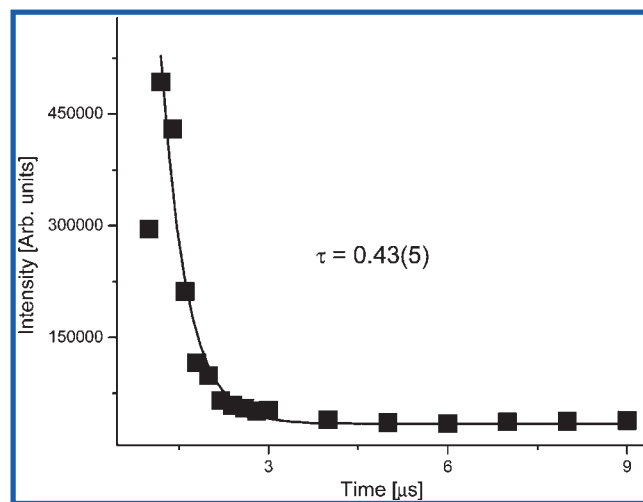


Figure 5. Time-resolved decay of OH in an air atmosphere (FOX-7).

in good agreement with our previous similar measurements²⁸ for RDX, TNT, HMX, and PETN. The only difference was that, for FOX-7, relatively strong OH emission was also observable in argon buffer gas. To the best of our knowledge, there is no other previous work describing time delayed observation of OH in LIBS.

The observation that these OH emission bands appear in the spectra with a 1 μs delay following instantaneous emission corresponding to the atomic lines of H and O indicates that OH is formed by subsequential reactions of primary breakdown products, not by direct fragmentation of the FOX-7 molecules. The quenching of OH emission observed (in both air and Ar atmospheres) after 4 μs can be explained by its reaction with the transient and extremely reactive cyanide radical (CN) or dicarbon

Table 2. Concentrations in Parts Per Billion (ppb) of the Compounds Identified by SIFT-MS in an Ar Atmosphere Inside the Experimental Chamber after Initiation of the Explosive Sample Using 10 Laser Pulses

name ^a	formula	molecular weight	ion	products <i>m/z</i>	background	ppb (sample 1) ^a	ppb (sample 2)
ammonia	NH ₃	17	O ₂ ^{•+}	17, 35	79	5	123
water	H ₂ O	18	H ₃ O ⁺	19, 37, 55, 73, 91	0.29%	0.96%	0.13%
acetylene	C ₂ H ₂	26	O ₂ ^{•+}	26	0	7	25
hydrogen cyanide	HCN	27	H ₃ O ⁺	28	4	121	105
formaldehyde	HCHO	30	H ₃ O ⁺	31	19	187	67
nitric oxide	NO	30	O ₂ ^{•+}	30	247	513	368
acetonitrile	CH ₃ CN	41	H ₃ O ⁺	42	0	0	6
acetaldehyde	C ₂ H ₄ O	44	H ₃ O ⁺	45, 63, 81	0	18	74
ethanol	C ₂ H ₆ O	46	H ₃ O ⁺	47, 65, 83	1378	4518	4194
nitrous acid	HONO	47	H ₃ O ⁺	30, 48, 66	39	202	115
nitrogen dioxide	NO ₂	48	O ₂ ^{•+}	46	345	246	696
acetone	C ₃ H ₆ O	58	NO ⁺	88	4	57	5

^a Sample 1 is a regular FOX-7 sample provided by Explosia. Sample 2 has been synthesized specifically for this study avoiding any use of ethanol.

monoxide (C₂O).²⁹ The lifetime of the OH radical was only 0.4 μs; however, its persistence for 4 μs corresponds to a continuous formation due to a sequence of reactions (including fragmentation of the HONO molecules, see the following sections). These observations are substantially different from the results of our previous study of RDX, HMX, PETN, and TNT,²⁸ in which the OH radical was only observed in air for a short interval of 1.5–2 μs following the laser pulse.

Vibrational and Excitation Temperatures. The vibrational temperature of the CN radicals produced by the FOX-7 explosive was determined from the relative line intensities within the available vibrational band. This calculation used the electronic transition of B²Σ_g⁻ → X²Σ_u⁺ and the emission intensities corresponding to the most intense vibrational transitions (0–0, 1–1, 2–2, 3–3). The vibrational temperature was calculated on the basis of the Boltzmann population distribution using the energy dependency of the intensities:

$$\ln[I_{\nu}/\lambda^3 f] = KE_{\nu} + Q \quad (1)$$

where I_{ν} is the intensity observed for the transition originating from the vibrational state with the vibrational quantum number ν , λ is the corresponding wavelength, f is the value of the Franck–Condon factor for the vibronic transition, and E_{ν} is the vibrational energy of the state ν . Linear regression of the experimental data, plotted as a Boltzmann plot, provides the slope K and the constant Q . The vibrational temperature can be finally calculated from the slope K using a simple equation:

$$T_{\text{vib}} = -1/kK \quad (2)$$

where k is the Boltzmann constant. The vibrational temperature of the (FOX-7 explosive) CN radicals determined using this method was approximately 5200 ± 800 K. This corresponds to the kinetic gas temperature typical for LIBS plumes.¹⁴

SIFT-MS Data. SIFT-MS data obtained using the reagent ions H₃O⁺ and O₂^{•+} for the samples directly from the reaction zone after the laser pulse (in an argon atmosphere) showed the presence of nitrogen dioxide (NO₂), nitrous acid (HONO), ammonia (NH₃), hydrogen cyanide (HCN), formaldehyde (HCHO), acetonitrile (CH₃CN), acetylene (C₂H₂), ethanol (CH₃CH₂OH), and dimethyldinitrobutane (DMNB). The mean absolute concentrations of these stable products obtained by sampling from a

point separated by 2.5 cm from the sample surface during the first 10 s after the LIBS event are given in Table 2 in units of parts per billion (ppb).

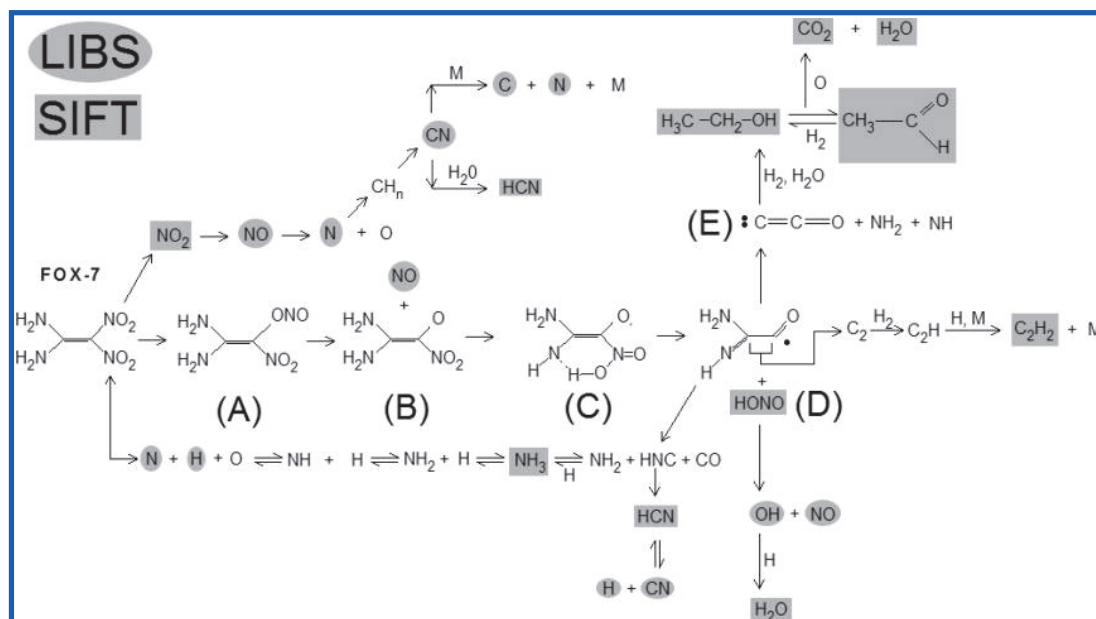
Over time, the concentrations of all of the products decreased due to their diffusion into the volume of the chamber. The concentrations obtained using the same experimental apparatus in the absence of any explosive samples are also given. Note that the levels of ethanol, NO, NO₂, HONO, and HCN were significantly elevated in all of the LIBS experiments.

The SIFT experiments confirm that ethanol was produced at a relatively higher concentration (one order of the magnitude higher) in comparison to the other reaction products (NO, NO₂) of the FOX-7 laser decomposition (sample 1 in Table 1). Thus, new sample material was synthesized strictly without the use of ethanol as a solvent to demonstrate that the detected ethanol was not present as an impurity in crystalline FOX-7 (sample 2 in Table 1). SIFT-MS analyses of the ablation plasma end products again confirmed the presence of relatively high concentrations of C₂H₅OH, demonstrating that ethanol is indeed a major component of FOX-7 explosion fumes.

Mechanism. An understanding of the decomposition mechanism plays a key role in the evaluation of properties of a new type of explosive. Because of its unique features, the decomposition mechanism of FOX-7 is expected to differ from that of RDX and HMX.^{30,31} However, the kinetics of elementary processes of ionization, excitation, and decomposition in the LIBS plasma occurs on the time scale of microseconds in qualitative agreement with previous work.¹⁴ A reaction scheme (Scheme 1) for the decomposition of FOX-7 and for the formation of the final stable products was constructed on the basis of the results presented in the previous sections and is discussed here.

Laser radiation causes fragmentation, ionization, and atomization of the molecules of the FOX-7 sample. The transient intermediate species H, CN, OH, NO, C, and N were observed on the basis of characteristic emission lines and bands in the optical spectra, and the stable end products C₂H₅OH, HCHO, HCN, HONO, NH₃, CH₃CN, C₂H₄O, C₂H₂, NO₂, NO, C₃H₆O, and H₂O were observed via the occurrence of characteristic product ions on the SIFT-MS chemical ionization mass spectra. Note that the major stoichiometric explosion products N₂ and CO₂ generated in macroscopic quantities were not a subject of this investigation, as their production is well understood³² and as

Scheme 1



they are always present in atmospheric air. Thus, these products are of very limited interest from the point of view of the identification of explosives based on their decomposition products.

In Scheme 1, the observed intermediate transient species are shown in circles, and the observed stable products formed by the reactions of the intermediate species are indicated by rectangles.

Gindulyte et al.¹⁶ suggested that the initial step of FOX-7 decomposition is a nitro-to-nitrite rearrangement (A in a Scheme 1) followed by the elimination of a NO molecule (B). We adopted this reaction pathway as the basis of Scheme 1.

The next step, according to this theory, is the migration of a H atom from the NH₂ group to NO₂ (C), followed by HONO elimination from the structure (C), resulting in the formation of a reasonably stable, conjugated radical (D). According to Gindulyte et al.,¹⁶ the weakest bond in this structure (D) is the central C–C bond. Finally, CO elimination may occur, and the remaining fragment may further break down into a NH₂ radical and a HNC molecule. Our experimental results support the validity of this scheme by direct observation of H₂O, NH₃, HCN (or HNC isomer that cannot be distinguished by SIFT-MS), NO, and HONO stable molecules in agreement with theoretical predictions,¹⁶ which also include CO molecules that cannot currently be detected by SIFT-MS. Note that the production of two molecules of N₂, CO, and H₂O from the FOX-7 molecule is exothermic (117 kcal/mol).

In addition to the products predicted by theory,¹⁶ the SIFT-MS measurements indicate that the final products of the decomposition are not only the molecules mentioned above but also ethanol, C₂H₅OH, in a relatively high concentration of several parts per million when sampled 2.5 cm from the surface. The possibility of contamination due to solvent was excluded by validation experiments with a sample of FOX-7 prepared without the use of ethanol (see section 3.3). The formation mechanism of ethanol is proposed in Scheme 1 as a reaction path in which the structure (D) does not fragment directly to CO, HNC, and NH₂ but where only the C–N bonds dissociate. The resulting

extremely reactive fragment (E), dicarbon monoxide C₂O, then reacts with atomic H or with H₂O molecules, producing ethanol or acetaldehyde. Both of these molecules were detected using SIFT-MS, with the concentration of ethanol being more than an order of magnitude greater. In the reactive environment of the plasma, ethanol finally oxidizes to CO₂ and H₂O.

Most of the observed species were small neutral radicals, with the exception of C⁺. Thus, the dominant chemical pathways are neutral, but we cannot completely exclude the role of ions in chemistry occurring on nanosecond time scales. Some specific reaction pathways deserve closer attention.

Oxides of nitrogen, NO₂ and NO, are formed either by direct decomposition of the parent molecule or by secondary reactions of atomic nitrogen with oxygen. The two related acids HNO₂ and HNO₃ are formed by secondary reactions of NO₂ and NO with OH radicals, water molecules, and hydrogen atoms.

CN radicals are formed in reactions of atomic nitrogen with carbon-containing species:

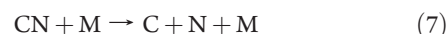
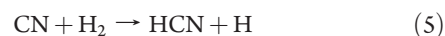


At high fume temperatures (thousands of degrees Kelvin), CN can also be formed by an endothermic reaction of atomic carbon with nitrogen:



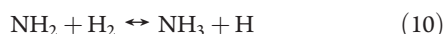
The rate constant for this reaction increases with temperature according to the Arrhenius law, with an activation energy of 46 kcal/mol³³ at $T = 5000$ K.

CN radicals observed by emission spectroscopy react with hydrogen or water molecules present in the plume:



forming one of the characteristic stable end products, HCN. The activation energy of reaction 5 is 4.7 kcal/mol,³⁴ and this reaction is easily accessible at $T > 4000$ K. CN is also destroyed by collision-induced dissociation (eq 7), which has a much larger activation energy (141 kcal/mol) but can occur by collisions with abundant gas present at atmospheric pressure. Thus, not all of the CN is necessarily converted to HCN.

NH radicals are formed either by direct elimination from the parent molecule or by reactions between atomic nitrogen and hydrogen.



This sequence of reactions leads to the formation of the observed ammonia.

CONCLUSIONS

The combined experiments using LIBS and SIFT-MS allowed for the analyses of atomic and molecular species produced by laser-induced breakdown of explosive compounds. Interpretations of the time-resolved emission spectra allowed for the construction of a reaction scheme of the early phases of the explosive decomposition. SIFT-MS provided the concentrations of trace amounts of characteristic stable end products. The formation mechanism of the stable products observed by SIFT-MS, including the oxides of nitrogen, hydrogen cyanide, acetylene, and ammonia, is plausibly explained on the basis of emission spectroscopy data. In addition to expanding our fundamental understanding of the chemical processes involved in a laser-induced breakdown of explosives, this study indicates that the decomposition of explosive molecules leads not only to the major stoichiometric products of N_2 , CO_2 , and H_2O but also to characteristic combinations of more complex products. These end products (exemplified by HCN and NH_3) are also present in the gas phase products generated after an explosion, and the methodology presented in this paper can thus offer a way for safe and non-destructive studies of characteristic explosion products, without the need for the initiation of hazardous quantities of explosives in the form of test charges. However, occurrence of secondary reactions between the products may influence the actual quantitative concentrations of individual end products and more research will be needed to relate products of LIBS to the products of actual explosions. The use of tablets of bulk explosives was found to be preferable to the use of thin films on metallic surfaces because of the elimination of parasitic metal atom emission. Our pilot studies using industrial explosives indicate that the composition of the end products of laser-generated plasma plumes correspond well to the composition of fumes collected after the explosion of a much larger (0.5 kg) charge. Thus, we plan to carry out further experimental research using actual mixtures of industrial explosives rather than pure compounds, which would make the combination of LIBS and SIFT-MS much more relevant to the examination of explosive products, without detonating dangerous explosives.

AUTHOR INFORMATION

Corresponding Author

*E-mail: civis@jh-inst.cas.cz. Phone: +420-286 591 766.

ACKNOWLEDGMENT

We gratefully acknowledge the financial support for this work provided by the Ministry of Trade and Industry of the Czech Republic, Project Tandem FT-TA4/124, and by GACR, Project No. 202/09/0800.

REFERENCES

- (1) Pasquini, C.; Cortez, J.; Silva, L. M. C.; Gonzaga, F. B. *J. Braz. Chem. Soc.* **2007**, *18*, 463.
- (2) Smith, D.; Španěl, P. *Mass Spectrom. Rev.* **2005**, *24*, 661.
- (3) Gottfried, J. L.; De Lucia, F. C.; Munson, C. A.; Miziolek, A. W. *Spectrochim. Acta, Part B* **2007**, *62*, 1405–1411.
- (4) Dudragne, L.; Adam, P.; Amouroux, J. *Appl. Spectrosc.* **1998**, *52*, 1321–1327.
- (5) DeLucia, F. C.; Samuels, A. C.; Harmon, R. S.; Walters, R. A.; McNesby, K. L.; LaPointe, A.; Winkel, R. J.; Miziolek, A. W. *IEEE Sens. J.* **2005**, *5*, 681–689.
- (6) Morel, S.; Leone, N.; Adam, P.; Amouroux, J. *Appl. Opt.* **2003**, *42*, 6184–6191.
- (7) Hybl, J. D.; Lithgow, G. A.; Buckley, S. G. *Appl. Spectrosc.* **2003**, *57*, 1207–1215.
- (8) Dixon, P. B.; Hahn, D. W. *Anal. Chem.* **2005**, *77*, 631–638.
- (9) Schade, W.; Bohling, C.; Hohmann, K.; Scheel, D. *Laser Part. Beams* **2006**, *24*, 241–247.
- (10) Harmon, R. S.; DeLucia, F. C.; LaPointe, A.; Winkel, R. J.; Miziolek, A. W. *Anal. Bioanal. Chem.* **2006**, *385*, 1140–1148.
- (11) Dikmelik, Y.; McEnnis, C.; Spicer, J. B. *Opt. Express* **2008**, *16*, 5332–5337.
- (12) DeLucia, F. C.; Gottfried, J. L.; Munson, C. A.; Miziolek, A. W. *Spectrochim. Acta, Part B* **2007**, *62*, 6.
- (13) Lopez-Moreno, C.; Palanco, S.; Laserna, J. J.; DeLucia, F.; Miziolek, A. W.; Rose, J.; Walters, R. A.; Whitehouse, A. I. *J. Anal. At. Spectrom.* **2006**, *21*, 55–60.
- (14) Sovová, K.; Dryahina, K.; Španěl, P.; Kyncl, M.; Civiš, S. *Analyst* **2010**, *135*, 1106.
- (15) Dorsett, H. *Aeronautical and Maritime Research Laboratory, DSTO-TR-1054*, 2000.
- (16) Gindulyte, A.; Massa, L.; Juany, L.; Karle, J. *J. Phys. Chem. A* **1999**, *103*, 11045.
- (17) Mayhew, C. A.; Sulzer, P.; Petersson, F.; Hidacher, S.; Jordan, A.; Märk, L.; Watts, P.; Märk, T. D. *Int. J. Mass Spectrom.* **2010**, *289*, 58.
- (18) Ostmark, H.; Bergman, H.; Ekvall, K. *J. Anal. Appl. Pyr.* **1992**, *24*, 163.
- (19) Sovová, K.; Ferus, M.; Matulková, I.; Španěl, P.; Dryahina, K.; Dvořák, O.; Civiš, S. *Mol. Phys.* **2008**, *106*, 1205.
- (20) McEnnis, C.; Dikmelik, Y.; Spicer, J. B. *Appl. Surf. Sci.* **2007**, *254*, 557.
- (21) Španěl, P.; Dryahina, K.; Smith, D. *Int. J. Mass Spectrom.* **2006**, *249*, 230.
- (22) Španěl, P.; Smith, D. *Eur. J. Mass Spectrom.* **2007**, *13*, 77.
- (23) Pearse, R. W. B.; Gaydon, A. G. *The Identification of Molecular Spectra*, 3rd ed.; Wiley: New York, 1963.
- (24) Babánková, D.; Civiš, S.; Juha, L. *Prog. Quantum Electron.* **2006**, *30*, 75.
- (25) Harb, T.; Kedzierski, W.; McConkey, J. W. *J. Chem. Phys.* **2001**, *115*, 5507.
- (26) Babánková, D.; Civiš, S.; Juha, L.; Bittner, M.; Cihelka, J.; Pfeifer, M.; Skála, J.; Bartnik, A.; Fiedorowicz, H.; Mikolajczyk, J.; Ryč, L.; Šedivcová, T. *J. Phys. Chem. A* **2006**, *110*, 12113.
- (27) Civiš, S.; Babánková, D.; Cihelka, J.; Sazama, P.; Juha, L. *J. Phys. Chem.* **2008**, *31*, 7162.
- (28) Sovová, K. Diploma Thesis, Charles University, Faculty of Science, Prague, Czech Republic, 2009.
- (29) Thweatt, W. D.; Erickson, M. A.; Hershberger, J. F. *J. Phys. Chem.* **2004**, *108*, 74.

- (30) Shalashilin, D. V.; Thomson, D. L. *J. Phys. Chem. A* **1997**, *101*, 961.
- (31) Wu, C. J.; Fried, L. E. *J. Phys. Chem. A* **1997**, *101*, 8675.
- (32) Španěl, P.; Dryahina, K.; Smith, D. *Int. J. Mass Spectrom.* **2006**, *249*, 230.
- (33) Babushok, V. I.; DeLucia, F. C.; Dagdigian, P. J.; Gottfried, J. L.; Munson, C. A.; Nusea, M. J.; Miziolek, A. W. *Spectrochim. Acta, Part B* **2007**, *62*, 1321.
- (34) Akhavan, J. *The Chemistry of Explosives*, 2nd ed.; The Royal Society of Chemistry: Cambridge, U.K., 2004.

Curriculum vitae

Personal

Born 28 December 1984, Mladá Boleslav

Higher education

- 2009 - present: PhD study: Physical chemistry
Charles University in Prague
Faculty of Science
Passed exams including Cambridge English: Preliminary (PET),
Physical chemistry, Mass spectrometry, Phytoremediation,
Passed final PhD state examination in physical chemistry, 25
March 2013
- 2007 - 2009: MSc study: Environmental chemistry, Charles University in
Prague
Faculty of Science
MSc thesis title: Study of explosive materials using
spectroscopic methods
- 2004 - 2007: BSc study: Environmental chemistry, Charles University in
Prague
Faculty of Science
BSc thesis title: High resolution FTIR spectroscopy and gas
chromatography study of decomposition products of PET
material

Previous employment

- 2009 – present: J. Heyrovský Institute of physical chemistry, AVCR, v. v. i.
Dolejškova 3, Prague
Department of mass spectrometry
Postgraduate student
- 2008: Institute of Physics, AVCR, v. v. i.
Application of spectroscopic measurements in the plasma
research
12 month part-time contract as laboratory assistant
- 2006 - 2009: J. Heyrovský Institute of physical chemistry, AVCR, v. v. i.
Department of Fourier transform (FT) and laser spectroscopy
Undergraduate student

Membership

- Czech society for mass spectrometry
- Jan Marek Marci spectroscopic society
- Association of the Czech Chemical Societies

Publications in peer reviewed journals with impact factor

1. Dryahina K., Španěl P., Pospíšilová V., **Sovová K.**, Hrdlička L., Machková N., Lukáš M. and David Smith: Quantification of pentane in exhaled breath, a potential biomarker of bowel disease, using selected ion flow tube mass spectrometry *Rapid Commun. Mass Spectrom.* **27**, 1983 (2013).
2. **Sovová K.**, Čepl J., Markoš A. and Španěl P.: Real time monitoring of population dynamics in concurrent bacterial growth using SIFT-MS quantification of volatile metabolites *Analyst* **138**, 4795 (2013).
3. Shestivska V., Španěl P., Dryahina K., **Sovová K.**, Smith D., Musílek M., Nemeč A.: Variability in the concentrations of volatile metabolites emitted by genotypically different strains of *Pseudomonas aeruginosa* *J. Appl. Microbiol.* **113**, 701 (2012).
4. **Sovová K.**, Shestivska V. and Španěl P.: Real-time quantification of traces of biogenic volatile selenium compounds in humid air by selected ion flow tube mass spectrometry *Anal. Chem.* **84**, 4979 (2012).
5. Smith D., **Sovová K.** and Španěl P.: A selected ion flow tube study of the reactions of H_3O^+ , NO^+ and O_2^{+} with seven isomers of hexanol in support of SIFT-MS *Int. J. Mass spectrom.* **319**, 25 (2012).
6. Shestivska V., Nemeč A., Dřevínek P., **Sovová K.**, Dryahina K. and Španěl P.: Quantification of methyl thiocyanate in the headspace of *Pseudomonas aeruginosa* cultures and in the breath of cystic fibrosis patients by selected ion flow tube mass spectrometry *Rapid Commun. Mass Spectrom.* **25**, 2459 (2011).
7. Civiš M., Civiš S., **Sovová K.**, Dryahina K., Španěl P., Kyncl M.: Laser Ablation of FOX-7: Proposed Mechanism of Decomposition *Anal. Chem.* **83**, 1069 (2011).
8. **Sovová K.**, Dryahina K., Španěl P.: Selected ion flow tube, SIFT, studies of the reactions of H_3O^+ , NO^+ and O_2^{+} with six volatile phytogetic esters *Int. J. Mass spectrom.* **300**, 31 (2011).
9. **Sovová K.**, Dryahina K., Španěl P., Kyncl M., Civiš S.: A study of the composition of the products of laser-induced breakdown of hexogen, octogen, pentrite and trinitrotoluene using selected ion flow tube mass spectrometry and UV-Vis spectrometry *Analyst* **135**, 1106 (2010).
10. **Sovová K.**, Ferus M., Matulková I., Dryahina K., Španěl P., Dvořák O., Civiš S.: A study of thermal decomposition and combustion products of disposable polyethylene terephthalate (PET) plastic using high resolution Fourier transform infrared spectroscopy, selected ion flow tube mass spectrometry and gass chromatography mass spectrometry *Molecular Phys.* **106**, 1205 (2008).

Proceedings included in WoS

11. Cihelka J., Matulková I., **Sovová K.**, et al.: Optical Emission Spectroscopy of High-Power Laser-Induced Dielectric Breakdown in Molecular Gases and Their Mixtures: Investigating Early Stages of Plasma Chemical Action in Planetary Atmospheres *Origins of life and evolution of biospheres* **39**, 227 (2009).
12. **Sovová K.**, Matulková I., Kamas M., et al.: SIFT-MS Analysis of Molecular Gas Mixtures Exposed to High-Power Laser Plasmas: Laboratory Simulation of High-Energy-Density Events in Early Earth's Atmospheres *Origins of life and evolution of biospheres* **39**, 249 (2009).

Lectures at scientific meetings

1. Summer school of mass spectrometry, Pec pod Sněžkou 20.9.-24.9. 2010: SIFT-MS: VOCs emitted by plants.
2. "SIFT-MS; current and proposed applications" ISTM, Medical School, Keele University, Thornburrow Drive, Stoke-on-Trent. Wednesday November 3rd 2010: SIFT-MS: VOC emissions from plants.
3. Second Ion Chemistry Meeting Dolní Malá Úpa, May 27 – 29. 2011: Real-time SIFT-MS detection of volatile forms of selenium released by plants.
4. Czech conference on mass spectrometry 19.-21.10. 2011, Hradec Králové: Selected Ion Flow Tube Mass Spectrometry.
5. 64. congress of the Association of Czech and Slovak Chemical Societies 25. - 27. June 2012 Olomouc: Selected Ion Flow Tube Mass Spectrometry.

Research projects

- Co-ordinating & responsible person of " Key Activity" number 7 (KA 7) (January 2013 – May 2014) in project: BIO-OPT-XUV (BOX) Research Team Advancement at the Faculty of Biomedical Engineering, Czech Technical University in Prague. Project duration: July 1, 2011 – May 30, 2014.
- Principal investigator of GAUK (Charles University Foundation) student project: Study of volatile compounds released by plants during phytoremediation of contaminated soil using selected ion flow tube mass spectrometry, SIFT-MS (2010-2013).
- Collaborator at: Selected ion flow tube mass spectrometry studies of volatile compounds emitted by bacterial cultures (PI Patrik Španěl, 2009-2012, Czech Science Foundation).
- Collaborator at: Research of new methods of detection of explosives (PI Svatopluk Civiš, 2007-2010, Czech ministry of trade and industry).

Short scientific visits in the UK and abroad

Keele University and Imperial College London (1 week in 2010)

Open University (SIFT-MS laboratory, Dr. C. Turner) (1 week in 2010)

Faculty of Bioscience Engineering - Organic Chemistry Environmental Organic Chemistry and Technology: EnVOC, Coupure links 653, 9000 Ghent – Belgium (1 week in 2012).

